

Bridge River Water Use Plan

**CARPENTER RESERVOIR PRODUCTIVITY
MODEL VALIDATION AND REFINEMENT:
DRAFT OF FINAL REPORT**

Reference: BRGMON#10

Final Implementation Year (Year 3)

Study Period: 2015-2018

Authors:

Limnotek and affiliated organizations

31 October 2018



**CARPENTER RESERVOIR
PRODUCTIVITY MODEL VALIDATION AND REFINEMENT
DRAFT OF FINAL REPORT**

Bridge – Seton Water Use Plan Study Number BRGMON#10

October 31, 2018



**CARPENTER RESERVOIR PRODUCTIVITY MODEL VALIDATION AND
REFINEMENT**

DRAFT OF FINAL REPORT

Bridge – Seton Water Use Plan Study Number BRGMON10

Submitted to
BC Hydro
Burnaby, B.C.

Prepared by:
Limnotek and associated organizations

October 31, 2018

Citation: Limnotek. 2018. Carpenter Reservoir Productivity Model Validation and Refinement (BRGMON10): Draft of final report. Report prepared for BC Hydro. 93p. plus appendices

*Authors of this report are listed according to task and affiliation under Acknowledgements on pages x and xi. The study was managed by St'at'imc Eco-Resources Ltd.

Cover photo: Carpenter Reservoir facing west, 2016. C. Perrin photo.

© 2018 BC Hydro.

No part of this publication may be reproduced, stored in a retrieval system, or transmitted, in any form or by any means, electronic, mechanical, photocopying, recording, or otherwise, without prior permission from BC Hydro, Burnaby, B.C.

EXECUTIVE SUMMARY

This report answers four management questions addressing uncertainties about relationships between water management actions and biological production in Carpenter Reservoir. Statistical modeling and a hydrodynamic model called CE-QUAL-W2 both using empirical data from 2015 and 2016 were developed to answer all questions as follows:

Question 1: Is light the primary factor regulating productivity of littoral habitat in Carpenter Reservoir?

Field measurements from 2015 and 2016 were used to build a regression model showing factors contributing to variance in accrual of periphyton biomass, the key indicator of biological production in littoral habitat. The model showed that periphyton biomass accrual is not sensitive to the range of light in the littoral zone but it was very sensitive to change in NO₃-N concentrations, a nutrient shown to limit algal production. ***These findings showed that light is not the primary factor regulating biological productivity of littoral habitat in Carpenter Reservoir.***

There are stable stony materials and unstable sand substrata in the littoral zone of Carpenter Reservoir. Almost no periphyton was found on sand so no model could be built using data from the sand. Samplers using sand as a substratum were subject to minor flows across the water – sand interface, similar to water movements in shallow water of the littoral zone. This physical disturbance may have been enough to inhibit development of an attached periphyton community. In contrast, a diverse algal assemblage did grow on stable substrata. The contrast in communities between these types of surfaces show that biological production is primarily defined by the physical composition of substrata. Stable materials support a robust and diverse assemblage of periphyton that can contribute to the littoral food web while unstable sandy materials subject to movement by water do not. Where the physical substrate supports periphyton, our findings show that periphyton is limited by NO₃-N concentration, not light.

These findings do not mean that sand does not support biological communities. An invertebrate community would be expected to be present in the sand, feeding on detrital organic matter derived from allochthonous sources and from settlement of organic matter produced in the overlying water column. In this case light would not be a factor in driving that production because the organic matter is produced elsewhere and is transported to the sand or it is derived through heterotrophic processes that do not need light for metabolism.

Question 2: Is light the primary factor regulating productivity of pelagic habitat in Carpenter Reservoir?

A combination of field observations and modeling was used to answer management question 2. The field measurements from 2015 and 2016 were used to build two regression models; one explaining factors contributing to variance in production of phytoplankton, the key indicator of biological production in pelagic habitat and the other explaining factors contributing to variance in biomass of zooplankton food for fish.

The phytoplankton model included light measured in two ways: photosynthetically active radiation (PAR) and turbidity under the premise that turbidity causes light attenuation. These variables were found to act differently on primary

production. A strong positive effect of PAR on primary production was greater than from other predictor variables. It showed that **rates of production changed with amount of irradiance occurring over the vertical profile of the photic zone**. An hypothesis was developed that turbidity induced limitation of phytoplankton growth by sequestration of nutrients by adsorption onto the very small particles that contribute to turbidity. This action by turbidity is a secondary and independent effect that was different from its effect on light attenuation and may explain independence of PAR and turbidity effects on primary production in the phytoplankton model.

The effect of PAR on primary production indirectly affected zooplankton biomass by being positively associated with primary production leading to change in phytoplankton biomass that is food for zooplankton. This indirect effect of light on zooplankton biomass was, however, very small and almost indistinguishable from sensitivity of zooplankton biomass to change in temperature. Similarly, turbidity influenced zooplankton potentially through action on feeding effectiveness but only in a small way compared to temperature.

In summary **light is a factor but not the main factor regulating biological production in pelagic habitat. PAR is the main variable driving this effect through its control of primary production**. Resulting phytoplankton biomass is a factor explaining variance in zooplankton biomass but **it's effect is of little consequence compared to water temperature that explains most of the variance in zooplankton biomass**. Water management actions that determine light in the water column are the same ones driving water temperature. Under exceptionally turbid conditions turbidity is high and temperature is low, mainly in the early part of the growing season. These conditions occur when water surface elevations are kept low in the spring and early summer. They will lower zooplankton biomass and reduce the amount of food for fish. In contrast, a management action that favours high water temperature and low turbidity (produced from high water surface elevation) will optimize production of zooplankton biomass and thus food for fish. Through these interactions it is not turbidity driving change. It is temperature.

Question 3: Is light penetration in Carpenter Reservoir impacted by changes in reservoir operations?

A combination of field observations and calibrated hydrodynamic modelling was used to answer management question 3. Observations from the field provided an understanding of the mechanisms controlling light penetration in Carpenter Reservoir and the hydrodynamic model was used to run scenarios based on historic operational data to assess whether changes in reservoir operation affect light penetration.

Results showed that thermal stratification isolates the surface layer of Carpenter Reservoir from cold and turbid inflows. Over the course of spring and summer, glacial fines in the surface layer settle, and the penetration of light increases. The difference in light penetration between years is primarily controlled by the initial turbidity in the surface layer at the start of summer stratification. The turbidity at the start of persistent stratification is lower when the water level in the reservoir is relatively high. In contrast, turbidity at the start of persistent stratification is relatively high when water level is low. At low water level the mixing of cold turbid inflows throughout the water column is enhanced. With a higher initial load of turbidity, it takes longer for the surface layer to clear over summer and average light penetration is reduced. These observations show

that reservoir operation, primarily the control of water surface elevation affects light penetration in Carpenter Reservoir.

Question 4: Can suspended sediment transport into Seton be altered by changes in Carpenter Reservoir operation?

The hydrodynamic model called CE-QUAL-W2, calibrated with field data from 2015 and 2016, was used to examine reservoir operation scenarios and their effect on the transport of suspended particles into Seton Lake and, for comparison, the Lower Bridge River. Analysis showed that turbidity in units of NTU could be modeled in place of suspended sediment concentration.

Flow to Seton Lake was turbid during freshet, followed by a decline over the summer months, followed by another peak in September. The first peak results from both the local inflow during freshet dominating the inflow from Downton Reservoir combined with high turbidity in the local inflow. Hence the first peak is largely not controlled by management actions. The second peak occurs after freshet when the total inflow into Carpenter Reservoir is dominated by the inflow and rising turbidity from Downton Reservoir. This second peak is controlled by management actions to regulate flow from Downton Reservoir. A conclusion is that the transport of suspended sediment into Seton Lake is affected by the operation of Carpenter and Downton Reservoirs. There are a number of factors that control both the timing and quantity of this load. They include the load of turbidity from Downton Reservoir (under management control), the load of turbidity from local tributaries (not under management control), the volume of the hypolimnion (under management control), and the flow rate to Seton Lake (under management control).

These same criteria will determine load of suspended sediment to the Lower Bridge River because the elevation of the outlet to the river is the same as that used to release water to Seton Lake and hydrodynamic processes delivering water and suspended particle load to the two outlets are the same.

Project Status

A summary of the status of BRGMON10 study findings is listed as follows:

Study objectives	Management questions	Status
Determine if light or other environmental variables affect periphyton production on stable and unstable substrata in Carpenter Reservoir.	Is light the primary factor regulating productivity of littoral habitat in Carpenter Reservoir?	Field measurements and statistical modeling using empirical data showed that light is not the primary factor regulating biological production in littoral habitat of Carpenter Reservoir. The primary factor regulating this production is type of substratum. Sand does not support an effective periphyton community. Stable substrata do support a robust periphyton community, which is regulated by NO ₃ -N concentration, a nutrient that limits algal production. This finding was shown by comparison of coefficients in regression modeling and biological interpretations. This management question has been answered
Determine if light or other environmental variables affect phytoplankton and zooplankton production in pelagic habitat in Carpenter Reservoir.	Is light the primary factor regulating productivity of pelagic habitat in Carpenter Reservoir?	Field measurements and statistical modeling using empirical data showed that photosynthetically active radiation is the primary factor regulating phytoplankton production, but temperature is the primary factor regulating zooplankton biomass (food for fish) in pelagic habitat of Carpenter Reservoir. Turbidity is not an important factor. These findings were shown by comparison of coefficients in regression modeling and biological interpretations. This management question has been answered.
Determine whether water management in Carpenter Reservoir affects light penetration or other environmental variables.	Is light penetration in Carpenter Reservoir impacted by changes in reservoir operations?	Two years of field data collection and hydrodynamic modeling showed that light penetration in Carpenter Reservoir is impacted by changes in reservoir operations. Control of inflow, outflow, and water surface elevation can modify light attenuation in the water column. This management question has been answered.
Determine if changes to reservoir operation affect the inflow of suspended sediment into Seton Lake.	Can suspended sediment transport into Seton be altered by changes in Carpenter Reservoir operation?	Suspended sediment transport to Seton Lake and to the Lower Bridge River can be altered by changes in the operation of Carpenter Reservoir. Two years of field data collection and hydrodynamic modeling showed that actions to keep the water surface elevations high, limit flow to Seton Lake and optimize storage in Downton Reservoir to minimize flow to Carpenter Reservoir are strategies that can help limit the transport of sediment to Seton Lake. Opportunities to implement these actions are reduced when the generating units at Shalalth must operate at full capacity and water must be

Study objectives	Management questions	Status
		<p>released from Downton Reservoir to maintain a safe water surface elevation according to seismic risks. Given that it is not commonly practical to avoid this flow routing, reduced sediment transport to Seton Lake may not be achievable.</p> <p>This management question has been answered.</p>

ACKNOWLEDGEMENTS

This project was performed under contract to BC Hydro as part of the Bridge River Water Use Plan Studies. Authors working on behalf of St'at'imc Eco-Resources included the following people:

Author	Task	Affiliation
C.J. Perrin, MSc. RPBio.	Study design, director of field operations, subject integration, reporting, client liaison	Limnotek
Roger Pieters, PhD	Study design, CE-QUAL-W2 modeling, reporting	University of British Columbia
Jennifer Harding, PhD	Study design, statistical analysis and modeling, reporting	Limnotek*
Dan Robb, PhD candidate	CE-QUAL-W2 modeling, study design, reporting	University of British Columbia
S. Bennett, MSc. RPBio.	Data compilation, statistical analysis	Limnotek

*Present address: Fisheries and Oceans Canada, Whitehorse, Yukon.

This project was performed under contract to BC Hydro as part of the Bridge River Water Use Plan Studies. The authors thank many people who contributed to the project as follows. Bonnie Adolf (Project Coordinator), Gilda Davis (contract manager), and Jude Manahan (bookkeeper) with St'at'imc Eco-Resources Ltd. (SER) are thanked for contract administration.

We thank the field crew including Annika Putt, Marc Laynes, Tyler Creasey, Allison Hebert, and several members of SER for energy and enthusiasm to complete long and often complicated days in the field. Allison Hebert worked with Shannon Harris to complete lab work and calculations for the primary production measurements. The field crew was assisted by L.J Wilson and Caroline Melville who were safety check-in people on most field days.

Chemical analyses of stream and lake water samples and periphyton biomass were completed at ALS Environmental under the management of Courtney Duncan. Danusia Dolecki performed the zooplankton enumerations and biomass measurements and Lech Dolecki completed the algal cell identifications, enumerations, and bio-volume measurements.

Odin Scholz (Split Rock Environmental Ltd.) and Brad Oleman (BC Ministry of Forests Lands and Natural Resource Operations) are thanked for support on access to meteorological data from the 5-Mile Forest Service weather station. We are grateful to Dr. David Levy, Fisheries Advisor to SER for numerous discussions regarding study scope and integration with other SER projects. Joes Goes is thanked for organizing

access for our crew to use the boat ramp at the east end of Anderson Lake. Mike Chung is thanked for assisting with data entry from field and lab sheets.

Several people from BC Hydro are thanked for attention to contract management with SER and for the provision of hydrology data from BC Hydro Power Records. They included Teri Neighbour, Dr. Ahmed Gelchu, Darin Nishi, Jeff Walker, and Matt Casselman. Jim Coles (Area Manager, BC Hydro), Rick Enegren (Dam Safety Engineer, B.C. Hydro), and Mark Thorsteinson (Dam Safety Engineer, B.C. Hydro) are thanked for approving our installation of meteorological instruments and samplers on the Terzaghi Dam and for approving our installation of samplers on the trash boom in Carpenter Reservoir.

GIS analysis and mapping in support of the CE-QUAL modeling was completed by Nicole Fink (GIS Specialist, BC Hydro) and Faizal Yusuf (Hydrotechnical Engineer, BC Hydro). Meaghan Leslie-Gottschligg produced the site location map. Special thanks goes to Dorian Turner of BC Hydro for arranging a location on grounds of the BRG1 generating station for us to install a solar radiation sensor and for organizing building space on the same property for our field crew to set up and operate a field lab. We also thank Adjoa Quanioo and Alex Huang, UBC co-op students, who helped with the CE-QUAL-W2 modelling as well as Thea Rodgers and Melanie Mewhort who helped with instrument servicing and data analysis and whose salaries were subsidized by the UBC Work Learn program.

TABLE OF CONTENTS

	Page
EXECUTIVE SUMMARY	iv
ACKNOWLEDGEMENTS	ix
TABLE OF CONTENTS	xi
LIST OF FIGURES	xiv
LIST OF TABLES.....	xx
1 INTRODUCTION.....	1
2 DESIGN	2
3 SITE DESCRIPTION.....	4
3.1 Location 4	
3.2 Catchment and Reservoir Areas.....	6
3.3 Reservoir bathymetry.....	6
4 METHODS	7
4.1 Field logistics.....	7
4.2 CE-QUAL-W2.....	8
4.2.1 Overview.....	8
4.2.2 Computational grid.....	9
4.2.3 Boundary conditions.....	12
4.2.3.1 Hydrology.....	12
4.2.3.2 Inflow temperature and chemistry	13
4.2.3.3 Meteorology	15
4.2.4 Reservoir conditions.....	15
4.2.4.1 Water column profiling	15
4.2.4.2 Instrument moorings	16
4.2.5 Initial conditions	16
4.2.6 Model testing.....	16
4.3 Biological measurements and modeling	17
4.3.1 Periphyton.....	17
4.3.2 Phytoplankton	21
4.3.3 Zooplankton	22
4.3.4 Regression analysis.....	23
4.3.5 Environmental variables	26
4.3.5.1 Periphyton and phytoplankton regression modeling	26
4.3.5.2 Zooplankton regression modeling	29
4.3.5.3 Descriptive environmental variables.....	30
5 RESULTS AND DISCUSSION	32
5.1 CE-QUAL-W2.....	32
5.1.1 Measured boundary conditions	32

5.1.1.1	Hydrology.....	32
5.1.1.2	Inflow temperature and chemistry	36
5.1.1.3	Meteorology	39
5.1.2	Measured reservoir conditions	39
5.1.2.1	Water column profiling	39
5.1.2.2	Instrument moorings	43
5.1.2.2.1	Temperature	43
5.1.2.2.2	Turbidity.....	44
5.1.3	Selection of scenarios	47
5.1.4	Modeled 2015 field year	51
5.1.4.1	Water temperature	51
5.1.4.2	Water chemistry	51
5.1.4.3	Tracers in 2015.....	55
5.1.5	Modeled 2016 field year	56
5.1.5.1	Water temperature	56
5.1.5.2	Water chemistry	59
5.1.5.3	Tracers in 2016.....	60
5.1.6	Management scenarios.....	61
5.2	<i>Biological modeling</i>	65
5.2.1	Periphyton.....	65
5.2.1.1	Stable substrata	65
5.2.1.1.1	Periphyton composition on stable substrata	65
5.2.1.1.2	Stable substrata regression model.....	65
5.2.1.2	Sand samplers	67
5.2.1.2.1	Periphyton composition on sand	67
5.2.1.2.2	Sand substrata regression model.....	68
5.2.2	Phytoplankton	69
5.2.2.1	Phytoplankton composition	69
5.2.2.2	Phytoplankton regression model.....	70
5.2.3	Zooplankton	73
5.2.3.1	Zooplankton composition	73
5.2.3.2	Zooplankton regression model.....	74
5.2.4	Sensitivity analysis	75
5.2.5	Biological response to management scenarios	76
6	ANSWERS TO MANAGEMENT QUESTIONS.....	79
6.1	<i>Question 1: Is light the primary factor regulating productivity of littoral habitat in Carpenter Reservoir?</i>	<i>79</i>
6.2	<i>Question 2: Is light the primary factor regulating productivity of pelagic habitat in Carpenter Reservoir?</i>	<i>80</i>
6.3	<i>Question 3: Is light penetration in Carpenter Reservoir impacted by changes in reservoir operations.....</i>	<i>82</i>
6.4	<i>Question 4: Can suspended sediment transport into Seton Lake be altered by changes in Carpenter Reservoir operations.....</i>	<i>84</i>

6.4.1	Approach	84
6.4.2	Outflow to Seton Lake	85
6.4.3	Outflow to the Lower Bridge River	86
6.4.4	Conclusion	87
6.5	CE-QUAL-W2 sources of error	88
7	LIST OF REFERENCES CITED	90
8	APPENDIX A: SPECIFICATIONS OF SUSPENDED AND BOTTOM MOORINGS	94
8.1	Mooring suspended from trash boom	94
8.2	Subsurface mooring	96
9	APPENDIX B. WINTER TEMPERATURES FROM THE SUSPENDED MOORING IN 2015 – 2016	98
10	APPENDIX C. METEROLOGICAL CONDITIONS IN 2015 AND 2016. 100	
11	APPENDIX D. SUPPLEMENTARY TRIBUTARY TEMPERATURE AND CHEMISTRY	102
11.1	Content of this appendix	102
11.2	Tributary temperature	102
11.3	Tributary water chemistry	103
12	APPENDIX E: CONTINUOUS TURBIDITY MONITORING	115
12.1	Appendix E-1: Continuous turbidity in the Middle Bridge River	115
12.2	Appendix E-2: Continuous turbidity in the reservoir	117
13	APPENDIX F: CE-QUAL-W2 model calibration	118
13.1	Approach 118	
13.2	Water temperature	121
13.3	Hypolimnetic Mixing	125
13.4	Specific Conductance	126
13.5	Turbidity 129	
13.6	Outflows 132	
13.7	Light attenuation	133
13.8	References cited in Appendix F	134
14	APPENDIX G: FIGURES SUPPORTING SCENARIOS MODELLED IN CE-QUAL-W2	135

LIST OF FIGURES

	Page
Figure 1. Sampling stations and landmarks in Carpenter Reservoir and associated lakes in the Bridge/Seton River system (Anderson Lake and Seton Lake). Stations C1 through C10 were stations for physical and chemical profiling along the longitudinal axis of Carpenter Reservoir. The “W” stations were tributary inflows and the “M” stations were meteorological stations. Periphyton moorings in Anderson Lake were labelled AW and AE and in Seton Reservoir they were labelled SN and SS. Chemistry and biological sampling stations in Anderson Lake were labelled A1 and A2 and in Seton Reservoir they were labelled S4 and S5.....	5
Figure 2. Image of the CE-QUAL-W2 computational grid. Width (B), density (ρ), pressure (P) and water quality state variables (Φ) are defined at cell centers. Horizontal velocity (U), longitudinal eddy viscosity (A_x) and diffusivity (D_x), and longitudinal shear stress (τ_{xx}) are defined at the right hand side of the cell. Vertical velocity (W) and vertical diffusivity (D_z) is defined at the bottom of the cell, and the vertical eddy viscosity is defined at the lower right corner of the cell. Adapted from Cole and Wells (2015).	10
Figure 3. Plan view of model segments. The Middle Bridge River flows into Segment 2. Terzaghi Dam is located at the east end of Segment 57. Segments 1 and 58 (not shown) are inactive boundary segments for use by the model.	11
Figure 4. Side view of Carpenter Reservoir showing the 56 active segments along the length of the reservoir and the 107 active layers. Boundary (inactive) layers are not shown. The Middle Bridge River enters on the left, and Terzaghi Dam is adjacent to the deepest segment on the right.	11
Figure 5. Cross channel profile of Segment 57, the last active segment before Terzaghi Dam. Shown are 107 active layers of 0.5 m each (layers 2 to 108). Layer 1 and 109 are inactive boundaries for use by the model. The top elevation of first active layer #2 is 651 mASL and the bottom elevation of the last active layer #108 is at 597.5 mASL.....	12
Figure 6. Cross channel profile of Segment 2, the shallowest active segment of the reservoir which received inflow from the Middle Bridge River. The top elevation of first active layer #2 was 651 mASL and the bottom elevation of the last active layer was 643.5 mASL. ...	12
Figure 7. Styrofoam array used to represent periphyton growth on stable substrata.	18
Figure 8. Sand pails used to host periphyton growth on sand in Carpenter Reservoir. Rigging on the pail handles was used to clip the pails onto lines of fixed length that were suspended from a boom. This arrangement provided a range of pail depths extending from close to the water surface to the bottom of the euphotic zone.	18
Figure 9. Total inflow to Carpenter Reservoir from LaJoie Dam averaged over 1961-2016 for each calendar day. Mean (heavy black line), maximum and minimum (medium black lines) and mean \pm one standard deviation (light black lines). The total inflow is shown in blue for 2015 and in red for 2016. There were three off-scale peaks consisting of a single point each.	32
Figure 10. Daily local inflow to Carpenter Reservoir, averaged over 1961-2016. Mean (heavy black line), maximum and minimum (medium black lines) and mean \pm one standard deviation (light black lines). The local inflow is shown in blue for 2015 and in red for 2016.	33
Figure 11. Flow release to Bridge generating stations during 1961 – 2016. Mean (heavy black line), maximum and minimum (medium black lines) and mean \pm one standard deviation (light black lines). The outflow is shown in blue for 2015 and in red for 2016.....	33

Figure 12. Water surface elevation in Carpenter Reservoir, 1960-2016 (a) and average water level by month in Carpenter Reservoir, 1960-2016 (b). Mean (heavy black line), maximum and minimum (medium black lines) and mean \pm one standard deviation (light black lines) are shown. The water level is shown in blue for 2015 and in red for 2016. The dashed lines mark the normal minimum (606.55 mASL) and maximum (651.08 mASL)..... 34

Figure 13. Average inflow from La Joie Dam, April to October, 1961 to 2017. The red lines show the mean and the mean \pm one standard deviation. 35

Figure 14. Average local inflow to Carpenter Reservoir, April to October, 1961 to 2017. The red lines show the mean and the mean \pm one standard deviation. 35

Figure 15. Average water level, Carpenter Reservoir, April to October, 1960 to 2017. The red lines show the mean and the mean \pm one standard deviation. 36

Figure 16. Tributary temperature (panels g and h), conductivity (panels i and j), and turbidity (panels k and l) contrasted between local inflow and inflow from La Joie in 2015 and 2016. Inflow (panels a and b), outflow (panels c and d), and reservoir water level (panels e and f) are shown for reference. 38

Figure 17. (a) Temperature, (b) conductivity, C25, (c) turbidity (corrected to bottle data), (d) dissolved oxygen, (e) dissolved oxygen as percent saturation, and (f) nominal chlorophyll profiles collected at Carpenter Reservoir station C2, May to October, 2015. The legend in the last panel gives the cast number, station and date. In (f), the dash lines marks the bottom of the photic zone (the 1% light level). 41

Figure 18. (a) Temperature, (b) conductivity, C25, (c) turbidity (corrected to bottle data), (d) dissolved oxygen, (e) dissolved oxygen as percent saturation, and (f) nominal chlorophyll profiles collected at Carpenter Reservoir station C2, April to October, 2016. The legend in the last panel gives the cast number, station and date. In (f), the dash lines marks the bottom of the photic zone (the 1% light level). 42

Figure 19. (a) Wind speed at Fivemile, (b) air temperature at Terzaghi Dam, (c) solar radiation at Terzaghi Dam, (d) inflows and (e,f) water temperature at log boom in Carpenter Reservoir, 16 April to 20 October 2015. From 22 May to 18 June, the deepest sensor was removed for repair of the turbidity wiper. Arrows mark the times of the sampling surveys. 45

Figure 20. (a) Wind speed at Fivemile, (b) air temperature at Terzaghi Dam, (c) solar radiation at Terzaghi Dam, (d) inflows and (e,f) water temperature (2 hour average) in Carpenter Reservoir, 13 April to 14 October 2016. Data from both the boom and subsurface moorings were interpolated to 1 m depths. Arrows mark the times of the sampling surveys. Time is in days of 2016. 46

Figure 21. Modelled photic zone depth and flow boundary conditions for all years 1961–2017; (a) photic zone depth; (b-f) flow boundary conditions and water level; (blue) clear surface layer (deep photic zone) through (red) turbid surface layer (shallow photic zone). The numbers on the right indicate the year of the flow boundary conditions and their colour corresponds to the colour of the lines in the figure. 48

Figure 22. Modelled photic zone depth and flow boundary conditions for all years 1961–2017; (a) photic zone depth; (b-f) flow boundary conditions and water level; (colours) selected years for model scenarios; (grey) years not selected for model scenarios. 50

Figure 23. Field year 1 (2015). Modelled water quality parameters at segment 53 (station C2). . 53

Figure 24. Field year 1 (2015). Snapshots of modelled temperature T, conductivity C25 and turbidity Tu along the length of the reservoir at selected dates. 54

Figure 25. Field year 1 (2015). Passive conservative tracers at segment 53 (station C2) from (a) initial water in the reservoir, (b) inflow from La Joie Dam, and (c) local tributary inflow. .	56
Figure 26. Field year 2 (2016). Modelled water quality parameters at segment 53 (station C2). .	57
Figure 27. Field year 2 (2016). Snapshots of modelled temperature T, conductivity C25 and turbidity Tu along the length of the reservoir at selected dates.....	58
Figure 28. (a) Linear and (b) log-linear plots comparing measured and modelled surface turbidity at segment 53 (station C2) for Field years 1 and 2 (2015 and 2016). (solid lines), modelled turbidity at 1 m depth; (circles), measured turbidity from the Sea-Bird profiles at 1 m depth; (dash line) log-linear least-squares fit for the measurements collected from May to July in 2015 and 2016.....	60
Figure 29. Field year 2 (2016). Passive conservative tracers at segment 53 (station C2) from (a) initial water in the reservoir, (b) inflow from La Joie Dam, and (c) local tributary inflow. .	61
Figure 30.(a-d) Flow boundary conditions, and (e) the water level for each model scenario. The grey region indicates the model period (22 May – 20 Oct).	62
Figure 31. Modelled (a) temperature, (b) turbidity, and (c) photic zone depth, all at 1 m depth at segment 53 (station C2), for each model scenario.....	64
Figure 32. Mean algal biovolume by division found on ball moorings, by incubation period in Carpenter Reservoir in 2015 and 2016. Error bars are standard deviations calculated from biovolume of all taxa combined.	65
Figure 33. Algal biovolume, by taxonomic group, found on sand moorings by incubation period in Carpenter Reservoir in 2015 and 2016. Error bars are standard deviations calculated from biovolume of all taxa combined.	68
Figure 34. Composition of phytoplankton biovolume in Carpenter Reservoir by month. Values are mean biovolume by algal division calculated from samples collected in 2015 and 2016 at stations C2 and C6. Error bars are standard deviations of mean biovolume among all taxa.	70
Figure 35. Arithmetic mean particle size in water samples, by station and month in 2015 (left) and 2016 (right).	72
Figure 36. Mean zooplankton biomass (\pm sd) by order and month in Carpenter Reservoir. Data are from duplicate samples collected at each of two stations on each monthly sampling episode in each of two years (2015 and 2016).	73
Figure 37. Predicted mean accrued periphyton biomass on stable substrata by scenario.....	77
Figure 38. Predicted mean growing season rate of primary production among water management scenarios in Carpenter Reservoir.....	78
Figure 39. Predicted mean growing season zooplankton biomass among water management scenarios in Carpenter Reservoir.....	79
Figure 40. Model results showing mean annual photic zone depth as a function of mean water level over the first 30 days of the model period. The blue circles show reservoir operational conditions from 1961-2017 subjected to meteorological and water quality forcing from 2015. The red circles show reservoir operational conditions from 1961-2017 subjected to meteorological and water quality forcing from 2016.	84
Figure 41. Hydrodynamic model outflow to Seton Lake for each scenario: (a) temperature, and (b) turbidity. The intakes to Seton Lake were shut down from mid-September to mid-October 2016, which shows up as a data gap in Scenario LowDR.	86

Figure 42. Hydrodynamic model outflow to the Lower Bridge River compared to model outflow to Seton: (a,b) temperature; (c,d) turbidity; (a,c) Scenario NormOP (2011); (b,d) Scenario LowDR (2016)..... 87

Figure 43. Temperature at 0.5 m, 5 m, and 10 m at the log boom in Carpenter Reservoir during October 20, 2015 through April 13, 2016. The dashed line marks the temperature of maximum density ($T_{MD} = 3.98^{\circ}\text{C}$). 99

Figure 44. Hourly (a) wind speed, (b) air temperature, (c) relative humidity, (d) precipitation and (e) total solar irradiance data available for Carpenter Reservoir during April to October 2015. The grey line in (d) is local inflow in units of $\text{m}^3 \cdot \text{s}^{-1}/100$ 100

Figure 45. Hourly (a) wind speed, (b) air temperature, (c) relative humidity, (d) precipitation and (e) total solar irradiance data available for Carpenter Reservoir during April to October 2016. The grey line in (d) is local inflow in units of $\text{m}^3 \cdot \text{s}^{-1}/100$ 101

Figure 46. Tributary temperature for (a, b) Middle Bridge and Hurley River (c,d) larger tributaries, and (e,f) smaller tributaries, for 2015 and 2016 respectively. 103

Figure 47. Monthly turbidity and total suspended solids concentrations in 2015 and 2016 in the Bridge River inflows. Flow rate in 2015 (a) and 2016 (b) is shown for reference. Turbidity data are corrected to lab values. 105

Figure 48. Monthly turbidity and total suspended solids concentrations in 2015 and 2016 in small tributaries and in the tailrace of the generating station. Turbidity data are corrected to lab values. 106

Figure 49. Turbidity versus total suspended solids (TSS) for tributaries to Carpenter Reservoir, 2015 and 2016. RED – Samples from Upper and Middle Bridge Rivers and the Bridge Tailrace. BLUE – Samples from the Hurley River and from Gun, Truax, Tyaughton, Marshall and Keary Creeks. The blue line gives the fit through zero to the blue data.. 107

Figure 50. Total dissolved phosphorus and soluble reactive phosphorus concentration (shown as PO_4) in 2015 and 2016 in the Bridge River inflows. Flow rate in 2015 (a) and 2016 (b) is shown for reference..... 108

Figure 51. Total dissolved phosphorus and soluble reactive phosphorus concentration in 2015 and 2016 in the small tributary inflows to Carpenter Reservoir and in outflow at the Bridge generating station. 109

Figure 52. Total dissolved phosphorus, soluble reactive phosphorus (shown as PO_4), and total phosphorus concentration in 2015 (left panels) and 2016 (right panels) in the Bridge River inflows. Flow rate in 2015 (a) and 2016 (b) is shown for reference..... 110

Figure 53. Total dissolved phosphorus, soluble reactive phosphorus (shown as PO_4), and total phosphorus concentration in the small tributary inflows to Carpenter Reservoir in 2015 (left panels) and 2016 (right panels)..... 111

Figure 54. Conductivity (shown as C25) and nitrate-N (shown as NO_3) concentration in 2015 (left panels) and 2016 (right panels) in the Bridge River inflows. Flow rate in 2015 (a) and 2016 (b) is shown for reference..... 113

Figure 55. Conductivity (shown as C25) and nitrate-N (shown as NO_3) concentration in 2015 (left panels) and 2016 (right panels) in the small tributary inflows to Carpenter Reservoir... 114

Figure 56. (a) Inflow, (b) YSI turbidity, and (c) hourly average turbidity from inflow to the top of Carpenter Reservoir, 14 April to 22 October, 2015. **MBAbove** marks the Middle Bridge River above the Hurley; **MBBelow** marks the Middle Bridge Below the Hurley, and **MBCConf** marks the Middle Bridge at confluence with Carpenter Reservoir. Flow in the Hurley was estimated as 25% of the local flow. 116

Figure 57. **(a)** Inflow, **(b)** YSI turbidity, and **(c)** hourly average turbidity from inflow to the top of Carpenter Reservoir, 13 April to 26 October, 2016. **MBAbove** marks the Middle Bridge River above the Hurley; **MBBelow** marks the Middle Bridge Below the Hurley, and **MBConf** marks the Middle Bridge at confluence with Carpenter Reservoir. Flow in the Hurley was estimated as 25% of the local flow. 117

Figure 58. Turbidity data recorded at the log boom in Carpenter Reservoir, 16 April to 20 October, 2015. The recorder was at 27.5 m depth before 18 June 2015, and at 30 m depth thereafter. The red + signs give the turbidity measured at 30 m by the Sea-Bird at Station C2. 118

Figure 59. Turbidity data recorded at the log boom in Carpenter Reservoir, 13 April to 14 October, 2016. The recorder was at located 1.8 m above the bottom on the subsurface mooring approximately 1 km downstream of the log boom. At the start of the mooring period the turbidity recorder was at a depth of 30.9 m. As the water level rose, the depth of water above the turbidity recorder increased to 43.6 m by the end of the mooring period. 118

Figure 60. Comparison of the temperature measured at the log boom (blue) and the temperature from segment 53 (station C2) of the model (red) at depths of (a) 0.5, (b) 5, (c) 15, (d) 20 and (e) 30 m during field Year 1 (2015) (left), and Field Year 2 (2016) (right). 122

Figure 61. Measured and modelled temperature profiles at station C1--C9 in 2015 (Field Year 1). 123

Figure 62. Measured and modelled temperature profiles at station C1--C9 in 2016 (Field Year 2). 124

Figure 63. Measured and modelled conductivity profiles at station C1--C9 in 2015 (Field Year 1). 127

Figure 64. Measured and modelled conductivity profiles at station C1--C9 in 2016 (Field Year 2). 128

Figure 65. Measured and modelled turbidity profiles at station C1--C9 in 2015 (Field Year 1). . 130

Figure 66. Measured and modelled turbidity profiles at station C1--C9 in 2016 (Field Year 2). . 131

Figure 67. Measured and modelled (a,b) temperature and (c,d) turbidity; in (a,c) 2015 and (b,d) 2016; at (blue) Bridge powerhouse on Seton Lake (to Seton) and (red) the Lower Bridge River downstream of Terzaghi Dam (to LBR); (solid lines) model output; (dashed lines) tributary temperature loggers; (markers) tributary sampling with the YSI probe; (mod) model output; (mes) measured values. The Bridge powerhouse units were shut from mid-September to mid-October which shows up as a data gap for the model output. From 14 Jul to 11 Aug 2016, the tributary temperature logger in the Lower Bridge River was malfunctioning, which shows up as a data gap for the measured data. 132

Figure 68. Scatter plot of light extinction coefficient versus turbidity. Each data point corresponds to one Sea-Bird profile where the extinction coefficient was calculated from the PAR measurements and the turbidity was the mean value from the water surface to the 1 percent light level. Measurements from Carpenter Reservoir, Seton Lake, and Anderson Lake are included in the regression. 133

Figure 69. Scenario 1, Clear Surface Layer (1973). Modelled water quality parameters at segment 53 (station C2). 135

Figure 70. Scenario 2, Turbid Surface Layer (1999). Modelled water quality parameters at segment 53 (station C2). 136

Figure 71. Scenario 3, Normal Operations (2011). Modelled water quality parameters at segment 53 (station C2). 137

Figure 72. Scenario 4, Low Downton Reservoir (2016). Modelled water quality parameters at segment 53 (station C2).....	138
Figure 73. Scenario 1, Clear Surface Layer (1973). Snapshots of modelled temperature T , conductivity C_{25} , and turbidity Tu	139
Figure 74. Scenario 2, Turbid Surface Layer (1999). Snapshots of modelled temperature T , conductivity C_{25} , and turbidity Tu	140
Figure 75. Scenario 3, Normal Operations (2011). Snapshots of modelled temperature T , conductivity C_{25} , and turbidity Tu	141
Figure 76. Scenario 4, Low Downton Reservoir (2016). Snapshots of modelled temperature T , conductivity C_{25} , and turbidity Tu	142
Figure 77. Scenario 1, Clear Surface Layer (1973). Passive conservative tracers at segment 53 (station C2) from (a) Initial water in the reservoir, (b) inflow from La Joie Dam, (c) Local tributary inflow.....	143
Figure 78. Scenario 2, Turbid Surface Layer (1999). Passive conservative tracers at segment 53 (station C2) from (a) Initial water in the reservoir, (b) inflow from La Joie Dam, (c) Local tributary inflow.....	144
Figure 79. Scenario 3, Normal Operations (2011). Passive conservative tracers at segment 53 (station C2) from (a) Initial water in the reservoir, (b) inflow from La Joie Dam, (c) Local tributary inflow.....	145
Figure 80. Scenario 4, Low Downton Reservoir (2016). Passive conservative tracers at segment 53 (station C2) from (a) Initial water in the reservoir, (b) inflow from La Joie Dam, (c) Local tributary inflow.....	146

LIST OF TABLES

	Page
Table 1. Catchment areas that drain into Carpenter Reservoir.....	6
Table 2. Morphometric and bathymetric measures for Carpenter Reservoir.	7
Table 3. Physical and chemical output computed by CE-QUAL-W2	9
Table 4. List of drainage and model segments for CE-QUAL-W2 modeling.....	10
Table 5. Catchments contributing to local inflow to Carpenter Reservoir.	13
Table 6. Dates of periphyton sampling series in 2015 and 2016	19
Table 7. Number of observations applied to periphyton accrual for stable substrata and unstable substrata regression analyses.....	23
Table 8. Number of observations applied to the phytoplankton production regression analyses.	24
Table 9. Number of observations applied to the zooplankton biomass regression model.....	24
Table 10. Hypotheses of response by periphyton accrual and phytoplankton production to selected environmental variables.	28
Table 11. Hypotheses for predictor variables included in the zooplankton analyses.....	30
Table 12. Layout of model runs.	51
Table 13. Water level, volume and volume change over the first 40 days of the model scenarios.	63
Table 14. Sensitivity of biological endpoints to change in predictor variables among each of the biological production models.	76
Table 15. Listing of instruments attached to the suspended vertical line mooring in Carpenter Reservoir during April 16 through October 20, 2015.....	94
Table 16. Listing of instruments attached to the suspended vertical line mooring in Carpenter Reservoir during October 20, 2015 through April 13, 2016 (winter deployment).....	95
Table 17. Listing of instruments attached to the suspended vertical line mooring in Carpenter Reservoir during April 13 through October 14, 2016.....	95
Table 18. Listing of instruments attached to the subsurface vertical line mooring in Carpenter Reservoir during April 13 through October 14, 2016.....	97
Table 19. Model parameters used in this study and the default CE-QUAL-W2 values. The column on the right indicates whether the parameters were based on field observations (obs) or selected as calibration parameters (cal).....	119
Table 20. Mean error and root-mean-square error (RMSE) of temperature, conductivity, and turbidity. CE-QUAL-W2 model output compared to field measurements from the moored thermistor chain attached to the log boom, the Sea-Bird profiles, and tributary sampling at the Bridge powerhouse outflow on Seton, and the Lower Bridge River downstream of Terzaghi Dam.	120

1 INTRODUCTION

The Bridge-Seton Water Use Plan Consultative Committee (CC) developed aquatic ecosystem objectives for the Bridge River watershed that included efforts to maximize the abundance and diversity of fish populations while establishing flow controls for hydroelectric power generation, among other interests (Bridge River WUP CC, 2003). The Bridge River watershed provides habitat for resident fish species, which are valued from commercial, recreational, and cultural perspectives. Tradeoffs occurred in the water use planning, resulting in decisions to manage water elevations in reservoirs of the Bridge River watershed (Downton, Carpenter, Seton), manage spills from the reservoirs, and define flows in rivers (Middle and Lower Bridge River, Seton River). The complete package of flow controls is collectively known as N2-2P. While N2-2P was accepted, the Bridge River WUP CC (2003) was constrained in making decisions by lack of information about the effects of change in flows on fish populations and biological production that support those populations. Despite this uncertainty, N2-2P was implemented on March 30, 2011 (Water Act Order 2011, Bridge River Power Development Water Use Plan, 17 March 2011) with a commitment to fund monitoring studies to fill data gaps and better inform people tasked with water management decisions in future years, including the St'át'imc people and St'át'imc Eco-Resources Ltd. (SER).

The Bridge River WUP CC (2003) developed a predictive model of biological productivity in Carpenter Reservoir to assist with defining the scope of monitoring and develop an understanding of links between water management decisions and biological production. The model was based on an assumption that light solely limited that biological production. During model development, the CC found that uncertainties about how water management actions may change the perceived light-driven biological production in pelagic and littoral habitats of Carpenter Reservoir could not be resolved because of many data gaps needed for model calibration. Studies were recommended to fill those data gaps and update or replace the existing model.

Four management questions were proposed by the CC as follows.

- 1) Is light the primary factor regulating productivity of littoral habitat in Carpenter Reservoir?
- 2) Is light the primary factor regulating productivity of pelagic habitat in Carpenter Reservoir?
- 3) Is light penetration in Carpenter Reservoir impacted by changes in reservoir operations?
- 4) Can suspended sediment transport into Seton be altered by changes in Carpenter Reservoir operation?

This report describes the development of a new model and its application to various water management scenarios using data that were collected in 2015 and 2016

and the complete hydrological record dating from the beginning of reservoir formation in 1962. Analysis of model output is used to answer the four management questions.

2 DESIGN

Biological production was defined by three metrics. Accrual of periphyton biomass and rate of production by phytoplankton were selected because photosynthetic algae in these assemblages (one attached and the other free living in the water column) are the only part of the reservoir food web that directly uses light, the main variable of interest among management questions, as an energy source for production of organic matter supplying the food web in Carpenter Reservoir. For question 1, algal production was measured as periphytic algal accrual in units of $\mu\text{g chl-a}\cdot\text{cm}^{-2}$ for set time periods (Perrin et al. 1987, Bothwell 1988) where chl-a is chlorophyll-a, a primary plant pigment that is commonly used as a measure of biomass in algae (Wetzel 2001, Behrenfeld et al. 2005). For question 2, algal production was production of phytoplankton measured as the amount of ^{14}C incorporated into algal biomass and expressed in units of $\text{mg C}\cdot\text{m}^{-3}\cdot\text{d}^{-1}$ (Steeemann Nielsen 1952, Wetzel 2001). These measurements of algal production in each of littoral and pelagic habitats are standard procedures. They show the amount of carbon fixed per unit area or volume per unit time. Fish populations that are of ultimate interest by the consultative committee ingest invertebrates or other fish as food sources. Invertebrates ingested by fish include zooplankton, benthic invertebrates that use bottom sediment as habitat and emerge through the water column during transition from larval and pupal stages to adults, benthic invertebrates that drift into the reservoir from tributary streams, and terrestrial insects that land on the water surface and fail to escape the surface tension. To facilitate bridging the gap between algal production and fish, zooplankton biomass was selected as the third metric to model. Zooplankton are sensitive to the hydrology of Carpenter Reservoir (Perrin and MacDonald, 1999), making them a good indicator of interactions between water management actions, natural hydrology, and food web processes supporting fish populations. The combination of the three metrics provided measures of primary and secondary production in Carpenter Reservoir.

Multiple regression analysis was used to model the relative importance of light and other habitat attributes that may drive biological production. Regression analysis retains the original units of measure and allows quantitative prediction of the dependent variable (primary production, periphyton accrual, zooplankton biomass) with estimated error.

The regression model had the following generic form:

$$y_i = \beta_0 + \beta_1 x_{i1} + \beta_2 x_{i2} \dots + \beta_j x_{ij} + \varepsilon_i$$

Equation 1

where

y_i is the value of a biological metric for an i th observation,

$x_{1...j}$ is the value of independent variable 1 and j is the number of independent variables,

β_0 is the intercept when all predictor variables (e.g. variables describing habitat attributes) have a value of zero,

β_1 is the regression slope for y on x_1 when all other predictor variables (other x 's) are held constant,

β_2 is the regression slope for y on x_2 when all other predictor variables (other x 's) are held constant,

β_j is the regression slope for y on x_j when all other predictor variables (other x 's) are held constant, and

ε_i is unexplained error associated with the i th observation.

One regression model for each biological dependent variable (periphyton accrual, phytoplankton primary production, zooplankton biomass) was calculated using biological metric values matched with light and other habitat attributes. The rationale for selection of those attributes is described in Section 4.3.5.1 and Section 4.3.5.2. To expand ranges of values of dependent variables that is desirable in regression modeling, similar data were collected from Anderson Lake and Seton Lake that are part of the Bridge/Seton Rivers system (Figure 1).

A second part of modeling involved building a CE-QUAL-W2 hydrodynamic simulation model (<http://www.cee.pdx.edu/w2/>) of Carpenter Reservoir. Output included physical and chemical variables known to drive biological production and were included as candidate independent variables in the regression modeling (see Section 4.3.5.1 and Section 4.3.5.2). Those variables were associated with light, nutrient concentrations, and temperature. CE-QUAL-W2 was built and calibrated using two years of detailed empirical data from Carpenter Reservoir and run among various water management scenarios. CE-QUAL-W2 output provided input to the regression equations for each scenario to show the potential effects of the different scenarios on biological production. Relative change in biological production between the management scenarios provided insight into the sensitivity of the biological communities to water management actions. Output from this linking of the two models was used to answer management questions 1 and 2 (Section 1). CE-QUAL-W2 alone was used to answer management questions 3 and 4.

3 SITE DESCRIPTION

3.1 Location

Carpenter Reservoir is situated within the original Bridge River floodplain between the Bendor Range of the Coast Mountains to the south and the Shulaps Range, Pearson Ridge, and Marshall Ridge of the Chilcotin Ranges to the north (Figure 1). The reservoir was formed with construction of the Mission Dam on the Bridge River in 1960. In 1965 it was renamed the Terzaghi Dam. The dam is located 40 km upstream of the confluence of the Bridge River and the Fraser River near Lillooet. The width of the original flood plain is up to 1.5 km. Substrata within the draw down zone consists of a thin sediment veneer overlying glacial silts and sand with localized gravel and cobble remnants. At drawdown the river typically erodes a profile of approximately 1 m below floodplain elevation, re-suspending substratum materials in the process. Deposits of organic debris including small branches and forest litter that is transported from upstream are evident in most locations where cut banks have formed.

The Terzaghi Dam is located at a narrow gap between bedrock outcrops at the eastern extent of the original Bridge River floodplain. The dam was constructed over an original diversion dam that was built in 1948 (BC Hydro 1995). The dam is an earthfill structure, 60 m high with a crest length of 366 m. A spillway with two gates and a free overflow section is located in rock on the right (facing downstream) abutment. A low-level outlet tunnel is located below the spillway.

Carpenter Reservoir is 50 km long and has an average width of 1 km at full pool with a longitudinal axis lying east west. It extends westward from the Terzaghi Dam along the original Bridge River floodplain. The reservoir surface area at full pool is $46.2 \times 10^6 \text{ m}^2$ but it declines to approximately half this area at full drawdown. The dewatered area at drawdown occurs along 25 km of the Bridge River floodplain in the western half of the reservoir. From the reservoir shorelines, ridges to the north rise to 2,445 m and peaks to the south are at elevations of more than 3,000 m.

The Terzaghi Dam is used to store water for power generation. Water in Carpenter Reservoir is diverted through two tunnels located 3 and 4 km respectively upstream of the dam. The tunnels pass through Mission Mountain to the south and through penstocks to powerhouses called BRG1 and BRG2 located at Shalalth on Seton Lake. Water is discharged from the powerhouses to Seton Lake.

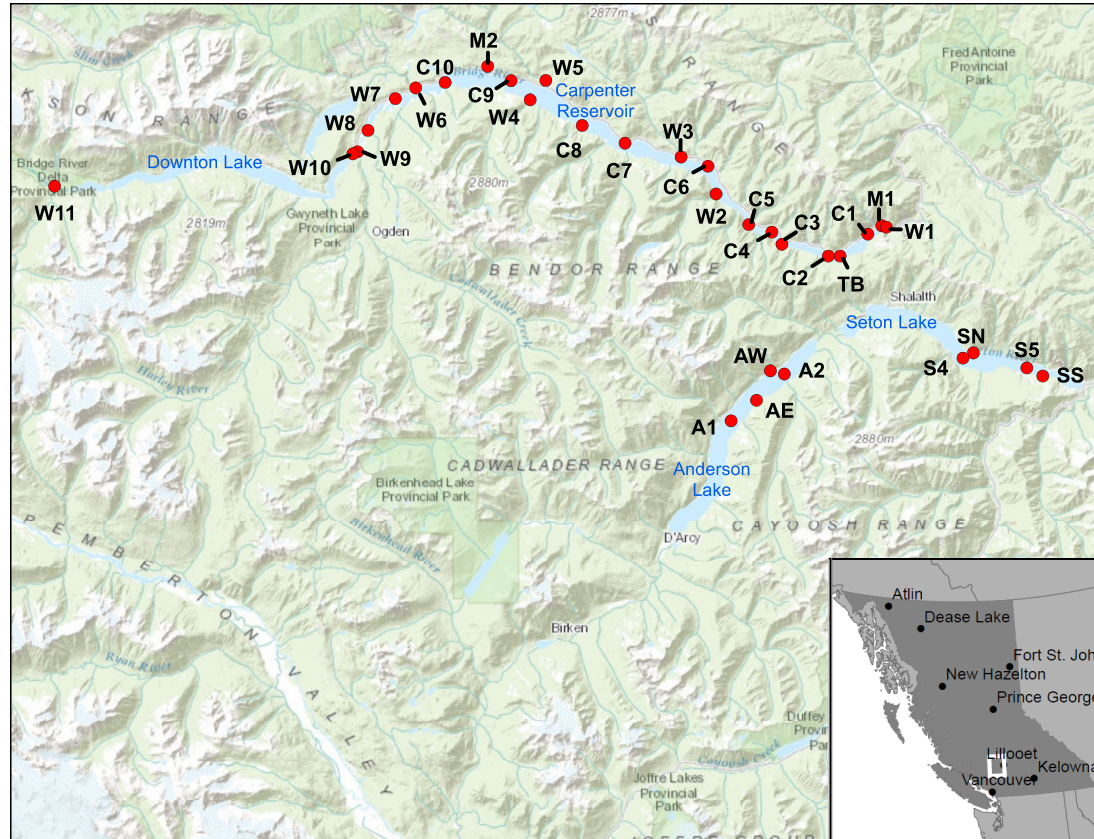


Figure 1. Sampling stations and landmarks in Carpenter Reservoir and associated lakes in the Bridge/Seton River system (Anderson Lake and Seton Lake). Stations C1 through C10 were stations for physical and chemical profiling along the longitudinal axis of Carpenter Reservoir. The “W” stations were tributary inflows and the “M” stations were meteorological stations. Periphyton moorings in Anderson Lake were labelled AW and AE and in Seton Reservoir they were labelled SN and SS. Chemistry and biological sampling stations in Anderson Lake were labelled A1 and A2 and in Seton Reservoir they were labelled S4 and S5.

3.2 Catchment and Reservoir Areas

Catchments that drain into the reservoir include the Middle Bridge River, the Hurley River, Gun Creek, Tyaughton Creek, Marshall Creek and numerous other streams (Table 1, Figure 1). The Middle Bridge River (MBR) upstream of the Hurley River confluence represents 26.7% of total catchment area for the reservoir. The MBR carries discharge from Downton Reservoir that receives eastward drainage from the Coast Mountains. The MBR also receives flow from the Hurley River (18.2% of total catchment area) at the town of Goldbridge. A tributary called Tyaughton Creek has a relatively large catchment area (20.5% of the total), but all is within the relatively dry Chilcotin Mountains where water yield is low compared to that from the MBR. Other local drainage represents 34.6% of the catchment area. Water from the west and south originates as glacial meltwater at alpine elevations of the Coast Mountains (1,800 to 3,000 m). Parent materials in much of the headwater areas are granitic and volcanic. The Bridge River is a 6th order system at the Carpenter Reservoir.

Table 1. Catchment areas that drain into Carpenter Reservoir.

Drainage Name	Area (ha)	Percent of total area
Drainage to La Joie Dam	99,069	26.7
Hurley River	67,640	18.2
Tyaughton Creek	75,973	20.5
Gun Creek	58,988	15.9
Other local drainage	60,007	18.7
TOTAL (to Terzaghi Dam and tunnel intakes)	371,029	100

3.3 Reservoir bathymetry

Daily surface elevation and live storage volume were downloaded directly from BC Hydro, System Control Centre (Power Supply Operations). The storage data were from a regression model produced by BC Hydro that determines live storage volume as a function of water surface elevation. Volumes for the model were determined from interpretation of air photos taken at a low water surface elevation. Water surface area determined at several elevations on the air photo using planimetry multiplied by depth interval between elevations provided volumes for those selected elevations. For a given elevation, the sum of strata volumes below that elevation provided live storage volume. The calculated model is run daily by BC Hydro to determine live storage volume from measurements of water surface elevation in the dam forebay at midnight.

In addition to this storage model, a more detailed bathymetric model, also known as a digital elevation model (DEM) was compiled by BC Hydro for this project. A DEM is a basic tool for setting up and running CE-QUAL-W2. The DEM supported calculations of water volumes in the whole reservoir and in various segments and bins for given water surface elevations. It was calculated by digitizing basin elevation maps of the

original Bridge River floodplain that was inundated following commissioning of the Terzaghi Dam.

A summary of morphometric features of the reservoir is shown in Table 2. The intake gates to the Seton Lake tunnels limit the lowest water surface elevation at 600.61m and 599.54 m (to bottom of gate). The original riverbed elevation immediately downstream of the Terzaghi Dam is approximately 609 m (Topographic map 92 J/16, 1992). This close proximity to the intake elevations shows the tunnels are located close to the original riverbed and that all storage volume is available as live storage (available to be withdrawn into the penstocks). Water depth in the region of the tunnels at full pool is 50m.

Table 2. Morphometric and bathymetric measures for Carpenter Reservoir.

Measure	Value at full pool (652 m)
Reservoir Length (km)	50
Average Reservoir Width (km)	1
Reservoir Area (ha)	46.2 x 10 ⁶ m ²
Maximum water depth (m)	55
Live storage volume (m ³)	91.13 x 10 ⁷ m ³
Dead storage volume	0
Total storage (m ³)	91.13 x 10 ⁷ m ³

4 METHODS

4.1 Field logistics

All field activities were staged out of Lillooet, British Columbia. A one-ton field truck was used to tow an 8 m long, welded aluminum work boat that was powered by twin v8 inboard engines and jet drives. The boat was equipped with davit and winch for deploying instruments and had ample deck space for limnological sampling. One route of access to Carpenter Reservoir was via the Lillooet Pioneer Road 40 (also known as the Bridge River Road) north from Lillooet. Rudimentary boat ramps on the reservoir located at Tyaughton Creek, a recreation site at Big Horn Creek, at Marshall Creek, and at the Terzaghi Dam were adequate for launching the boat. Seton Lake was accessed from a public boat launch near Lillooet. Anderson Lake was accessed via Seton Lake. To do so, two crew members piloted the boat up Seton Lake, met other crew members at the public boat launch in Shalalth who drove the truck and trailer from Lillooet along the Bridge River Road to Carpenter Reservoir and over Mission Mountain to Shalalth. The boat was loaded onto the trailer, towed to Anderson Lake, and launched from a beach at Seton Portage. A second route of access to Carpenter Reservoir was from Seton Portage via the Mission Mountain Road. This route was used following sampling on Seton Lake and Anderson Lake.

All stream sampling sites were accessed via truck at or near road crossings or by boat at points of discharge into Carpenter Reservoir.

4.2 CE-QUAL-W2

4.2.1 Overview

CE-QUAL-W2 is a hydrodynamic and water quality model for rivers, lakes, reservoirs and estuaries. CE-QUAL-W2 laterally averages calculations (across channel) with segments along the length of the water body, and bins from the surface to the bottom. This structure makes CE-QUAL-W2 particularly suited for modelling long and narrow water bodies such as Carpenter Reservoir. Lateral averaging reduces the model to 2-dimensions, capturing the important physics along the length of the reservoir while ensuring the run time for the model is reasonable for a desktop computer. This also makes it possible to explore a range of reservoir operation scenarios. CE-QUAL-W2 has been widely used, having been applied to over 200 reservoirs in the United States, and more than 100 other reservoirs worldwide (<http://www.ce.pdx.edu/w2/>). The source code for CE-QUAL-W2 is publicly available and is currently being developed and maintained at Portland State University (<http://www.ce.pdx.edu/w2/>) for the US Army Corp of Engineers. In addition, CE-QUAL-W2 is widely accepted in the scientific literature, making it ideal for our purposes.

CE-QUAL-W2 solves laterally averaged equations of fluid flow for conservation of mass, and conservation of momentum along the length of the reservoir. The model assumes that the reservoir is well mixed across channel, a reasonable assumption in a narrow reservoir like Carpenter Reservoir. The model will solve transport equations for temperature, conductivity, turbidity, and nutrients in Carpenter Reservoir, which are included in the list of relevant environmental variables for the biological regression modeling (Section 4.3.5). Conductivity is not on that list but it is needed for solving mass transport equations.

CE-QUAL-W2 requires input data describing the physical and chemical state of the reservoir over time periods when it will be run. The time was May through October of a given year or scenario. This duration covers the time from lowest water surface elevation and volume in early spring to highest water surface elevation and volume in the fall and the time of most annual biological production, assuming relatively small rates of biological production in the winter. Input data was collected in 2015 and 2016 from all main river and tributary inflows, multiple profiling stations along the longitudinal axis, meteorological stations and outflows as described in the following sections.

CE-QUAL-W2 was run from spring through to fall, to simulate the evolution of the biologically productive season. The model was started on the date of the first sampling trip and it ended on the date of the last sampling trip, 22 May 2015 (day 142) to 20 October 2015 (day 293) or 12 May 2016 (day 133) to 14 October 2016 (day 281). The water quality variables computed by the model are given in Table 3.

Table 3. Physical and chemical output computed by CE-QUAL-W2

Physical or chemical water quality variable computed by CE-QUAL-W2	Comments
Temperature, T (°C)	
Conductivity at 25°C ($\mu\text{S}/\text{cm}$) called C25 in the text	Conductivity is used in place of total dissolved solids or salinity. It acts as a conservative tracer to identify water masses.
Turbidity (NTU) Called Tu in the text	Turbidity is used to model glacial fines in the model. See Section 2.4.6.1.2, Section 3.4.3, and Appendix AWQ.
Nutrient concentrations ($\mu\text{g}\cdot\text{L}^{-1}$) Includes soluble reactive phosphorus (SRP), also known as orthophosphate ($\text{PO}_4\text{-P}$) plus total dissolved P (TDP), total phosphorus (TP), and nitrate ($\text{NO}_3\text{-N}$).	There is no consumption of nutrients specified in the model. $\text{NH}_4\text{-N}$ is not included in the model because that form of N was mostly undetectable in analysis of water samples.
Tracers -Tracer 1: initial water in the reservoir -Tracer 2: inflow from La Joie Dam -Tracer 3: local tributary inflow	Tracers are used to identify the origin of water in the reservoir.

4.2.2 Computational grid

CE-QUAL-W2 ran on a computational grid of cells (Figure 2). To do so it required information on boundary conditions such as river inflow and meteorological data. The model was set up with inflow from La Joie Dam, inflow from the local drainage, outflow to the Bridge River powerhouses, and outflow from Terzaghi Dam. The local inflow was distributed along the length of the reservoir from Terzaghi Dam to the Middle Bridge River in 13 local drainage segments that were further divided into model segments of equal length, with a maximum segment length of 1000 m (Table 4).

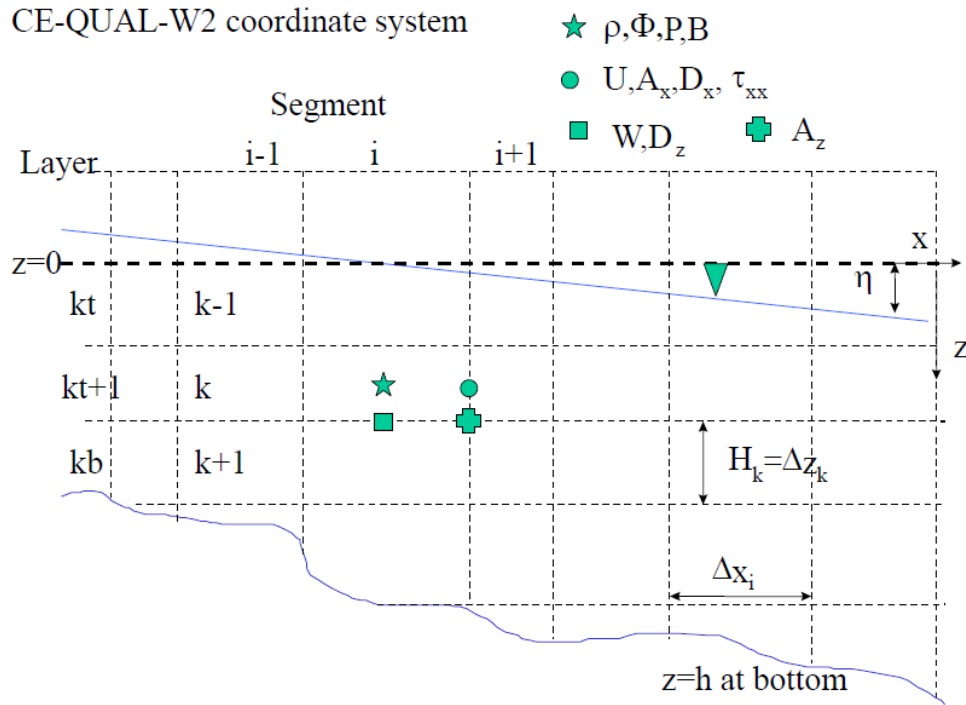


Figure 2. Image of the CE-QUAL-W2 computational grid. Width (B), density (ρ), pressure (P) and water quality state variables (Φ) are defined at cell centers. Horizontal velocity (U), longitudinal eddy viscosity (A_x) and diffusivity (D_x), and longitudinal shear stress (τ_{xx}) are defined at the right hand side of the cell. Vertical velocity (W) and vertical diffusivity (D_z) is defined at the bottom of the cell, and the vertical eddy viscosity is defined at the lower right corner of the cell. Adapted from Cole and Wells (2015).

Table 4. List of drainage and model segments for CE-QUAL-W2 modeling.

Reservoir sampling station that defined boundaries of drainage segments	Model segments	Comment
empty	1	Upstream boundary segment (inactive)
C10B	2-5	Segment 2: Inflow from La Joie Dam
C10A	6-12	
C9	13-18	
C8	19-25	
C7	26-31	
C6B	32-35	
C6A	36-39	
C5	40-43	
C4	44-45	
C3	46-48	
C2B	49-51	
C2A	52-54	Segment 53: Outflow to Bridge powerhouses
C1	55-57	Segment 57: Adjacent to Terzaghi Dam
empty	58	Downstream boundary segment (inactive)

The model consisted of 56 horizontal segments along the length of the reservoir (Figure 3). The segment lengths varied from 700 m to 1000 m. Each segment was divided into vertical layers regularly spaced at 0.5 m intervals (Figure 4). The deepest segment, next to the dam, was divided vertically into 107 layers (Figure 5), and the shallowest segment farthest from the dam had 15 vertical layers (Figure 6). The model had one additional inactive (empty) segment at the upstream and downstream boundaries and one inactive layer at the top and bottom boundaries.

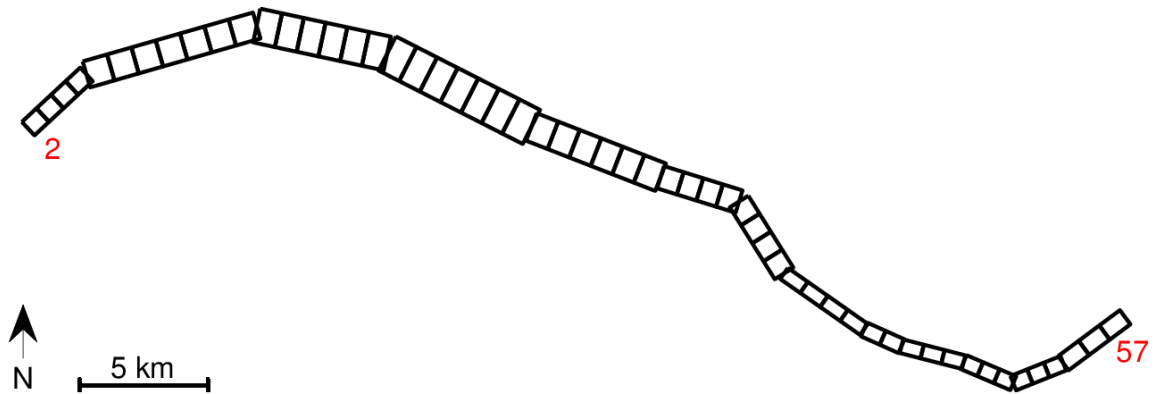


Figure 3. Plan view of model segments. The Middle Bridge River flows into Segment 2. Terzaghi Dam is located at the east end of Segment 57. Segments 1 and 58 (not shown) are inactive boundary segments for use by the model.

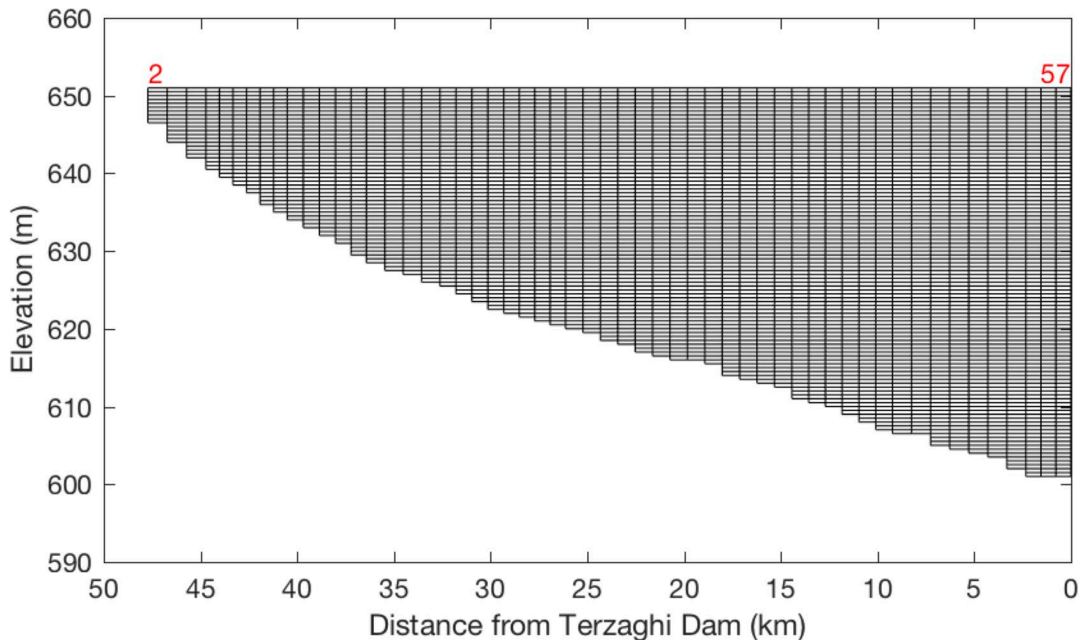


Figure 4. Side view of Carpenter Reservoir showing the 56 active segments along the length of the reservoir and the 107 active layers. Boundary (inactive) layers are not shown. The Middle Bridge River enters on the left, and Terzaghi Dam is adjacent to the deepest segment on the right.

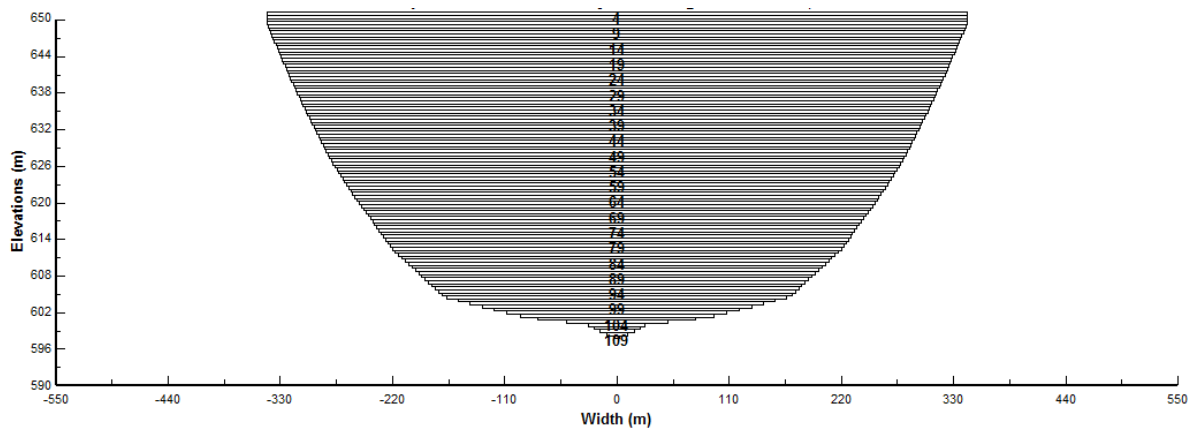


Figure 5. Cross channel profile of Segment 57, the last active segment before Terzaghi Dam. Shown are 107 active layers of 0.5 m each (layers 2 to 108). Layer 1 and 109 are inactive boundaries for use by the model. The top elevation of first active layer #2 is 651 mASL and the bottom elevation of the last active layer #108 is at 597.5 mASL.

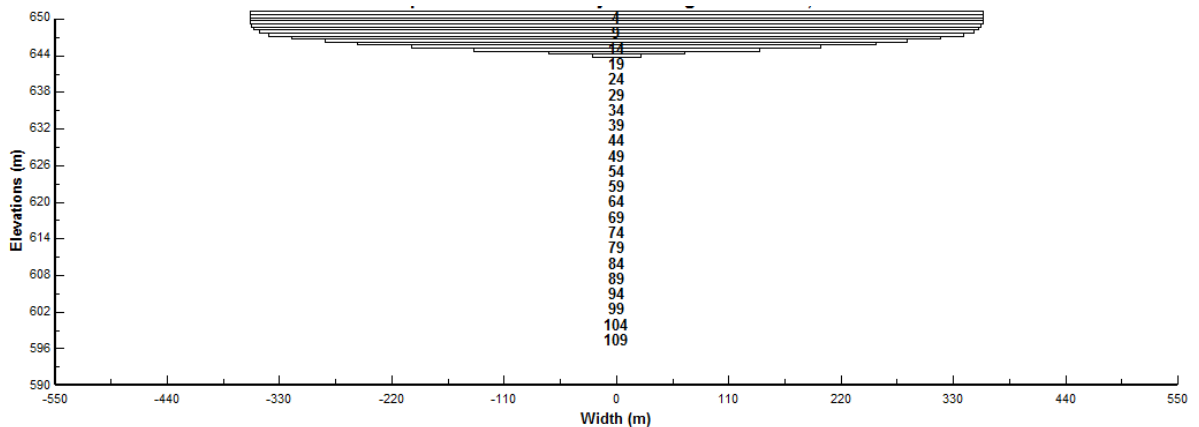


Figure 6. Cross channel profile of Segment 2, the shallowest active segment of the reservoir which received inflow from the Middle Bridge River. The top elevation of first active layer #2 was 651 mASL and the bottom elevation of the last active layer was 643.5 mASL.

4.2.3 Boundary conditions

4.2.3.1 Hydrology

Hydrologic data were obtained from BC Hydro for the period of 1961-2016 for flow data and 1960-2016 for water level. The data included inflows from La Joie Dam, outflows to the Bridge River powerhouses, outflows from Terzaghi Dam, inflows from local drainage, and reservoir water level. Daily averaged data were interpolated to the hourly time step of the model. The model was set up with the following flow boundary conditions:

1. Release from La Joie Dam,
2. Local inflow from thirteen catchments distributed along the length of the reservoir,
3. Outflow to the Bridge River powerhouses, and
4. Release from the Terzaghi Dam.

Inflow from surrounding catchments was divided into segments based on catchment area (Table 5).

Table 5. Catchments contributing to local inflow to Carpenter Reservoir.

Drainage segment	Drainage segment area (ha)	% of local drainage area ⁽¹⁾	Tributaries that were sampled ⁽²⁾	% coverage of drainage segment area by sampled tributaries
C11	68,824	26	Hurley River (T, WQ)	99
C10B ⁽³⁾	3,881	1	Sucker Creek (T)	76
C10A ⁽³⁾	64,716	24	Gun Creek (T,WQ) McDonald Cr (T). Girl Creek (T)	90 3 1
C9 ⁽³⁾	6,366	2	Truax Creek (T,WQ)	83
C8 ⁽³⁾	78,753	30	Tyaughton Creek (T, WQ)	96
C7	12,756	5	none	none
C6B	12,213	5	Marshall Creek (T,WQ)	75
C6A	5,933	2	Keary Creek (T,WQ)	72
C5	6,803	3	none	none
C4	577	0.2	none	none
C3	1,989	1	none	none
C2B	1,476	1	none	none
C2A	714	0.3	none	none
C1	1,863	1	none	none
Total	266,864	100	none	none

⁽¹⁾ Does not include drainage to La Joie Dam.

⁽²⁾ Tributary was sampled for (T) temperature, and (WQ) water quality.

⁽³⁾ Local inflow to drainage segment C8 to C10A were added to model segment 2.

4.2.3.2 Inflow temperature and chemistry

For drainage segments with one sampled tributary (Table 5), the temperature, turbidity, C25 and nutrient concentration data from that tributary was used for that entire drainage segment. For drainage segments with multiple tributaries, an area weighted average was used for that drainage segment. For drainage segments with no sampled tributaries (Table 5), chemical values were set to those of Keary Creek, which is representative of the other small tributaries. Temperature data for these segments were set to Gun Creek. The monthly water chemistry data were linearly interpolated to the model time step. In this process one anomalous and exceptionally high value of turbidity was found in Tyaughton Creek on 23 May 2015 (251 NTU). It could not be statistically

supported and was replaced with a value from Gun Creek in order to balance the turbidity budget during this time. All other measured values were used.

Chemistry of the inflow from the La Joie Dam (release from Downton Reservoir), the Hurley River, Gun Creek, and Tyaughton Creek was measured, representing 81.3% of the total drainage into Carpenter Reservoir. Three smaller tributaries that contribute to the balance of the local drainage were also sampled, one from the north side of Carpenter Reservoir, Marshall Creek, and two from the south side, Truax Creek and Keary Creek.

Sampling of the Middle Bridge River that flows from the La Joie Dam was done at three locations:

- Middle Bridge River above the Hurley, sampling below La Joie Dam but above the confluence with the Hurley River;
- Middle Bridge River below the Hurley; and
- Middle Bridge River where it discharges into the wetted reservoir.

Data were also collected from the outflows from Carpenter Reservoir, and from the Upper Bridge River for comparison.

Water chemistry of all these tributaries was sampled monthly from May to October in 2015 and 2016. A YSI model 6920 multisensor Sonde was used to measure temperature, conductivity, pH and turbidity. Water samples were collected for analysis of soluble reactive phosphorus (SRP), total dissolved phosphorus (TDP), total phosphorus (TP), total ammonia (NH₄-N), nitrate (NO₃-N), total nitrogen (TN), total suspended solids (TSS), and quality assurance tests for pH and turbidity at ALS Environmental as described in Section 4.3.5. Turbidity from the YSI sensor was corrected by a factor of 0.81 to match the turbidity measured in the lab that was considered more reliable. Conductivity measured by the YSI sensor was corrected to a more accurate sensor on an instrument called a Sea-Bird Electronics SBE19plusV2 CTD (conductivity, temperature, depth) profiler that was used for physical and chemical profiling along the central axis of the reservoir that is described in Section 4.2.4.1. That correction factor was 0.8 as determined through a conductivity budget for the reservoir. All figures in this report show corrected data.

Each tributary temperature was measured using an internally recording Onset Hobo Water Temperature Pro logger (U22-001) with accuracy of 0.2 °C, recording every 20 to 60 minutes.

A turbidity recorder was moored in the Middle Bridge River upstream of Carpenter Reservoir (UTM 10U 511,946 Easting 5,634,532 Northing). The recorder consisted of an RBR Virtuoso, connected to a Seapoint optical backscatter sensor (OBS). A custom metal frame was fabricated that protected the logger and sensor while

ensuring the sensor was exposed to flow. The entire apparatus laid flat on the river bed and was anchored with sufficient mass to ensure it did not move while exposed to all river flows. The apparatus performed successfully. Data were recorded every 2 minutes. In 2015 the OBS was deployed without a wiper. In 2016 a Zebra Hydro wiper was added.

4.2.3.3 Meteorology

In 2015 and 2016, three sources of meteorological data were available near Carpenter Reservoir as follows:

1. BC Hydro sensors at the Terzaghi Dam including hourly wind speed, wind direction and air temperature,
2. A meteorological station set up on the Terzaghi Dam but separate from the BC Hydro instruments. This station included an Onset Hobo Micro Station Data logger (H21-002) recording data from a Photosynthetically Active Radiation (PAR) sensor (S-LIA) and a Solar Radiation sensor (S-LIB). An Onset Hobo Pro (U23) was used to measure air temperature and relative humidity,
3. BC Wildfire Service weather station called Five-mile located halfway up the reservoir at 50° 54' 39" N, 122° 41' 20" W, elevation 865 m. Measurements at that station included wind speed and direction, air temperature and relative humidity.

CE-QUAL-W2 was forced with wind from the Five-mile site, along with air temperature, relative humidity, and solar radiation from Terzaghi Dam.

4.2.4 Reservoir conditions

4.2.4.1 Water column profiling

Depth profiles of conductivity and temperature were collected from casts of a Sea-Bird Electronics SBE19plusV2 CTD profiler. This instrument, designed for oceanographic work, provides high accuracy (0.005 °C), high resolution (0.0001 °C) and stable temperature needed for CE-QUAL-W2 modeling. The particular design of the conductivity cell gives rise to unprecedented accuracy and stability at low conductivity, with excellent results in fresh water. As the profiler is lowered through the water column, it collects four samples a second which are recorded internally for upload after the survey. Additional sensors on the Sea-Bird included a WETlabs EC0 combined fluorometer and turbidity meter, a Biospherical PAR sensor, and a SBE43 dissolved oxygen sensor. PAR is the acronym for photosynthetically active radiation which includes wavelengths of 400 – 700 nanometers, the spectrum used by plants including aquatic algae in photosynthesis. Data from these added sensors as well as temperature were used for modeling of biological endpoints that are described in Section 4.3.5. To ensure unshaded PAR was collected, Sea-Bird casts were always done on the sunny side of the boat.

Surveys of the reservoir were conducted monthly from May to October 2015, and April to October 2016. Sea-Bird profiles were collected at all of the 10 stations along the 50 km length of the reservoir that had a water depth >10 m, providing a snapshot of the reservoir each month, and giving a detailed view of the gradients along the reservoir. Data from the Sea-Bird turbidity sensor were corrected by a factor of 0.85 by comparison to water samples that were analyzed in the lab; corrected data is shown in all figures.

4.2.4.2 Instrument moorings

Continuous temperature and turbidity at multiple depths is required to compile the CE-QUAL-W2 model. These data were measured in 2015 and 2016 on a fixed temperature mooring attached to a trash boom located upstream of the intakes to the Bridge 1 and 2 powerhouse intakes. The mooring was attached to the boom at the location with greatest depth (UTM 10U 551,263 Easting 5,624,112 Northing). The mooring was deployed during 16 April to 20 October 2015, and 13 April to 14 October 2016.

In 2016, an additional subsurface temperature mooring was installed to better measure turbidity and temperature near the bottom of the reservoir. The subsurface mooring was deployed at a location approximately 1 km downstream of the log boom (10U 552,594 Easting; 5,624,640 Northing) from 13 April to 14 October 2016.

The moorings consisted of lines with temperature recorders attached. There was also a turbidity recorder attached to the deepest part of the boom mooring in 2015, and to the subsurface mooring in 2016. Mooring details are provided in Appendix A (Report Section 8).

4.2.5 Initial conditions

The model required initial conditions to specify the state of the reservoir at the start of the model run. Model runs were initialized with water temperature, electrical conductivity (C25¹) and turbidity measurements from the Sea-Bird profile at station C2 along with nutrient concentrations (SRP, TDP, TP and NO₃-N) from water samples at station C2. Model runs started on the same date as the monthly Sea-Bird profiles and water samples in May of the given field season. In 2015, the start date was 22 May and in 2016, it was 12 May.

4.2.6 Model testing

The performance of the model relied heavily on the quality and extent of the field data. The model required field data for two important purposes: (1) to impose initial and boundary conditions, and (2) for model calibration and validation. The approach taken herein was to calibrate the model to the first year of field data from 2015 and then to demonstrate the model's predictive capability by validating against the field data from 2016 without further adjustment of the model parameters. The model showed the same

¹ Electrical conductivity at 25 °C (C25) is a measure of total dissolved solids (TDS) and salinity (S).

agreement with field data as found in other modelling studies of reservoirs; see Appendix F (report section 13) for detail.

4.3 Biological measurements and modeling

4.3.1 Periphyton

Periphyton accrual was measured on installed substrates (Bothwell 1989, Perrin et al. 1987) using a novel and simple substrate sampling system. There are two common types of substrata in Carpenter Reservoir: stony materials that occur on benches and slopes and sandy materials that are present in the original river valley. The stony material is stable and is not susceptible to movement from water flow. The sand is unstable and is susceptible to movement. We used a different customized sampler for each of these “stable” and “unstable” types of substrata.

To represent stable substrata, we deployed a 2.5-cm diameter open cell Styrofoam ball clipped at each of six equidistant positions to a 3/8” braided nylon vertical mooring line over a depth that extended over the depth of the euphotic zone (Figure 7). A Styrofoam ball was collected at the end of two months of incubation at a given station and depth for measurement of periphyton biomass accrual (mass/area/time).

To represent unstable substrata, a pail two thirds full of sand (sand surface area of 551.5cm²) was suspended at each of six different depths from a 3/8” braided nylon vertical line with the deepest sampler situated at the bottom of euphotic zone (Figure 8). Sand for the pails was collected in early April of each year (2015 and 2016) from exposed sand within the Carpenter drawdown zone. All sand was collected from a depth >10 cm to avoid presence of surface algal biomass in the samplers. Enough sand was stock piled in April for use in samplers through October of each year. That sand was exposed to air for most of the previous winter. This configuration allowed sand in a bucket to be sampled at the end of two months of incubation at a given station and depth for measurement of periphyton biomass accrual (mass/area/time).



Figure 7. Styrofoam array used to represent periphyton growth on stable substrata.



Figure 8. Sand pails used to host periphyton growth on sand in Carpenter Reservoir. Rigging on the pail handles was used to clip the pails onto lines of fixed length that were suspended from a boom. This arrangement provided a range of pail depths extending from close to the water surface to the bottom of the euphotic zone.

The Styrofoam and sand samplers were deployed during three time series corresponding with spring, summer, and fall in each of 2015 and 2016 (Table 6). A sampling time series involved installation of the samplers on the first day and sampling two months later. On the transition day between sampling series, samples from the preceding series were collected and new substrata for the following series were installed.

Table 6. Dates of periphyton sampling series in 2015 and 2016

Year	Sampling series number	Season	Start date	End date
2015	Series 1	Spring	April 16, 2015	June 18, 2015
2015	Series 2	Summer	June 18, 2015	August 12, 2015
2015	Series 3	Fall	August 12, 2015	October 20, 2015
2016	Series 4	Spring	April 13, 2016	June 17, 2016
2016	Series 5	Summer	June 17, 2016	August 12, 2016
2016	Series 6	Fall	August 12, 2016	October 14, 2016

One Styrofoam sampler having six Styrofoam balls, five at different depths in the euphotic zone and one deeper than the euphotic zone was installed at two replicate stations in each of Carpenter Reservoir, Seton Lake, and Anderson Lake in each of 2015 and 2016. In Seton Lake the stations were S4 and S5 and in Anderson Lake they were A1 and A2 (Figure 1). Sand samplers were not installed in Seton or Anderson Lakes because they do not have sand substrata in littoral zones. In Seton and Anderson Lakes where there is little change in water surface elevation, the Styrofoam sampler line was secured between an anchor and submerged float. Depth of the Styrofoam balls was the difference between water depth at the sampler that was continuously logged using a Reefnet Sensus Ultra Logger (Reefnet Inc. Mississauga Ontario) attached to the mooring anchor and distance from the logger to the Styrofoam ball. In Carpenter Reservoir the two stations were two separate positions along a trash boom labelled as TB in Figure 1 that crosses the reservoir near station C2. By attaching the moorings to the trash boom in Carpenter Reservoir where there was a continuous increase in water depth in spring through fall, the samplers maintained constant depth during incubation.

Each Styrofoam sampler was deployed with clean Styrofoam balls. One Styrofoam ball (surface area = 19.63 cm²) from each depth on each mooring was retrieved after two months of incubation (mean \pm standard error; 62.75 days \pm 0.54). Each ball with adhered biomass was placed into a labelled plastic vial, immediately packed on dry ice, and shipped frozen to the lab. Each ball was analyzed for biomass measured as chlorophyll-a concentration on the whole ball and corrected for ball surface area. Chlorophyll-a was extracted in 5 ml of 90% acetone and stored in the dark for 20 to 24 hours at -20 °C. The Styrofoam dissolved in the acetone leaving only the chlorophyll extract in solution. Fluorescence of the acetone extract was measured before and after the addition of three drops of 10% HCl in a Turner Designs™ Model 10-AU fluorometer that was calibrated with a solution of commercially available chlorophyll-a. Calculations

to determine chlorophyll-a concentration were made using equations reported by Parsons et al. (1984). Three blank balls that were not deployed at sampling sites were processed the same way. In each case, chlorophyll-a concentration on the blank replicates was below the detection limit of the fluorometer and assumed to be zero.

The sand was sampled after approximately 60 days of incubation (62.14 days \pm 0.98). Each pail was hauled to the surface at a rate of approximately 0.25 m·s⁻¹. When the pail broke surface, the pail was carefully lifted on board the boat to avoid spilling water capping the sand. The water was then decanted off the sand using a hand pump and tubing device that was custom fabricated for this purpose. The device only withdrew clear water over top of the sand, not particles from the sand surface. This process left undisturbed sand without the water cap. The open end of a 12-dram plastic vial was pushed 2 cm into a random place on the sand, a clean plastic slide was inserted under the vial opening to prevent loss of sample and the vial with contents was removed. The vial was capped, immediately frozen on dry ice for shipment to the lab and analyzed for chlorophyll-a concentration (corrected by sample surface area) using the same methods as for the Styrofoam samples.

An additional sample was collected from each ball and sand sampler closest to the surface at the end of the mooring incubation for analysis of species composition. In the laboratory, each sand sample was shaken vigorously for 1 minute, emptied into a graduated cylinder and the volume of the sample solution was recorded. Then the sample was diluted according to the amount of sediment in the sample to avoid covering the algal cells by the sediment. The different volumes of aliquots were pre-settled in settling chambers to determine proper concentration of subsamples used for counting. Processing of the ball samples first required the modification of an existing sample jar lid for adaptation to a "Waterpik Flossing System". This system was used for accurately clearing the porous Styrofoam surface of algae and debris using high-pressure water injection. The modification of the sample jar lid required the drilling of two small holes. One hole (approximately 3mm in size) was needed for a snug fit of rubberized Waterpik system injection nozzle. The other smaller hole on the opposite end of the lid was made to allow for air to escape as the sample jar would fill up with water without allowing the splash of sample contents to escape. After a modified sample jar was prepared, a sample with an original and unmodified lid was shaken vigorously for 30 seconds and had its contents emptied into a graduated cylinder. The volume of the liquid contents was then recorded. Next, the Styrofoam ball was taken out using forceps and mounted onto a skewer and placed back in the jar. The skewer prevented the Styrofoam ball from spinning and moving around during Waterpik pressure wash. The jar was then closed using the modified pressure wash lid. The Waterpik flossing system was set to its maximum setting of 12 PSI spray and the nozzle was then inserted through the larger hole in the lid. While observing the direction of spray, the nozzle was adjusted accordingly to pressure wash the entire hemisphere of the Styrofoam ball. After one hemisphere had been thoroughly power washed, the lid was opened and the position of

the skewer mounted Styrofoam ball was inverted. The pressure washing procedure was repeated to wash the other hemisphere of the Styrofoam ball. Once the Styrofoam ball had been thoroughly washed, the lid was removed and the Styrofoam ball was then held by the skewer within the sample jar. Lastly, the ball was gently scrubbed using an electric toothbrush to remove any remaining visible debris off and rinsed into sample jar using the gentle spray of filtered water from a squeeze bottle.

Algal cell counts and measurement of biovolume by species was conducted the same way for each of the sand and ball samples once sample was prepared in the settling chambers. Chamber contents were settled for 24 hours. Cell counts and biovolume measurements were completed at 500x magnification under an Olympus CK20 Inverted Microscope. Only cells containing cytoplasm were enumerated. A minimum of 100 cells of the most abundant species and a minimum of 300 cells in total were counted per sample. Biovolume, by species, was determined by multiplying cell counts by the volume of representative geometric shapes or combination of shapes that most closely approximated cell shape.

4.3.2 Phytoplankton

Phytoplankton production also known as primary production was measured *in situ* as the rate of uptake of ^{14}C into algal biomass. A water sample that was collected with a Niskin bottle from each of six depths over the profile of the euphotic zone was transferred directly into two light and one dark 300 ml acid-cleaned BOD glass bottles assigned as a group of bottles to each depth; hence there were six sets of two light and one dark bottle. Each BOD bottle was rinsed three times with the sample before filling. The water samples were maintained under low light conditions during all manipulations until the incubation was started (within 1 h of the water collections). Water in the BOD bottles were inoculated with 0.185 MBq (5 μCi) of $\text{NaH}^{14}\text{CO}_3$ New England Nuclear (NEC-086H). The cluster of BOD bottles for each depth was attached to an acrylic plate and suspended at each of the six depths from which the water samples were taken. These samples were then incubated *in situ* for 4-5 h between the hours of 1000 and 1500 to allow the carbon uptake to proceed. Following retrieval of the incubation array, the BOD bottles were transported to facilities at BC Hydro in Shalalth in a cool dark box.

The incubations were terminated by parallel filtration of 100 ml of sample onto 0.2 and 0.75 μm polycarbonate Nucleopore™ filters. Each folded wet filter and retained biomass was placed in a 7 ml scintillation vial and stored in the dark until processing at the University of British Columbia.

In the fumehood, 100 μL of 0.5 N HCl was added to each vial to eliminate the unincorporated inorganic $\text{NaH}^{14}\text{CO}_3$. The scintillation vials were then left uncapped in the fumehood for approximately 48 h until dry. After 5 ml of Scintisafe® scintillation fluor was added to each vial, and stored in the dark for >24 hours, the samples were counted using a Beckman® Model #LS 6500 liquid scintillation counter. Each vial was counted for 10 minutes in an external standard mode to correct for quenching. The specific

activity of the stock was determined by adding 100 μL ^{14}C -bicarbonate solution to scintillation vials containing 100 μL of ethanoalamine and 5 ml Scintisafe® scintillation cocktail.

Calculation of rates of carbon incorporation followed methods reported by Parsons et al. (1984) and Ichimura et al. (1980). Daily rates of primary production were calculated by multiplying the hourly primary productivity by the incubation time and by the ratio of the solar irradiance during the incubation to the solar irradiance of the incubation day where solar irradiance was measured using a Li-Cor irradiance meter. Corrections for solar irradiance over periods of time were determined from ambient irradiance logged using the Onset PAR sensor and Micro Station data logger installed at a meteorological station at the Terzaghi Dam during sampling (May – October of each year). The difference between the ^{14}C incorporation in the light bottles (includes photosynthetic and non-photosynthetic uptake) and the ^{14}C incorporation in the dark bottle (includes only non-photosynthetic ^{14}C uptake) indicated carbon uptake by photosynthesis.

At the same stations where chlorophyll-a concentration was measured, a 125 ml aliquot depth-integrated water sample was collected monthly during May through October of each year for phytoplankton cell enumeration by species. These data were used to describe the assemblage of algae contributing to primary production. The depth-integrated water sample was prepared by mixing equal aliquots of water from at least three depths in the euphotic zone, collected using a VanDorn water bottle. The aliquots were dispensed to a glass amber jar, preserved with acid-Lugol's solution, and stored in a cool and dark location until the algal cells were counted. Prior to the enumeration, the samples were gently shaken for 60 seconds and allowed to settle in 25 mL chambers for a minimum of 8 hrs (Utermohl 1958). Counts of algal cells, by taxa, were done using an inverted phase-contrast plankton microscope. Cells of large micro-plankton (20-200 μm) were counted at 250X magnification. All cells within one 10-15 mm random transect were counted at 1560X magnification. In total, 250-300 cells were counted in each sample. The biovolume of each taxon was the cell count multiplied by the volume of a simple geometric shape corresponding most closely with the size and shape of the algal taxon. Canter-Lund and Lund (1995) and Prescott (1978) were used as taxonomic references.

4.3.3 Zooplankton

Zooplankton biomass was measured monthly from May to October from duplicate vertical hauls of a 153 μm mesh Wisconsin net having a 30 cm intake opening. The depth of haul was 30m or the complete water column where and when water depths were <30m (28.69 m \pm 0.51). The net was raised at a speed of approximately 0.5 $\text{m}\cdot\text{s}^{-1}$. The zooplankton were washed into the cod-end of the net and anaesthetized to prevent egg shedding in a wash of Club Soda before being added to a 10% sugared formalin solution. Each zooplankton sample was split using a Folsom plankton splitter to a

subsample volume containing post-naupliar stages of >100 of the most abundant taxa of crustaceans. For each sub-sample, the species were enumerated at 5-100x magnification under a GSZ-Zeiss stereo microscope. The number of attached eggs were counted. Sub-sample counts were then extrapolated to the total sample. Biomass of zooplankton were determined from length-to-weight regressions reported by McCauley (1984) using lengths measured with a digitizing system. Up to 25 random length measurements per taxon were taken per sample, and the final biomass was expressed as μg dry weight per sample. The amount of zooplankton biomass per sample was converted to volumetric zooplankton biomass (μg dry weight $\cdot\text{L}^{-1}$) using the known volume of water that was filtered by the Wisconsin net. This value was corrected to the amount of biomass in a 1 m^2 column of water over the depth of water at the sampling site to yield areal biomass in units of mg dry weight $\cdot\text{m}^{-2}$. Each haul for measurement of zooplankton biomass was considered a separate observation for regression analysis.

4.3.4 Regression analysis

Regression modeling was used to answer management questions 1 and 2. There were 42 to 78 observations of the dependent variables and associated independent and coincident environmental variables among all models (Table 7, Table 8, Table 9). Some losses or additions of observations were encountered as explained in the tables but these changes did not detract from what were ample sample sizes for regression analysis.

Table 7. Number of observations applied to periphyton accrual for stable substrata and unstable substrata regression analyses.

Reservoir or Lake	Type of periphyton mooring	Number of moorings	Number of samples per mooring	Number of sampling episodes per year	Number of years	Extras or loss	Number of observations
Carpenter	Styrofoam ball	2	6	3	2	+6*	78
Carpenter	Sand	12	1	3	2	-4**	68
Anderson	Styrofoam ball	2	6	3	2	-12***	60
Seton	Styrofoam ball	2	6	3	2	-1****	71

*samples added as depth of euphotic zone increased.

**four pails lost due to touching bottom and tipping.

***samples lost due to vandalism

****one sample lost from mooring

Table 8. Number of observations applied to the phytoplankton production regression analyses

Reservoir or Lake	Number of stations	Number of bottle depths per station	Number of sampling episodes per year	Number of years	Extras or loss	Number of observations
Carpenter	1	5	5 in 2015, 6 in 2016	2	-3*	58
Anderson	1	5	4 in 2015, 6 in 2016	2	+2*	52
Seton	1	4	4 in 2015, 6 in 2016	2	+6*	46

*samples added or deleted when BOD bottle depths were changed with variation in depth of the euphotic zone.

Table 9. Number of observations applied to the zooplankton biomass regression model

Reservoir or Lake	Number of stations	Number of hauls	Number of sampling episodes per year	Number of years	Extras or loss	Number of observations
Carpenter	2	2	6 in 2015, 5 in 2016	2	0	44
Anderson	2	2	5 in 2015, 6 in 2016	2	-2*	42
Seton	2	2	6 in 2015, 5 in 2016	2	0	44

*wind and large swells prevented reliable samples to be collected in June at one station in 2015,

We checked for multicollinearity among all variables for each response variable using variance inflation factors (VIF) and correlation coefficients (Zuur et al. 2010). Variables with a VIF score greater than 3 and a correlation coefficient greater than 0.6 were not included in the same model to avoid overfitting due to high multicollinearity (Zuur et al. 2009). All model combinations were considered with this caveat in mind and the top model was selected using an information theoretic approach using AICc (Grueber et al. 2011). Top models were also confirmed by evaluating model fit using pseudo R^2 of the fixed effects and by examining the p-values of individual model parameters. All models were inspected visually to ensure they met the assumptions of linear regressions. We also \log_{10} transformed each response variable as well as PAR and zooplankton biomass when they were included as predictor variables. By using a \log_{10} transformation of the biological variables and light we satisfied the assumption of normality and more accurately modeled biological growth and the relationship between light attenuation and increasing depth.

Preliminary analysis revealed low fit of models to the data (R^2) when the data from each water body (Carpenter, Seton, and Anderson) was combined into single source models. We believe this outcome was caused by variation and processes in each lake/reservoir being too different to create a unified model. We opted to create lake-specific models for each response variable. In so doing, a unique model of periphyton accrual on a stony surface was developed for each of Anderson Lake, Carpenter Reservoir, and Seton Lake. The same was done for phytoplankton production and zooplankton biomass. This approach, combined with the addition of random effects and a weights function to model variation in the residuals, more accurately reflected the differences in each lake/reservoir (i.e. lower $\Delta AICc$ /better model fits/higher R^2). The separate models for Anderson Lake and Seton Lake were not needed to answer the management questions for BRGMON10 and were not further considered.

All regression analyses were performed in R (R Development Core Team, 2011) and fitted using maximum likelihood. All models were first presented with standardized coefficients (subtracting the mean from each observation and then dividing by the standard deviation) shown as the β values in Equation 1. Absolute values of standardized coefficients within a given model were directly compared to determine relative importance of each independent variable acting on the dependent variable without concern over different units of measurement. For example, an independent variable coefficient β_1 with a value of 0.2 in standardized units had less effect on a dependent variable than an independent variable β_2 with a coefficient value of -0.3 because the absolute value of β_2 was greater than the absolute value of β_1 . Models with unstandardized coefficients were used to show sensitivity of the dependent variables (periphyton biomass accrual, phytoplankton production, zooplankton biomass) to change in the independent variables because the models with unstandardized coefficients show output in original units. Directional effects were determined from the unstandardized coefficients, not the standardized coefficients. For example, in a model with unstandardized coefficients, if the coefficient for independent variable β_1 was -0.2 and the coefficient for independent variable β_2 was 0.2, variable β_1 had a negative effect on the dependent variable and variable β_2 had a positive effect on the dependent variable. Sensitivity of a dependent variable to change in values of independent variables that could be changed according to management actions was defined as:

$$S = \left| \frac{P_d}{P_i} \right|$$

Equation 2

Where:

S was sensitivity of a dependent variable to change in value of an independent variable within the range of values of independent variables encountered in the surface layer where biological production was active,

P_d was the percent difference between a maximum and minimum value of the dependent variable and

P_i was the percent difference between a maximum and minimum value of the independent variable found among management scenarios (defined in Section 5.1.3)

Values of S that were <1 showed low sensitivity of the dependent variable to change in the independent variable and values of S that were >1 showed high sensitivity of the dependent variable to change in the independent variable.

To examine the effect of different management scenarios on dependent variables, the values of the independent variables were changed according to output of the same variables in simulations of the CE-QUAL-W2 model as described in Section 2 according to a range of management scenarios laid out in Section 5.1.3. Unstandardized coefficients in original units were used in the regression equations to predict an outcome using values of independent variables in original units. For the phytoplankton production predictions, all scenarios were run to a constant depth of 14m, which was the greatest photic zone depth found during measurements in 2015 and 2016. This standardization meant that for scenarios producing a photic zone depth less than 14m, the phytoplankton production would include values of zero at depths greater than the photic zone. Consequently, a scenario producing a small photic zone yielded a lower mean rate of phytoplankton production over the standard 14m depth even if rates were similar to or higher within the photic zone compared to another scenario producing a deeper photic zone. This approach corrected for differences in photic zone depth among scenarios.

4.3.5 Environmental variables

4.3.5.1 Periphyton and phytoplankton regression modeling

There is no question that light or more correctly PAR limits photosynthesis that drives biological production in lakes and reservoirs (Wetzel 2001) as described in initial modeling by the Bridge River WUP CC (2003). A general rule is that photosynthesis is active where PAR occurs at intensities of more than 1% of irradiance at the water surface (Wetzel 2001). In addition to the basic physics of light attenuation in clear water, PAR attenuation may be affected by particles in water. In Carpenter Reservoir, those particles include inorganic fines that are carried in suspension from upstream due to erosion by glaciers and snow fields in the headwaters of the Bridge River and by particle mobility within the drawdown zone of Downton and Carpenter Reservoirs. The particles, measured as turbidity or suspended solids concentration, intuitively should increase PAR attenuation in the water column, resulting in a shallower depth of photosynthetic production (i.e. a shallower euphotic zone) than would occur if turbidity was lower.

In addition to PAR, autotrophic production is driven by nutrient supply (Guildford and Hecky 2000, Wetzel 2001). Low concentrations of phosphorus (P) and nitrogen (N) naturally occurring in Carpenter Reservoir (Perrin and MacDonald 1999) maintains low biomass of aquatic algae and limits overall biological production. This natural “oligotrophic” status is caused by low supply of phosphorus from erosion of parent materials in the Bridge River headwaters, tight adsorption of oxidized phosphate to mineral particles contributing to turbidity and low supply of inorganic nitrogen that mainly comes from atmospheric sources. This condition means that bacterial and algal cells that are at the base of the food web will sequester virtually any bioavailable form of P (i.e. soluble reactive P) and N (i.e. $\text{NH}_4\text{-N}$ and $\text{NO}_3\text{-N}$) to sustain biological growth, thus driving the limited nutrient supply even lower in the water column. This rationale means that availability of bio-available N and P measured in concentration units (mass/volume) must be considered in the regression modeling.

Temperature will affect the physiological growth rates of algae (e.g. Bothwell 1988, Goldman and Carpenter 1974, Wetzel 2001) and drive density stratification that can affect availability of nutrients between independent mixed layers. That stratification can be modified by water residence time that in turn is defined by rates of inflow, outflow, and reservoir volume. There are two different processes here; one is associated with metabolic growth of algal cells while the other is associated with hydrodynamic forcing that changes temperature driven kinetics of algal growth. Both are important but they are fundamentally associated with known effects of temperature on algal growth. Hence, temperature must also be considered in modeling biological production in Carpenter Reservoir.

Interactions between light, temperature, and nutrients may synergistically or antagonistically affect autotrophic production. For example, influx of organic and inorganic material associated with high flows to a reservoir can increase the transport of inorganic fines carrying a load of adsorbed nutrients. Those nutrients may increase nutrient-limited growth of algal cells but only if they are exchangeable with other ions and thus become bio-available (Liess et al. 2015, Guildford and Hecky 2000, Wetzel 2001). Conversely, the added turbidity may reduce PAR and lower rates of primary production. High flow from seasonal snow melt may produce the same responses. Temperature change will affect density stratification that can affect availability of nutrients between independent mixed layers, which is also defined by water residence time that in turn is defined by rates of inflow, outflow, and reservoir volume. The assumption about light limitation of biological production by Bridge River WUP CC (2003) was a statement about turbidity affecting the amount of habitat in Carpenter Reservoir where photosynthesis can occur. While turbidity and its potential effect on PAR is important, these interactions with nutrient supply and temperature must also be considered when determining effects of water management actions on biological production.

Several variables associated with light, temperature, and nutrients were included in modeling periphyton and phytoplankton production (see Section 2 for introduction to regression modeling) (Table 10). For periphyton, light was measured as accumulated

PAR over a period of incubation of the Styrofoam balls or sand at a given depth. For phytoplankton, light was measured as PAR occurring during the day of primary production and biomass measurement again at a given depth. All *in situ* PAR was measured monthly at each of the two stations on each lake/reservoir and at times of primary production measurements from casts of a SeaBird SBE19Plus CTD (SeaBird Electronics, Bellevue WA) on the sunny side of the boat. For both periphyton and phytoplankton, a regression equation was developed between *in situ* PAR and PAR measured continuously using an Onset PAR sensor and Micro Station data logger installed at a meteorological station at the Terzaghi Dam. That equation was used to estimate continuous PAR *in situ* from the atmospheric PAR. For periphyton, mean temperature and mean turbidity was calculated from the same monthly casts during May through October of the SeaBird at each station and depth in each year. Among these SeaBird casts, one was always done at the same station and day for each measurement of primary production. Nutrient concentrations were the mean soluble reactive phosphorus (SRP) concentration and mean NO₃-N concentration calculated from monthly samples collected from the epilimnion at each station. The epilimnetic sample was collected at a depth <2m at each place and time using a Niskin bottle. NH₄-N was not considered useful as an N source for modeling even though it is actively taken up by algae (Suttle and Harrison 1988) because it was found below the method detection limit of 5 µg·L⁻¹ on all dates. Without detection it could not be included in the models.

Table 10. Hypotheses of response by periphyton accrual and phytoplankton production to selected environmental variables.

Predictor Variable	Unit	Hypothesis	Predicted Periphyton Response	Level ^a	Reference
PAR	µMol·m ⁻²	PAR limits growth and production of photosynthetic algae	Positive	By depth, station and sampling day	(Lamberti and Steinman 1997, Wetzel 2001)
Temperature	°C	Affects metabolic activity and consequently periphyton growth	Positive	By depth, station and sampling day	(Allan and Castillo 2007; Bothwell, 1988; Lamberti and Steinman 1997, Wetzel 2001)
Phosphorus (soluble reactive phosphorus)	mg·L ⁻¹	Phosphorus limits periphyton growth	Positive to a threshold	By station and sampling day	(Perrin et al 1987; Rosemond et al 1993, Wetzel 2001)
Nitrate-N	mg·L ⁻¹	Nitrate is a nutrient that can limit algal growth	Positive to a threshold	By station and sampling day	(Perrin and Richardson 1997; Rosemond et al. 1993)
Turbidity	NTU	Turbidity increases light scatter and subsequently decreases light availability for algal production	Negative	By depth, station and sampling day	(Leland, 1995)

Note: ^a Level refers to the level at which the predictor variable was measured (e.g. by depth, station and sampling day means the predictor variable was measured once per depth, station and month coinciding with the response variable).

4.3.5.2 **Zooplankton regression modeling**

There were biological and abiotic variables potentially explaining zooplankton biomass (Table 11). Descriptions of methods of measurement are as follows.

Phytoplankton biomass measured as chlorophyll-a concentration shows food available for zooplankton in the pelagic food web. This biomass measurement was done monthly during May through October of each year at each of the 6 to 7 depths through the euphotic zone at C2 (Carpenter Reservoir), A1 (Anderson Lake), and S4 (Seton Lake). Each sample was collected from the specific depths using a Niskin bottle with sample dispensed into a 250 ml amber glass sample bottle. A depth-integrated sample was collected monthly also during May through October of each year over the entire euphotic zone at sites C6 (Carpenter), A2 (Anderson) and S5 (Seton) in 2015 and 2016. A depth-integrated sample was collected by dispensing an aliquot of set volume from a sample collected with the Niskin bottle from each of six depths into a 250 ml amber glass sample bottle. Chlorophyll-a concentration was determined by *in vitro* fluorometry (Yentsch and Menzel, 1963) from each sample (discrete depth or depth-integrated). Two aliquots from each sample bottle were parallel filtered through 0.2 and 0.75 µm polycarbonate Nucleopore™ filters as was done for the aliquots used for primary production analysis using a vacuum pressure differential of <100 mm of Hg. Care was taken to limit light exposure of the chlorophyll samples during field handling of water samples and laboratory analysis. The water filtrations were completed on the day of sample collection at the Shalalth field lab. The filters with phytoplankton biomass were stored in the dark at –20°C prior to analysis at the University of British Columbia. Chlorophyll-a was extracted in 5 ml of 90% acetone and stored in the dark for 20 to 24 hours at –20°C. Fluorescence of the acetone extract was measured before and after the addition of three drops of 10% HCl in a Turner Designs™ Model 10-AU fluorometer that was calibrated with a solution of commercially available chlorophyll-a. Chlorophyll-a concentration was determined using equations reported by Parsons et al. (1984).

Temperature and turbidity for the zooplankton modeling was the same data collected for modeling periphyton and phytoplankton (see Section 4.3.5.1). These data were included because of known sensitivities by *Daphnia* sp, the main cladoceran in Carpenter Reservoir to variation in temperature and photoperiod that may be influenced by turbidity (Korpelainen 1986, Schwartz and Ballinger 1980). Turbidity may be expected to directly and negatively affect zooplankton abundance (e.g. Sellami et al. 2011).

Water residence time and amount of drawdown were considered potential predictors of zooplankton biomass. If water residence time was less than time needed for zooplankton to complete a growth or life cycle, it would limit potential production of food for fish. This limitation is closely linked to the amount of drawdown in the sense that large drawdown limits the area of pelagic habitat while little drawdown increases that habitat area. For modeling we assigned a 78-day mean water residence time and 78-day mean drawdown in meters as potential independent variables where the term of 78 days was considered to capture most life cycle growth of *Daphnia* sp. that is the most

common zooplankton genus in Carpenter Reservoir (Pietrzak et al. 2013). Water residence time was calculated as total volume divided by mean annual rate of outflow using mean daily flow data from BC Hydro. Drawdown was calculated as top water surface elevation minus water elevation on a given day using water elevation data from BC Hydro.

Table 11. Hypotheses for predictor variables included in the zooplankton analyses.

Predictor Variable	Unit	Hypothesis	Level*	Reference
Phytoplankton biomass (chlorophyll-a retained on 0.2 µm filter)**	µg·L ⁻¹	Food source for zooplankton	By station and sampling day	(Burks et al. 2002)
Temperature	°C	Affects physiology and population ecology of zooplankton	By station and sampling day	(Burks et al. 2002)
Turbidity	NTU	Turbidity can reduce phytoplankton production and result in less food for zooplankton	By station and sampling day	(Burks et al. 2002)
78-day mean water residence time	Days	Longer residence time provides longer growing period for zooplankton within the reservoir	Reservoir and sampling day	(Korpelainen, 1986; Schwatz, and Ballinger, 1980)
78-day mean drawdown	m	Less habitat available for zooplankton as drawdown increases	Reservoir and sampling day	(Korpelainen, 1986; Schwatz, and Ballinger, 1980)

*Level refers to the level at which the predictor variable was measured (e.g. by depth, station and sampling day means the predictor variable was measured once per depth, station and month coinciding with the response variable).

**phytoplankton biomass was captured on each of 0.2 µm and 0.75 µm filters, creating two separate sets of data, one for 0.2 µm and 0.75 µm biomass. For regression modeling we used the 0.2 µm data to capture a large size range of phytoplankton biomass potentially available as zooplankton food.

4.3.5.3 Descriptive environmental variables

While only bioavailable oxidized inorganic forms of N and P were included in the regression modeling, a full suite of total and dissolved nutrients concentration was measured in the water samples to support interpretation of the model output. One water sample was collected monthly during May through October of each year at a depth of 1m and within the hypolimnion at each of the two stations on each lake/reservoir using a Niskin bottle. The nutrient analyses included TN (total nitrogen), TP (total phosphorus), TDP (total dissolved phosphorus), nitrate-nitrogen (NO₃-N), ammonium (NH₄-N), and SRP (soluble reactive phosphorus). Dissolved inorganic nitrogen (DIN) was the sum of NO₃-N and NH₄-N concentrations. Water for TDP, nitrate, ammonium, and SRP were filtered in the field at the time of collection through Waterra 0.45 µm FHT-45

polyethersulphone filters

(http://www.waterra.com/pages/Product_Line/filters/filters_2011.html) using an Alexis peristaltic pump (<http://pegasuspumpcompany.com/alexis-peristaltic-pumps>). All samples were submitted within 24 hours to ALS labs in Burnaby for analysis using standard methods (APHA 2014).

Complete profiles of temperature, PAR, turbidity, dissolved oxygen, and fluorescence from surface to bottom at each station were measured monthly during May through October each year using the Sea-Bird Electronics SBE19plusV2 CTD. These profiles were always done at the same time of phytoplankton production measurements.

Euphotic zone depth (depth at which PAR is 1% of surface PAR), over which photosynthesis is active was calculated from the SeaBird casts or from casts of the LiCor irradiance meter that is described in Section 4.3.2. These data were supported with measurement of water transparency using a standard 20 cm diameter Secchi disc deployed over the shaded side of the boat. Secchi depth was the mean value of the depth of disappearance of the disc when lowered through the water column and depth of reappearance of the disc when subsequently raised.

The irradiance profiles were used to calculate the light extinction coefficient according to the following standard equation (Wetzel 2001):

$$n = ((\ln I_0) - (\ln I_z))/z$$

Equation 3

Where:

n is the light extinction coefficient

I_0 is irradiance at the water surface and

I_z is irradiance at depth z

The particle size distribution in water discharged from BR1 (flowing into Seton Lake) was sampled along with water flowing into Downton Reservoir (Upper Bridge River) and water flowing into Carpenter Reservoir (Middle Bridge River) on the same monthly frequency as the lake and stream sampling. Representative aliquots were taken and diluted with background electrolyte (2% and 8% NaCl) to obtain samples for counting using a Micromeritics Elzone 280PC. Samples were tested over 2 ranges, ~1.3-25 microns and 11-200 microns. At the low end of the low range, particles <1 µm and commonly near 0.5 µm were still detected even though the nominal cut-off was about 1.3 µm. All particle size distribution analyses were run at the University of British Columbia Department of Mining Engineering.

5 RESULTS AND DISCUSSION

5.1 CE-QUAL-W2

5.1.1 Measured boundary conditions

5.1.1.1 Hydrology

Water release from Downton Reservoir to Carpenter Reservoir from the LaJoie Dam during 1961-2016 was uniform with an overall mean of $41.1 \text{ m}^3\cdot\text{s}^{-1}$ and little seasonality (Figure 9). There were small increases in flow during February-March and August-September. The year to year variability was greatest in August, at which time brief periods of high flows were not unusual. In 2015, the daily inflow followed mean flow through most of the year, except for above average flow in March to mid-April, and again during mid-July to mid-August. In 2016, the inflow remained higher than average during late March to late September and was a record high during late May to mid-July. These high water releases from LaJoie in 2016 were the result of a decision by BC Hydro to reduce recently discovered seismic risk on the dam by lowering water levels in Downton Reservoir.

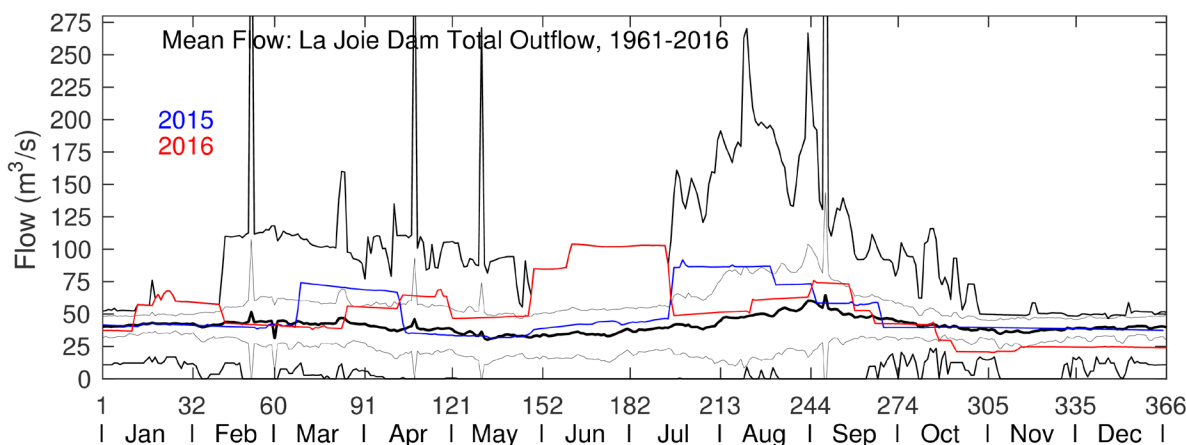


Figure 9. Total inflow to Carpenter Reservoir from LaJoie Dam averaged over 1961-2016 for each calendar day. Mean (heavy black line), maximum and minimum (medium black lines) and mean \pm one standard deviation (light black lines). The total inflow is shown in blue for 2015 and in red for 2016. There were three off-scale peaks consisting of a single point each.

Local inflow to Carpenter Reservoir showed distinct seasonality (Figure 10) with an overall average flow from 1961-2016 of $50.8 \text{ m}^3\cdot\text{s}^{-1}$, slightly greater than the average release from LaJoie Dam. Peak flows with a long tail occurred in July and August driven by glacial snowmelt. In 2015, freshet was early with above average flows during early May to early June, but below average inflows during mid-June to the end of August. Flow in fall 2015 was average interspersed with three large peaks resulting from rainstorm events. In 2016, freshet was also early with above average flows in April and May, but below average inflows during mid-June to mid-July. In fall of 2016, inflows were average except for a November rainstorm which produced anomalous flows for several days.

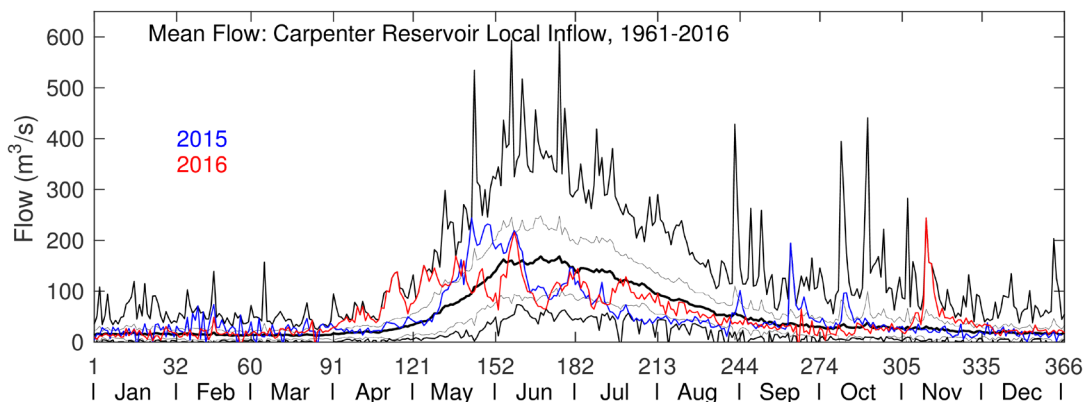


Figure 10. Daily local inflow to Carpenter Reservoir, averaged over 1961-2016. Mean (heavy black line), maximum and minimum (medium black lines) and mean ± one standard deviation (light black lines). The local inflow is shown in blue for 2015 and in red for 2016.

Approximately 96% of water released from Carpenter Reservoir passes through two tunnels to two power generating stations located at Shalalth on Seton Lake. The average flow to Seton Lake during 1961-2016 was $87.4 \text{ m}^3 \cdot \text{s}^{-1}$. The flow was highest in winter with a smaller but broad peak during August and September (Figure 11). Average flows occurred in 2015 except in mid-June to mid-July when flow was significantly higher than average. In 2016, average flows occurred during January to March and above average flows occurred in April to mid-July. The Bridge generating stations were shut down for maintenance for 25 out of 30 days during 13 September to 12 October, 2016.

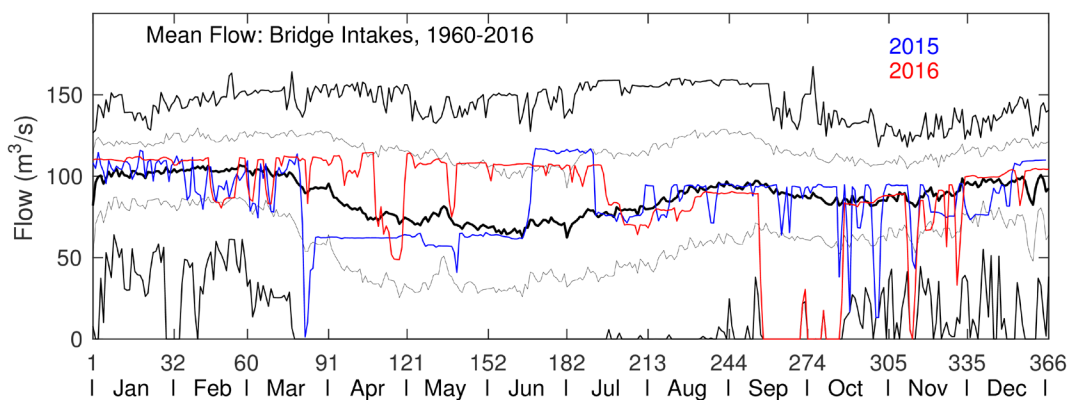


Figure 11. Flow release to Bridge generating stations during 1961 – 2016. Mean (heavy black line), maximum and minimum (medium black lines) and mean ± one standard deviation (light black lines). The outflow is shown in blue for 2015 and in red for 2016.

Water level in Carpenter Reservoir had a strong seasonal cycle, declining in fall and winter to sustain power generation, reaching a minimum in May, and rising rapidly in spring with storage of freshet inflow (Figure 12). There was cyclical inter-annual variability in the maximum water level, with periods of relatively high water (e.g. 1982-1985) alternating with periods of relatively low water (e.g. 2007-2009). The water level in 2015 was average, except for above average water level from April to June, and

slightly above average water levels in the fall. In 2016, the water level was above average from January to mid-May and below average from early July to late September.

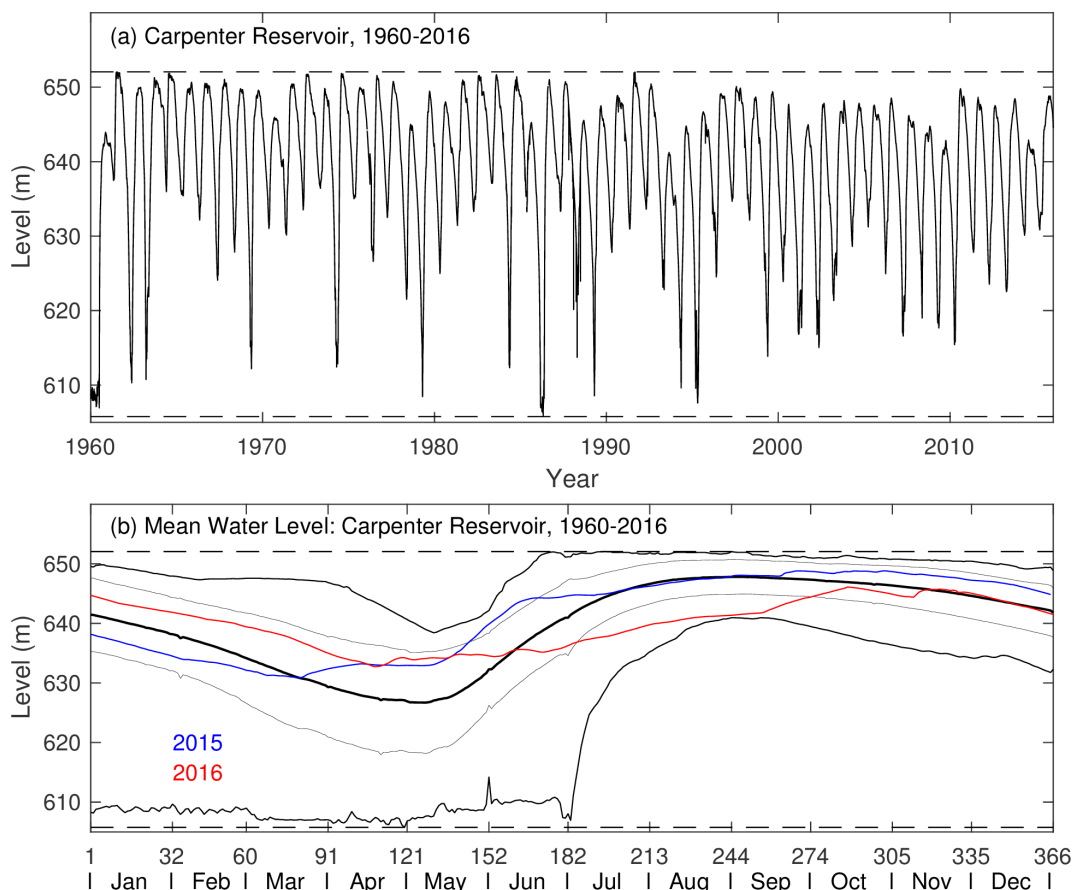


Figure 12. Water surface elevation in Carpenter Reservoir, 1960-2016 (a) and average water level by month in Carpenter Reservoir, 1960-2016 (b). Mean (heavy black line), maximum and minimum (medium black lines) and mean \pm one standard deviation (light black lines) are shown. The water level is shown in blue for 2015 and in red for 2016. The dashed lines mark the normal minimum (606.55 mASL) and maximum (651.08 mASL).

Hydrology during the biologically productive time of year, which was the time modelled using CE-QUAL-W2, is shown in Figure 13, Figure 14, and Figure 15. The 2015 inflow from La Joie Dam was higher than average and in 2016 it was even higher, the fourth highest on record (Figure 13). In contrast, the year before (2014) had relatively low inflow. In both 2015 and 2016, the local flow was average, while in 2014 it was below average (Figure 14). In 2015, the water level was above average from April to October, while it was closer to average during the previous five years and close to average in 2016.

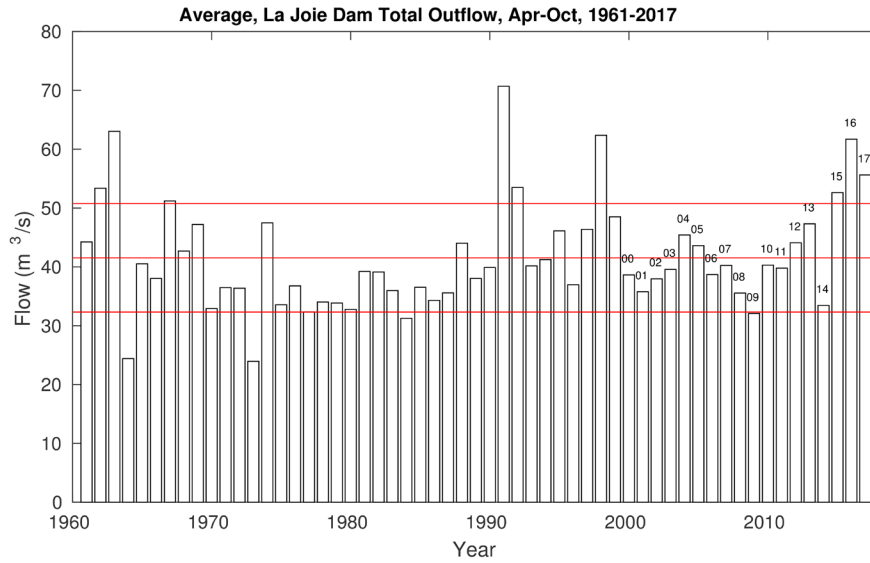


Figure 13. Average inflow from La Joie Dam, April to October, 1961 to 2017. The red lines show the mean and the mean \pm one standard deviation.

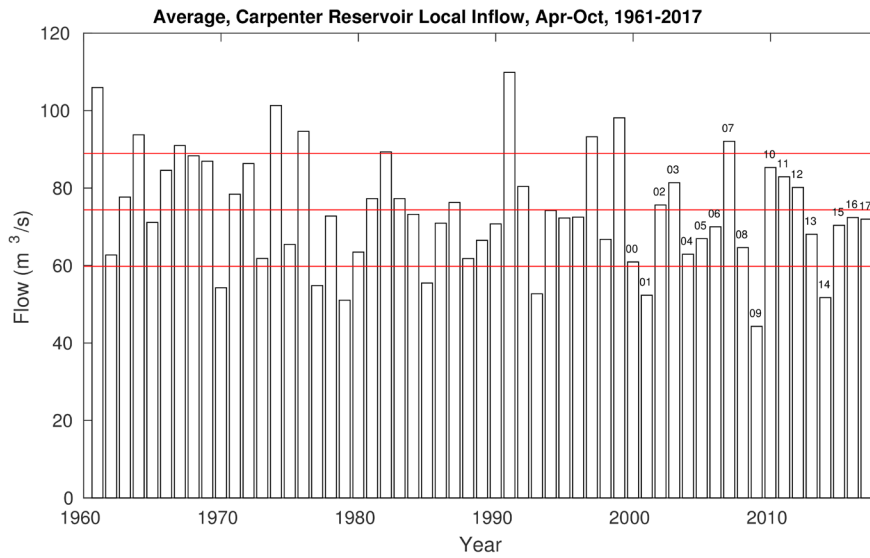


Figure 14. Average local inflow to Carpenter Reservoir, April to October, 1961 to 2017. The red lines show the mean and the mean \pm one standard deviation.

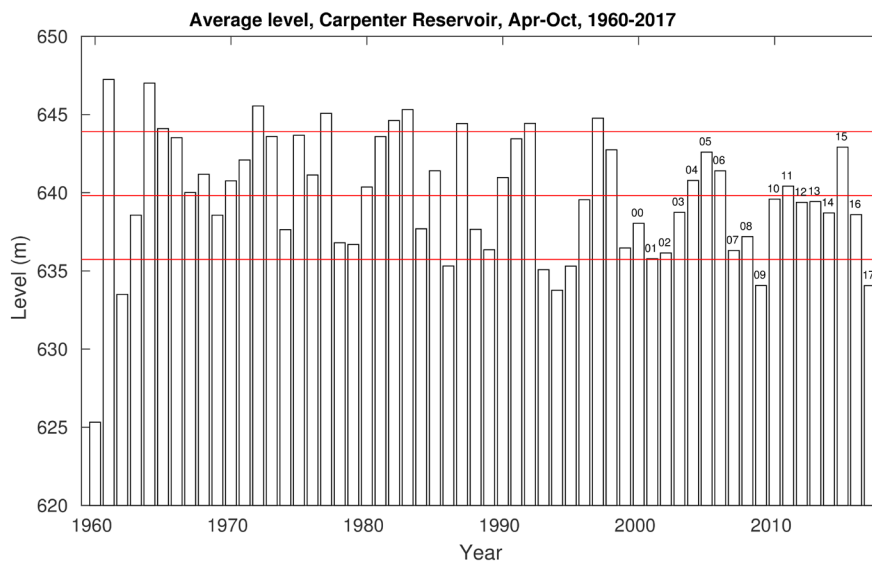


Figure 15. Average water level, Carpenter Reservoir, April to October, 1960 to 2017. The red lines show the mean and the mean \pm one standard deviation.

5.1.1.2 Inflow temperature and chemistry

During the modelled time period of May through October, temperature of inflow from La Joie Dam was in a range of 5 - 11°C while temperature of the tributaries had greater temporal variations (Figure 16). Temperature was used to determine the plunge depth of water flowing into the reservoir (e.g. Pieters and Lawrence 2011). For example, if a tributary was cold, and entrainment during plunging was low, then the tributary inflow will plunge into the hypolimnion (deep water); however, if the tributary was warm, it entered the epilimnion (surface layer). If the tributary temperature was intermediate, it can slot in at the thermocline. In summer, tributary temperatures varied by over 5°C in the course of a day, and the plunge depth varied accordingly.

In a lotic (river) environment, particles of many sizes are transported downstream (subject to bed, slope and flow conditions in a given river). In a lentic environment such as in Carpenter Reservoir, larger particles that contribute mass to TSS in the river settle rapidly, while the smaller (<2 μm) glacial particles that contribute to light scattering remain suspended. Because only small particles remain suspended in the reservoir, and because light scattering is a better measure of the small particles of interest, turbidity was used in place of TSS in the CE-QUAL-W2 model. (For further detail, including a comparison of TSS and turbidity, see Appendix D (Report Section 11) In the model a settling rate of 6 $\text{m}\cdot\text{month}^{-1}$ was used, which gives the best match to the observed turbidity.

Flow, water level, as well as tributary temperature, conductivity and turbidity are summarized for 2015 and 2016 in Figure 16 with further detail provided in Appendix D (Report Section 11). In 2015, the turbidity of the inflow from La Joie Dam began around 10 NTU in May and rose steadily to just over 100 NTU in October. In 2016, the turbidity of the inflow from La Joie Dam also increased from May onwards, though in 2016 it

leveled off in the fall. Relatively low turbidity in the smaller inflow tributaries without seasonal trend showed that inflow from La Joie Dam (Downton Reservoir) was the primary source of turbidity to Carpenter Reservoir. One exception was a high turbidity event in the small tributaries on 23 May 2015 following a rainstorm the previous evening (Figure 16k). Detail of this turbidity is provided in Appendix E (Report section 12).

Time course changes in conductivity and the various forms of N and P during 2015 and 2016 are shown in Appendix D (Report section 11.3). In general, SRP and TDP concentrations in the tributaries to Carpenter Reservoir were close to or less than the method detection limit of $1 \mu\text{g}\cdot\text{L}^{-1}$ of SRP and $2 \mu\text{g}\cdot\text{L}^{-1}$ of TDP. TP concentration was greater than concentrations of soluble P, which shows that much of the phosphorus load to Carpenter Reservoir was bound to particles and was not biologically available. Similar results are seen in other glacial systems (Pieters et al. 2017). $\text{NO}_3\text{-N}$ concentrations were $<60 \mu\text{g}\cdot\text{L}^{-1}$ in all inflows to Carpenter Reservoir with concentrations commonly lower in the small tributaries compared to the main inflow Bridge River. The $\text{NO}_3\text{-N}$ concentrations declined through freshet, which may be related to depletion of nitrate from snowpack and shallow soil before the end of freshet (cf Sebestyen et al., 2008). This snowpack contribution of $\text{NO}_3\text{-N}$ is important because all $\text{NO}_3\text{-N}$ in the Bridge River system, where there are no anthropogenic discharges of contaminated water, comes from atmospheric sources. Unlike phosphorus that comes from weathering of parent materials, there are no mineral sources of $\text{NO}_3\text{-N}$.

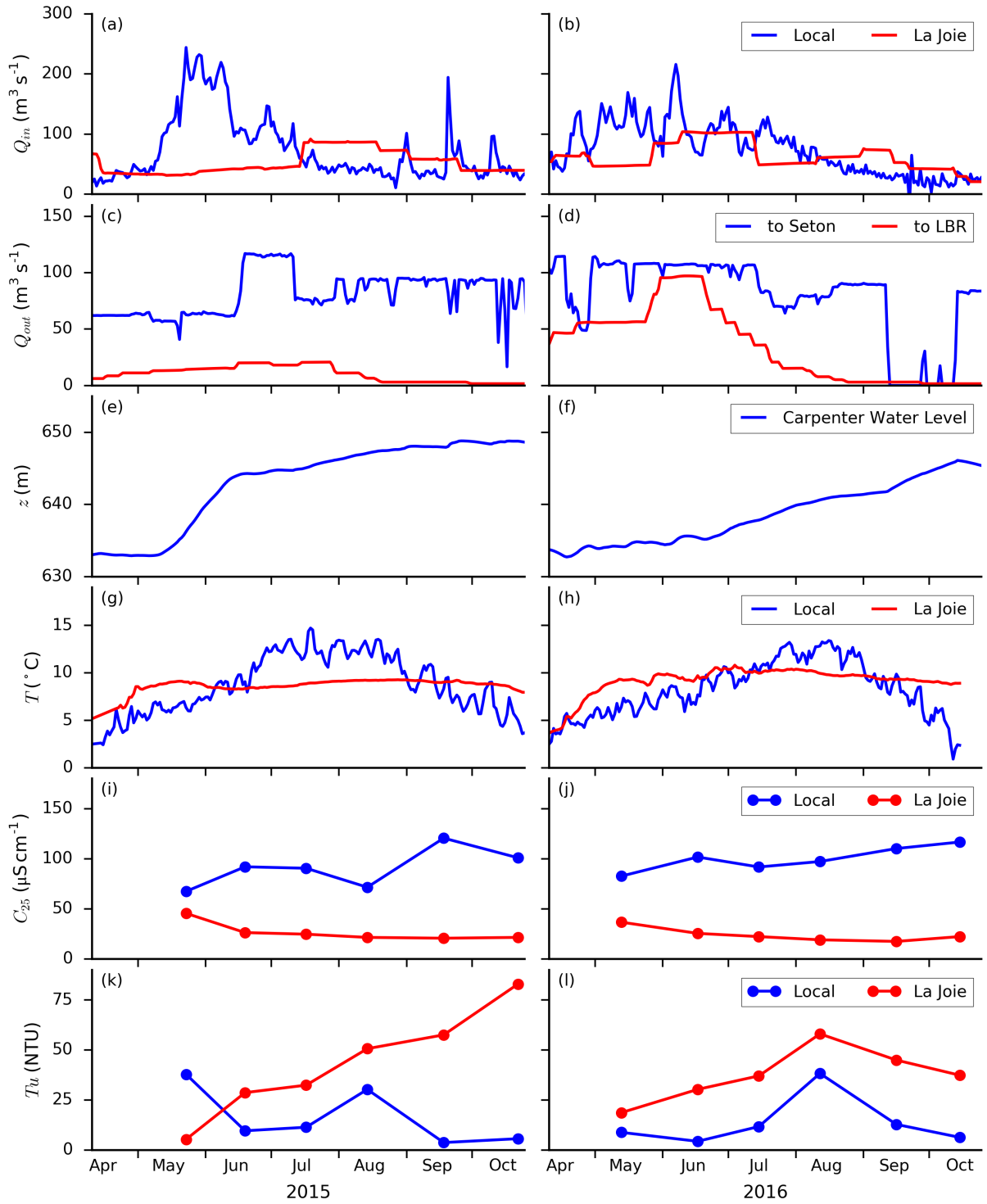


Figure 16. Tributary temperature (panels g and h), conductivity (panels i and j), and turbidity (panels k and l) contrasted between local inflow and inflow from La Joie in 2015 and 2016. Inflow (panels a and b), outflow (panels c and d), and reservoir water level (panels e and f) are shown for reference.

5.1.1.3 Meteorology

Meteorological data for 2015 and 2016 are shown in Appendix C (Report Section 10). Wind speed at Terzaghi Dam, often reaching over $10 \text{ m}\cdot\text{s}^{-1}$, was higher than at Five-mile, likely the result of funnelling in the narrow region near the dam. Wind data from Fivemile were used in the CE-QUAL-W2 model because they were considered more representative of the whole reservoir that was mostly not exposed to wind funnelling.

Air temperatures were similar at the different meteorological stations (Appendix C, Report Section 10). In 2015, there were 31 days with the daily maximum temperature over 30°C . In particular, there were 15 consecutive days with temperature over 30°C (26 June to 10 July 2015), with a maximum air temperature of 37°C on 27 June 2015. In 2016, air temperature followed similar seasonal trends as 2015, except it was a slightly cooler, having only 14 days with a maximum air temperature over 30°C .

5.1.2 Measured reservoir conditions

5.1.2.1 Water column profiling

On 22 May 2015, temperature at the reservoir surface was 15°C and temperature stratification consisted of a broad gradient to the bottom (Figure 17). By 18 June 2015, two layer stratification was observed, with a surface mixed layer (epilimnion), a sharp thermocline between 12 and 14 m, and cooler deep water (hypolimnion) below 14 m. On 16 July and 12 August 2015, temperature of the surface layer was close to 20°C . By 17 September 2015, the surface layer had cooled to 15°C . By 20 October, the surface layer had deepened to over 25 m and cooled to 12°C , just above the temperature of the deep water, 11°C . Fall turnover would be expected shortly after this last profile. These observations show that Carpenter Reservoir undergoes a cycle of thermal stratification, which is typical of reservoirs. This cycle will be seen in more detail in the mooring data (Section 5.1.2.2).

The conductivity at 25°C (C25) remained relative steady in the surface layer from May to August, 2015 (Figure 17b). This observation was the first clue that the surface layer was relatively isolated during this time, and consistent with the plunging of cold inflow to depth. In contrast, the conductivity in the deep water declined during May to September 2015 due to lower-conductivity inflow.

From May to July, 2015, turbidity of the epilimnion declined steadily to a low of 0.6 NTU, and remained relatively low in August (Figure 18c). This finding was a surprise, given the high load of glacial inflow. Only in the fall did the turbidity of the surface layer begin to rise, likely the result of deepening, which mixes in more turbid water from below. In contrast, the turbidity in the hypolimnion was high, up to 35 NTU in September.

The dissolved oxygen concentrations in 2015 were high (Figure 17d) and close to saturation (Figure 17e), indicating little or no oxygen demand at the water-sediment interface. This finding would be expected for an oligotrophic system with short residence

time. On 16 July, when the thermocline was in the photic zone, there was a small peak in oxygen (>120 % saturation) at the thermocline, and a corresponding small peak in chlorophyll fluorescence (Figure 17f), both suggestive of an episodic high rate of photosynthesis.

Chlorophyll concentration in 2015 measured using fluorescence was $<2 \mu\text{g}\cdot\text{L}^{-1}$, which was a low value consistent with an oligotrophic system having low biological production (Figure 17f). In May, there was a broad peak to $1.7 \mu\text{g}\cdot\text{L}^{-1}$ at the base of the photic zone, suggestive of a localized spring bloom. In remaining months of 2015 the fluorescence was lower with smaller peaks near depths of the 1% light level (e.g. bottom of the photic zone).

The CTD profiles in 2016 showed a similar seasonal cycle as observed in 2015 (Figure 18). In 2016, profiles were started a month earlier than in 2015, at which time the reservoir had little temperature stratification (Figure 18a), and relatively uniform but high turbidity (Figure 18c). In June, July and August 2016, the thermocline was not as strong as in 2015, either a result of different weather conditions and possibly the result of higher inflow from La Joie Dam during June and July 2016 (e.g. Figure 16a and b). However, in 2016 the surface layer (epilimnion) underwent the same pattern observed in 2015: once the reservoir was thermally stratified, the turbidity of the surface layer declined steadily from 6 NTU in May 2016 to a low of 0.7 NTU in September, again suggesting the surface layer was isolated from turbid inflows during this time.

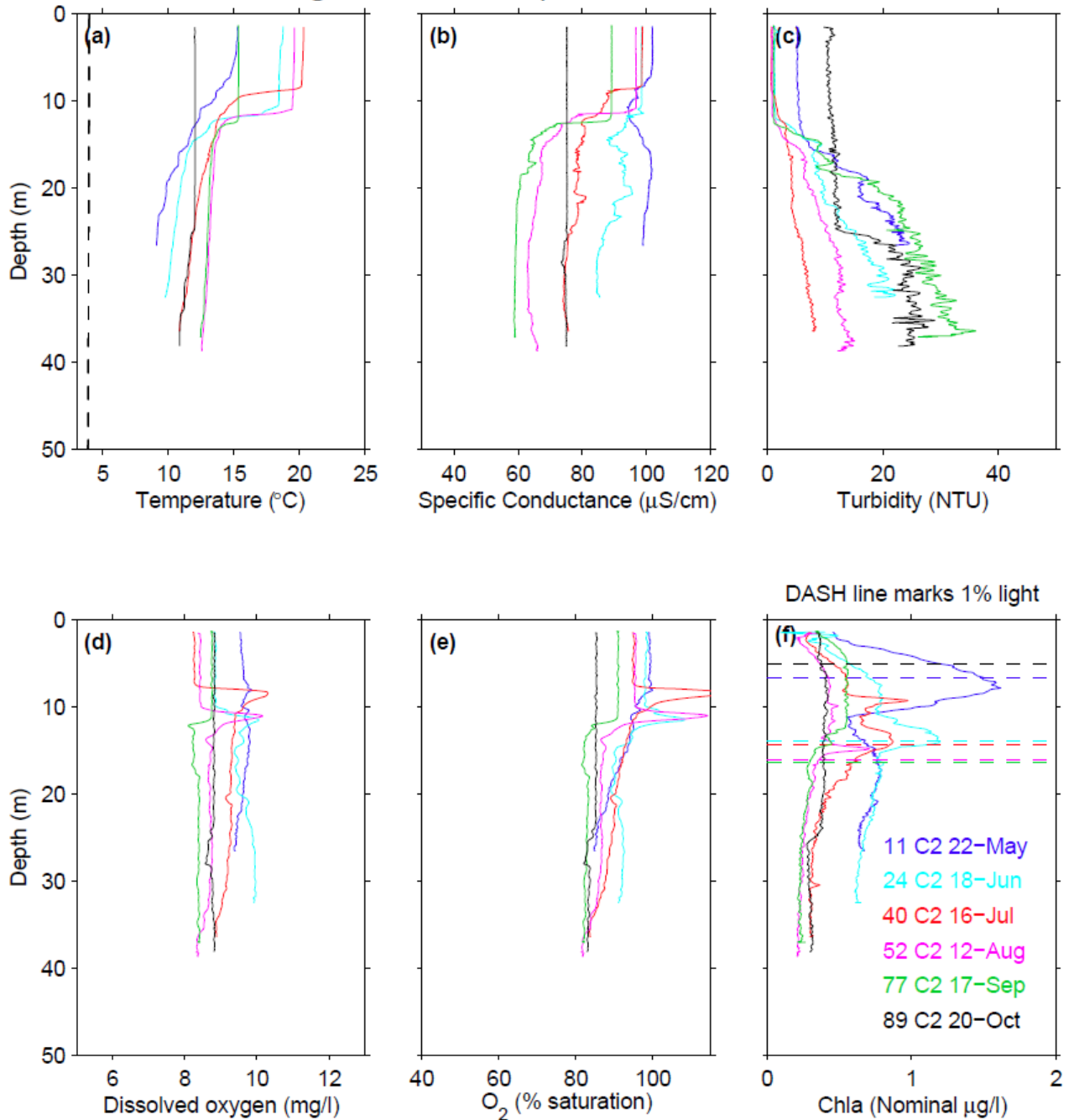


Figure 17. (a) Temperature, (b) conductivity, C25, (c) turbidity (corrected to bottle data), (d) dissolved oxygen, (e) dissolved oxygen as percent saturation, and (f) nominal chlorophyll profiles collected at Carpenter Reservoir station C2, May to October, 2015. The legend in the last panel gives the cast number, station and date. In (f), the dash lines marks the bottom of the photic zone (the 1% light level).

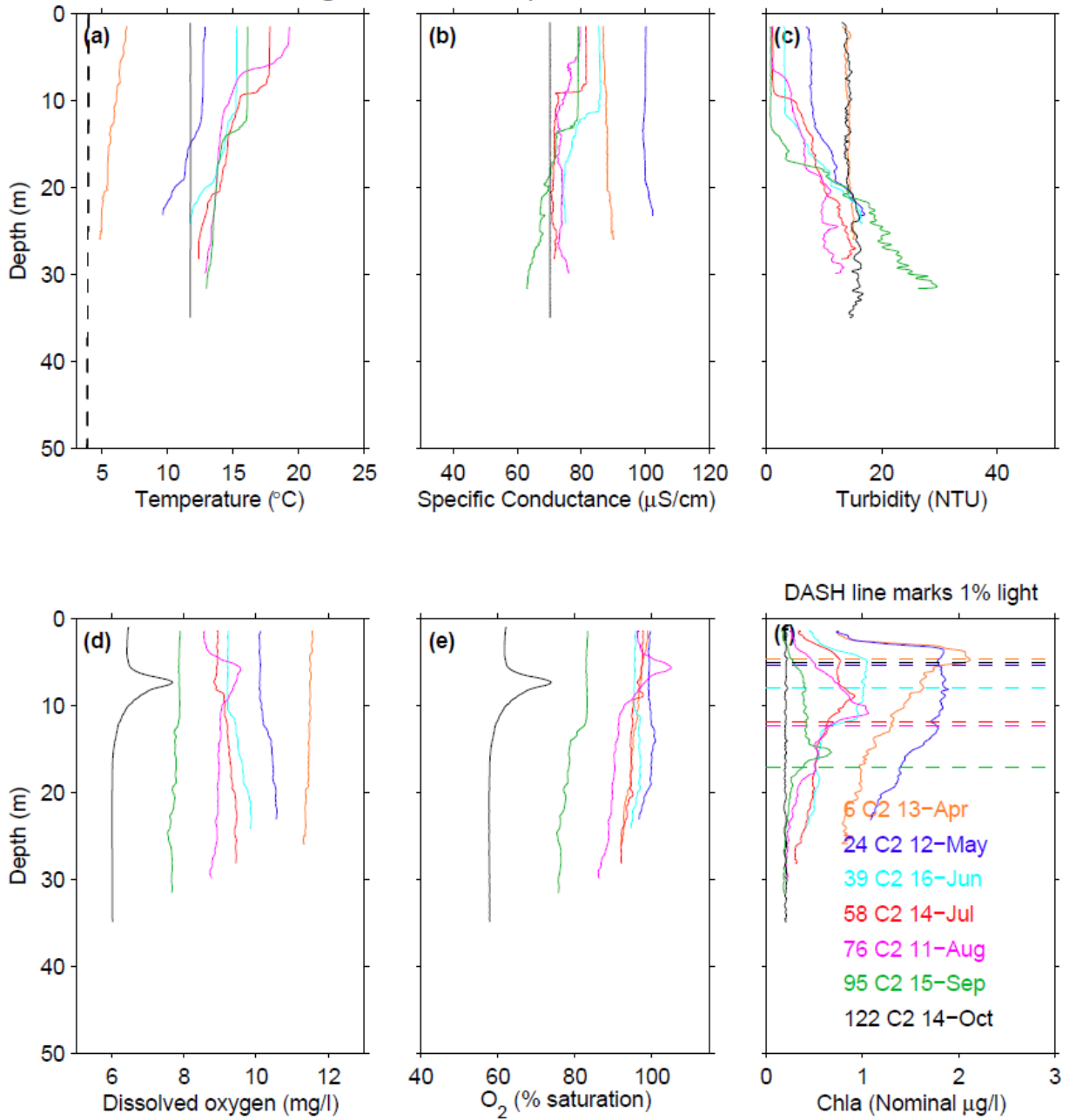


Figure 18. (a) Temperature, (b) conductivity, C25, (c) turbidity (corrected to bottle data), (d) dissolved oxygen, (e) dissolved oxygen as percent saturation, and (f) nominal chlorophyll profiles collected at Carpenter Reservoir station C2, April to October, 2016. The legend in the last panel gives the cast number, station and date. In (f), the dash lines marks the bottom of the photic zone (the 1% light level).

5.1.2.2 Instrument moorings

5.1.2.2.1 Temperature

Water temperature measured by the instruments hung from the log boom in 2015 are shown in Figure 19 along with wind speed, air temperature, solar radiation and inflow, shown for reference. The water temperature is shown as both a line plot (Figure 19e) and a contour plot (Figure 19f). In the line plot, each line of a given color plots the temperature at a given depth. From 22 May to 18 June 2015, the deepest temperature sensor was removed as part of repair of the turbidity wiper. In the contour plot, the color shows water temperature. Note, the contour program interpolates data between the measured depths. For example, the contour plot shows a smooth gradient between the data from the sensor at 10 m to that at 15 m depth. However, through most of the summer, there is a sharp gradient in temperature at the thermocline, located at 12 to 14 m depth as seen in the Sea-Bird profiles (Figure 17a); this is not resolved in the contour plot. Additional sensors were added in 2016 to better resolve the thermocline (Appendix A, Report Section 8).

At the start of the mooring period on 16 April 2015, the reservoir had just begun to stratify with temperature ranging from 5.5 to 7.4 °C. The reservoir reached maximum stratification during the exceptionally hot period from 26 June to 10 July 2015, with a surface layer temperature well above 20°C and temperature at 0.5 m peaking at 24.9°C during a period of low wind on 3 July 2015 (day 184). Temperature of the deep water also increased over the summer, reaching a maximum of about 13°C in late August 2015 (Figure 19).

In September, the surface mixed layer cooled steadily and deepened to 15 m on 20 September 2015 (day 263). By mid-October, little stratification remained with temperature ranging from 11.3 to 12.2 °C on 20 October 2015 (Figure 19).

In 2016, two temperature moorings were deployed, one hung from the log boom (top 20 to 25 m) and one moored on the bottom near the log boom (bottom 12 m). Account was taken of the gradual deepening of the bottom mooring as the water level increased, and the data from both moorings were interpolated to 1 m depths. The interpolated temperatures are shown in Figure 20, along with wind speed, air temperature, solar radiation and inflow, shown for reference.

At the start of the mooring period on 13 April 2016, the reservoir had just begun to stratify with temperature ranging from 4.6 to 7.3 °C. Unlike 2015, when the maximum temperature stratification occurred from the end of June to early July (during a period of prolonged hot weather), in 2016 the maximum stratification occurred from late July to early August, with the temperature at 0.5 m peaking to 22.9 °C on 28 July 2016 (day 575) and to 23.2 °C on 12 August 2016 (day 590). The temperature of the deep water also increased over the summer, with the temperature at 30 m reaching a maximum of 13.6 °C in early September 2016.

In September, the surface layer cooled steadily and deepened to 10 m by 8 September 2016 (day 617), and to 20 m by 8 October 2016 (day 647). By mid-October, little stratification remained with temperature ranging from 11.5 to 11.9 °C on 14 October 2016, when the mooring was recovered.

5.1.2.2.2 Turbidity

A continuous record of turbidity was measured in the deep water of the reservoir from April to October in both 2015 and 2016. In both years turbidity was high, varying from 10 to 40 NTU and there was agreement with bottle data (for detail see Appendix E-2, Section 12.2).

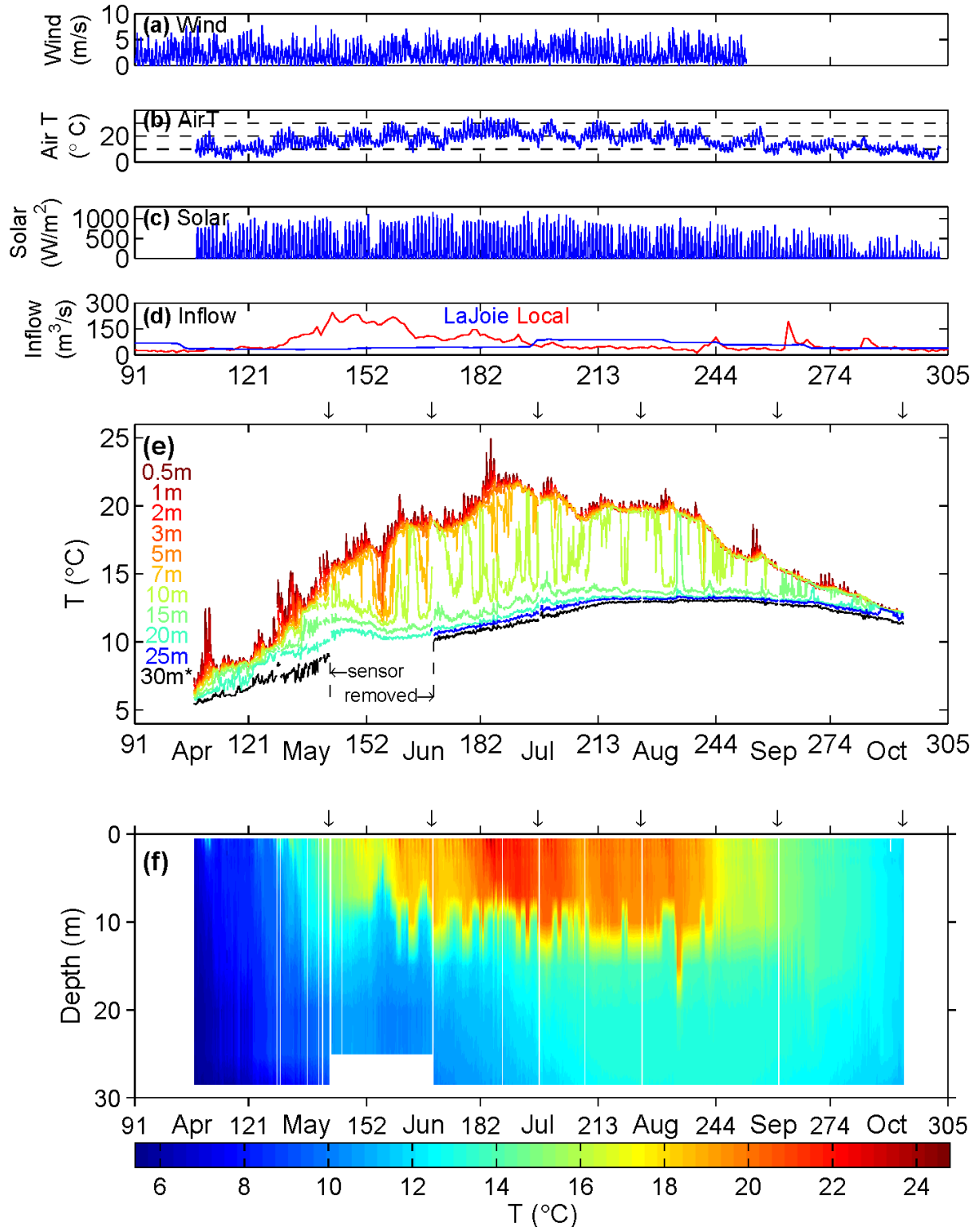


Figure 19. (a) Wind speed at Fivemile, (b) air temperature at Terzaghi Dam, (c) solar radiation at Terzaghi Dam, (d) inflows and (e,f) water temperature at log boom in Carpenter Reservoir, 16 April to 20 October 2015. From 22 May to 18 June, the deepest sensor was removed for repair of the turbidity wiper. Arrows mark the times of the sampling surveys.

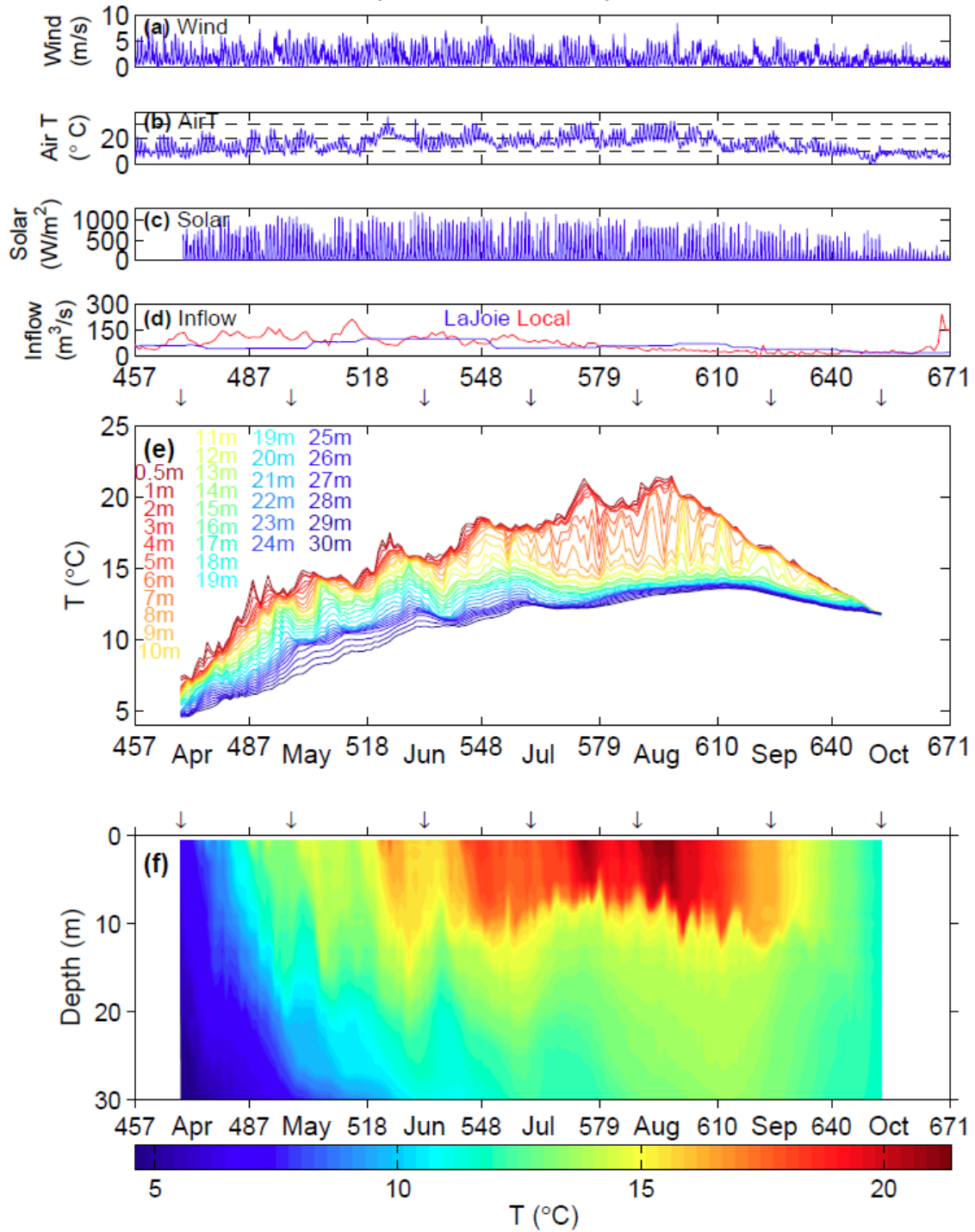


Figure 20. (a) Wind speed at Fivemile, (b) air temperature at Terzaghi Dam, (c) solar radiation at Terzaghi Dam, (d) inflows and (e,f) water temperature (2 hour average) in Carpenter Reservoir, 13 April to 14 October 2016. Data from both the boom and subsurface moorings were interpolated to 1 m depths. Arrows mark the times of the sampling surveys. Time is in days of 2016.

5.1.3 Selection of scenarios

Two sets of model runs were explored. The first set reproduced measurements from the 2015 and 2016 field years. In each case the model run started and ended with the first and last field sampling dates for the given field year. These runs were used to calibrate and validate the model, as described in Appendix F (report section 13). The behaviour of the reservoir observed during 2015 and 2016 is described in Section 5.1.4 and Section 5.1.5 respectively. The second set included four scenarios of different forcing of daily mean inflow from La Joie Dam, local inflow, outflow to the Bridge powerhouses (on Seton Lake), and outflow to the Lower Bridge River to examine change in light availability (turbidity) in relation to flow. Light was the focus because it is the topic of the management questions. These flows, along with the initial water level at the start of the model runs, reproduced the water level for the given year. Since meteorological and water quality data were not available for years having the different flow conditions, those data from 2015 were used. Similar results (not shown) were obtained using forcing from 2016, which provides confirmation that light availability in Carpenter Reservoir is impacted by reservoir operation; *i.e.*, the interannual variability in meteorological and water quality data alone cannot explain the variability in light availability.

Choosing from the hydrologic (flow) conditions from prior years (1961-2017) provided a way to explore a wide range of realistic flow conditions. Since the meteorological and water quality data were not available for these years, these runs do not represent water quality conditions during those years, rather they represent scenarios of what might be observed using the calibrated CE-QUAL-W2 simulations. Subjecting various operational conditions (1961-2017) to the same set of meteorological and water quality data provided a basis for comparison between scenarios by removing the effect of interannual variability in these meteorological and water quality data, thereby, isolating the effect of reservoir operation.

To relate changes in reservoir operation to changes in light availability (turbidity), we simulated the flow conditions in each year of the flow record (1961-2017). We identified years where the model results showed high and low turbidity in the surface layer, corresponding to shallow and deep photic zone depths, respectively. The goal was to identify the reservoir operations associated with extremes in photic depth, *i.e.*, light availability. For each year in the flow record², the modelled photic depth at station C2 and corresponding flow conditions were produced (Figure 21). At the start of the model runs, all the photic depths were the same (≈ 7 m), since the initial turbidity data at station C2 was set to the Sea-Bird profile of 22 May 2015. By mid-June, the photic depths varied from 2 m to 12 m, depending on the flow conditions for the given year. From mid-June to the end of August, the photic depths typically increased. During this period, the surface layer was relatively isolated from the cooler and more turbid inflows that plunged

² Note that 1962, 1972, 1974, 1982, and 1991 were not included as these years had a large volume of spill from Terzaghi Dam during the model period, which is not considered here.

into the deep water. As a result, the turbidity in the surface layer (originating from early in spring before the reservoir stratifies) declined as suspended particles settled. Only in the fall did the photic depth begin to decline, likely due to deepening of the surface layer as more turbid water is mixed in from below.

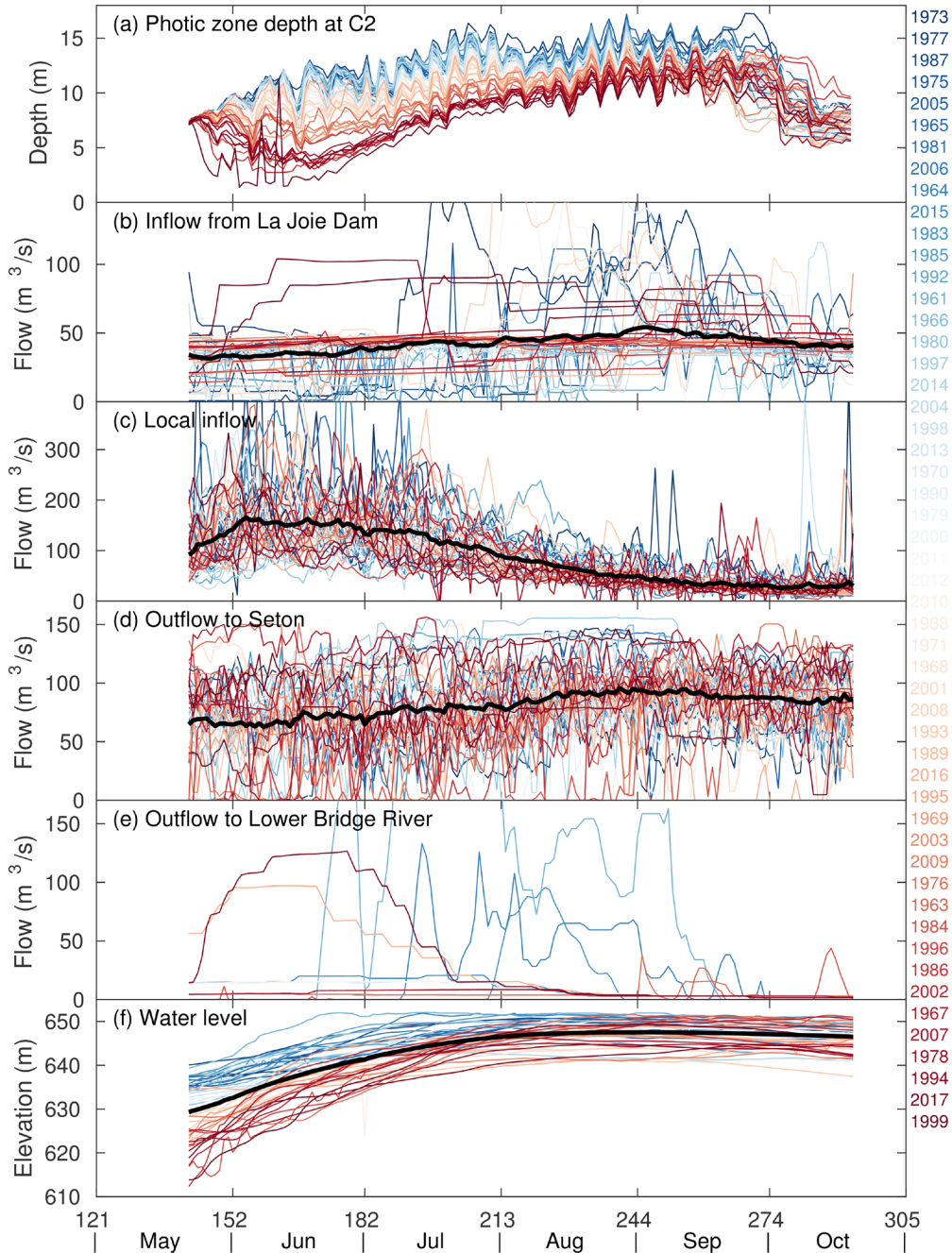


Figure 21. Modelled photic zone depth and flow boundary conditions for all years 1961–2017; (a) photic zone depth; (b-f) flow boundary conditions and water level; (blue) clear surface layer (deep photic zone) through (red) turbid surface layer (shallow photic zone). The numbers on the right indicate the year of the flow boundary conditions and their colour corresponds to the colour of the lines in the figure.

We ranked each year based on the average photic zone depth during the model period (right column in Figure 21). Rankings were from deepest (blue) to shallowest (red) photic zone depth, corresponding to clearest (blue) to most turbid (red) surface layer, respectively. The rankings clustered around water level (Figure 21f). Model runs with a clearer surface layer began with a higher water level, and vice versa the runs with a turbid surface layer began with a lower water level. There was also some clustering in the flow from La Joie Dam, where lower inflow from La Joie Dam in the first part of the model period favoured a clearer surface layer during that time (Figure 21b). For other characteristics, such as local inflow (Figure 21c) and outflow to Seton (Figure 21d), there was no obvious clustering between the extremes. The rankings and clustering were very similar for model runs using the meteorological and water quality forcing of 2016 (not shown).

This analysis allowed us to identify flow conditions resulting in extremes in surface layer turbidity, thereby, resulting in extremes in light availability. Out of the 52-year flow record (52 model runs), the clearest surface layer was in 1973 and the most turbid was in 1999. We selected these two model runs as scenarios (representative of their clusters). We hereafter refer to these scenarios as Clear Surface Layer (ClearSL) and Turbid Surface Layer (TurbSL), respectively.

To examine how far the extremes (ClearSL and TurbSL) deviate from typical conditions, we selected a Normal Operations (NormOP) Scenario. Out of the 52 model runs, the 26th clearest surface layer was in 2011; inflows, outflows, and water levels in 2011 were very close to the mean daily values over the period of record, and these flow conditions were generally representative of other runs with median surface layer clarity.

Due to dam safety, a requirement was put in place to lower the normal maximum water level in Downton Reservoir from 749.81 to 734.0 m until La Joie Dam undergoes seismic upgrades (BC Hydro 2016). This requirement resulted in outflows to the Lower Bridge River that were sustained at a higher level over a longer period of time than in previous years (Figure 21). Since the reservoir operations in 2016 and 2017 may be the new norm until upgrades are complete, we selected a Low Downton Reservoir (LowDR) scenario, to examine how the lower normal maximum water level may impact turbidity and light availability in Carpenter Reservoir in the near future.

To summarize, Figure 22 shows the scenarios as in Figure 21, except that it highlights the four scenarios using coloured lines overlying grey lines which represent all the other years. Table 12 shows a list of the scenarios with corresponding flow conditions.

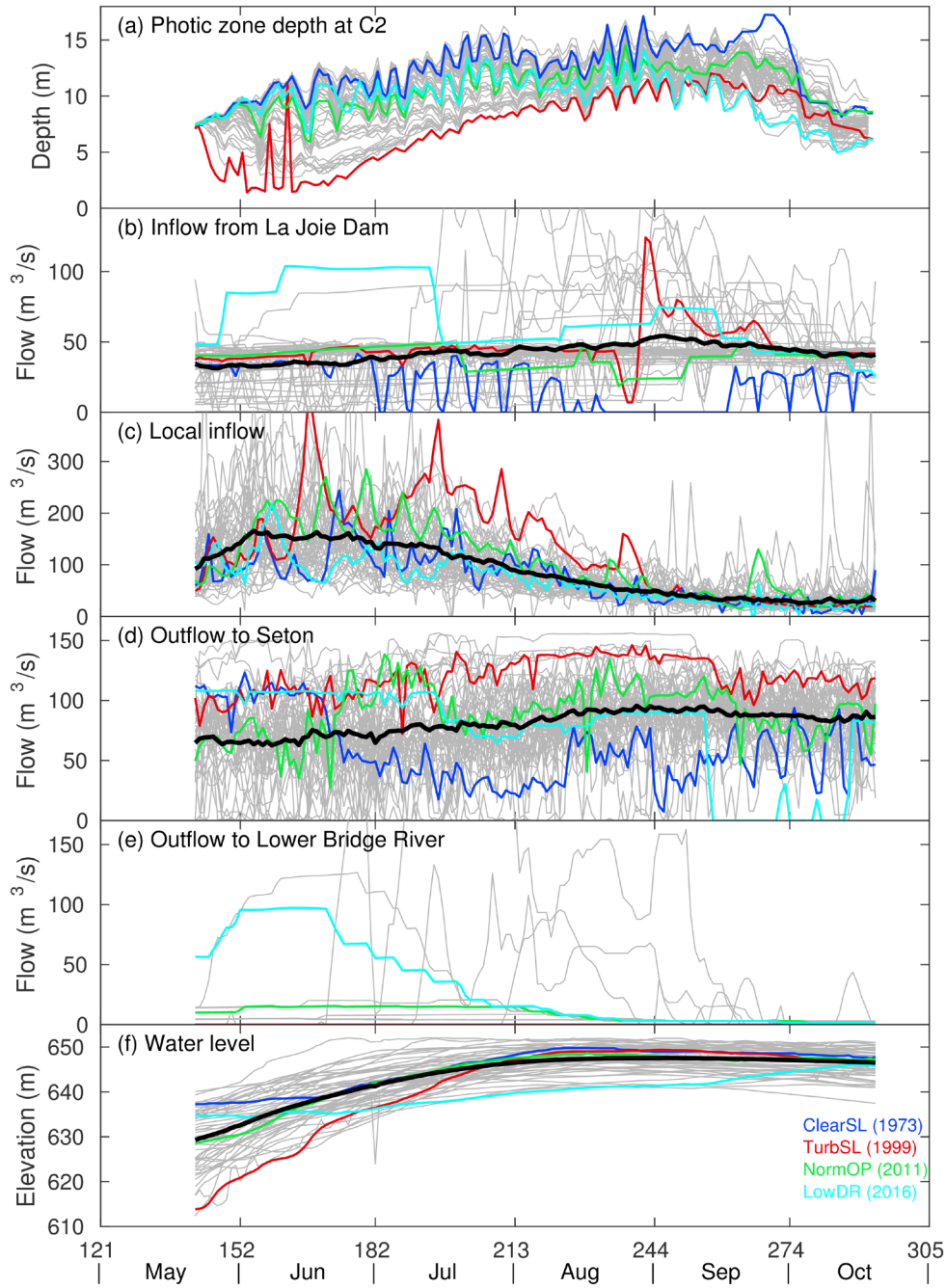


Figure 22. Modelled photic zone depth and flow boundary conditions for all years 1961–2017; (a) photic zone depth; (b-f) flow boundary conditions and water level; (colours) selected years for model scenarios; (grey) years not selected for model scenarios.

Table 12. Layout of model runs.

Scenario	Name	Flow forcing (reservoir operation)*	Met and WQ forcing**	Start date	End date	La Joie Outflow (Apr-Oct)	Local Inflow (Apr-Oct)	Initial Water level (22 May)
2015	2015 Field year 1	2015	2015	22May	20Oct	High	Average	Average
2016	2016 Field year 2	2016	2016	12May	14Oct	Very High	Average	Average
1	Clear surface layer (ClearSL)	1973	2015	22May	20Oct	Very Low	Low	High
2	Turbid surface layer (TurbSL)	1999	2015	22May	20Oct	Above average	High	Low
3	Normal operations (NormOP)	2011	2015	22May	20Oct	Average	Above average	Average
4	Low level in Downton R. (LowDR)	2016	2015	22May	20Oct	Very High	Average	Average

* The model was run with the reservoir operation conditions for a given year, namely the inflows and outflows for the given year, which gives the matching water level.

** Gives the year for the model start and end date, reservoir initial condition, meteorological forcing, and tributary temperature, conductivity, turbidity, and nutrients used in the model run.

The rationale for selection of scenarios and list of scenarios was submitted to BC Hydro for approval. BC Hydro agreed to the scenarios in email discussions occurring on August 24, 2017, August 25, 2017, August 31, 2017, September 1, 2017, September 5, 2017, and October 12, 2017 (M. Casselman, BC Hydro, personal communications).

5.1.4 Modeled 2015 field year

5.1.4.1 Water temperature

Water temperature computed by the model is shown as both line and contour plots in Figure 23 and as snapshots in time in Figure 24 (left column). Results showed general and acceptable agreement with the measured data shown in Figure 19 and Appendix F (report Section 13.2). Seasonal evolution of the thermocline can be seen as the epilimnion warms in summer and then cools and deepens in the fall. In addition, there are times when the depth of the thermocline oscillated over periods of 4 to 6 days, likely due to prolonged variations in the wind on the reservoir surface. For example, wind from the west will push the warm surface layer toward Terzaghi Dam, deepening the layer of warm water near the dam (Figure 24d). When the wind ends, the warm layer near the dam will become shallower again (Figure 24g). These temporal oscillations are shown as peaks and valleys at the thermocline in Figure 23b.

5.1.4.2 Water chemistry

The modelled turbidity is shown as a time series in Figure 23c. The initial turbidity in the reservoir was set to the Sea-Bird turbidity measurements at station C2 on 22 May 2015. The initial turbidity was approximately 4 NTU in the top 10 m, increasing to

approximately 20 NTU in the deepest water (> 20 m). From May to August the turbidity of the surface layer (epilimnion) decreased from 4 to 0.7 NTU, similar to the decline observed in the field data. In contrast, turbidity in the deep water was much higher. Appendix D shows very high turbidity in all local tributaries in May 2015 (specifically on 23 May 2015, after a rainstorm the previous evening) (Figure 48). This tributary inflow, which plunged to depth, contributed to the elevated turbidity in the deep water during May and early June. Appendix D also shows that turbidity in flow from La Joie Dam rose steadily from ~ 10 NTU in May to > 100 NTU in October 2015 (Figure 47e). This inflow from La Joie Dam contributed to the increased turbidity in the deep water toward the end of the model period. This pattern of the declining and then rising turbidity of the deep water was also observed in the Sea-Bird profiles (Figure 17).

The C25 of the surface water remained relatively steady through summer, consistent with the field data and again suggesting isolation of the surface layer (Figure 23d). The C25 of the surface began to decline in the fall as the surface layer was mixed down, and as deeper water – with lower C25 – was included in the surface layer. In deep water, C25 first increased during freshet (May to early June), reflecting tributary inflows with higher C25 concentrations that was largely absent before freshet (Figure 23). From July onward, C25 of the deep water declined as a result of the plunging of cold inflow from La Joie Dam with lower C25. The declining C25 of the deep water was also observed in the Sea-Bird profiles (Figure 17b). At times, the inflow of water from local tributaries with slightly elevated C25 was seen at the bottom of the reservoir, for example, in the snapshot of 16 July 2015 (Figure 24h). Note how water with lower C25 from La Joie Dam slotted in above this.

Total dissolved phosphorus (TDP) concentration from the model is shown in Figure 23e. The initial TDP concentration was at the method detection limit of $2 \mu\text{g}\cdot\text{L}^{-1}$. Relatively high TDP concentrations from La Joie can be seen at depth, through June and July. During this time the TDP concentration in the surface layer remained relatively constant. During August and September, the TDP concentration increased at depth. Small increases in TDP concentration at the surface did not occur until late September and October. This observation suggests that supply of soluble phosphorus to the surface layer does not occur until the fall, and that TDP from both the La Joie and tributary inflows may ‘short circuit’ to the deep outlet without being available to the photic zone during much of the productive growing season. This subsurface flow of soluble phosphorus may cause biological production in downstream Seton Lake and the Lower Bridge River to be greater than in Carpenter Reservoir and that Carpenter Reservoir is mainly a conduit of that phosphorus from upstream sources.

Model results for $\text{NO}_3\text{-N}$ are shown in Figure 23f. The initial concentration was near $10 \mu\text{g}\cdot\text{L}^{-1}$, a very low concentration that shows little input from upstream and atmospheric sources. During freshet, $\text{NO}_3\text{-N}$ concentration more than doubled at depth in association with plunging inflow from La Joie. The higher $\text{NO}_3\text{-N}$ concentrations in that inflow may be attributed to mobilization of $\text{NO}_3\text{-N}$ accumulated in melting snowpack and

forest soils. Declining $\text{NO}_3\text{-N}$ concentration at all depths later in the summer is consistent with depletion of the snowpack source of $\text{NO}_3\text{-N}$ and demand by phytoplankton in the surface layer.

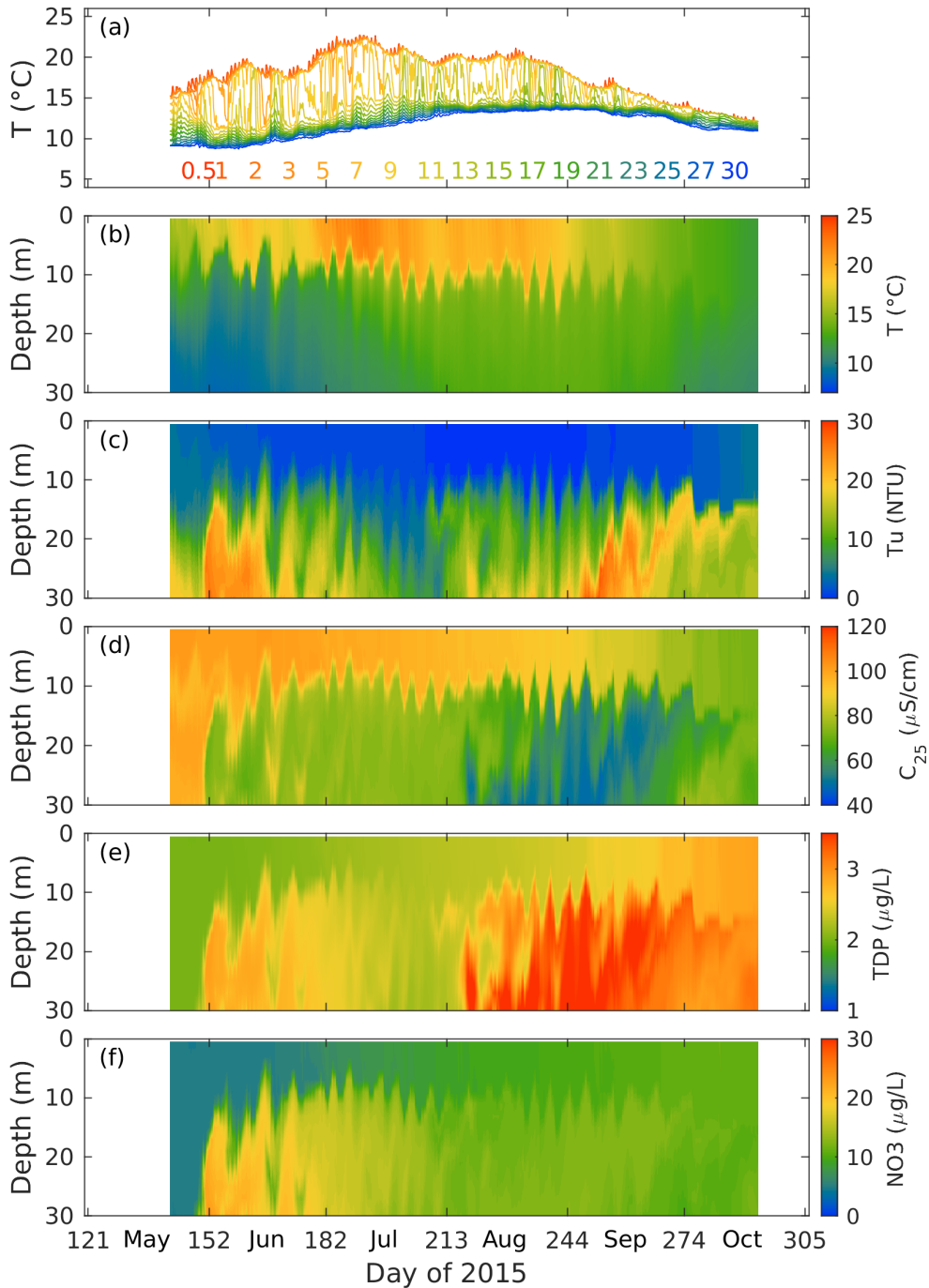


Figure 23. Field year 1 (2015). Modelled water quality parameters at segment 53 (station C2).

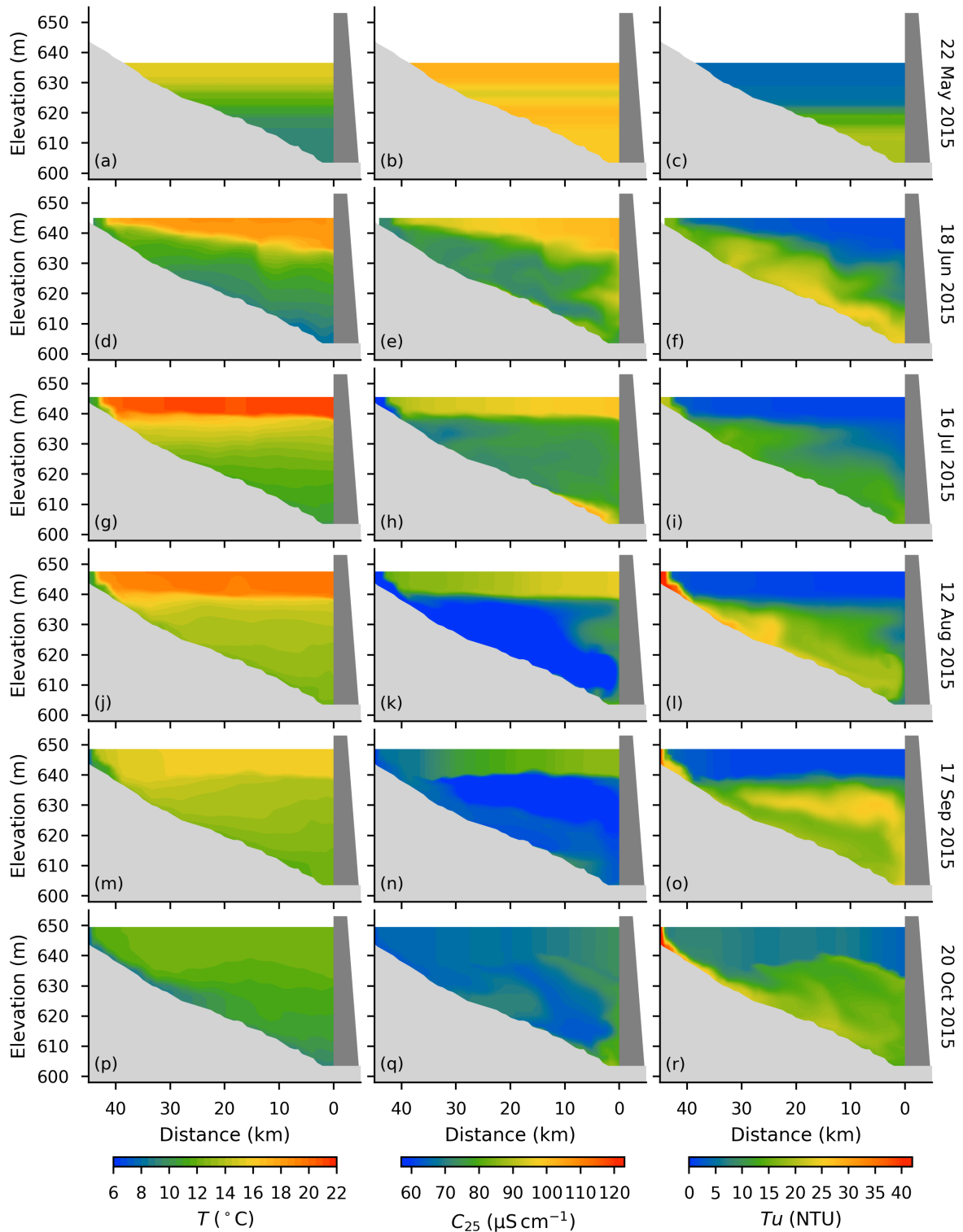


Figure 24. Field year 1 (2015). Snapshots of modelled temperature T , conductivity C_{25} and turbidity Tu along the length of the reservoir at selected dates.

5.1.4.3 Tracers in 2015

Tracers – the transport of inert scalars – were added to the model to track (1) the fraction of water in the reservoir at the start of the model run, (2) the fraction of water coming from La Joie Dam and (3) the fraction of local flow (including the Hurley River). Tracers can help in understanding various mechanisms including the transport of plunging inflows, transport from the hypolimnion to the epilimnion, and the residence times of specific inflows.

The three tracers for Field year 1 (2015) are shown in Figure 25. The contours show the fraction of water originating from (a) the initial water in the reservoir, (b) the inflow from La Joie Dam, and (c) the local tributary inflow, all shown at station C2 (segment 53). At each depth and for each time, the sum of the values in panels a, b and c is equal to one.

At the beginning of the simulation on May 22, the fraction of initial water was one, and the fraction of water originating from the La Joie and local tributary inflows were both equal to zero. During freshet (May to mid-June), all inflows plunged deep into the reservoir and, by July, replaced almost all of the initial water in the hypolimnion. As the summer progressed and local tributary inflow decreased, the water in the hypolimnion was largely replaced by inflow from La Joie Dam. From mid-August to mid-September, the lenses of tributary water around 10 m depth suggests insertion of tributary water to the thermocline with the cooler inflow from La Joie below.

Very little water from the inflows entered the surface layer before September. This result suggests that, for most of the productive season, the turbidity in the surface layer is controlled by the initial turbidity in the reservoir, and by the settling of turbidity from the surface layer, rather than by the turbidity of the inflows. Recall the Sea-Bird profiles showed a decrease in turbidity in the surface layer, each month, from May to July (Figure 17), despite high inflow turbidity. By October, the Sea-Bird profiles showed a large increase in turbidity in the surface layer. The tracer results show that by October, much of the initial water in the surface layer was replaced by turbid inflow from La Joie Dam, in agreement with Sea-Bird profile observations.

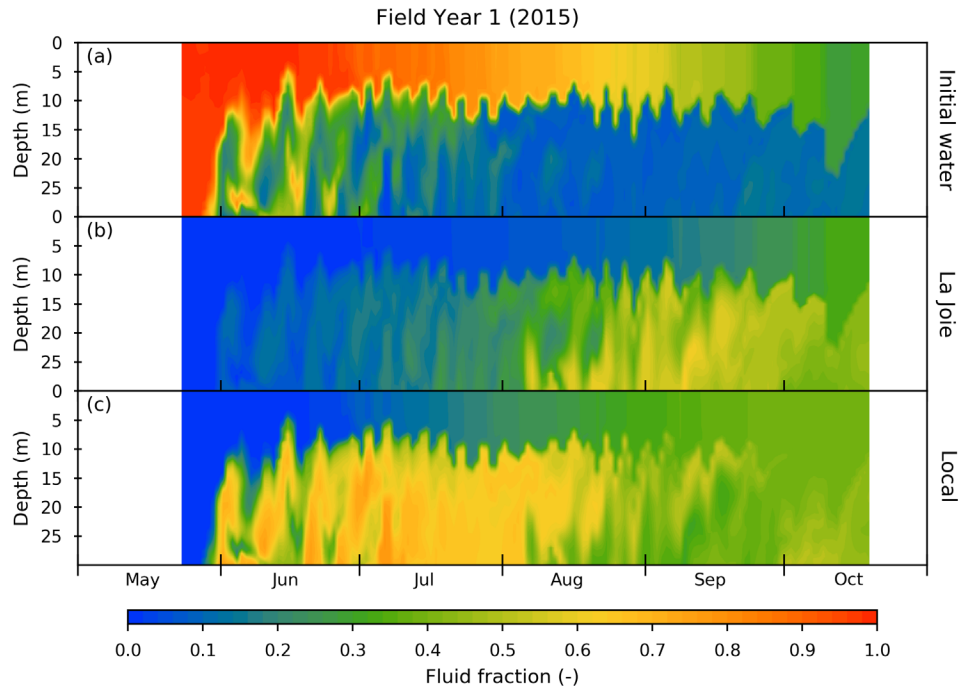


Figure 25. Field year 1 (2015). Passive conservative tracers at segment 53 (station C2) from (a) initial water in the reservoir, (b) inflow from La Joie Dam, and (c) local tributary inflow.

5.1.5 Modeled 2016 field year

5.1.5.1 Water temperature

Modelled water temperature for 2016 is shown as both a line and contour plot in Figure 26b and as temporal snapshots in Figure 27 (left column). The modelled temperature shows general agreement with the moored temperature data (Figure 19 and Appendix F (report section 13.2)). Discrepancies between the measured and modelled data are similar to those in Field year 1 (2015) with the exception of June 2016, when the modelled surface temperature was warmer and the deep water was cooler than observed; this occurred during a period of high outflow from Carpenter Reservoir as will be discussed below.

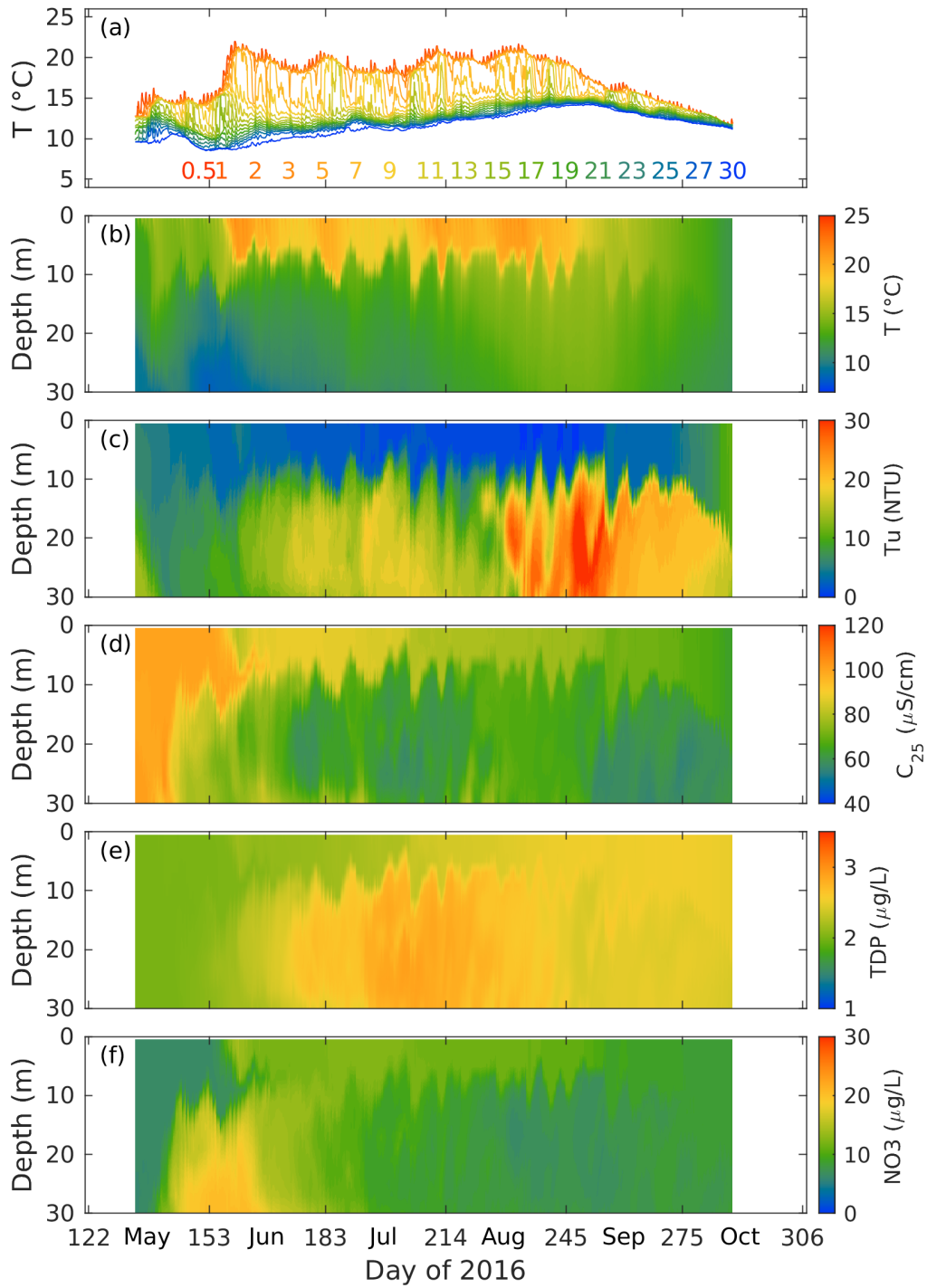


Figure 26. Field year 2 (2016). Modelled water quality parameters at segment 53 (station C2).

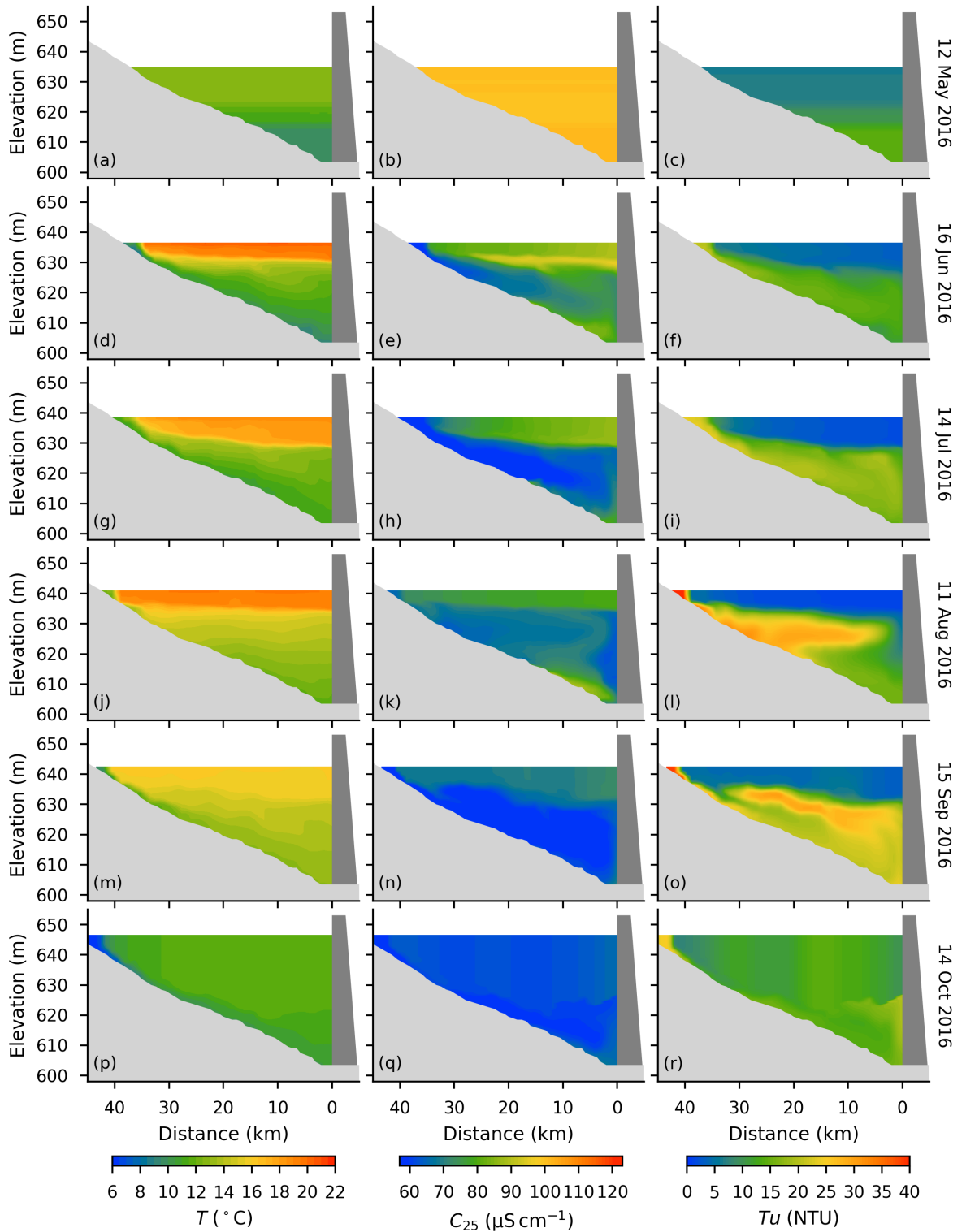


Figure 27. Field year 2 (2016). Snapshots of modelled temperature T, conductivity C₂₅ and turbidity Tu along the length of the reservoir at selected dates.

5.1.5.2 **Water chemistry**

The modelled turbidity is shown in Figure 26c and Figure 27 (right column). The initial turbidity in the reservoir was set to the Sea-Bird turbidity measurements at station C2 on 12 May 2016, which was 8 NTU in the top 10 m, increasing to 16 NTU at depth (> 20 m). At the start of the simulation, the turbidity in the local tributary inflow was <10 NTU, lower than in May 2015 (Figure 23).

The modelled changes in turbidity in the surface layer over the productive season follow the same trend as the Sea-Bird profiles (Figure 18c) and Appendix F (report Section 13.5). Though it is hard to see in Figure MODWQ16c, the model results for 2016 show the onset of higher turbidity in the surface layer earlier in the productive season than in 2015. As a result of the lower turbidity of the tributary inflows in 2016, the plunging of cold turbid tributary inflow in May and June 2016 (Figure 26c) is less apparent than in 2015 (Figure 23c).

C25, TDP concentration, and $\text{NO}_3\text{-N}$ concentration in 2016 showed similar patterns to those in 2015, with several exceptions. First, C25 in the surface layer declined earlier in 2016 (Figure 26d) than in 2015 (Figure 23d). Second, TDP concentration in the hypolimnion was lower in the last half of the simulation in 2016 (Figure 26e), compared to 2015 (Figure 23e). This difference reflects lower TDP concentrations measured in the flow from La Joie Dam, from August to October 2016 (Appendix D, Report Section 11.3); these concentrations were used as part of the inflow boundary conditions in the model. Third, $\text{NO}_3\text{-N}$ concentration rose more rapidly in the surface layer in 2016 (Figure 26f) than in 2015 (Figure 23f), again reflecting the slightly earlier replacement of the surface mixed layer with tributary inflow in 2016.

To summarize, both the measured and modelled turbidity at 1 m — representative of the surface mixed layer — is shown for 2015 and 2016 in Figure 28a. The observed and modelled turbidity decline from May to August. The decline in turbidity is close to a straight line when the data are log-linear plotted (Figure 28b). The slope of the dash line is -0.032 days^{-1} and corresponds to Stokes settling for particles with a diameter of 2 μm . To see a clearing of the surface mixed layer — with a low in 2015 of 0.6 NTU — was surprising given the high turbidity of the inflows.

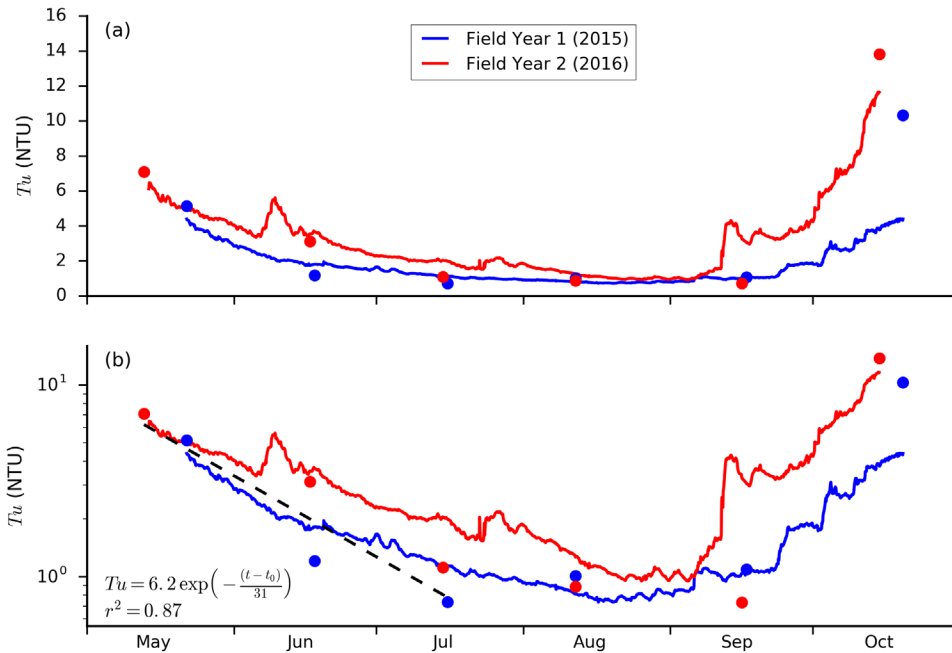


Figure 28. (a) Linear and (b) log-linear plots comparing measured and modelled surface turbidity at segment 53 (station C2) for Field years 1 and 2 (2015 and 2016). (solid lines), modelled turbidity at 1 m depth; (circles), measured turbidity from the Sea-Bird profiles at 1 m depth; (dash line) log-linear least-squares fit for the measurements collected from May to July in 2015 and 2016.

5.1.5.3 Tracers in 2016

The modelled tracers for 2016 are shown in Figure 29. Compared to 2015, both higher inflows from La Joie Dam and higher outflow from Terzaghi Dam in June resulted in an earlier replacement of the initial water in the hypolimnion. By one month into the simulation, over 90% of the initial water was replaced in the hypolimnion. In addition, water originating from La Joie Dam and the local inflows entered the surface layer earlier in the productive season.

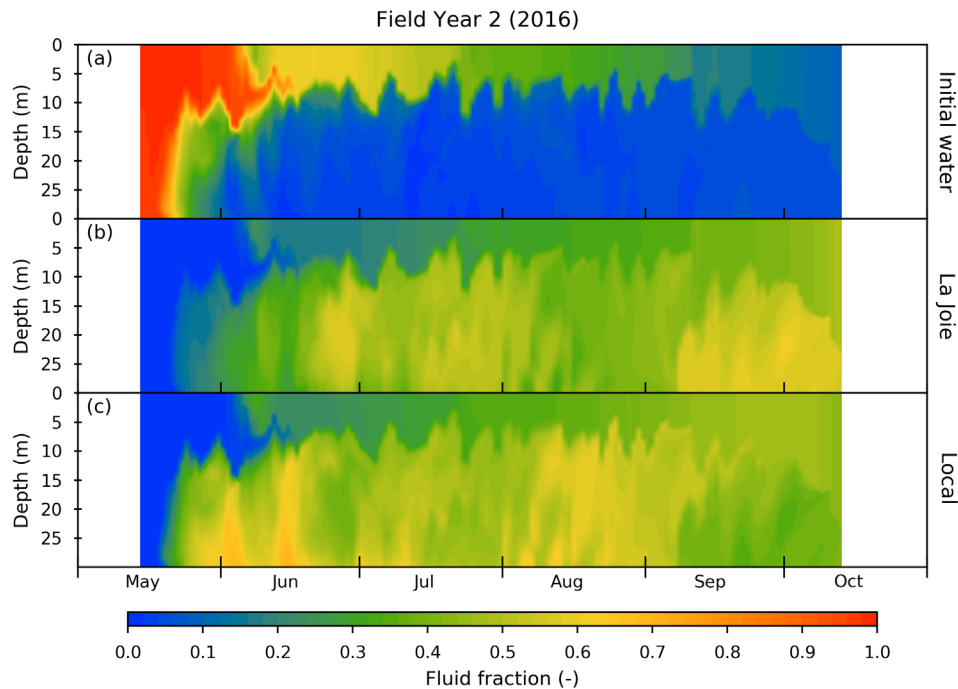


Figure 29. Field year 2 (2016). Passive conservative tracers at segment 53 (station C2) from (a) initial water in the reservoir, (b) inflow from La Joie Dam, and (c) local tributary inflow.

5.1.6 Management scenarios

Four scenarios were selected for modeling as described in Section 5.1.3 and can be summarized as follows:

1. Scenario 1, clear surface layer scenario (ClearSL) represents the deepest mean annual photic zone depth out of the set of reservoir operations from 1961-2017.
2. Scenario 2, turbid surface layer scenario (TurbSL) represents the shallowest mean annual photic zone depth out of the set of reservoir operations.
3. Scenario 3, normal operations scenario (NormOP) represents average reservoir operations
4. Scenario 4, low Downton Reservoir scenario (LowDR) represents reservoir operations with a lower normal maximum water level (734.0 m) in Downton Reservoir.

Flow boundary conditions and resulting water levels for each scenario are shown in Figure 30. Scenario 1 (ClearSL) is characterized by relatively low inflows, low water release in late June through October, and maintenance of high water surface elevations in Carpenter Reservoir. Scenario 2 (TurbSL) has opposite conditions of relatively high inflows, high water release, and low water surface elevations. Scenario 3 (NormOP) has average inflows, water release, and water surface elevations. Scenario 4 (LowDR) has high water release from LaJoie to keep water levels in Downton at a low level, moderate

to high water release to Seton and high water release to the Lower Bridge River. The high water releases are required in this scenario to maintain water levels in Carpenter Reservoir while accepting high inflows from LaJoie.

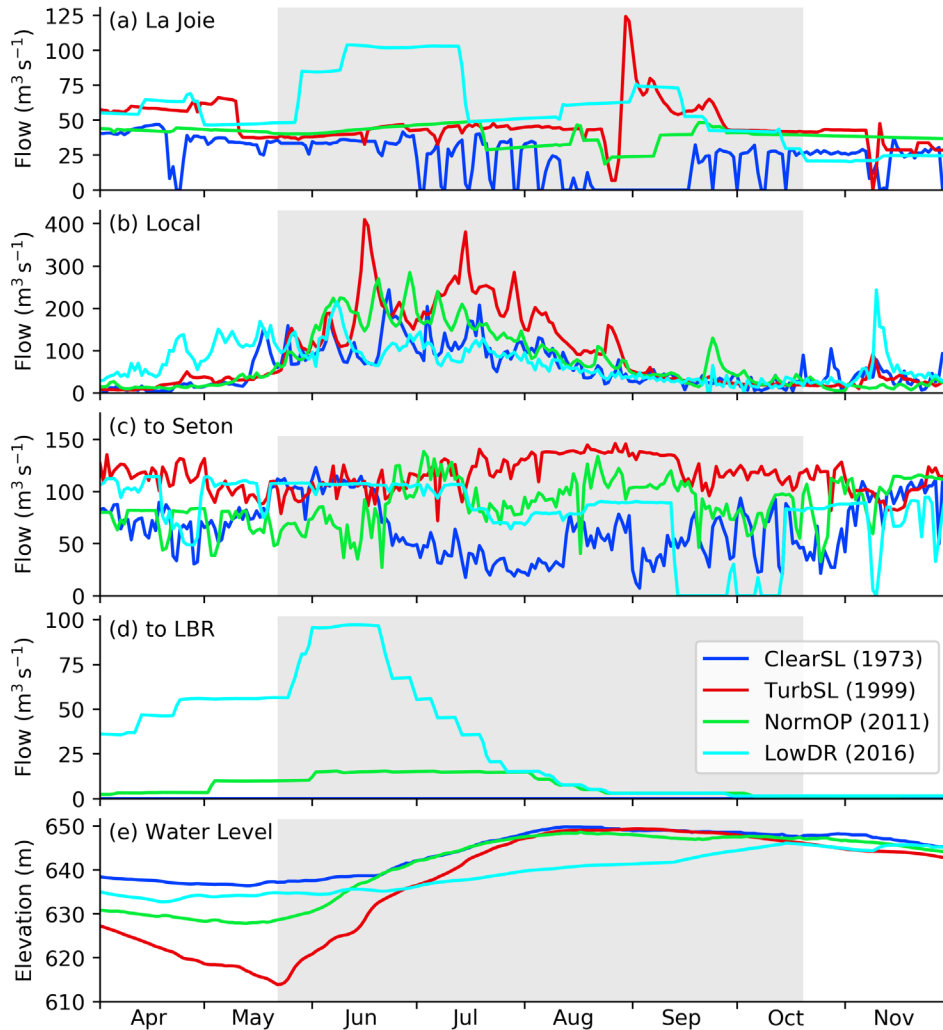


Figure 30.(a-d) Flow boundary conditions, and (e) the water level for each model scenario. The grey region indicates the model period (22 May – 20 Oct).

Detailed imaging of time series, snapshot, and tracer plots for each scenario are provided in Appendix G (report Section 14).

Water temperature among scenarios showed the same cycle of seasonal stratification as was observed in 2015 (Figure 23) and 2016 (Figure 26). The exception was Scenario TurbSL where the development of temperature stratification was inhibited in the first month because of low water level, which left the reservoir with a small volume and shallow depth (<10 m), (see Figure 70 and Figure 74). Once the water level rose sufficiently by mid-June the regular pattern of thermal stratification resumed.

A comparison of modelled surface water temperature, surface turbidity, and photic zone depth between scenarios is shown in Figure 31. The surface temperature was similar in all four scenarios, which is to be expected given that all the scenarios are driven by the same meteorological data, namely that of 2015. The only difference was in Scenario TurbSL from mid-May to late-June, when water level was very low, and surface temperature was reduced due to mixing with cold inflows. At the beginning of the model run (22 May), the turbidity at 1 m depth was ~5 NTU for all scenarios. By June, the surface turbidity declined slightly to ~4 NTU for all scenarios, except for Scenario TurbSL, which had risen to ~25 NTU. The results suggest that turbid inflows entered the surface layer more readily in Scenario TurbSL than in the other three scenarios, again due to low water level. Low water volume in the spring during scenario TurbSL may contribute to this effect. Between 22 May and 1 July, the reservoir volume for TurbSL increased by a factor of 14, compared to a factor of 3.2 for Scenario NormOP and 1.4 for Scenario ClearSL (Table 13) coinciding with a large decline in surface turbidity during TurbSL and little change in turbidity among the other scenarios. Time course change in photic zone depth was the inverse of turbidity in TurbSL; it declined to only about 2m during the peak of turbidity but then increased gradually to reach 14m near the end of the end of September before declining again when turbidity increased with mixing of the water column in the fall.

Table 13. Water level, volume and volume change over the first 40 days of the model scenarios.

Scenario	Water level (m)		Volume (Mm ³)		V_{May22} / V_{Jul1}
	22 May	1 July	22 May	1 July	
ClearSL	637.22	642.15	435	622	1.4
TurbSL	613.85	636.52	30	411	13.6
NormOP	628.62	642.11	193	620	3.2
LowDR	634.82	636.27	356	403	1.1

Tracer results for TurbSL indicate that initial water in the reservoir is completely flushed by mid-June (Appendix G, Figure 78). Even if all the initial water remained in the reservoir during TurbSL, the initial water would make up a small proportion of the total water in the reservoir. This result is quite different from the other three cases, where the surface layer is composed predominantly of initial water until the fall, when the thermocline deepens, mixing water from the inflows from below (Appendix G Figure 77, Figure 79, Figure 80). However, in Scenario TurbSL, once thermal stratification is established by mid-June, the surface layer then becomes isolated from subsequent inflows, and the turbidity declines, approaching that of the other scenarios by the end of August (Appendix G, Figure 78).

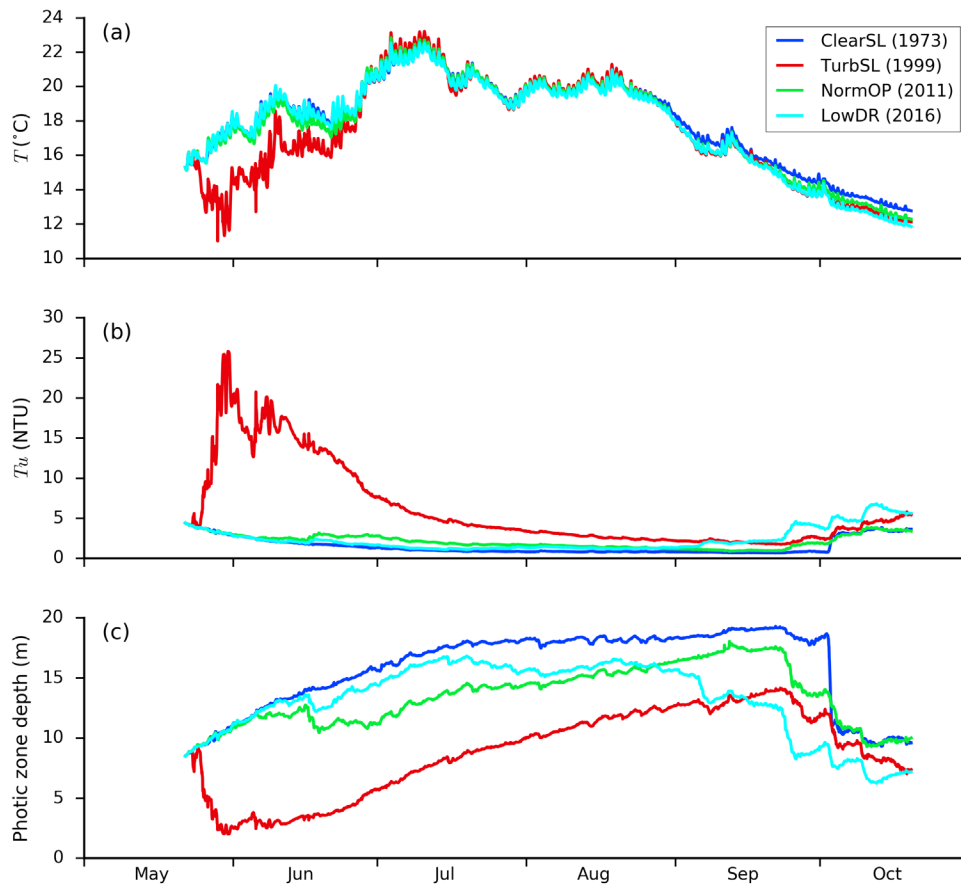


Figure 31. Modelled (a) temperature, (b) turbidity, and (c) photic zone depth, all at 1 m depth at segment 53 (station C2), for each model scenario.

The LowDR scenario is particularly relevant for present time because this is the policy that BC Hydro is following until seismic upgrades to the LaJoie Dam can be completed a few years from now. In LowDR, turbidity in the surface layer is low, as long as water surface elevation is kept high, as shown in Figure 30. The same policy was applied for scenarios ClearSL and NormOP. However, by mid-September the LowDR surface turbidity increases and exceeds that of Scenario TurbSL, albeit at values 5 times less than during the spring for TurbSL. In the LowDR scenario, the Bridge powerhouses are shut down, and outflow to the Lower Bridge River is minimal during mid-September to mid-October. As a result, the reservoir filled with turbid water released from La Joie Dam. In the other three scenarios, during the same time period, the inflows were less than or equal to the outflows, so the turbid water passed through the reservoir and mixed less into the surface layer. Also noteworthy is that turbidity in Scenario LowDR begins to increase sooner than the other three scenarios, which produces a sooner decline in photic zone depth during the growing season, eventually leading to the smallest photic zone depth among all scenarios in September and October (Figure 31).

5.2 Biological modeling

5.2.1 Periphyton

5.2.1.1 Stable substrata

5.2.1.1.1 Periphyton composition on stable substrata

Periphyton algae found on the ball moorings in Carpenter Reservoir were mostly comprised of taxa from the class Bacillariophyceae (diatoms) and division Chlorophyta (green algae) (Figure 32). The diatoms are ubiquitous to all lakes and reservoirs. They represented 44%, 61% and 31% of the attached algal communities in spring, summer, and fall respectively. Most common diatoms were *Achnanthes linearis*, *Achnanthes minutissima*, *Amphipleura pellucida*, *Asterionella formosa*, *Diatoma elongatum*, *Eunotia tenella*, several *Fragilaria* sp., *Melosira* sp., *Nitzschia* sp., *Rhopalodia gibba*, and *Synedra ulna*. The chlorophytes (*Spirogyra* sp. and *Mougeotia* sp) made up most of the rest with a minor contribution from the Phylum Cyanobacteria (blue green algae). Most common blue greens were *Anabaena* sp. *Aphanisomenon* sp., and *Lyngbya* sp (only in fall 2016),

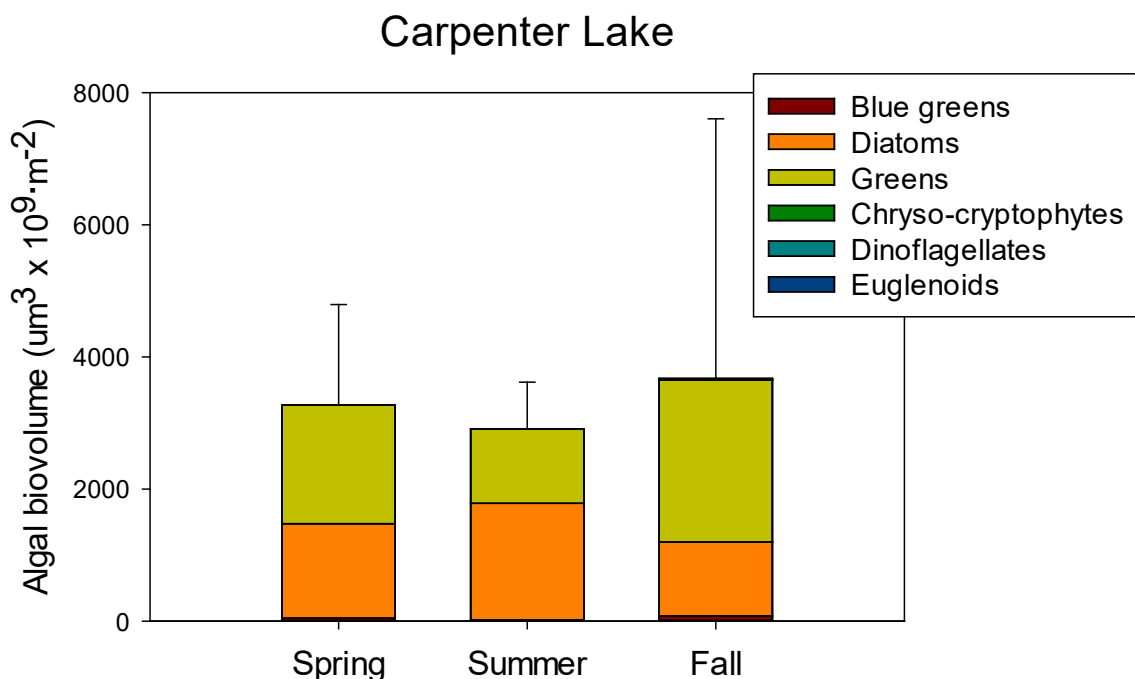


Figure 32. Mean algal biovolume by division found on ball moorings, by incubation period in Carpenter Reservoir in 2015 and 2016. Error bars are standard deviations calculated from biovolume of all taxa combined.

5.2.1.1.2 Stable substrata regression model

Periphyton biomass on stable substrata was positively and only explained by $\text{NO}_3\text{-N}$ concentration ($R^2=0.7$) (Equation 4). Sampling series (the time of sampling) was added as a random effect as part of selecting the best model but that addition did not increase fit of the model to the data and was not further considered. There was no need

to develop a regression equation using standardized coefficients (used to rank independent variables) because there was only one independent variable. The equation with **unstandardized coefficients** (used for prediction in original units) had the form:

$$\text{Periphyton Chla} = -0.76 + 10^{(0.189 * [NO_3 - N])} - 1$$

Equation 4

This model shows that the amount of PAR within the littoral zone was not limiting the rate of periphyton accrual on the stable substrata. NO_3 -N concentration was the main driver of periphyton growth. The littoral zone refers to shallow water habitat where macrophyte and non-macrophyte primary production occurs, determined at least in part by the vertical extent of light penetration associated with water clarity and change in water surface elevation (Wetzel 2001). This definition means that the littoral zone in Carpenter Reservoir is the shallow habitat of reservoir shorelines extending to a water depth at which light is sufficient to support photosynthesis that produces biomass on substrata. By this definition, light would not be expected to limit periphyton production in the littoral zone because sampling always occurred where light was potentially sufficient to drive photosynthesis. Light could be important if there was a gradient of responses in primary production to a gradient of irradiance in the littoral zone. The lack of PAR as an independent variable in the periphyton model showed that periphyton accrual was not sensitive to change in PAR over that gradient of accumulated light during the term of incubation of the substrata in the littoral zone where PAR occurred at intensities between 100% (water surface) and 1% (bottom of the photic zone) of surface irradiance.

The molar ratio of bio-available N:bio-available P in water can indicate the relative supply of N and P, the two nutrients that potentially limit growth of algae, whether it is periphyton or phytoplankton (Wetzel 2001). Nutrient limited growth kinetics are the same between both types of algae. Bio-available N can be approximated as the sum of NO_3 -N and NH_4 -N. NO_2 -N can be included but is transient in the oxidation of NH_4 -N to NO_3 -N so does not need to be considered. Bio-available P can be approximated as soluble reactive P (called SRP, which is mostly the phosphate anion) concentration when it is detectable or by total dissolved P (TDP) when SRP is undetectable. When TDP is undetectable, total phosphorus (TP) can be used but only with recognition that refractory phosphorus that is not available for biological uptake is part of TP. Rhee (1978) showed that for a given species of algae there is a sharp transition between P-limited and N-limited growth. The particular N:P ratio at which the transition between N and P-limitation occurs is species dependent, varying from as low as 7:1 for some diatoms (Rhee and Gotham 1980) to as high as 45:1 for some blue-greens (Healey 1985). Below a molar N:P of 20, the growth of most algal species will be limited by N whereas P-deficient growth is prevalent at molar N:P ratios greater than 50 (Guildford and Hecky, 2000). Because an optimum N:P ratio (above which P limitation

occurs and below which N limitation occurs) can vary widely among freshwater algae, the range between 20 and 50 may be regarded as a transition range in a community where the growth of some species will be P-limited and others will be N-limited.

Among the inflows to Carpenter Reservoir, molar N:P can be calculated using $\text{NO}_3\text{-N}$ as the N source ($\text{NH}_4\text{-N}$ was not detectable) and SRP can be used as the P source. The overall mean $\text{NO}_3\text{-N}$ concentration among both years and dates was $16.6 \mu\text{g}\cdot\text{L}^{-1}$ in the inflow from the Middle Bridge River and $14.8 \mu\text{g}\cdot\text{L}^{-1}$ among the small tributaries. SRP concentration was $1.8 \mu\text{g}\cdot\text{L}^{-1}$ and $1.1 \mu\text{g}\cdot\text{L}^{-1}$ in the same sources respectively. These concentrations resulted in a molar N:P of 20 in the discharge from the Middle Bridge River and 30 in the smaller tributaries, which indicates N deficiency for growth of most species of algae in water that is discharged into the reservoir. The very low concentrations of both SRP and $\text{NO}_3\text{-N}$ show that addition of either N or P will quickly drive an algal assemblage into growth limitation by the other nutrient, which infers general co-limitation of N and P for many algal species in the supply of water to Carpenter Reservoir.

Within the epilimnion where chemical measurements were made for both the periphyton and phytoplankton models, the mean $\text{NO}_3\text{-N}$ concentration was $5.5 \mu\text{g}\cdot\text{L}^{-1}$ and SRP concentration was $1.0 \mu\text{g}\cdot\text{L}^{-1}$, which was the method detection limit. These mean concentrations are very low but potentially higher than actual values because concentrations could not be detected in several samples. If we accept the detected values, they reveal a molar N:P of 12, which shows more extreme N deficiency of algal growth than was found in the inflow streams. This change in N deficiency between streams and surface layer in the reservoir shows stripping of inorganic N in the reservoir. This finding means that any N that is biologically available will be quickly sequestered during photosynthetic biological production. It also means that much of the bioavailable N that does occur will not be detectable using wet chemistry and that biological response is the better indicator of change in nutrient availability in the water column of Carpenter Reservoir. Periphyton is a good indicator of that response (Bothwell 1989).

This rationale showing potential N deficiency in the nutrient supply to periphyton algae is consistent with Equation 4 in showing the importance of $\text{NO}_3\text{-N}$ in controlling periphyton accrual. It shows that nutrient limitation was the most important factor determining biological production in the littoral zone of Carpenter Reservoir.

5.2.1.2 Sand samplers

5.2.1.2.1 Periphyton composition on sand

The periphyton community composition on sand was completely different and less dense than the community found on ball moorings in Carpenter Reservoir. Sand periphyton in the spring was entirely made up of *Cryptomonas* sp., a chryso-cryptophyte (Figure 33) while in the summer, the community shifted to diatoms dominated by *Stauroneis* sp. and some *Rhopalodia* sp. The community in the fall was approximately 5x larger than either of the previous seasons and was comprised primarily of

Cryptomonas sp. (a flagellate; 87% of total biovolume). The remaining portion was a combination of *Cymbella* sp. and *Stauroneis* sp., both diatoms. Chryso-cryptophytes are flagellated free swimming phytoplankton, not attached periphyton. This finding shows that the cells were not growing on the sand but were associated with the bottom of the water column at the sand surface.

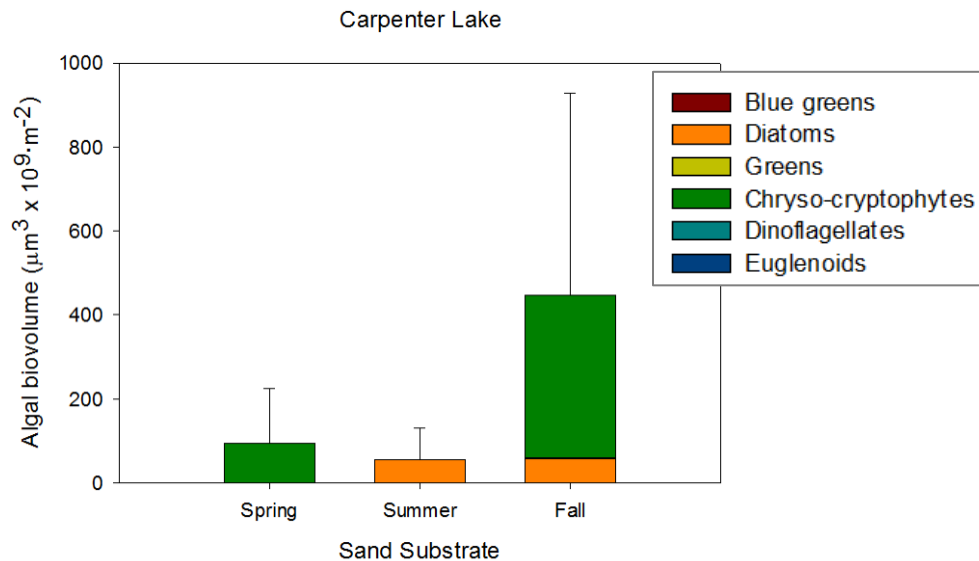


Figure 33. Algal biovolume, by taxonomic group, found on sand moorings by incubation period in Carpenter Reservoir in 2015 and 2016. Error bars are standard deviations calculated from biovolume of all taxa combined.

5.2.1.2.2 Sand substrata regression model

Given that most algae found in the sand cores were motile chryso-cryptophytes, we know that the cells were not stationary. The cells were moving in association with the bottom of the water column at the sand surface. With this behaviour, an assemblage of algae from a sand core cannot be assumed to be growing and accruing on the sand at a single place as on the ball moorings on which only attached taxa were found. The assemblage on sand was potentially disconnected from the littoral food web that is driven by processes in the substratum, not over top of it.

This finding introduces considerable caution in developing a regression model to examine habitat attributes driving periphyton accrual on sand. If the algal community in the samples was not stationary and directly associated with habitat attributes in the sampled mooring, any association between a habitat attribute and the algal biomass may be spurious and not actually linked even if a significant statistical model is found. The 10 times lower algal biovolume found in the sand samples (Figure 33) than on the ball moorings (Figure 32) further shows that sand was not conducive to supporting an

attached algal community. For these two reasons (poor representation by an attached algal community and little algal biovolume) a regression model for the sand mooring was not developed. Any model may not be representative of the attached littoral community and not reliable for exploring potential effects of management actions on biological assemblages in the sand substrata.

5.2.2 Phytoplankton

5.2.2.1 Phytoplankton composition

Phytoplankton biovolume in Carpenter Reservoir was greatest in May ($664 \mu\text{m}^3 \cdot 10^3 \cdot \text{ml}^{-1}$) and it steadily declined to $182 \mu\text{m}^3 \cdot 10^3 \cdot \text{ml}^{-1}$ in October in combined data from 2015 and 2016 (Figure 34). Taxa were mostly from the Chrysophyceae, Cryptophyceae (the cumulative biovolume of these classes of flagellates is commonly called the chryso-cryptophytes) and class Bacillariophyceae (diatoms). These taxa are common in nutrient deficient lakes and reservoirs of British Columbia. The chryso-cryptophytes represented 50% to 64% of the phytoplankton community and the diatoms were 18-28% of the community in all months except in June when they were 7% of the community biovolume during May – October. Most common chryso-cryptophytes were *Kephyrion* sp., *Ochromonas* sp., *Uroglena* sp., *Chromulina* sp., *Chrysochromulina* sp., and *Cryptomonas* sp. and the common diatoms were *Asterionella formosa*, *Fragilaria crotonensis*, and *Aulacoseira* sp. The division Chlorophyta (green algae) were common in June (33% of total biovolume) but rarer in other months. Most common taxa were *Chlamydomonas* sp. and *Ankistrodesmus* sp. Relatively rare taxa included Cyanobacteria (blue-green algae), euglenoids (*Euglena* sp.) and dinoflagellates (e.g. *Gloeodinium* sp., *Peridinium* sp., and *Ceratium* sp.).

Carpenter

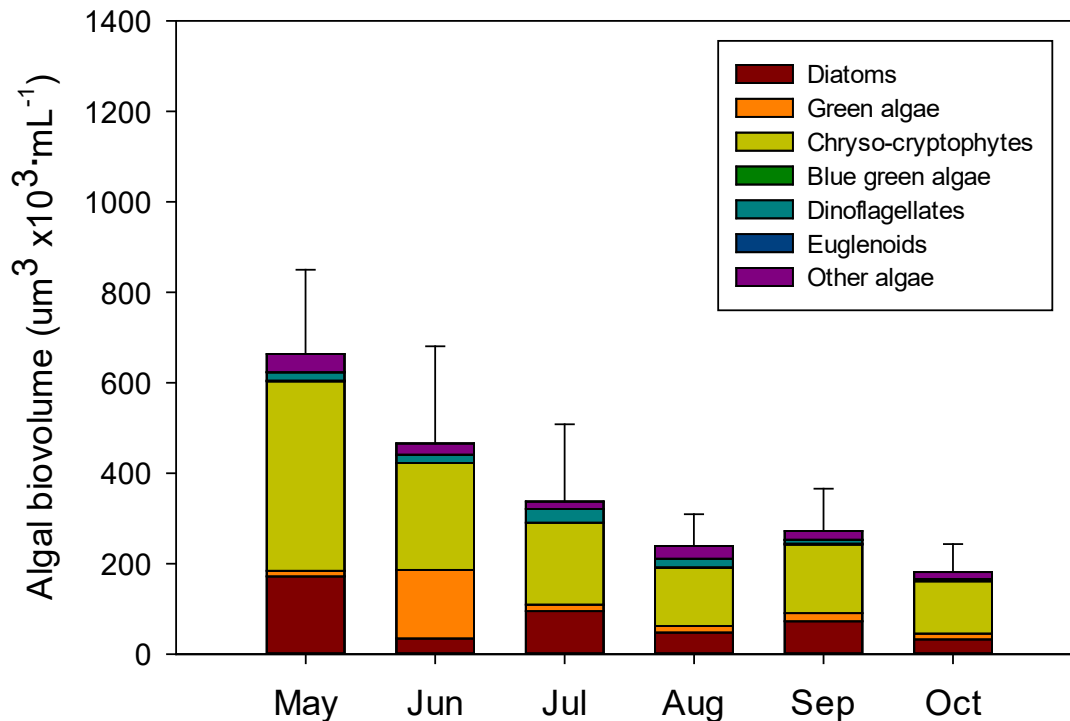


Figure 34. Composition of phytoplankton biovolume in Carpenter Reservoir by month. Values are mean biovolume by algal division calculated from samples collected in 2015 and 2016 at stations C2 and C6. Error bars are standard deviations of mean biovolume among all taxa.

5.2.2.2 Phytoplankton regression model

Primary production in Carpenter Reservoir was related to PAR, turbidity and temperature ($R^2 = 0.78$) (Equation 5 and Equation 6). The regression equation using **standardized coefficients** (used to rank independent variables) was:

$$Phytoplankton\ PP = 0.896 + PAR^{0.327} + 10^{-0.112 \cdot temperature} + (PAR^{-0.669} * 10^{-0.669 \cdot temperature}) + 10^{-0.032 \cdot turbidity} - 1$$

Equation 5

The equation with **unstandardized coefficients** (used for prediction in original units) had the form:

Phytoplankton PP

$$= 0.193 + PAR^{10.154} + 10^{0.036*temperature} + (PAR^{-0.565} * 10^{-0.565*temperature}) + 10^{-0.032*turbidity} - 1$$

Equation 6

Among the independent variables, PAR had a greater effect on primary production than did temperature, which in turn had greater effect than turbidity. Turbidity had about 10 times less importance than did PAR. This distinction means that even in the presence of turbidity over the average values that were measured in the photic zone of pelagic habitat (0.2 – 14.6 NTU), PAR drives most primary production. Note that turbidity in the photic zone is much less than turbidity found deeper in the water column because turbid water flowed along the bottom of the reservoir below the photic zone where phytoplankton were growing (see Sections 5.1.4 and 5.1.5). Equation 5 and Equation 6 show that the effect of PAR on primary production is independent of the effect of turbidity on primary production within the range of euphotic zone depths of 100% of surface irradiance to 1% of surface irradiance. If turbidity is 1 NTU over all depths of the photic zone, increasing PAR will exert a positive effect on primary production with higher rates occurring at higher PAR and lower rates occurring at lower PAR according to light attenuation within the turbidity affected photic zone. Similarly, if turbidity is higher at 10 NTU, for example, PAR will still exert control over primary production at that level of turbidity. The strong interaction of PAR and temperature in the model shows that PAR is statistically dependent on temperature or vice versa temperature is statistically dependent on PAR. This dependency happens because the two variables change with position in the water column and thus are interactively dependent. This interaction is different from collinearity that was found not to be present between PAR and temperature. If collinearity was present, the model would be unstable and one of the two variables would have to be removed.

The independence of PAR and turbidity acting on phytoplankton production means these two factors affected phytoplankton production in different ways. PAR is a direct and unequivocal measure of irradiance available for photosynthesis. Hence, PAR is the key indicator of light. Turbidity is a measure of light scattering, not available light for biological production. It is also an indirect indicator of particle concentration. This distinction in measurement between PAR and turbidity means that turbidity was potentially showing something different from changing light available for phytoplankton production. In Carpenter Reservoir, turbidity is caused by suspensions of very small inorganic particles. Raw data from the lab showed particle sizes ranging from approximately 0.5 µm to over 100 µm with mean values being 13 – 37 µm in the Upper Bridge River, 6 – 45 µm in the inflow to Carpenter Reservoir from the Middle Bridge River, and 2 – 9 µm in the tailrace of the Bridge generating station (outflow of Carpenter Reservoir) (Figure 35). The smaller particles in the Carpenter outflow compared to upstream sites shows settlement of larger particles in Carpenter Reservoir, contributing

to sand aggradation that is obvious at drawdown. Some distributions had colloidal materials (size $\leq 1 \mu\text{m}$ as defined by Gottselig et al 2017). Given that small particles can scavenge phosphorus by adsorption (Gottselig et al 2017) it is possible that turbidity was an indicator of nutrient scavenging that potentially contributed to limitation of algal growth. Phosphorous has a particular affinity to small particles and is one of the nutrients that can limit biological production in an oligotrophic system like Carpenter Reservoir.

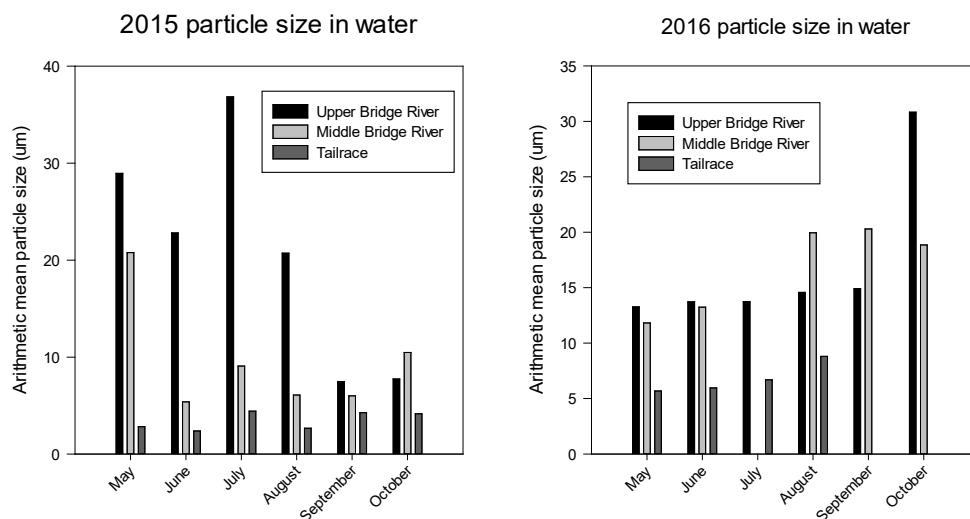


Figure 35. Arithmetic mean particle size in water samples, by station and month in 2015 (left) and 2016 (right).

Phytoplankton production was positively related to temperature (positive coefficient in the model with unstandardized coefficients), which is consistent with present understanding that primary production increases with rising temperature when there is no interference from other factors (Goldman and Carpenter 1974).

Given that concentrations of $\text{NO}_3\text{-N}$ and SRP were near to or less than method detection limits, they were not found with sufficient variance to be detected by the model as factors explaining variance of phytoplankton production. This dilemma does not mean that nutrient supply was not important in driving primary production. Along with $\text{NO}_3\text{-N}$ concentration, SRP concentration may have been relatively high in the spring but below detection. As phytoplankton grew during the summer, further demand for bio-available N and P would occur and drive the concentrations even lower but would not be detectable in the wet chemistry. This process may occur in Carpenter Reservoir because the surface mixed layer was not exchanged during time of measurements in spring through late summer (Section 5.1.4 and Section 5.1.5) thus allowing biological demand to change nutrient supply in the surface mixed layer. Increasing nutrient limitation during the growing season is consistent with lower primary production in late summer, producing the time course change in phytoplankton biovolume shown in Figure 34. This

hypothesis is supported by work of Bothwell (1988) who showed that algal growth rates can change by several fold over ranges of concentrations of a growth-limiting nutrient (phosphorus in work of Bothwell) that are below method detection limits of modern wet chemistry techniques, including those used in this study.

5.2.3 Zooplankton

5.2.3.1 Zooplankton composition

Mean zooplankton biomass among the two years and two stations (C2 and C6) increased 7 fold from May (310 mg dry weight·m⁻²) to September (2,251 mg dry weight·m⁻²) and then declined to 333 mg dry weight·m⁻² in October (Figure 36). Cladoceran biomass increased during the growing season, making up 87% of total zooplankton biomass by September and 80% in October. *Daphnia rosea* occurred in greatest biomass among cladocerans with smaller biomass comprised of *Daphnia pulicaria*, *Eubosmina longispina*, and *Leptodora kindtii*. Incidental biomass of *Diaphanosoma brachyurum*, *Sida crystallina*, and *Daphnia galeata* was found. In May, the cyclopoid and calanoid copepods comprised 75% of total zooplankton biomass but declined to 13% by September and 21% in October. The copepod occurring in greatest biomass was *Acanthodiaptomus denticornis*. Rarer taxa were *Epischura nevadensis* and *Cyclops scutifer*.

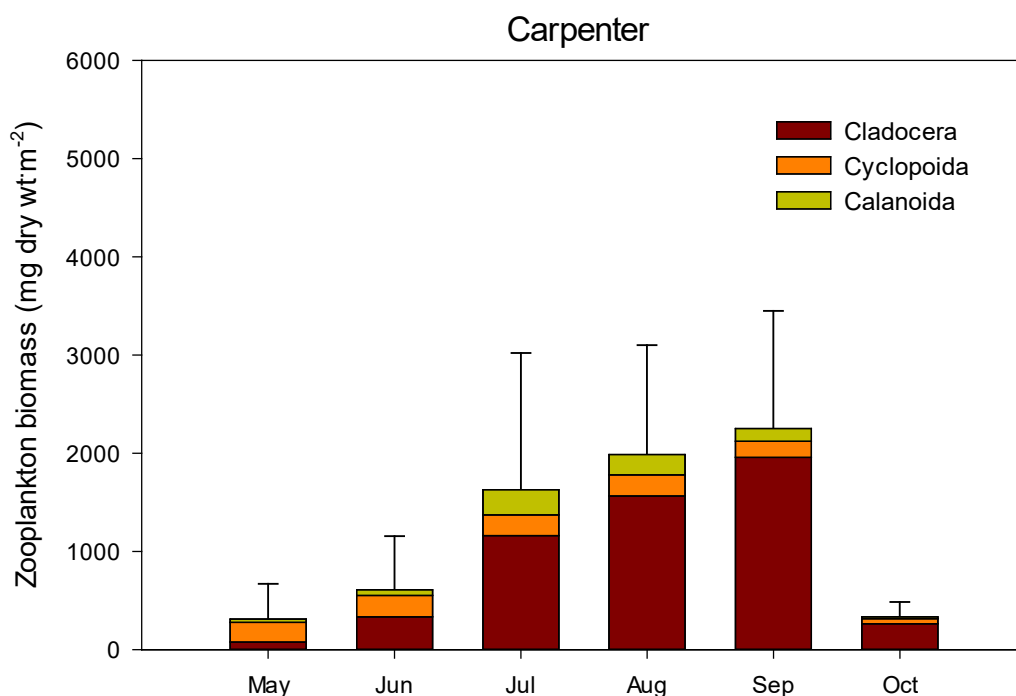


Figure 36. Mean zooplankton biomass (±sd) by order and month in Carpenter Reservoir. Data are from duplicate samples collected at each of two stations on each monthly sampling episode in each of two years (2015 and 2016).

5.2.3.2 Zooplankton regression model

Zooplankton biomass in Carpenter Reservoir was related to phytoplankton biomass, temperature, and turbidity ($R^2 = 0.90$) (Equation 7). The regression equation using **standardized coefficients** (used to rank independent variables) was:

$$\text{Zooplankton biomass} = 2.964 + 10^{-0.170 \cdot \text{Chlorophyll } a} + 10^{0.860 \cdot \text{Temperature}} + 10^{-0.337 \cdot \text{Turbidity}}$$

Equation 7

The equation with **unstandardized coefficients** (used for prediction in original units) had the form:

$$\text{Zooplankton biomass} = 0.365 + 10^{-0.176 \cdot \text{Chlorophyll } a} + 10^{0.23 \cdot \text{Temperature}} + 10^{-0.032 \cdot \text{Turbidity}}$$

Equation 8

Among the independent variables, temperature had the greatest effect on zooplankton biomass followed by turbidity and phytoplankton biomass. The model showed that zooplankton biomass increased as temperatures increased over the growing season. The community shifted mainly from small copepods to the larger cladocerans over this time series. Lower biomass was found when turbidity was high and vice versa greater biomass occurred at times of lower turbidity. This relationship was related to the inverse seasonality between turbidity that was high in the spring and lower late in the growing season (Section 5.1.4 and Section 5.1.5) and zooplankton biomass that was low in the spring and high at the end of the growing season in relation to the time course development of the cladocerans. Phytoplankton biomass as food for zooplankton was a small factor explaining variation in zooplankton biomass.

It is noteworthy that physical factors driving phytoplankton production (Section 5.2.2.2) were the same ones driving zooplankton biomass independent of phytoplankton production. Turbidity negatively affected both phytoplankton production and zooplankton biomass. Temperature negatively affected phytoplankton production but positively affected zooplankton, creating offsetting processes in the interaction between the production of phytoplankton and zooplankton. Given that availability of phytoplankton biomass was of small importance in contributing to variance in zooplankton biomass, any offsetting of phytoplankton biomass by temperature was of little consequence to zooplankton.

The direct negative effect of turbidity on zooplankton biomass shown in Equation 7 and Equation 8 can be related to processes affecting zooplankton growth and survival,

which is different from the potential role of fine particle turbidity affecting nutrient limitation of primary production in Carpenter Reservoir (Section 5.2.2.2). Light attenuation by turbidity may alter vertical migration behaviour of zooplankton (Hylander et al. 2011) and particles contributing to turbidity may impair filter-feeding function (Koenings et al. 1990), leading to reduced feeding rates (Hart 1988). These factors were potentially occurring in Carpenter Reservoir in relation to variation in turbidity.

5.2.4 Sensitivity analysis

Sensitivity of each dependent variable (periphyton on stable substrata, phytoplankton production, zooplankton biomass) to independent variables in the respective models was calculated as shown in Equation 2, which provided a way to compare relative importance of habitat attributes driving the biological endpoints. Only independent variables that could be changed by management actions were considered ($\text{NO}_3\text{-N}$ concentration, turbidity, temperature). To be consistent, all runs of the regression models were done using data from the top 14m of the water column where biological production was most active (the photic zone). Effect of change in each one of the independent variables was done with the others fixed at mean values in the raw data used for building the regression models. Only models with unstandardized coefficients were used in the calculations because they were used for prediction of outcomes in original units.

Results in Table 14 show large differences in the importance of predictor variables. Periphyton accrual was highly sensitive to its only predictor variable, which was $\text{NO}_3\text{-N}$ concentration that occurred over a small range of <5 to $6.2 \mu\text{g}\cdot\text{L}^{-1}$ (measurements only from the surface mixed layer that applies to the littoral zone). Both phytoplankton production and zooplankton biomass were highly insensitive to change in turbidity, which covered a range of 0.2 -19 NTU in the photic zone. Note that much higher turbidity occurred in the reservoir but it occurred at depths exceeding those in the photic zone where data were truncated to make the sensitivity comparisons. In contrast, phytoplankton production and zooplankton biomass were very sensitive to change in water temperature. For example, an increase in surface layer temperature from 12°C early in the growing season to 20°C later in the summer contributed to a 112% increase in rates of primary production. A 50% increase in temperature (10°C to 15°C) resulted in a 1300% change in zooplankton biomass, which showed extreme sensitivity within the modeling framework.

Table 14. Sensitivity of biological endpoints to change in predictor variables among each of the biological production models.

Model	Sensitivity (<i>S</i> , Equation 2) by predictor variable*			Conclusion
	NO ₃ -N concentration	Turbidity	Temperature	
Periphyton on stable substrata	3.5	Not a predictor variable	Not a predictor variable	High sensitivity to NO ₃ -N concentration
Phytoplankton production	Not a predictor variable	-0.008	1.53	Very low sensitivity to turbidity. High sensitivity to temperature
Zooplankton biomass	Not a predictor variable	<0.001	26	Extremely low sensitivity to turbidity. Very high sensitivity to temperature

*values <1 indicate low sensitivity to change in value of the predictor variable, values >1 indicate high sensitivity to change in value of the predictor variable

5.2.5 Biological response to management scenarios

Four water management scenarios and the 2015 and 2016 years were selected for modeling as described in Section 5.1.3. For reference, the modeled hydrodynamic attributes of the scenarios were described in Section 5.1.6. For each scenario, CE-QUAL-W2 produced mean values of output variables that were input variables for the biological regression models (Section 5.2.1.1.2, Section 5.2.2.2, Section 5.2.3.2). We used the mean growing season values in the surface layer cropped to 14m, the maximum photic zone depth among observations used to produce the biological models, for each of these variables to estimate each of periphyton accrual in the littoral zone, rates of primary production in the pelagic zone, and yield of zooplankton biomass in the pelagic zone using each of the respective biological models with unstandardized coefficients.

For periphyton, we selected NO₃-N concentrations in CE-QUAL-W2 output from the surface mixed layer cropped to 14m. With the exception of output for 2016 the NO₃-N concentrations were at or below the method detection limit of 5 µg·L⁻¹. The mean concentration in 2016 was 6.5 µg·L⁻¹. This finding means that the differences in water management among scenarios did not affect the main driver of periphyton accrual, NO₃-N concentration except in 2016 (Figure 37). The 2016 year effect was potentially due to early replacement of the surface mixed layer with tributary inflow carrying higher NO₃-N concentrations than was present in the surface mixed layer of the reservoir (Section 5.1.5.2). The 1.5 µg·L⁻¹ increase in mean NO₃-N concentration in 2016 caused more than a doubling in periphyton biomass due to the high sensitivity of periphyton algae to NO₃-N concentration (Table 14). There might have been further variation in periphyton accrual among scenarios but due to limitations of wet chemistry, lower NO₃-N

concentrations could not be resolved, making detection of further periphyton responses to management scenarios undetectable. Regardless, all values would be very low and close to those shown in Figure 37. A conclusion is that management scenarios did not affect periphyton accrual except in 2016 due to the anomaly in NO₃-N concentration.

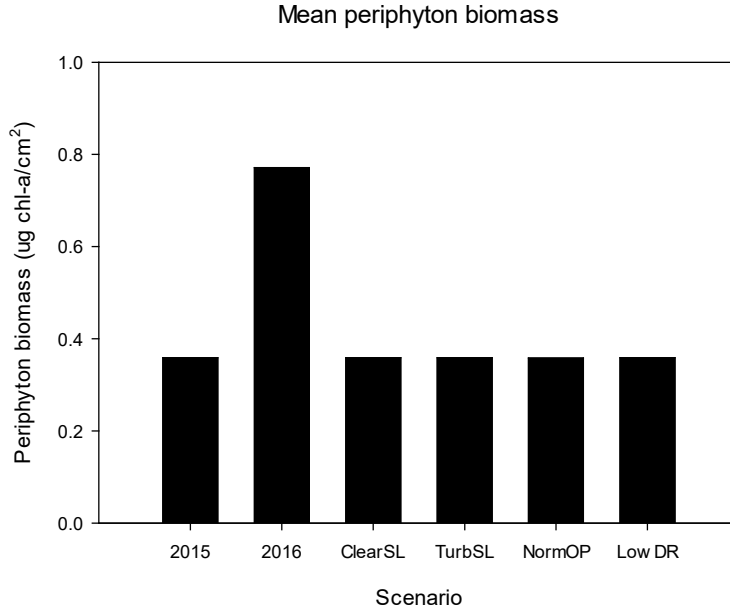


Figure 37. Predicted mean accrued periphyton biomass on stable substrata by scenario.

Phytoplankton production in the surface mixed layer varied by only 0.66 mgC·m³·d⁻¹ among all scenarios (range of 4.02 to 4.68 mgC·m³·d⁻¹) (Figure 38). This insensitivity to change in management action was due to little change in surface temperature among scenarios, which was the main driver of primary production. Variation in turbidity caused by management actions was not important because turbidity contributed little to variation in primary production (Table 14).

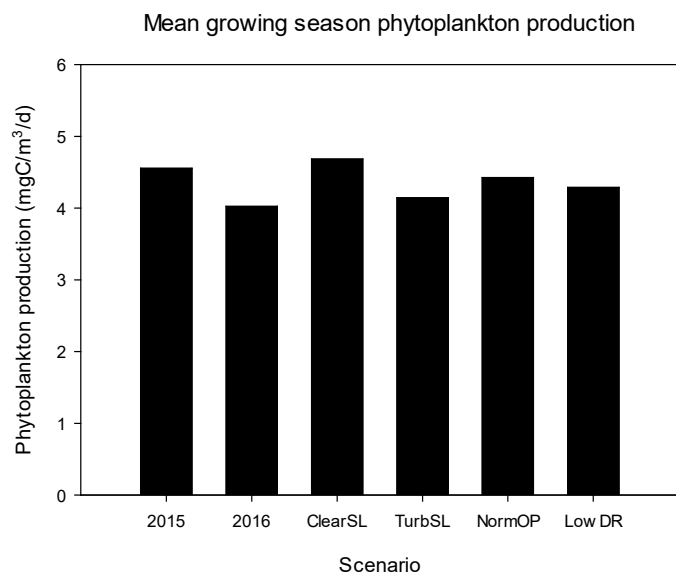


Figure 38. Predicted mean growing season rate of primary production among water management scenarios in Carpenter Reservoir.

Zooplankton biomass responded more among scenarios than did phytoplankton production and periphyton biomass accrual (Figure 39). Recall that zooplankton was highly sensitive to change in temperature and had very low sensitivity to turbidity (Table 14). Phytoplankton biomass, a predictor in the zooplankton model (Equation 8), was set at average levels among scenarios ($1 \mu\text{g chl-a}\cdot\text{L}^{-1}$) to focus on the effect of hydrodynamic management actions on zooplankton biomass in Figure 39. Zooplankton biomass declined between 2015 and 2016 mainly due to lower mean surface water temperature in 2016 (mean of 14.6°C in 2016 compared to 15.6°C in 2015). Turbidity was also higher in 2016 than in 2015 but turbidity had little effect on zooplankton biomass so this difference was not relevant. In the ClearSL scenario, zooplankton biomass reached the highest among all scenarios mainly due to high water temperature that was produced with little exchange of water in the surface layer during the growing season. In contrast TurbSL produced low water temperature and relatively high turbidity in the surface layer. The low temperature was predicted to strongly curtail zooplankton development, thus producing overall low biomass, close to that found in 2016. Zooplankton biomass in NormOP and LowDR was predicted to be intermediate among values found in the other scenarios due to intermediate mean growing season surface temperature of 15.2°C and 15.1°C respectively.

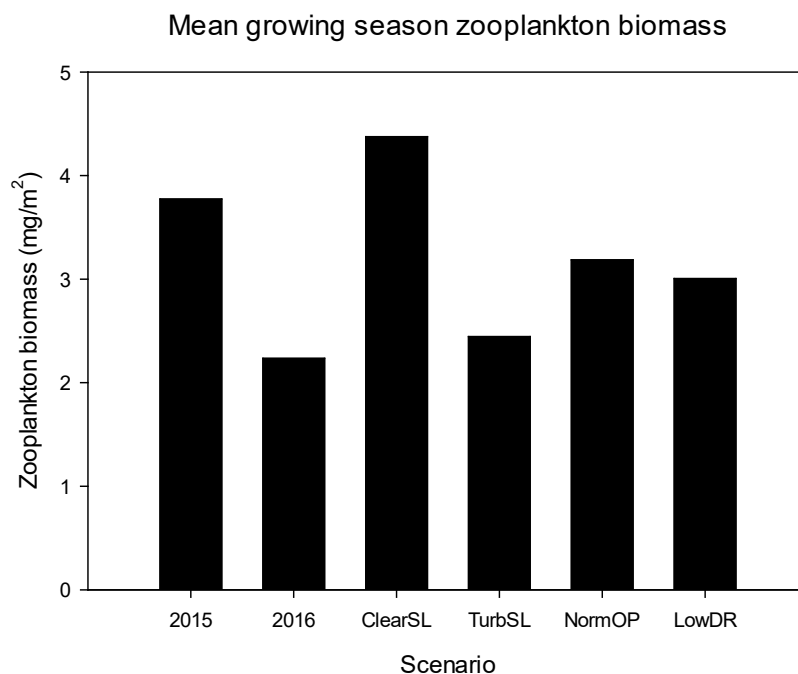


Figure 39. Predicted mean growing season zooplankton biomass among water management scenarios in Carpenter Reservoir.

6 ANSWERS TO MANAGEMENT QUESTIONS

6.1 Question 1: Is light the primary factor regulating productivity of littoral habitat in Carpenter Reservoir?

A combination of field observations and modeling was used to answer management question 1. The field measurements from 2015 and 2016 were used to build a regression model showing factors contributing to variance in accrual of periphyton biomass, the key indicator of biological production in littoral habitat as defined in Section 2. Periphyton will theoretically respond directly to variation in light as part of photosynthesis. Our model showed that periphyton biomass accrual was not sensitive to the range of light in the littoral zone but it was very sensitive to change in NO₃-N concentrations. These findings show that light is not the primary factor regulating biological productivity of littoral habitat in Carpenter Reservoir.

There are two types of substrata in the littoral zone of Carpenter Reservoir, stable lithic substrata and unstable sand. Almost no periphyton community was found on sand following a two-month incubation at several littoral depths so no model could be built using data from the sand. The samplers were suspended from a cross-reservoir boom and thus were subject to wind-activated movement. This movement created minor flows across the water – sand interface in the samplers, similar to water movements in shallow water of the littoral zone. This physical disturbance may have been enough to inhibit development of an attached periphyton community. Even without water movement, species of attached algae in Carpenter Reservoir that were common on the

stable substrata samplers may not have been well adapted to growing on sandy materials. In contrast, a diverse algal assemblage did grow on the stable Styrofoam substrata. The contrast in communities between these types of surfaces show that biological production is primarily defined by the physical composition of substrata. Stable materials support a robust and diverse assemblage of periphyton that can contribute to the littoral food web while unstable sandy materials subject to movement by water do not. Where the physical substrate supports periphyton, our findings show that periphyton is limited by $\text{NO}_3\text{-N}$ concentration, not light.

These findings do not mean that sand does not support biological communities. Indeed, an invertebrate community would be expected to be present in the sand as well as in stony substrata. Those animals would feed on detrital organic matter derived from allochthonous sources and from settlement of organic matter produced in the overlying water column. Limited production of periphyton on sand only means that autotrophic epilithic biological production may be small compared to the amount of organic matter coming from other sources for support of sand – based invertebrate production. In this case light would not be a factor in driving that production because the organic matter is produced elsewhere and transported to the sand or it is derived through heterotrophic processes that do not need light for metabolism.

6.2 Question 2: Is light the primary factor regulating productivity of pelagic habitat in Carpenter Reservoir?

A combination of field observations and modeling was used to answer management question 2. The field measurements from 2015 and 2016 were used to build two regression models; one explaining factors contributing to variance in production of phytoplankton, the key indicator of biological production in pelagic habitat and the other explaining factors contributing to variance in biomass of zooplankton food for fish as defined in Section 2.

The phytoplankton model included light measured in two ways: PAR and turbidity under the premise that turbidity causes light attenuation. These variables were found not to be intercorrelated. They were independent predictors, which means they acted differently on primary production. PAR was a direct and most accurate measure of light available for photosynthesis. Its effect on primary production was greater than from other predictor variables (temperature and turbidity). Its strong positive effect on primary production showed that rates of production changed with amount of irradiance occurring over the vertical profile of the photic zone. This finding means that depth will change the amount of habitat where primary production can occur. That depth may be potentially modified by the amount of turbidity in the water column.

The independence of PAR and turbidity showed that turbidity acted on primary production in a way that was different from what is commonly assumed to be light limitation. If light effects on primary production were caused by turbidity the same way as PAR, intercorrelation of PAR and turbidity would be found because PAR is a direct and

unequivocal measure of light for photosynthesis. This outcome did not happen. Given that much of the suspended solids that contributed to light scattering that was measured as turbidity were very small, some less than 1 μm , a hypothesis is that adsorption of phosphorus increased with rising turbidity and decreased with declining turbidity, thus inducing change in limitation of phytoplankton growth by phosphorus. This action by turbidity is a secondary and independent effect that was different from its effect on light attenuation and may explain independence of PAR and turbidity effects on primary production in the phytoplankton model.

The effect of PAR on primary production indirectly affected zooplankton biomass as shown in the zooplankton model (Equation 7 and Equation 8). Increasing PAR favoured primary production, which could increase phytoplankton biomass. That biomass favoured zooplankton biomass. This indirect effect of light on zooplankton biomass was, however, very small and almost indistinguishable from sensitivity of zooplankton biomass to change in temperature. Similarly, turbidity influenced zooplankton potentially through action on feeding effectiveness but only in a small way compared to temperature.

Among variables affected by management scenarios, temperature stood out as the main factor driving zooplankton biomass. Generation time in zooplankton is inversely related to temperature (Gillooly 2000), which means that higher temperature will shorten generation time and increase rate of biomass production for a given body size. Among wide ranging lake zooplankton populations temperature along with body size and food supply are well established factors driving zooplankton production, including taxa found in Carpenter Reservoir (Shuter and Ing 1997). Our sensitivity analysis supported this evidence in showing very high sensitivity of zooplankton biomass, the end product of change in generation time, to change in temperature. There was less but still significant involvement by food supply measured as phytoplankton biomass, which is also consistent with findings of Shuter and Ing (1997). One reason for low involvement of food supply may be extreme nutrient limitation at all times in Carpenter Reservoir, thus producing little variation in food supply which reduces sensitivity in modeling. Temperature was the main driver in part because it did occur with sufficient variance that could be linked to coincidental variation in zooplankton biomass. Low temperature in the spring favoured low biomass of small bodied cyclopoids and higher temperature later in the growing season favoured higher biomass of large bodied cladocerans. Those large bodied zooplankton are important because they are most easily captured as prey by planktivorous fish. This association means that rising temperature is an important factor favouring production of food for fish.

In summary light is a factor but not the main factor regulating biological production in pelagic habitat. PAR is the main variable driving this effect through its control of primary production. Resulting phytoplankton biomass is a factor explaining variance in zooplankton biomass but its effect is of little consequence compared to water temperature that explains most of the variance in zooplankton biomass. Water

management actions that determine light in the water column are the same ones driving water temperature. Under exceptionally turbid conditions (Scenario TurbSL) turbidity is high and temperature is low, mainly in the early part of the growing season. These conditions occur when water surface elevations are kept low in the spring and early summer. They will lower zooplankton biomass and reduce the amount of food for fish. In contrast, a management action that favours high water temperature and low turbidity (produced from high water surface elevation) will optimize production of zooplankton biomass and thus food for fish. Through these interactions it is not turbidity driving change. It is temperature.

6.3 Question 3: Is light penetration in Carpenter Reservoir impacted by changes in reservoir operations

A combination of field observations and hydrodynamic modelling was used to answer management question 3. Observations from the field provided an understanding of the mechanisms controlling light penetration in Carpenter Reservoir and the hydrodynamic model was used to run scenarios based on historic operational data to assess whether changes in reservoir operation affect light penetration. Light penetration is defined here as the depth of the photic zone, which is the depth at which light decreases to 1% of that at the surface.

Over the summer months, Carpenter Reservoir undergoes thermal stratification with the development of a warm epilimnion (surface layer) above a cool, turbid hypolimnion (deep water). Despite the high input of glacial fines, the observations showed that once persistent summer stratification was established, the turbidity of the surface layer decreased (Figure 28), and depth of the photic zone increased, over spring and summer (Figure 31).

The main source of turbidity was water released from La Joie Dam, which was more turbid than the local tributaries with the exception of May 2015, when turbidity in the local tributaries was higher during freshet (Figure 16). The turbid inflows were cooler (denser) than the surface layer, and, as a result, the inflows plunged into the deep water, bypassing the photic zone, and short-circuited through the reservoir toward the deep outlets. The conductivity measurements confirmed the relative isolation of the surface layer: during stratification, the conductivity of the surface layer was relatively constant, in contrast to the deep water where the conductivity decreased due to lower conductivity inflows.

To understand the link between changes in reservoir operation and light penetration in Carpenter Reservoir, we simulated the flow conditions from prior years (1961-2017) to explore a set of realistic operational scenarios. The analysis showed that model runs with a clearer surface layer began with a higher water level, and model runs with a more turbid surface layer began with a lower water level. The relationship between photic zone depth and initial water level is shown in Figure 40. Here we used the average water level during the first 30 days of the model period; the results were

similar using, for example, the initial water level. The results showed that the photic zone depth (light penetration) is a function of the starting or spring water level ($R^2 = 0.75$).

Recall that the meteorological and water quality data were only available for two field seasons, 2015 and 2016. As a result, we simulated each year of the reservoir operations record (1961-2017) by forcing the model with the inflows, outflows, and initial water level from those years, but with meteorological and water quality data from 2015 (blue, Figure 40). This approach effectively removed the inter-annual variability in the meteorological and water quality data from the simulations to isolate the effect of reservoir operation. A complete set of reservoir operational scenarios (1961-2017) was also run using the meteorological and water quality forcing of 2016, which gave similar results (red, Figure 40). Note, there was no correlation between photic depth and the total inflow from La Joie ($R^2 = 0.08$), the total local inflow ($R^2 = 0.08$), or the total outflow to Seton ($R^2 = 0.01$).

In conclusion, thermal stratification isolates the surface layer of Carpenter Reservoir from cold and turbid inflows. Over the course of spring and summer, glacial fines in the surface layer settle, and the penetration of light increases. The difference in light penetration between years is primarily controlled by the initial turbidity in the surface layer at the start of persistent summer stratification. The turbidity at the start of persistent stratification is lower when the water level in the reservoir is relatively high at that time; and the turbidity at the start of persistent stratification is elevated if the water level is low at that time. At low water level the depth of the reservoir is shallower, the volume of the reservoir is over ten times smaller (Table 13), and the mixing of cold turbid inflows throughout the water column is enhanced. With a higher initial load of turbidity, it takes longer for the surface layer to clear over summer (Figure 31), and average light penetration is reduced. These observations show that reservoir operation, primarily the control of water surface elevation, does affect light penetration in Carpenter Reservoir.

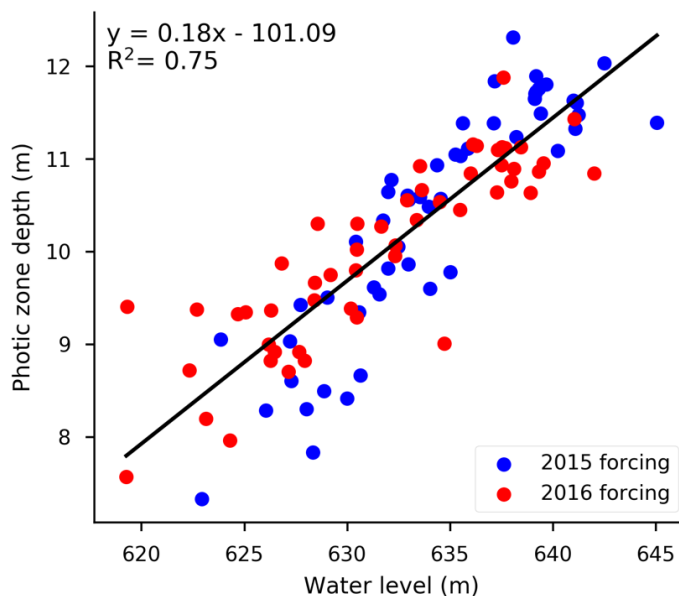


Figure 40. Model results showing mean annual photic zone depth as a function of mean water level over the first 30 days of the model period. The blue circles show reservoir operational conditions from 1961-2017 subjected to meteorological and water quality forcing from 2015. The red circles show reservoir operational conditions from 1961-2017 subjected to meteorological and water quality forcing from 2016.

6.4 Question 4: Can suspended sediment transport into Seton Lake be altered by changes in Carpenter Reservoir operations

6.4.1 Approach

To address this question, we used CE-QUAL-W2 to explore a variety of reservoir operation scenarios and their effect on the transport of suspended particles into Seton Lake and, for comparison, the Lower Bridge River. Turbidity in units of NTU was used in place of suspended sediment concentration for reasons given in Section 5.1.1.2 and Appendix D. Note that, in the model for the Field years (2015 and 2016), there was agreement between observed and modelled turbidity for both the outflow to Seton and the Lower Bridge River (see Appendix F).

The four scenarios of management actions that were described in Section 5.1.3 were used to address management question 4 as they were for question 3. These scenarios provided extremes in reservoir operation (ClearSL and TurbSL), normal operations (NormOP), and near-term operations based on low water level in Downton Reservoir (LowDR).

Three points need to be considered:

1. The outflow to Seton Lake is taken from segment 53, which is 3.5 km from the Terzaghi Dam. The outflow to the Lower Bridge River is taken from segment 56,

which was adjacent to the Terzaghi Dam. The sill elevation of outflows to both Seton Lake (600.61, 599.54 mASL for BR1 and BR2) and the Lower Bridge River (599.69 mASL) were approximately the same. As a result of their proximity in both location and elevation, we would expect the outflow turbidity to both Seton Lake and the Lower Bridge River to be similar.

2. Outflow from a stratified water column occurs from a range of depths which is controlled by the density stratification and flow rate. CE-QUAL-W2, takes this selective withdrawal into account. Thus, the water withdrawn will not be identical to that at the outlet elevation, but a blend from adjacent depths.
3. Elevation of the outflows is at the bottom of the reservoir. Note that we are only modelling the turbidity suspended in the water column, and that the potential for sediment pickup from the bed of the reservoir is not included. Given continuous flow at the bottom caused by withdrawal, loose sediment at the water – substrata interface was expected to be minimal and not a factor in the modeling.

6.4.2 Outflow to Seton Lake

The modelled temperature and turbidity of the outflow to Seton Lake is shown for each scenario in Figure 41. At the start of the model run, the outflow temperature was approximately 10°C for all scenarios with the exception of Scenario TurbSL, in which it was approximately 14°C. The initial temperature was set to the Sea-Bird profile of 22 May 2015; recall the depth of the reservoir was shallow (< 10 m) at the start of Scenario TurbSL, so the initial temperature of the whole water column was set to that of the epilimnion on 22 May 2015. The deep temperature in Scenario TurbSL adjusted within the first few days of the simulation, and by late May, the outflow temperature was 10-11°C for all scenarios. As the temperature of inflows from La Joie Dam and local tributaries increased through mid-August (Figure 16g), the outflow temperature to Seton increased as well. The seasonal trend continued with slight cooling in the fall. At the start of the model run, the turbidity in the outflow to Seton was approximately 10-15 NTU for all scenarios as set by the initial conditions. As the initial water near the withdrawal was replaced with water from the inflows, the turbidity to Seton changed depending on the scenario. Recall that all four scenarios use as boundary conditions the turbidity of inflows measured in 2015. Recall also, that the local tributaries had relatively high turbidity in May 2015, in contrast to the turbidity from La Joie Dam which was high in fall 2015 (Figure 16k). The effect of this pattern can be seen in the turbidity of the outflow to Seton with a peak in the first month of the model run, and a peak again in the fall.

For Scenario TurbSL, the change in turbidity was most dramatic because the small initial volume of the reservoir was most affected by the elevated turbidity in the local inflows during freshet (Figure 16k). For the other three scenarios, the response was slower because of the larger initial volume of the reservoir (Table 13).

The seasonal variation in turbidity of the outflow to Seton Lake can be characterized as a peak during freshet, followed by a decline over the summer months,

followed by another peak in September. The first peak results from both the local inflow rate during freshet dominating the inflow from La Joie (Figure 30), and the high turbidity in the local inflow in May (Figure 16k). The second peak occurs after freshet when the total inflow into Carpenter Reservoir is dominated by the inflow from La Joie Dam. Furthermore, turbidity from La Joie Dam increases over the productive season, so the load from La Joie Dam is high later in the summer (Figure 16k).

While the first turbidity peak is controlled by unregulated local inflow (natural variability), the second peak is, in part, controlled by reservoir operations. This can be seen by comparing the magnitude of each peak in Figure 41b to the flow from La Joie Dam (Figure 30a). Scenario ClearSL has the lowest turbidity to Seton in the late summer and early fall; it also has the lowest inflow from La Joie Dam. Scenario NormOp has the second lowest turbidity and the second lowest inflow from La Joie Dam. The highest turbidity to Seton occurred in Scenario LowDR, where the inflow from La Joie was highest.

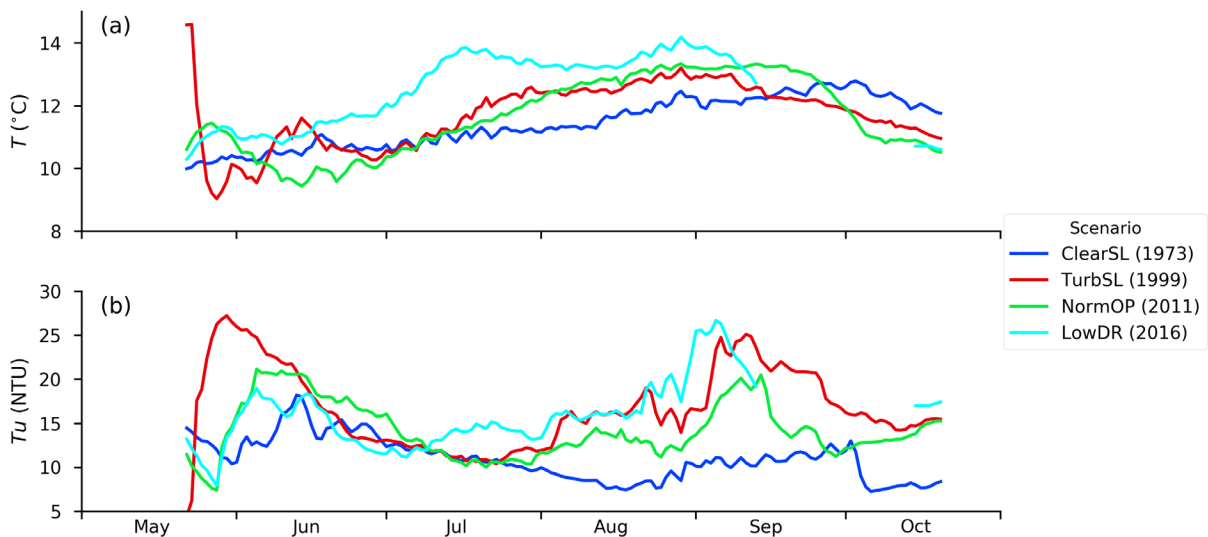


Figure 41. Hydrodynamic model outflow to Seton Lake for each scenario: (a) temperature, and (b) turbidity. The intakes to Seton Lake were shut down from mid-September to mid-October 2016, which shows up as a data gap in Scenario LowDR.

6.4.3 Outflow to the Lower Bridge River

For outflow to the Lower Bridge River, data were only available for two of the scenarios (NormOP and LowDR) because there was no outflow to the Lower Bridge River during Scenarios ClearSL and TurbSL. When there is no water release, the model provides no data.

The temperature and turbidity of the outflow to the Lower Bridge River are compared to that of the outflow to Seton Lake in Figure 42. The temperature and

turbidity data are very similar with an RMS difference of 1.0 and 0.8 °C, and 2.7 and 3.0 NTU for Scenarios NormOP and LowDR, respectively. This outcome was expected given the proximity of the outflows.

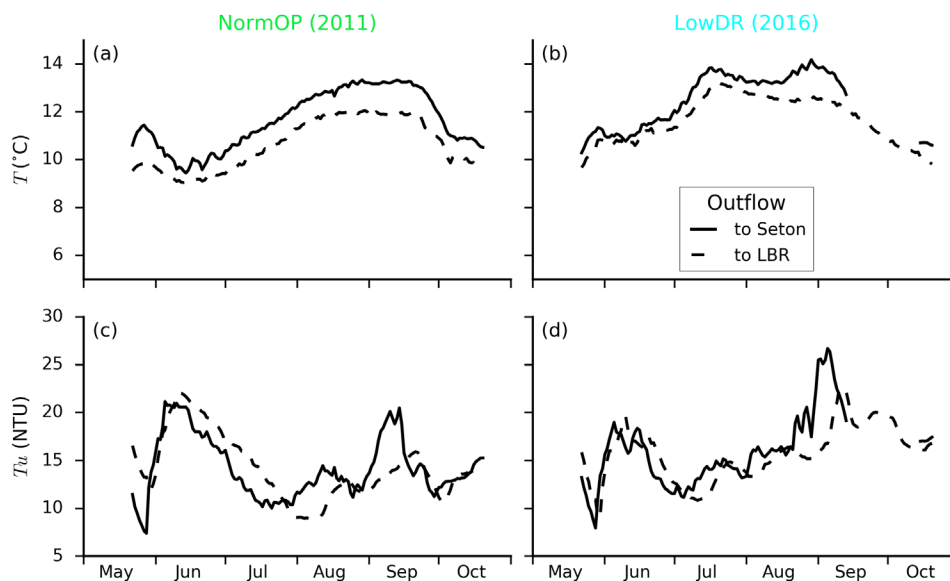


Figure 42. Hydrodynamic model outflow to the Lower Bridge River compared to model outflow to Seton: (a,b) temperature; (c,d) turbidity; (a,c) Scenario NormOP (2011); (b,d) Scenario LowDR (2016).

6.4.4 Conclusion

To address this question, we used the same approach of hydrodynamic modelling as was used to answer Question 3. Again, turbidity was used to characterize and model suspended sediments, which are dominated by glacial fines in Carpenter Reservoir.

The model showed seasonal variation in turbidity transported to Seton consisting of two distinct peaks (Figure 41b). The first peak in May to June, is dominated by elevated turbidity in the local (unregulated) inflow during freshet (cf. May 2015, Figure Figure 16k). The second peak, in September, is dominated by the increased flow and turbidity from La Joie Dam. The first peak is affected by natural inflows (the timing and turbidity of freshet in local inflow) and initial water level in the reservoir, and the second peak is affected by the volume (and turbidity) of water from La Joie Dam. During scenario ClearSL, the first peak was small because of low freshet inflow and the second peak was almost absent because there was no flow from La Joie from mid-August to mid-September (Figure 30a). In contrast, for the Scenario TurbSL, the turbidity transported to Seton was high in early June, because of the small volume of the reservoir at that time (Table 13), and the turbidity was high in early September because of high outflows from La Joie Dam (Figure 30a).

In the previous section, we saw how the turbidity and photic depth in the surface layer was controlled by the relative isolation of the surface layer through spring and summer. In contrast, the transport of turbidity to Seton Lake depends on the fate of the cold, turbid inflows which plunge below the surface layer, which mix into and are transported along the deep water of the reservoir, and are withdrawn into penstocks from the bottom of Carpenter Reservoir just upstream of Terzaghi Dam. As a result of these processes the load of turbidity to Seton Lake depends on four things as follows:

1. The load of turbidity from La Joie (under management control),
2. The load of turbidity from local tributaries (not under management control),
3. The volume of the hypolimnion (under management control), and
4. The flow rate to Seton Lake (under management control).

Given that three of these processes are under management control, a conclusion is that the transport of suspended sediment into Seton Lake is affected by the operation of Carpenter and Downton Reservoirs. There are a number of factors that control both the timing and quantity of this load. In Scenario TurbSL, the load to Seton Lake was 3 times higher than in Scenario ClearSL. In this case, the load from local tributaries increased by a factor of 2, and the load from La Joie Dam increased by a factor of 3. During a year such as that of TurbSL, options for the operation of the reservoirs may be restricted due to the need to move water through the system, thereby greatly limiting management control.

Note that results described above are specific to using the boundary conditions of 2015, were somewhat different using the boundary conditions of 2016, and would change given the tributary water quality data for any given year. The collection of tributary data during years with other extreme flow conditions would be needed to further explore the relationship between the sediment load to Seton Lake and reservoir operations.

6.5 CE-QUAL-W2 sources of error

The hydrodynamic model successfully reproduced the temperature, conductivity and turbidity observed in 2015 and 2016. The agreement was similar to that in the literature (Appendix F). The model was then used to simulate scenarios using flow conditions from other years. To do this, the water quality and meteorological data of 2015 (and 2016, not shown) were used to drive the initial and boundary conditions for the scenarios.

Ideally, the model would be run for scenarios having data inputs that are within the range of data values that were used to calibrate the model. However, the extremes in flow conditions (e.g. low water level) are what drive differences in surface water clarity in Carpenter Reservoir (Question 3) and differences in turbidity exported to Seton Lake

(Question 4). To the extent that these extremes are not represented in the field data, the model, of necessity, is extrapolating. This approach is not unusual and is a recognized limitation. For example, the mixing in the small volume of water at very low water level has not been calibrated against field data under those conditions. However, the changes to the parameters in the model have been modest, and it is fair to expect the hydrodynamic model to give a reasonable estimate of behaviour in this small volume.

Model results were particularly sensitive to tributary turbidity that was used to force the model. The noticeable effect of the slightly higher turbidity readings in the unregulated tributaries of 23 May 2015 was important. Greater importance was turbidity from the primary source, which was water released from the La Joie Dam, especially under flow extremes. Just as the turbidity exported from Carpenter Reservoir to Seton Lake can vary widely, it would be anticipated that there would be similar variation in the export of turbidity from Downton Reservoir, that may range beyond what was observed in the 2015 and 2016.

7 LIST OF REFERENCES CITED

- Allan, J. D., and M. M. Castillo. 2007. The abiotic environment. In *Stream Ecology: structure and function of running waters* (2nd ed.). Dordrecht, The Netherlands: Springer.
- American Public Health Association (APHA), American Water Works Association (AWWA) and Water Environment Federation (WEF). 2014. Standard methods for the examination of water and wastewater. Available at: www.standardmethods.org.
- BC Hydro. 1995. Dam Safety Investigations. Terzaghi Dam deficiency investigation. Summary report and appendices. BC Hydro. Maintenance, Engineering and Projects. Report No. H2479.
- BC Hydro. 2016. Dam Safety Program Report 2015-2016, prepared by S. Rigbey. Report No. F2016.
- Behrenfeld, M.J., E. Boss, D.A. Siegel, and D.M. Shea. 2005. Carbon-based ocean productivity and phytoplankton physiology from space. *Global Biogeochemical Cycles*. 19: 1-14.
- Bothwell, M.L. 1988. Growth rate responses of lotic periphytic diatoms to experimental phosphorus enrichment: The influence of temperature and light. *Canadian Journal of Fisheries and Aquatic Sciences*. 45: 261-270.
- Bothwell, M.L. 1989. Phosphorus – limited growth dynamics of lotic periphyton diatom communities: Areal biomass and cellular growth rate responses. *Canadian Journal of Fisheries and Aquatic Sciences*. 46: 1293-1301.
- Bridge River WUP CC. 2003. Bridge River Water Use Plan Consultative Committee Report (WUP CC). Compass Resource Management and BC Hydro. A report produced for BC hydro Water Use Planning group. (Executive Summary available on website: http://www.bchydro.com/content/dam/hydro/medialib/internet/documents/environment/pdf/wup_bridge_river_executive_summary_pdf.pdf)
- Burks, R. L., D. M. Lodge, E. Jeppesen, and T. L. Lauridsen. 2002. Diel horizontal migration of zooplankton: costs and benefits of inhabiting the littoral. *Freshwater Biology*, 47, 343–365.
- Canter-Lund, H. and J.W.G. Lund. 1995. *Freshwater Algae – Their Microscopic World Explored*. BioPress Ltd. Bristol, U.K.
- Cole, T. M. and S. A. Wells. 2015. CE-QUAL-W2: A Two-Dimensional, Laterally Averaged, Hydrodynamic and Water Quality Model, Version 3.72, User Manual. Department of Civil and Environmental Engineering, Portland State University, Portland, Oregon. 797pp.
- Gillooly, J.F. 2000. Effect of body size and temperature on generation time in zooplankton. *Journal of Plankton Research*. 22: 241-251.
- Goldman, J.C. and E.J. Carpenter. 1974. A kinetic approach to the effect of temperature on algal growth. *Limnology and Oceanography*. 19: 756-766.

- Gottselig, N., V. Nischwitz, T. Meyn, W. Amelung, R. Bol, C. Halle, H. Vereecken, J. Siemans, and E. Klumpp. 2017. Phosphorus binding to nanoparticles and colloids in forest stream waters. *Vadose Zone Journal*. doi:10.2136/vzj2016.07.0064.
- Grueber, C. E., Nakagawa, S., Laws, R. J., & Jamieson, I. G. (2011). Multimodel inference in ecology and evolution: challenges and solutions. *Journal of Evolutionary Biology*, 24(4), 699–711. <http://doi.org/10.1111/j.1420-9101.2010.02210.x>Zuur, A. F., Ieno, E. N., & Elphick, C. (2010). A protocol for data exploration to avoid common statistical problems. *Methods in Ecology and Evolution*, 1, 3–14.
- Guildford, S.J. and R.E. Hecky. 2000. Total nitrogen, total phosphorus, and nutrient limitation in lakes and oceans: Is there a common relationship? *Limnology and Oceanography*. 45: 1213-1223.
- Hart, R.C. 1988. Zooplankton feeding rates in relation to suspended sediment content: potential influences on community structure in a turbid reservoir. *Freshwater Biology*. 19: 123-139.
- Healey, F.P. 1985. Interacting effects of light and nutrient limitation on the growth rate of *Synechococcus linearis* (Cyanophyceae). *Journal of Phycology* 21:134-146.
- Koenings, J.P., R. Burkett, and J. Edmundson. 1990. The exclusion of limnetic Cladocera from turbid glacier-meltwater lakes. *Ecology*. 71: 57-67.
- Hylander, S., T. Jephson, K. Leuret, J. Von Einem, T. Fagerberg, E. Balseiro, B. Modenutt, M. Sol Souza, C. Laspumaderes, M. Jonsson, P. Ljungberg, A. Nicolle, P. Andes Nilsson, L. Ranaker, and L. Hansson. 2011. Climate-induced input of turbid glacial meltwater affects vertical distribution and community composition of phyto- and zooplankton. *Journal of Plankton Research* 33: 1239-1248.
- Ichimura, S., T.R. Parsons, M. Takahashi and H. Seki. 1980. A comparison of four methods for integrating ¹⁴C-primary productivity measurements per unit area. *J. Oceanogr. Soc. Jap.* 36: 259-262.
- Korpelainen, H. 1986. The effects of temperature and photoperiod on life history parameters of *Daphnia magna* (Crustacea: Cladocera). *Freshwater Biology*, 16, 615–620.
- Lamberti, G. A., and A. D. Steinman. 1997. A comparison of primary production in stream ecosystems. *Journal of the North American Benthological Society*, 16(1), 95–104.
- Leland, H. V. 1995. Distribution of phytobenthos in the Yakima River basin, Washington, in relation to geology, land use and other environmental factors. *Canadian Journal of Fisheries and Aquatic Sciences*, 52(5), 1108–1129.
- Liess, A, C. Faithful, B. Reichstein, O. Rowe, J. Guo, R. Pete, G. Thomsson, W. Uszko, and S. N. Francoeur. 2015. Terrestrial runoff may reduce microbenthic net community productivity by increasing turbidity: a Mediterranean coastal lagoon mesocosm experiment. *Hydrobiologia*, 753(1), 205-218.
- Parsons, T.K., Y. Maita and C.M. Lalli. 1984. *A Manual of Chemical and Biological Methods for Seawater Analysis*. Pergamon Press, Oxford. 173 p.

- Perrin, C.J., M.L. Bothwell and P.A. Slaney. 1987. Experimental enrichment of a coastal stream in British Columbia: effects of organic and inorganic additions on autotrophic periphyton production. *Canadian Journal of Fisheries and Aquatic Science* 44:1247-1256.
- Perrin, C. J., & Richardson, J. S. 1997. N and P limitation of benthos abundance in the Nechako River, British Columbia. *Can. J. Fish. Aquat. Sci.*, 54, 2574–2583.
- Perrin, C.J. and R.H. Macdonald. 1999. A phosphorus budget and limnology in Carpenter Lake Reservoir, 1995-96. Report prepared by Limnotek Research and Development Inc., Vancouver, B. C., for R.P. Griffith & Associates, Sidney, B.C. 72 p.
- Pieters, R., A. Law and G. Lawrence. 2017. *Tributary Water Quality, Kinbasket and Revelstoke Reservoirs*, 2014 and 2015. Prepared for BC Hydro, Revelstoke, BC. January 18, 2017, 40 pp.
- Pieters, R. and G.A. Lawrence. 2011. Plunging inflow and the summer photic zone in reservoirs. *Water Quality Res. J. of Canada* 47: 268-275.
- Pietrzak, B., A. Bednarska, M. Markowska, M. Rojek, E. Szymanska, and M. Slusarczyk. 2013. Behavioural and physiological mechanisms behind extreme longevity in *Daphnia*. *Hydrobiologia*. 715: 125-134.
- Prescott, G.W. 1978. *How to Know the Freshwater Algae*. 3rd Edition. Wm. C. Brown Company. Dubuque, IA.
- R Development Core Team. 2011. R: a language and environment for statistical computing. R Foundation for Statistical Computing, Vienna, Austria.
- Rhee, G. Y. 1978. Effects of N:P atomic ratios and nitrate limitation on algal growth, cell composition, and nitrate uptake. *Limnology and Oceanography* 23:10-25.
- Rhee, G. Y., and I.J. Gotham. 1980. Optimum N:P ratios and coexistence of planktonic algae. *Journal of Phycology* 16:486-489.
- Rosemond, A. D., P. J. Mulholland, and J. W. Elwood. 1993. Top-down and bottom-up control of stream periphyton: effects of nutrients and herbivores. *Ecology*, 74(4), 1264–1280.
- Schwartz, S. S., and R. E. Ballinger. 1980. Variations in life history characteristics of *Daphnia pulex* fed different algal species. *Oecologia*, 44: 181–184.
- Sebestyen, S. D., E. W. Boyer, J. B. Shanley, C. Kendall, D. H. Doctor, G. R. Aiken, and N. Ohte. 2008. Sources, transformations, and hydrological processes that control stream nitrate and dissolved organic matter concentrations during snowmelt in an upland forest, *Water Resour. Res.*, 44, W12410, doi:10.1029/2008WR006983
- Sellami, I., J. Elloumi, A. Hamza, M. A. Mhamdi, and H. Ayadi. 2011. Local and regional factors influencing zooplankton communities in the connected Kasseb Reservoir, Tunisia. *Water SA*. 37: 201-212.
- Shuter, B.J. and K.K. Ing. 1997. Factors affecting the production of zooplankton in lakes. *Canadian Journal of Fisheries and Aquatic Science* 54: 359-377.

- Steemann Nielsen, E. 1952. The use of radioactive carbon (^{14}C) for measuring organic production in the sea. *J. Cons. Int. Explor. Mer.* 18:117-140.
- Suttle, C.A. and P.J. Harrison. 1988. Ammonium and phosphate uptake rates, nitrogen: Phosphorus supply ratios, and evidence for N and P limitation in some oligotrophic lakes. *Limnology and Oceanography* 33: 186-202.
- Utermohl, H. 1958. Zur Vervollkommnung der quantitativen Phytoplankton methodik. *Int. Verein. Limnol. Mitteilungen* No. 9.
- Water Act Order. 2011. Province of British Columbia Water Act Order. Water Act Sections 87 and 88. License file numbers 0212289, 0115688, 0161431, 0210947, 0202694, 0265200, 0199585, 3005073, 3005075, 3005074.
- Wetzel, R.G. 2001. *Limnology*. Academic Press. San Diego.
- Yentsch, C.S. and V.W. Menzel. 1963. A method for the determination of phytoplankton chlorophyll-a and phaeophytin by fluorescence. *Deep-Sea Res.* 10: 221-231.
- Zuur, A. F., E. N. Ieno, and C. Elphick, C. 2010. A protocol for data exploration to avoid common statistical problems. *Methods in Ecology and Evolution*, 1: 3–14.
- Zuur, A. F., Ieno, E. N., Walker, N. J., Saveliev, A. A., & Smith, G. M. 2009. *Mixed effects models and extensions in ecology with R*. New York: Springer

8 APPENDIX A: SPECIFICATIONS OF SUSPENDED AND BOTTOM MOORINGS

8.1 Mooring suspended from trash boom

The suspended mooring consisted of a line with temperature recorders attached to the log boom upstream of the intakes to the Bridge 1 and 2 powerhouses. The mooring was attached to the boom at the location with greatest depth (UTM 10U 551,263 Easting 5,624,112 Northing). The line consisted of 1.8 m of ¼" galvanized chain at the top and 5/8" Samson Quik-Splice for the remainder. The Quick-Splice line was a 12 strand single braid polyolefin rope with low stretch (specific gravity 0.94, weight 11.9 kg/100 m). The bottom of the mooring was weighted using 30 lbs of steel (1 X 10 lb weight lifting ring purchased from Canadian Tire and a 20 lb cannonball).

The depths of the temperature recorders for three time intervals selected for temperature logging are given in Table 15, Table 16, and Table 17. Most of the temperature recorders were Onset U22-001 Hobo Water Temp Pro v2 (HWTP) temperature loggers with accuracy of ± 0.2 °C and resolution of 0.02 °C. The Onset HWTPs recorded one measurement every 20 minutes. Also included were two high accuracy RBR Solo T temperature recorders, with accuracy ± 0.002 °C, resolution of < 0.05 m°C, and recording every 3 seconds. At the bottom of the mooring a RBR Solo D depth recorder was included to monitor movement of the mooring, recording every 6 seconds.

Table 15. Listing of instruments attached to the suspended vertical line mooring in Carpenter Reservoir during April 16 through October 20, 2015.

Depth (m)	Instruments
	16 Apr - 20 Oct 2015
0.5	HWTP 1068-5988
1	RBR Solo T 75933
2	HWTP 1068-5976
3	HWTP 1068-5977
5	HWTP 1068-5978
7	HWTP 1068-5979
10	HWTP 1068-5980
15	HWTP 1068-5981
20	RBR Solo T 76651
~20 ⁽¹⁾ 25 ⁽²⁾	HWTP 1068-5982
27 ⁽³⁾ 30 ⁽²⁾	RBR Solo T 76652 RBR Solo D 78474 RBR Virtuoso 54153 with Seapoint turbidity 14839

⁽¹⁾ Tied up near 20 m from 16 April to 18 June; these data not used.

⁽²⁾ From 18 June to 20 October.

⁽³⁾ From 16 April to 22 May; removed for service from 22 May to 18 June.

Table 16. Listing of instruments attached to the suspended vertical line mooring in Carpenter Reservoir during October 20, 2015 through April 13, 2016 (winter deployment).

Depth	Instruments
(m)	20 Oct 2015 – 13 Apr 2016
0.5	HWTP 1011-0014
5	HWTP 1011-0083
10	HWTP 1011-0084

Table 17. Listing of instruments attached to the suspended vertical line mooring in Carpenter Reservoir during April 13 through October 14, 2016.

Depth	Instruments
(m)	13 Apr – 14 Oct 2016
0.5	HWTP 1068-5988
1	RBR Solo T 75933
2	HWTP 1068-5976
3	HWTP 1068-5977
5	HWTP 1068-5978
7	HWTP 1068-5979
8	HWTP 1038-8898
9	HWTP 1038-8899
10	HWTP 1068-5980
11	HWTP 1038-8900
12	HWTP 1038-8901
13	HWTP 1038-8902
14	HWTP 1038-8903
15	HWTP 1068-5981
16	HWTP 1038-8904
18	HWTP 1039-4321
20	RBR Solo T 76651 RBR Solo D 78475
22	HWTP 1039-4322 ⁽¹⁾
25	HWTP 1068-5982 ⁽¹⁾

⁽¹⁾ Bottom 5 m segment added 14 July 2016.

In 2015, the mooring line included an RBR Virtuoso turbidity recorder, connected to a Seapoint optical backscatter sensor (OBS) with a Zebra Hydro Wiper. Data was recorded every 2 minutes. The turbidity recorder was at the same depth as the Solo T

and Solo D at the bottom of the mooring (Table 15). In 2016, the turbidity recorder was attached to the subsurface mooring (see below).

On 23 April 2015, the bottom Solo T sensor, along with the Solo D and turbidity recorder were deployed at 27 m depth, just above the bottom (28.5 m). After deployment in April, the water level in Carpenter Reservoir declined slightly. On the first sampling trip on 22 May 2015 (day 142) the mooring was inspected, and the bottom sensors were found to have dragged along the bottom. The instruments were undamaged except for the wiper arm, which was badly bent. The bottom three instruments were removed for service, a replacement wiper arm was built, and the instruments were reattached at 30 m during the subsequent sampling trip on 18 June 2015 (day 169).

In 2015, the mooring was pulled up to the surface each month to inspect the turbidity sensor; data during these times were removed. Data from the depth recorder showed brief periods when the bottom of the mooring was shallower than expected; this could have resulted from the log boom shifting to a shallow location, or from drag on the mooring as the boom moved from one location to another. Data during the worst cases were removed.

Upon recovery of the main mooring line on 20 October 2015, three temperature recorders were attached to the log boom for the winter. The recorders were hung from individual lines consisting of chain to 1 m, and 3/8" static cord from 1 m to a steel weight ring (10 lb) at the bottom (Table 16).

In 2016, additional temperature sensors were added to the boom line between 8 and 16 m in order to better resolve the thermocline. At deployment on 13 April 2016, the line was only 20 m long to avoid the dragging on the bottom. On 14 July 2016, an additional 5 m of line was added with sensors at 22 and 25 m.

8.2 Subsurface mooring

To better measure turbidity and temperature near the bottom of the reservoir, a subsurface mooring was deployed in 2016 at a location approximately 1 km downstream of the log boom (10U 552,594 Easting; 5,624,640 Northing). This mooring had 60 lb of steel anchor; then a line of 5/8" Samson Quik-Splice ran from the anchor to a 12" trawl float 2 m above the bottom; finally a line of 3/8" static cord ran to an 8" trawl float at 12.5 m above the bottom. A 3/8" Samson double-braid nylon ground line, was connected from the anchor at the bottom of the mooring to a tree on the south shore of the reservoir; the mooring was recovered using this line. The instruments on the subsurface mooring are given in Table 18.

Table 18. Listing of instruments attached to the subsurface vertical line mooring in Carpenter Reservoir during April 13 through October 14, 2016.

Distance from bottom	Depth⁽¹⁾	Instruments
(m)	(m)	13 Apr – 14 Oct 2016
12	20.6	HWTP 1068-5985
7	25.6	HWTP 1068-5986
1.8	30.8	RBR Virtuoso 54153 with Seapoint turbidity 14839
1.7	30.9	RBR Solo T 76652 RBR Solo D 78474
0.3	32.3	HWTP 1068-5987
0	32.6	Bottom

(1) From a water level of 633.45 m ASL on 13 April 2016.

9 APPENDIX B. WINTER TEMPERATURES FROM THE SUSPENDED MOORING IN 2015 – 2016.

Following removal of the suspended mooring on 20 October 2015, a smaller mooring with three temperature recorders attached at depths of 0.5, 5 and 10 m was installed to record temperature during late fall 2015 through early spring 2016.

The time course change in temperature during winter is shown in Figure 43. When the temperature sensors were installed, the top 10 m was well mixed at 12°C. Based on the data from the previous mooring removed on 20 October 2015, there was little temperature stratification and fall turnover likely began in late October. The top 10 m cooled steadily and remained well mixed throughout the fall; during this time both wind and cooling contributed to mixing. The reservoir reached the temperature of maximum density ($T_{MD} = 3.98 \text{ }^{\circ}\text{C}$) on 24 December 2015 (day 358), after which it alternated between brief periods of mixing and reverse stratification. Below T_{MD} , cooling gives rise to less dense and stable water, which resists mixing by the wind. The data suggests ice-on was complete around 3 January 2016 (day 368) when the water stopped cooling, and a period of relatively steady temperature began. Relatively steady water temperature ended around 6 February 2016 (day 402), when the 0.5 m sensor began to warm; the 0.5 m sensor reached the temperature of the 5 m sensor on 8 February 2016 (day 404), and that of the 10 m sensor on 14 February 2016 (day 410). From these data, it is hard to pinpoint when exactly ice-off occurred, though it likely happened by late February. From late-February through March, 2016, the top 10 m of the reservoir warmed toward TMD; during this time both wind and warming contributed to mixing. There was a strong diurnal cycle at 0.5 m, with strong cooling at night (stable) and occasional warming during the day (unstable). The top 10 m reached TMD on 30 March 2016 (day 455). As the surface continued to warm, there were periods of stable temperature stratification and periods of mixing. While it is hard to tell when the summer temperature stratification began from just the top 10 m, it probably started in early April, and had definitely occurred by 13 April 2016, when the deeper moorings were installed.

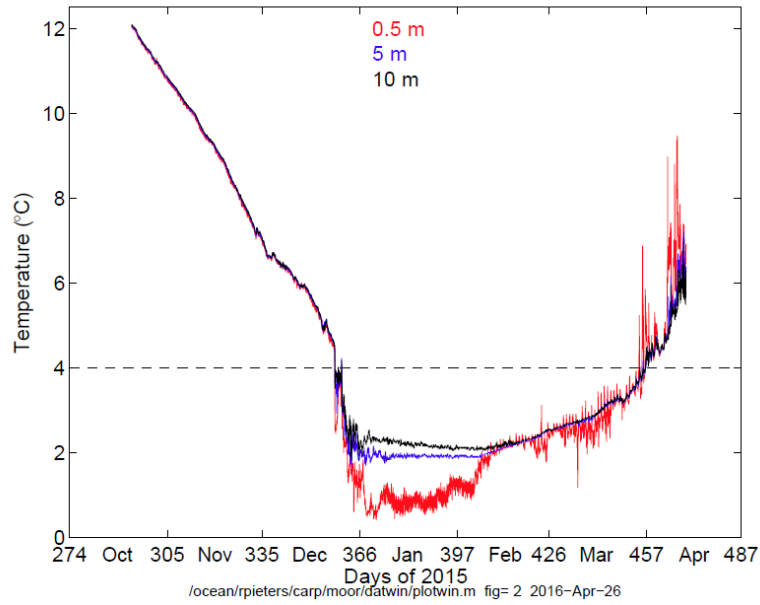


Figure 43. Temperature at 0.5 m, 5 m, and 10 m at the log boom in Carpenter Reservoir during October 20, 2015 through April 13, 2016. The dashed line marks the temperature of maximum density ($T_{MD} = 3.98^{\circ}\text{C}$).

10 APPENDIX C. METEOROLOGICAL CONDITIONS IN 2015 AND 2016.

This appendix provides a graphic overview of meteorological conditions in 2015 (Figure 44) and 2016 (Figure 45).

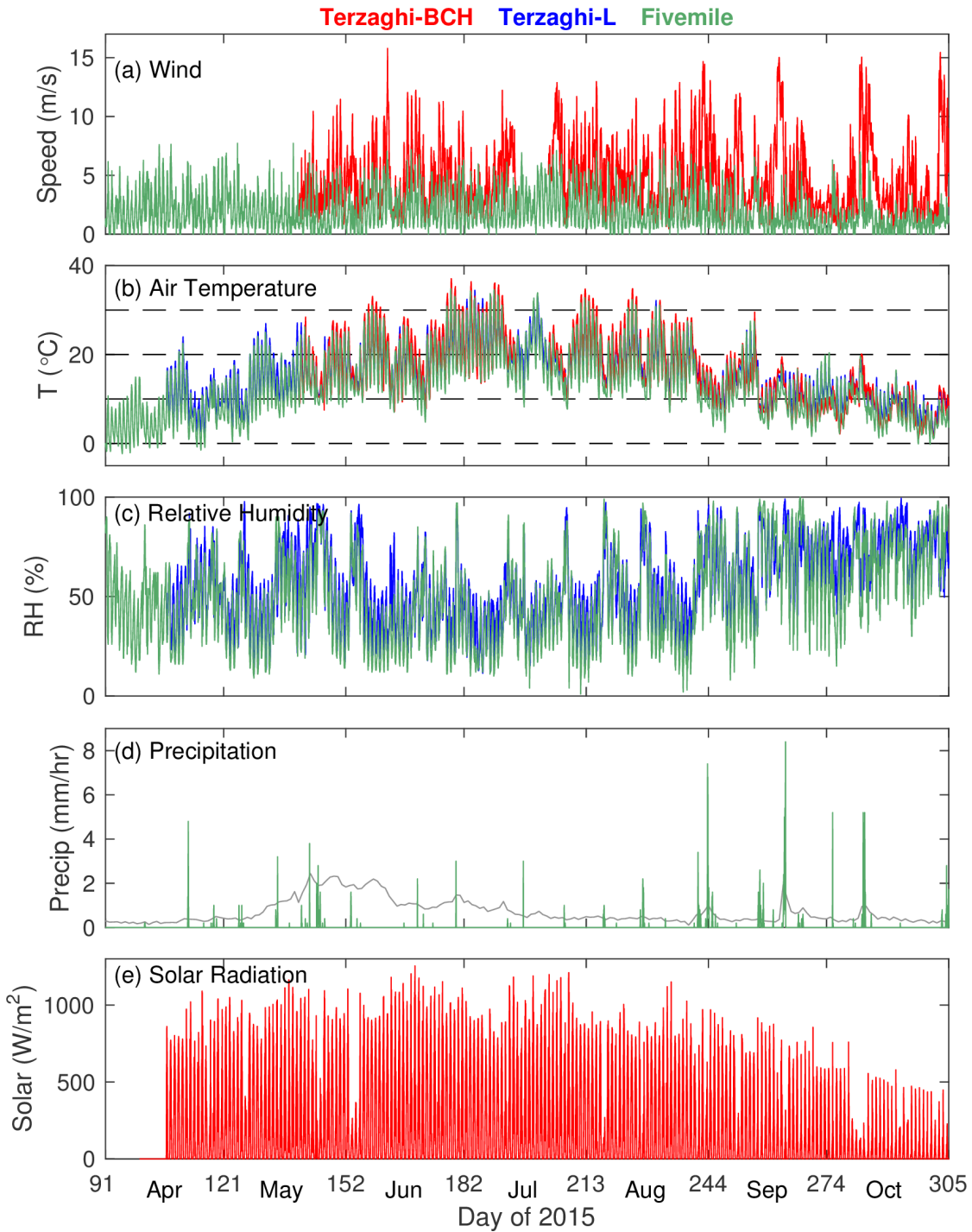


Figure 44. Hourly (a) wind speed, (b) air temperature, (c) relative humidity, (d) precipitation and (e) total solar irradiance data available for Carpenter Reservoir during April to October 2015. The grey line in (d) is local inflow in units of m³·s⁻¹/100.

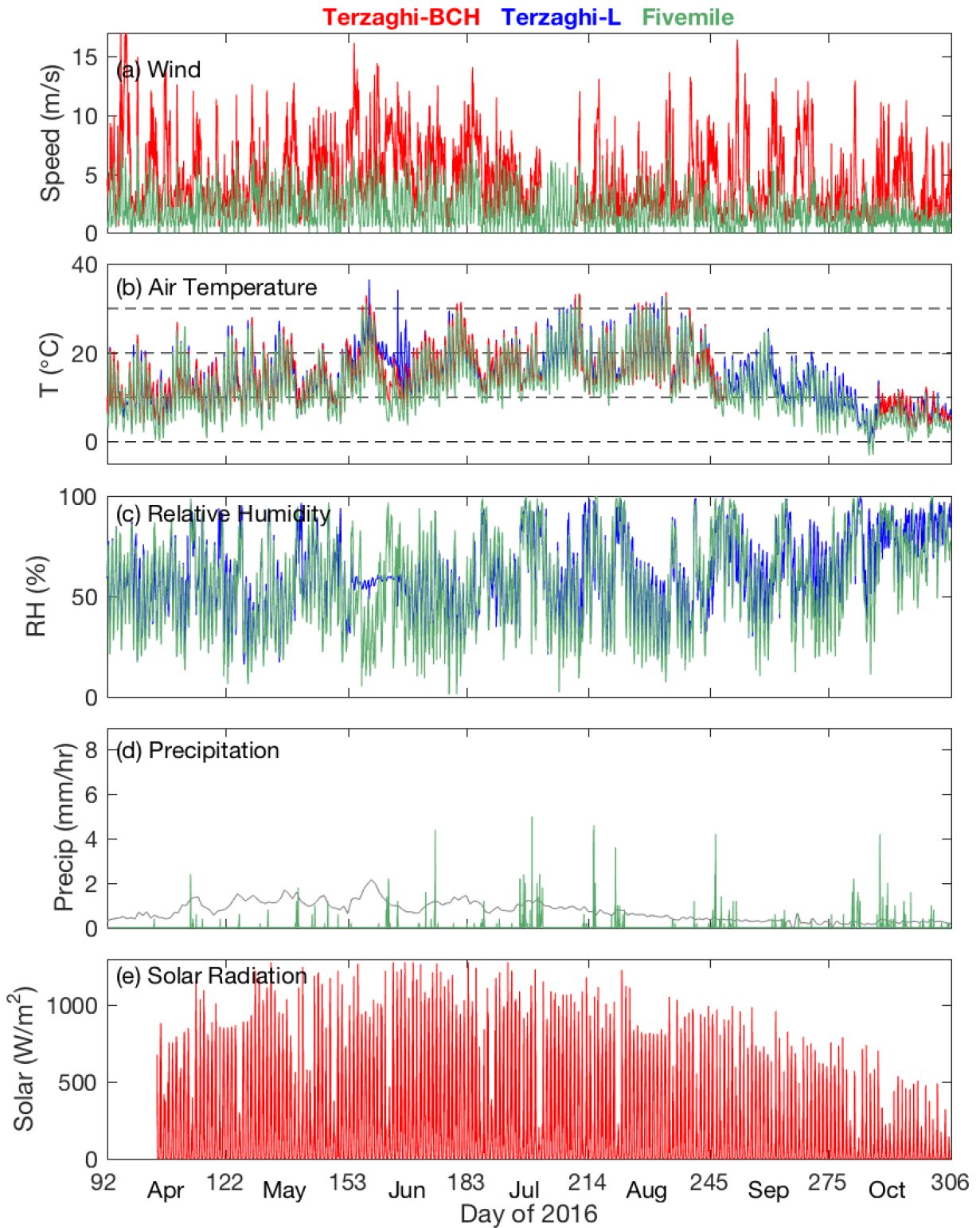


Figure 45. Hourly (a) wind speed, (b) air temperature, (c) relative humidity, (d) precipitation and (e) total solar irradiance data available for Carpenter Reservoir during April to October 2016. The grey line in (d) is local inflow in units of m³·s⁻¹/100.

11 APPENDIX D. SUPPLEMENTARY TRIBUTARY TEMPERATURE AND CHEMISTRY.

11.1 Content of this appendix

Several volumes of temperature and chemical attribute data were collected using instruments and by manual water sampling. These data were used in building the models and thus are relevant to show as supplementary information to support observations in the main report. Descriptions of those data appear in this appendix.

11.2 Tributary temperature

From May to October, in both 2015 and 2016, temperature of the inflow from La Joie Dam was 8 - 11°C (blue lines in Figure 46 a and b). In contrast, temperature of the Hurley River, the main inflow tributary to the Middle Bridge River, had strong seasonal, weekly and daily variations (red lines in Figure 46 a and b). Mixing of the Hurley River into the Middle Bridge River resulted in an intermediate temperature (green lines in Figure 46 a and b). Among the other larger tributaries, temperature in Gun Creek was lower than in Tyaughton Creek (Figure 46, c and d). The temperatures of three smaller tributaries varied from warmer (Keary) to cooler (Truax Creek) with Truax Creek and Keary Creek having greater seasonal variation than Marshall Creek (Figure 46 e and f).

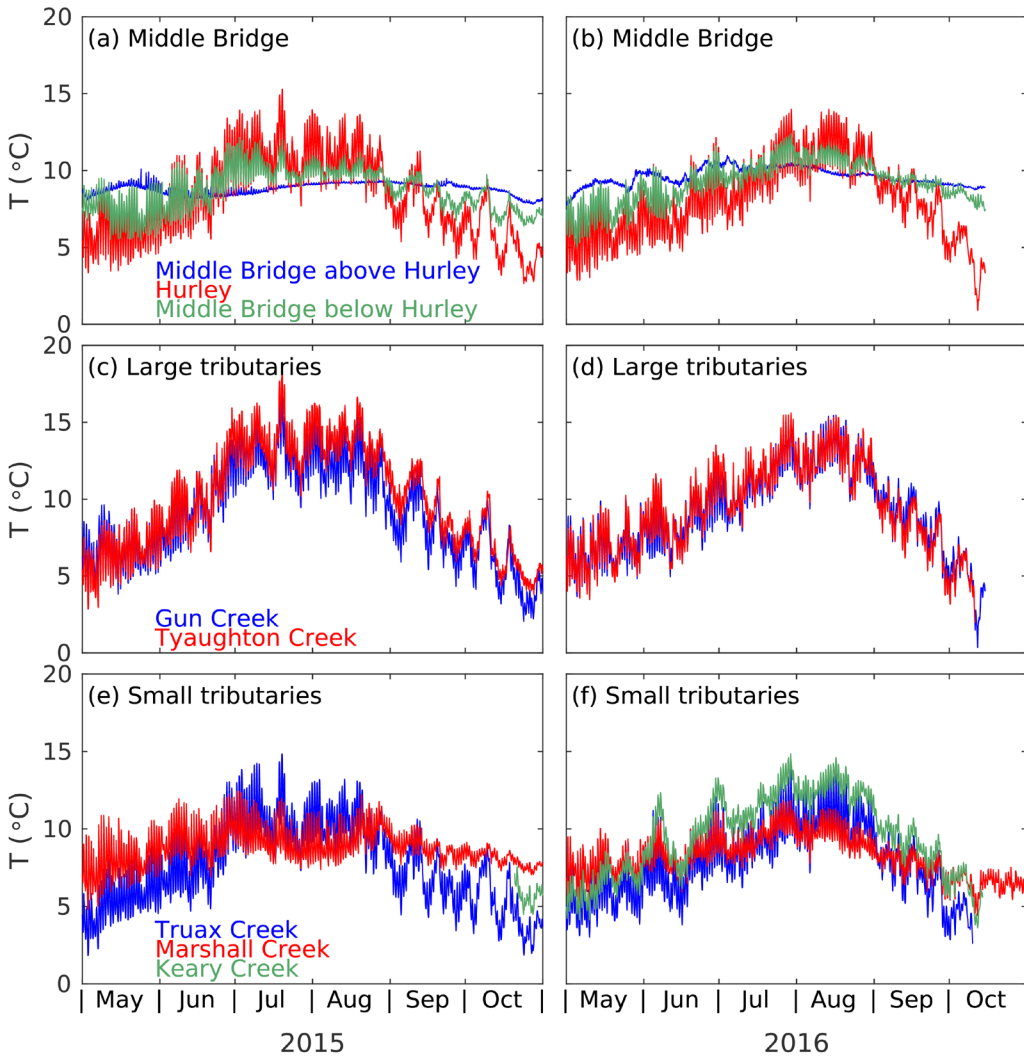


Figure 46. Tributary temperature for (a, b) Middle Bridge and Hurley River (c,d) larger tributaries, and (e,f) smaller tributaries, for 2015 and 2016 respectively.

11.3 Tributary water chemistry

The monthly values of total suspended solids (TSS) and turbidity are shown for the Upper Bridge, Middle Bridge and Hurley Rivers in Figure 49 and for the other tributaries to Carpenter Reservoir in Figure 48. TSS and turbidity are important measures of glacial fines which control the penetration of light in Carpenter Reservoir. Total suspended solids and turbidity are complementary but different physical measurements. Total suspended solids is a direct measure of the weight of the suspended solids: a filter is weighed, an aliquot of water sample is passed through the filter, the filter is dried and weighed again, and the solids content is determined as the change in the weight of the filter. The procedure is not only time consuming but the results have poor resolution when the difference in weight is small, namely for samples with low amounts of suspended solids, and for samples with small particles. In contrast, turbidity, which measures the amount of scattered light, is easy to measure with an

optical sensor. However, the amount of scattered light depends on the size, shape, colour and texture of the particles, which makes turbidity an indirect measure of suspended solids. Even a reservoir-specific relationship between TSS and turbidity usually shows significant scatter, and Carpenter Reservoir was no exception. In the Upper Bridge River, the Middle Bridge River, and in the Bridge Tailrace, the values of turbidity and TSS were not correlated (Figure 47 and Figure 49). Values were higher than in the smaller tributaries (Figure 48) where turbidity was a linear function of TSS concentration (Figure 49) although fit of a linear model to the data was mainly controlled by the highest reading, which does not instill confidence that a true functional relationship was present.

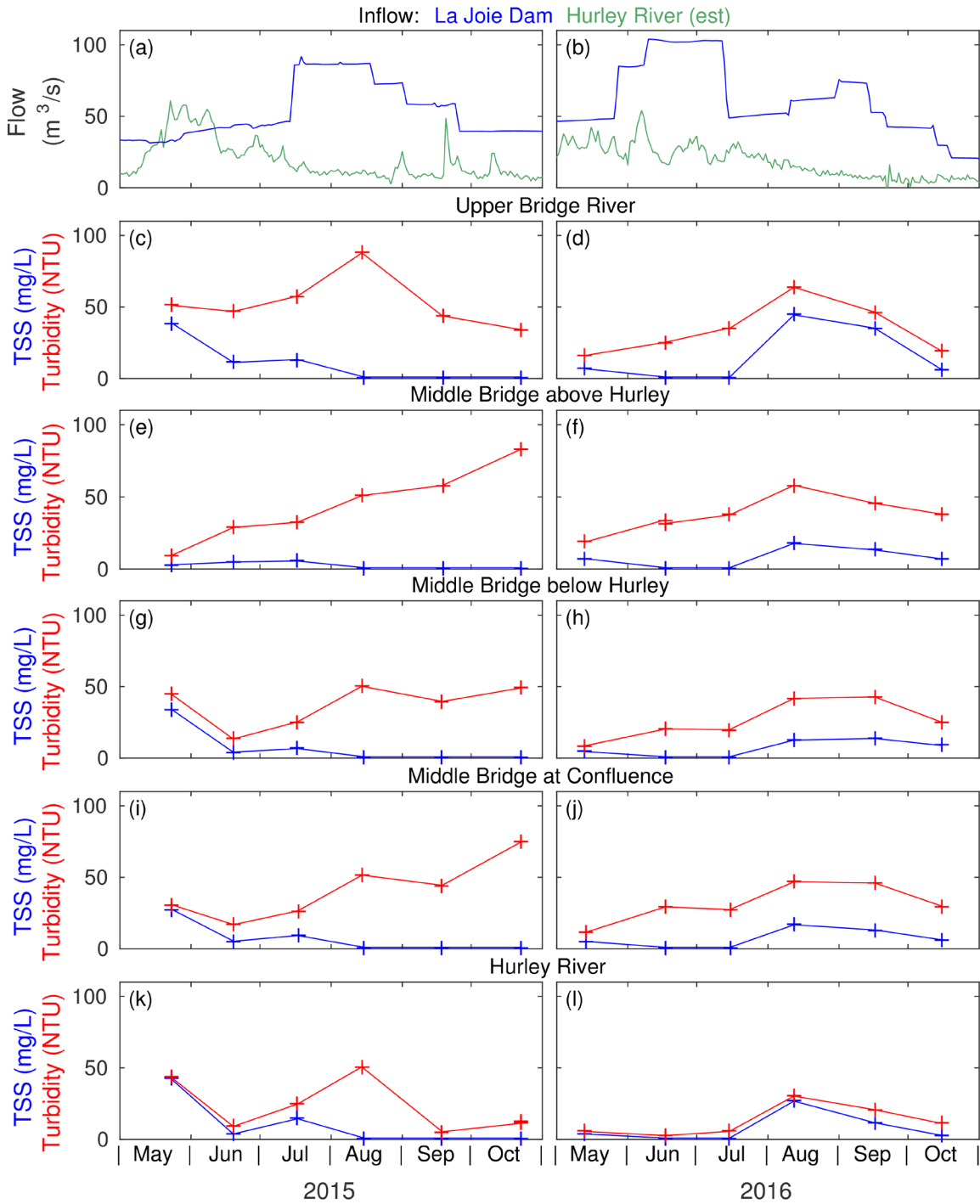


Figure 47. Monthly turbidity and total suspended solids concentrations in the Bridge River inflows. Flow rate in 2015 (a) and 2016 (b) is shown for reference. Turbidity data are corrected to lab values.

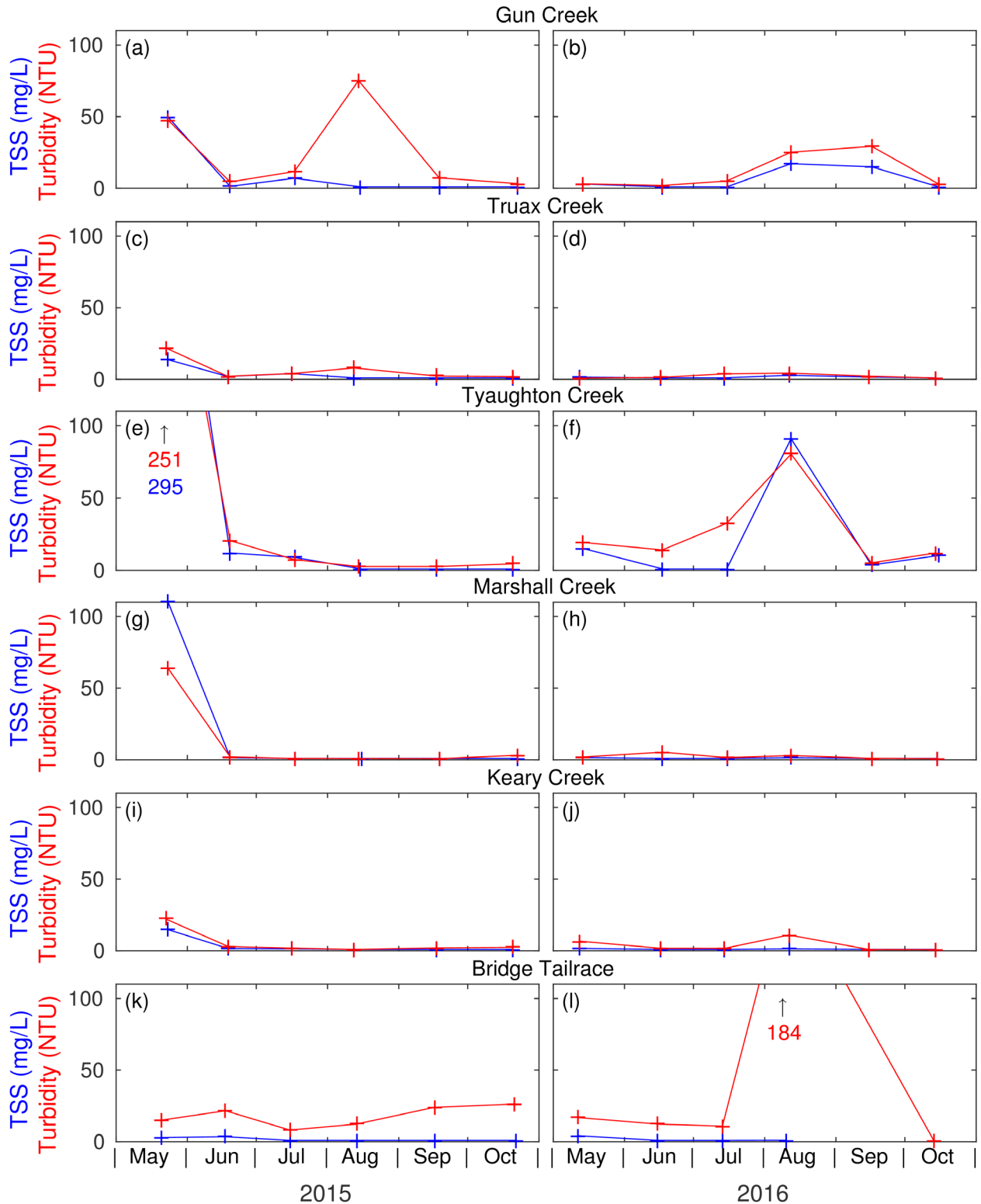


Figure 48. Monthly turbidity and total suspended solids concentrations in 2015 and 2016 in small tributaries and in the tailrace of the generating station. Turbidity data are corrected to lab values.

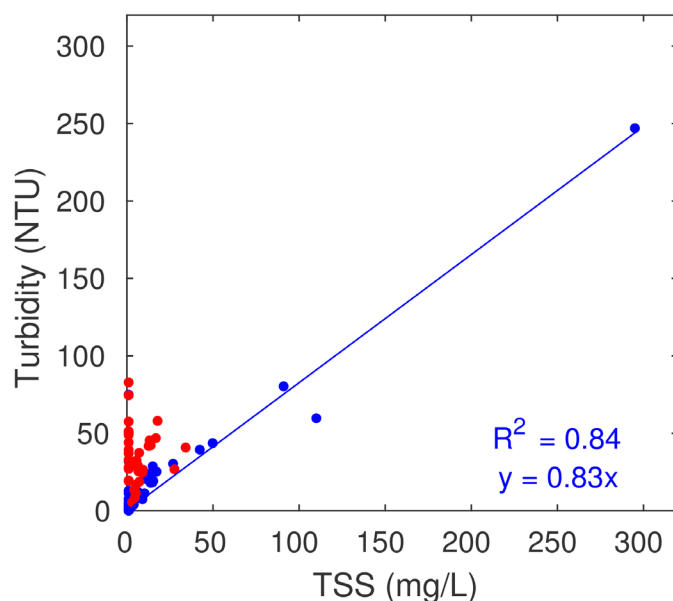


Figure 49. Turbidity versus total suspended solids (TSS) for tributaries to Carpenter Reservoir, 2015 and 2016. RED – Samples from Upper and Middle Bridge Rivers and the Bridge Tailrace. BLUE – Samples from the Hurley River and from Gun, Truax, Tyaughton, Marshall and Keary Creeks. The blue line gives the fit through zero to the blue data.

Soluble phosphorus (SRP and TDP) concentrations were mostly $<5 \mu\text{g}\cdot\text{L}^{-1}$ among the Bridge River sites except in July 2015 in the Upper Hurley River where values up to $8 \mu\text{g}\cdot\text{L}^{-1}$ were found (Figure 50). The Bridge River itself had higher concentrations of soluble phosphorus than did the Hurley River (Figure 50) and smaller inflow tributaries where soluble P concentrations were close to or less than the method detection limit of $1 \mu\text{g}\cdot\text{L}^{-1}$ SRP and $2 \mu\text{g}\cdot\text{L}^{-1}$ of TDP (Figure 51). Soluble P concentrations in the tailrace from the generating station were also close to the method detection limits except in the fall 2015 when concentrations up to $5 \mu\text{g}\cdot\text{L}^{-1}$ of TDP and $2 \mu\text{g}\cdot\text{L}^{-1}$ of SRP were found (Figure 51).

Total phosphorus concentration was greater than concentrations of soluble P mainly in the Bridge River inflow to Carpenter Reservoir (Figure 52). This difference shows that much of the phosphorus load to Carpenter Reservoir was bound to particles and was not biologically available. Only the simple phosphate anion is available for uptake by biota. Rising concentrations of TP during May through October in 2015 in the Middle Bridge River but not in the Upper Bridge River shows that TP associated with particles originated in Downton Reservoir. This Downton Reservoir effect on TP concentration was not found in 2016. Smaller or no difference between TP and soluble P concentration was found in the small tributary inflows compared to the Bridge River (compare Figure 53 and Figure 52).

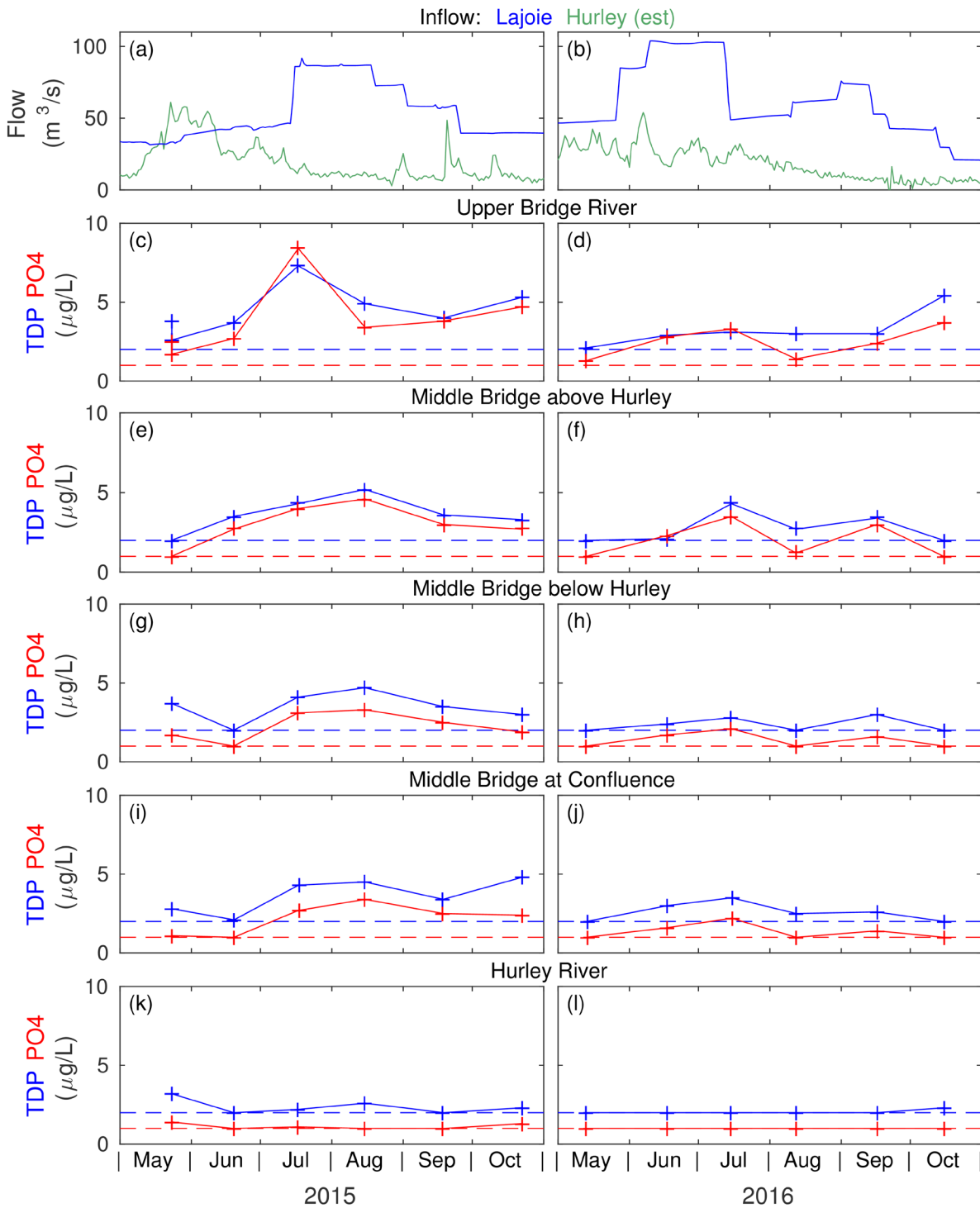


Figure 50. Total dissolved phosphorus and soluble reactive phosphorus concentration (shown as PO₄) in 2015 and 2016 in the Bridge River inflows. Flow rate in 2015 (a) and 2016 (b) is shown for reference.

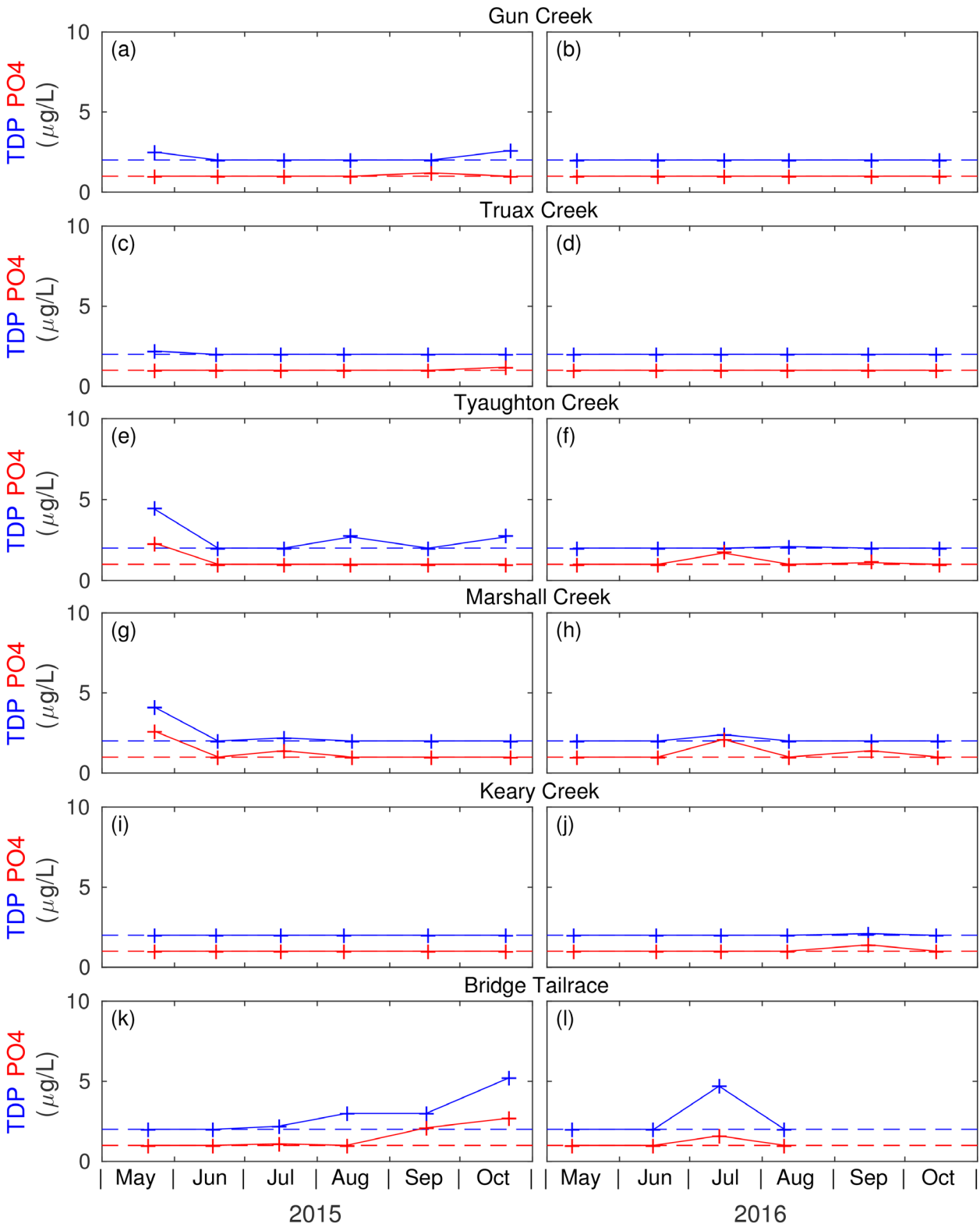


Figure 51. Total dissolved phosphorus and soluble reactive phosphorus concentration in 2015 and 2016 in the small tributary inflows to Carpenter Reservoir and in outflow at the Bridge generating station.

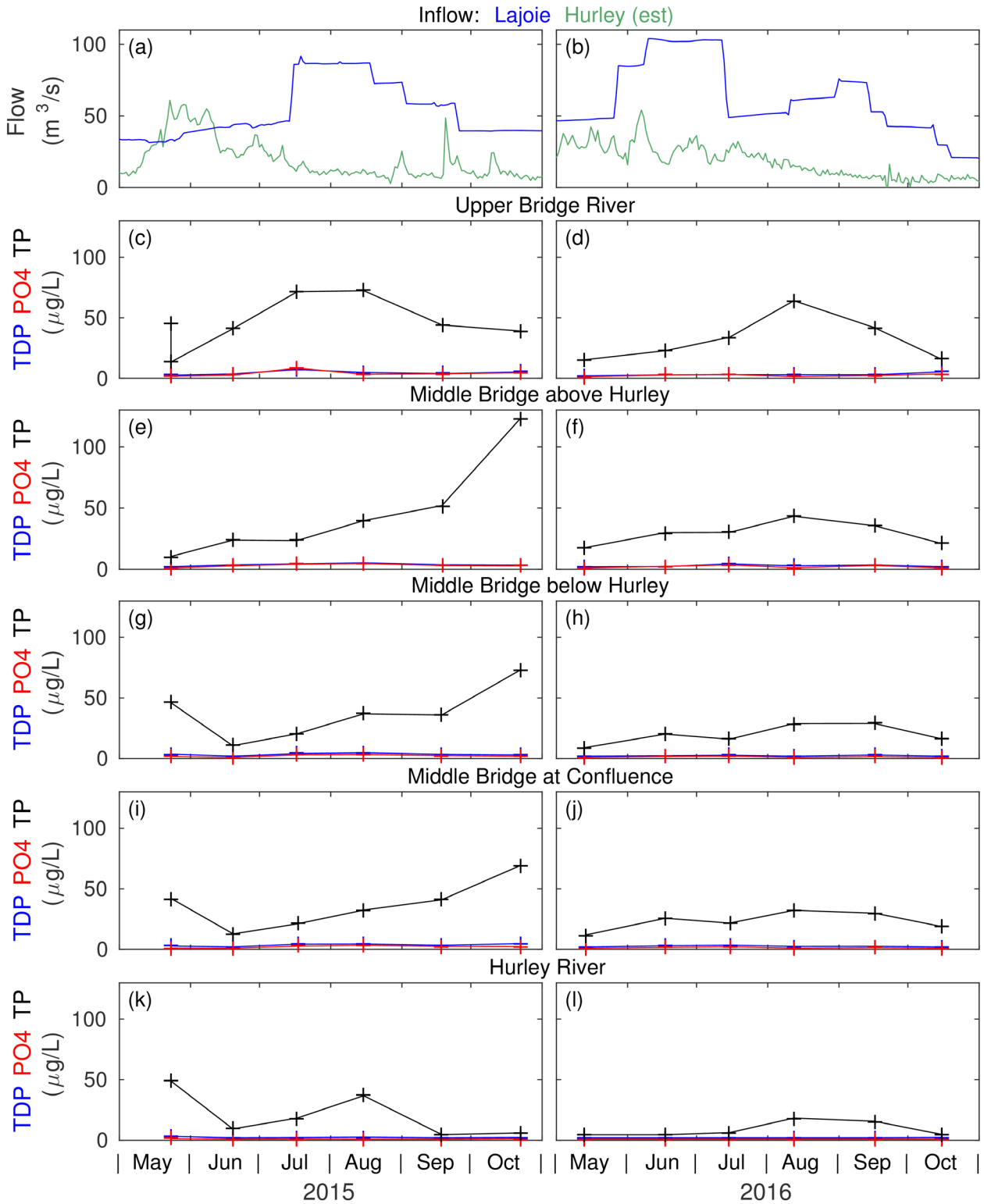


Figure 52. Total dissolved phosphorus, soluble reactive phosphorus (shown as PO₄), and total phosphorus concentration in 2015 (left panels) and 2016 (right panels) in the Bridge River inflows. Flow rate in 2015 (a) and 2016 (b) is shown for reference.

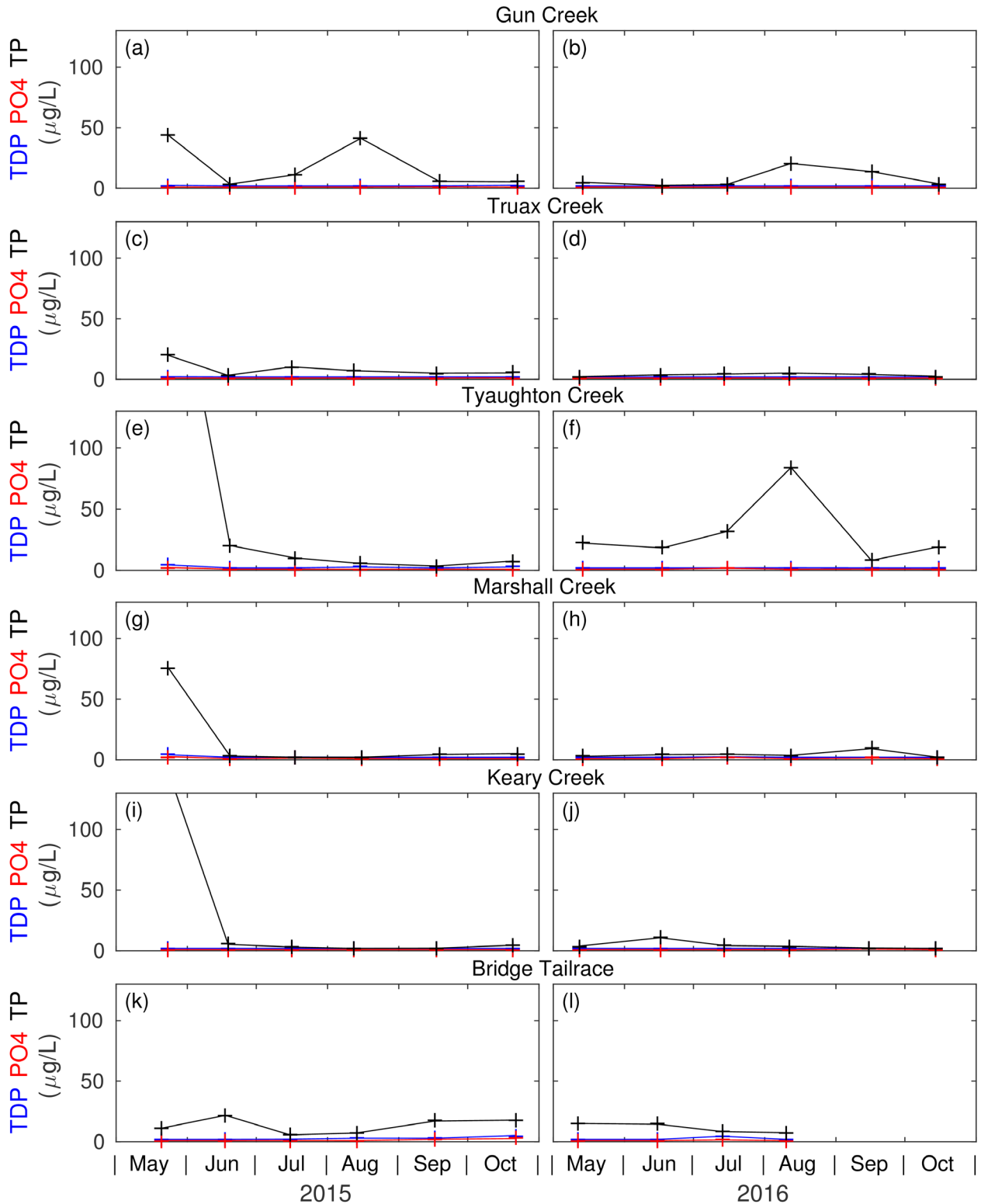


Figure 53. Total dissolved phosphorus, soluble reactive phosphorus (shown as PO₄), and total phosphorus concentration in the small tributary inflows to Carpenter Reservoir in 2015 (left panels) and 2016 (right panels).

Nitrate-N concentrations (the only form of inorganic N that was found above method detection limits) were $<60 \mu\text{g}\cdot\text{L}^{-1}$ in all inflows to Carpenter Reservoir with concentrations commonly lower in the small tributaries compared to the main inflow Bridge River (Figure 54 and Figure 55). In contrast, conductance was greater in the small tributaries than in the inflow from the Middle Bridge River (compare Figure 54 and Figure 55). This difference in conductance by source infers greater base cation and other ion content in the small tributaries compared to the Middle Bridge River, inferring different parent materials and weathering of those parent materials. Similar conductance between the Upper Bridge River and the inflow to Carpenter Reservoir shows that the whole Bridge River drainage was chemically different from the smaller tributary inflows and that processes in Downton Reservoir did not alter the base cation and other ion content that contributes to conductance.

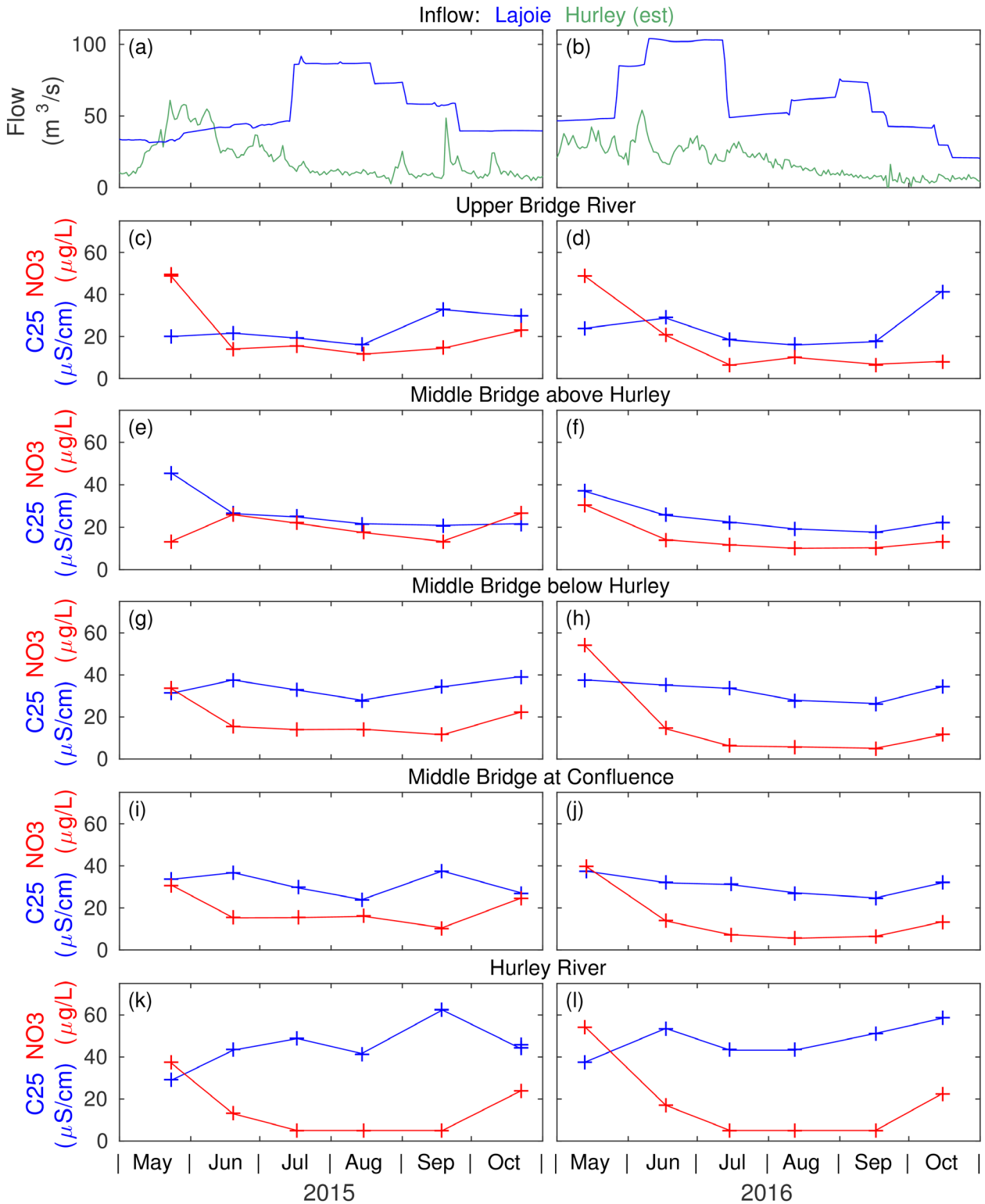


Figure 54. Conductivity (shown as C25) and nitrate-N (shown as NO₃) concentration in 2015 (left panels) and 2016 (right panels) in the Bridge River inflows. Flow rate in 2015 (a) and 2016 (b) is shown for reference.

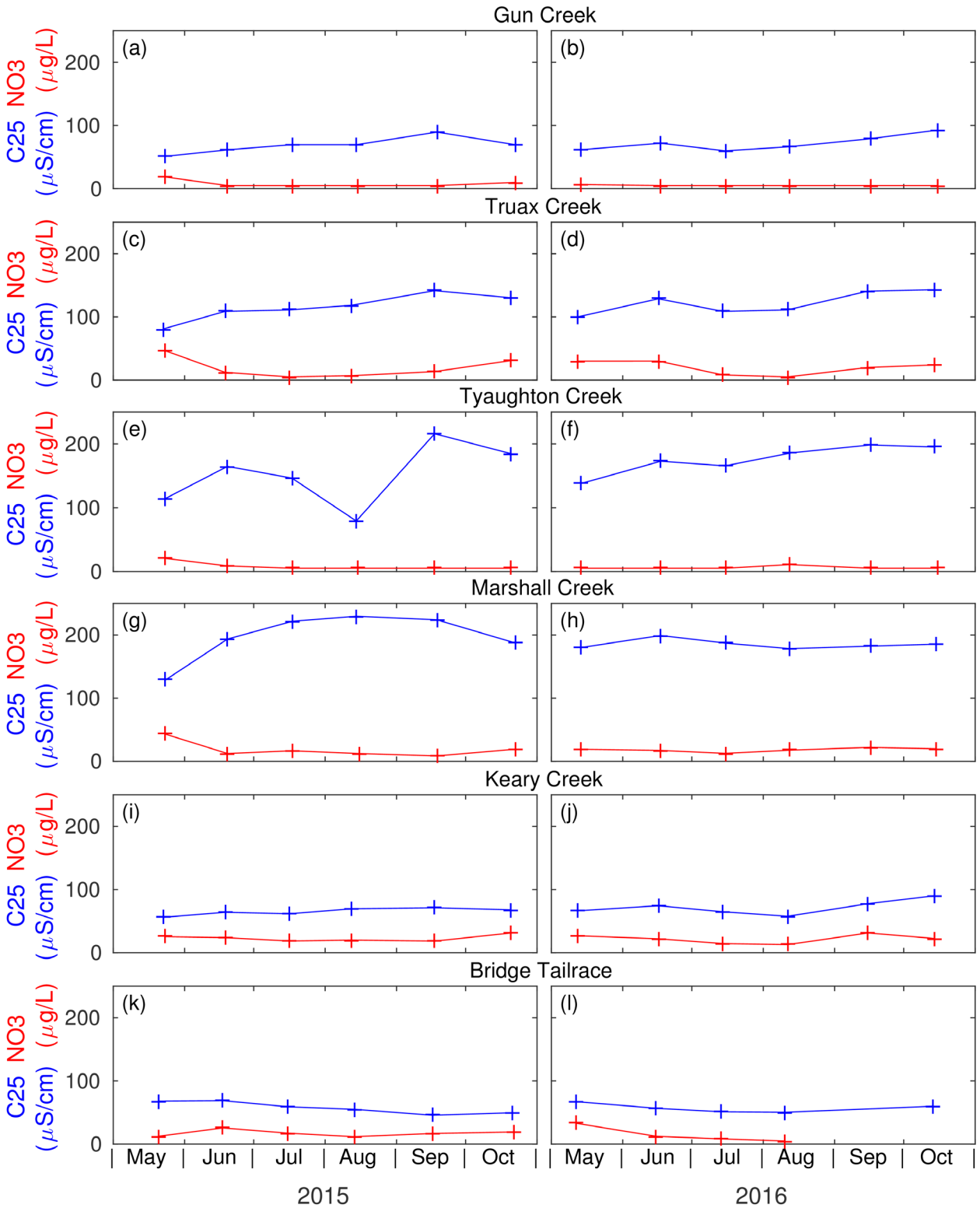


Figure 55. Conductivity (shown as C25) and nitrate-N (shown as NO₃) concentration in 2015 (left panels) and 2016 (right panels) in the small tributary inflows to Carpenter Reservoir.

12 APPENDIX E: CONTINUOUS TURBIDITY MONITORING

12.1 Appendix E-1: Continuous turbidity in the Middle Bridge River

Data from the turbidity recorder moored in the Middle Bridge River below the Hurley River are shown in Figure 56 and Figure 57 for 2015 and 2016, respectively. The sensor was deployed without a wiper in 2015, and with a wiper in 2016. In 2015, the sensor face was cleaned at the time of the spot readings (except for 22 October 2015 when the water was too deep to recover the mooring). At times, this monthly cleaning of the sensor resulted in an abrupt change in the turbidity readings (e.g. in May and September 2015, Figure 56), which suggests fouling affected the readings. In 2016, the monthly cleaning did not abruptly change the readings, which showed the wiper was effective in removing fouling of the sensor.

Monthly turbidity data for closely spaced sites associated with inflow of the Middle Bridge River to Carpenter Reservoir are shown in Figure 56b and Figure 57b. Turbidity in the Middle Bridge River above the Hurley represents inflow from La Joie Dam. This turbidity increased through spring and summer and remained elevated in fall (red in Figure 56b and Figure 57b). Turbidity in the water coming from La Joie Dam was generally higher than the turbidity measured in the Hurley River (green in Figure 56b and Figure 57b). The exception was during the onset of spring freshet in May 2015, when the turbidity in the Hurley River was higher. Middle Bridge below the Hurley is the combination of the La Joie and Hurley inflows, and the turbidity of the Middle Bridge below the Hurley (blue in Figure 56b and Figure 57b) generally falls between that of the two sources. Turbidity of the Middle Bridge at the confluence with Carpenter Reservoir (cyan in Figure 56b and Figure 57b) is close to that of the Middle Bridge below the Hurley (with the exception of October 2015), which suggests that, for these dates, the Middle Bridge River did not pick up significant additional turbidity as it flowed through the drawdown zone.

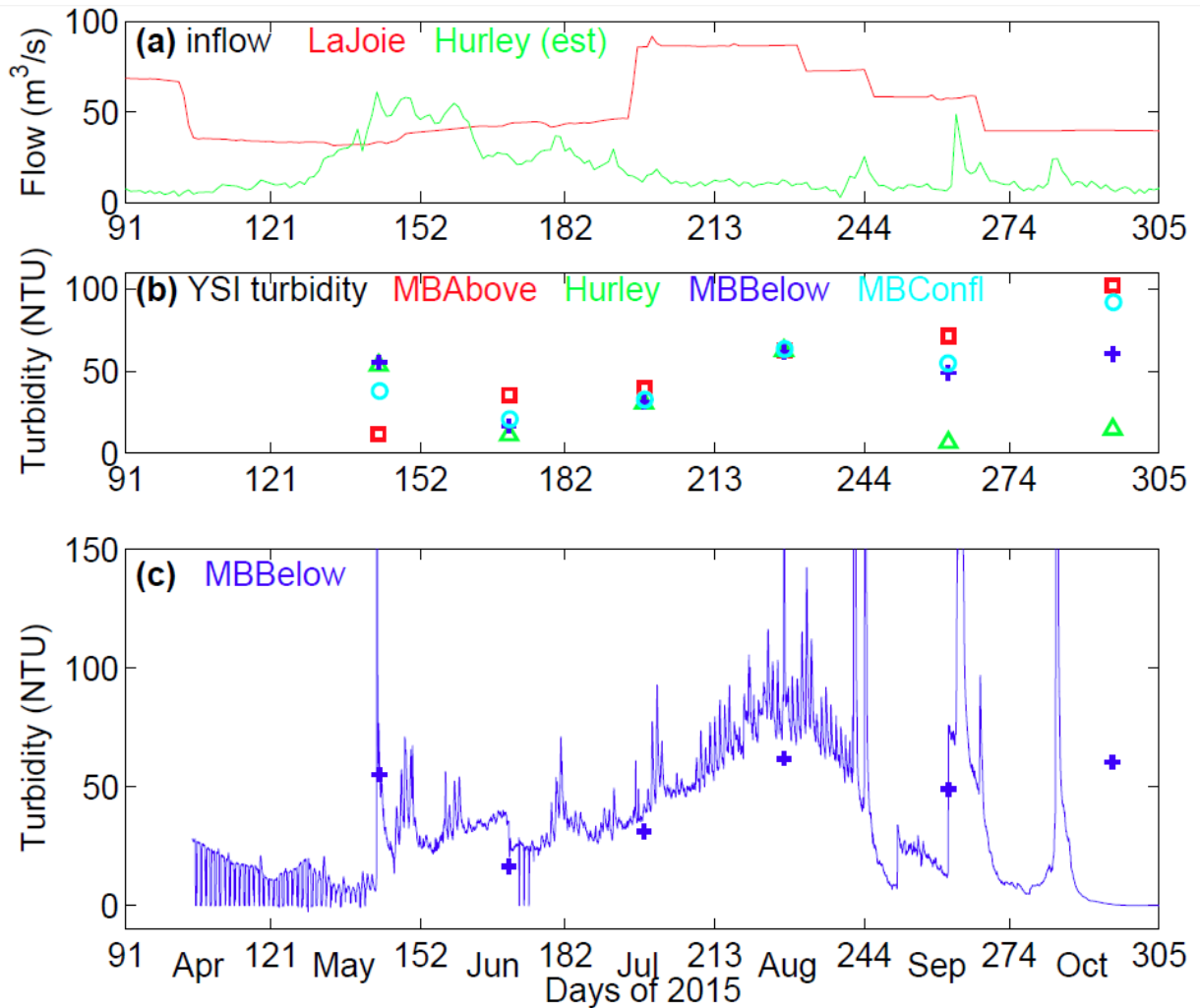


Figure 56. (a) Inflow, (b) YSI turbidity, and (c) hourly average turbidity from inflow to the top of Carpenter Reservoir, 14 April to 22 October, 2015. **MBAbove** marks the Middle Bridge River above the Hurley; **MBBelow** marks the Middle Bridge Below the Hurley, and **MBConf** marks the Middle Bridge at confluence with Carpenter Reservoir. Flow in the Hurley was estimated as 25% of the local flow.

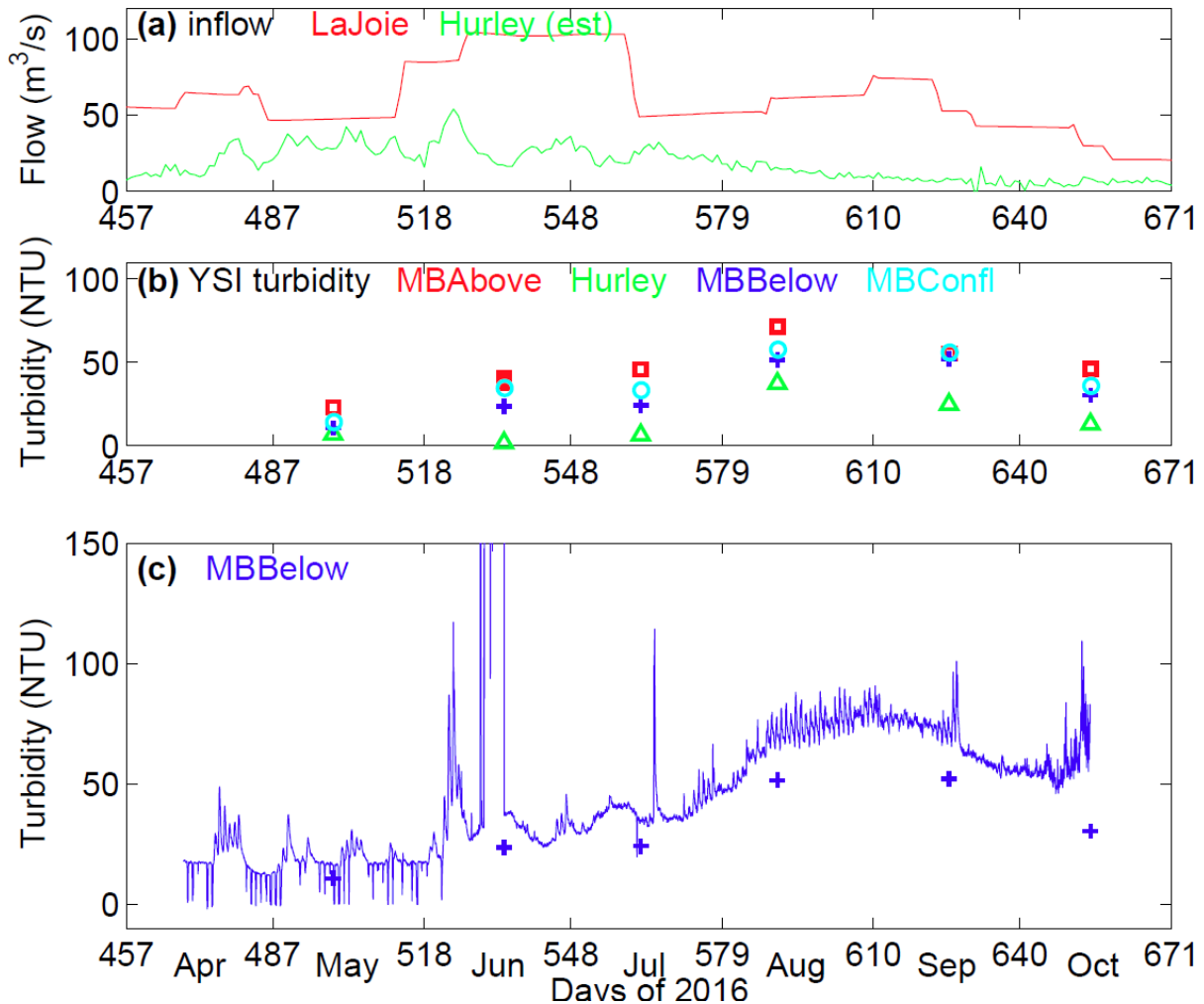


Figure 57. (a) Inflow, (b) YSI turbidity, and (c) hourly average turbidity from inflow to the top of Carpenter Reservoir, 13 April to 26 October, 2016. **MBAbove** marks the Middle Bridge River above the Hurley; **MBBelow** marks the Middle Bridge Below the Hurley, and **MBConf** marks the Middle Bridge at confluence with Carpenter Reservoir. Flow in the Hurley was estimated as 25% of the local flow.

12.2 Appendix E-2: Continuous turbidity in the reservoir

A continuous record of turbidity was measured in the deep water of the reservoir from April to October in both 2015 and 2016. In 2015, the turbidity recorder was attached at approximately 30 m depth to the mooring at the log boom, see Figure 58. In 2016, the turbidity recorder was attached 1.8 m above the bottom on the subsurface mooring (Figure 59). In both years, the turbidity varied from 10 to 40 NTU with episodic values exceeding 60 NTU.

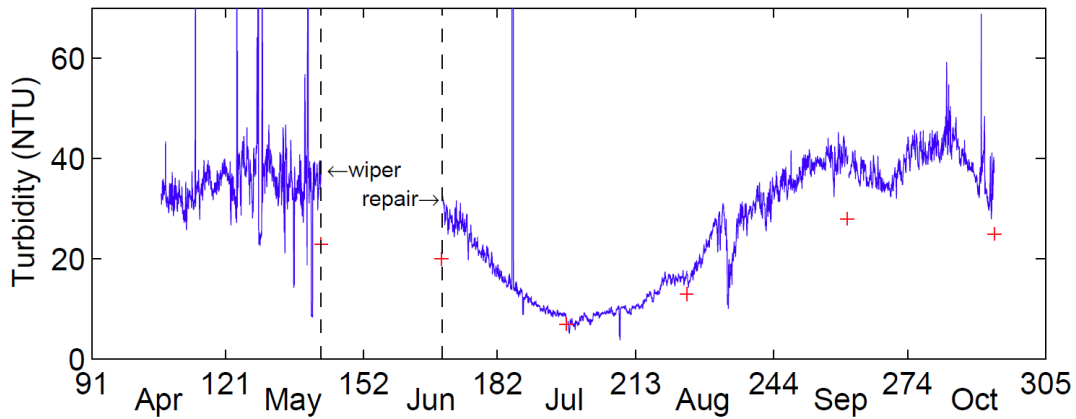


Figure 58. Turbidity data recorded at the log boom in Carpenter Reservoir, 16 April to 20 October, 2015. The recorder was at 27.5 m depth before 18 June 2015, and at 30 m depth thereafter. The red + signs give the turbidity measured at 30 m by the Sea-Bird at Station C2.

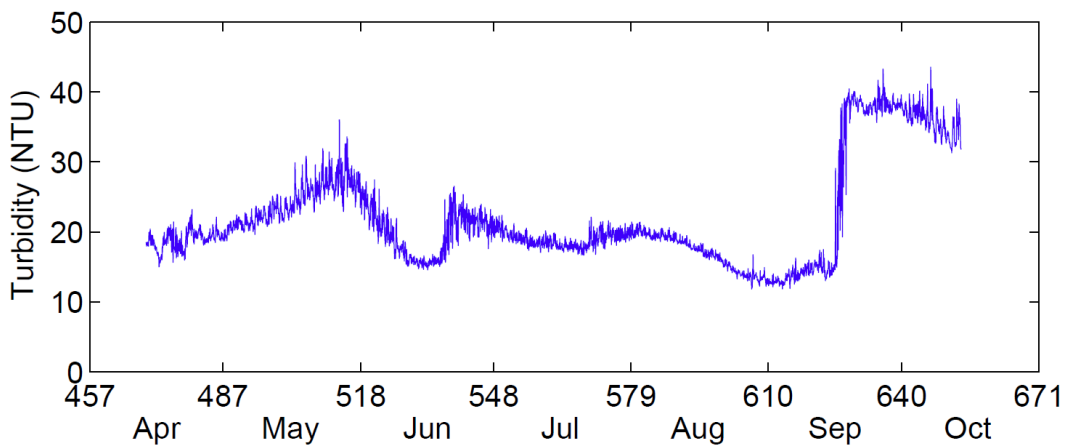


Figure 59. Turbidity data recorded at the log boom in Carpenter Reservoir, 13 April to 14 October, 2016. The recorder was at located 1.8 m above the bottom on the subsurface mooring approximately 1 km downstream of the log boom. At the start of the mooring period the turbidity recorder was at a depth of 30.9 m. As the water level rose, the depth of water above the turbidity recorder increased to 43.6 m by the end of the mooring period.

13 APPENDIX F: CE-QUAL-W2 model calibration

13.1 Approach

CE-QUAL-W2 (Version 3.7.2 that was used for this project) has many adjustable parameters. Where appropriate, input parameters were determined from observations. Many other parameters were set to the default values suggested in the user’s manual or to values from similar studies in literature. A few parameters were adjusted to closely match the field data. These and other selected parameters are summarized in Table 19.

Table 19. Model parameters used in this study and the default CE-QUAL-W2 values. The column on the right indicates whether the parameters were based on field observations (obs) or selected as calibration parameters (cal).

Parameter Description		Value	Default	Based on
Inorganic suspended solids				
SSS	Settling velocity ($\text{m}\cdot\text{day}^{-1}$)	0.2	1	cal
SEDRC	Sediment resuspension	OFF	OFF	
Mixing parameters				
FRICT	Chezy coefficient ($\text{m}^{0.5}\cdot\text{s}^{-1}$)	70	70	
AX	Longitudinal eddy viscosity ($\text{m}^2\cdot\text{s}^{-1}$)	1	1	
DX	Longitudinal eddy diffusivity ($\text{m}^2\cdot\text{s}^{-1}$)	1	1	
AZMAX	Maximum vertical eddy viscosity ($\text{m}^2\cdot\text{s}^{-1}$)	1	1	
FI	Internal friction coefficient (-)	0.015	0.015	
Scaling of meteorological forcing				
SHD	Shading coefficient (-)	1	1	
WSC	Wind sheltering coefficient (-)	0.7	1	cal
Heat exchange at air-water interface coefficients				
AFW	Wind function ($\text{W}\cdot\text{m}^{-2}\cdot\text{mm Hg}^{-1}$)	5	9.2	
BFW	Wind function ($\text{W}\cdot\text{m}^{-2}\cdot\text{mm Hg}^{-1}(\text{m}\cdot\text{s}^{-1})-\text{CFW}$)	7	0.46	cal
CFW	Wind function (-)	1	2	
Heat exchange at sediment-water interface				
TSED	Sediment temperature ($^{\circ}\text{C}$)	7	10	cal
CBHE	Coefficient of bottom heat exchange ($\text{W}\cdot\text{m}^{-2}\cdot^{\circ}\text{C}$)	0.3	0.3	
Light attenuation in water column				
EXH20	Light extinction coefficient of water † (m^{-1})	0.185	0.25	obs
EXSS	Turbidity-specific light extinction coefficient ($\text{m}^{-1}\cdot\text{NTU}^{-1}$)	0.081	0.1	obs
BETA	Fraction of solar radiation absorbed at water surface (-)	0.45	0.45	

†The parameter EXH20 is the light extinction coefficient due to water and dissolved substances.

The first step in model calibration was comparison of the measured and modelled water temperature, followed by specific conductance, and finally turbidity. Since water temperature controls the stratification and plays a key role in many physical, chemical, and biological processes, model calibration began with this quantity. Following water temperature, passive conservative scalars (e.g. specific conductance) were next, followed by the more challenging quantities, such as suspended particle concentration that was modelled as turbidity.

The modelled results were not expected to perfectly match the field observations for a variety of reasons, two of which are highlighted herein. First, by definition, a model is a simplified representation of a system — the system here being the spatial and temporal evolution of temperature, conductivity, turbidity, and nutrient concentration in Carpenter Reservoir. The model, CE-QUAL-W2, includes many of the important physical

processes that drive this system; however, some must be approximated, parameterized, or omitted, otherwise the model would be impractical and would complicate the understanding of the real system. Second, field observations were measured at a specific location and time; whereas the model is discretized into a finite number of spatial cells and time steps. Within a given cell and between subsequent time steps, the natural system will vary; however, the model contains a single value for each model variable within each cell at each timestep. That is, the field observations represent point measurements at specific times; whereas, the model results represent spatially-averaged values at discrete time steps. Most notably, CE-QUAL-W2 is a laterally-averaged model, meaning that variations in the cross-stream (lateral) direction are neglected. This approximation is valid for long and narrow water bodies, such as Carpenter Reservoir. Other studies have had success using laterally-averaged models for water bodies with similar geometries to Carpenter (e.g. Gelda et al. 2015; Bonalumi et al. 2012), which provides confidence in the modeling approach.

The model was calibrated manually by adjusting a subset of parameters until the computed results best matched the field observations in 2015 and 2016. We evaluated the performance of the model based on two goodness-of-fit statistics: the mean error (ME) and the root-mean-square error (RMSE). ME is the average difference between the modelled values and measured data and is a measure of model bias. RMSE is the square root of the mean of the squared differences between the modelled values and measured data and is a measure of model accuracy. ME and RMSE results for each of water temperature, specific conductance, and turbidity are given in Table 20. Further detail is given in the following sections.

Table 20. Mean error and root-mean-square error (RMSE) of temperature, conductivity, and turbidity. CE-QUAL-W2 model output compared to field measurements from the moored thermistor chain attached to the log boom, the Sea-Bird profiles, and tributary sampling at the Bridge powerhouse outflow on Seton, and the Lower Bridge River downstream of Terzaghi Dam.

Measurement source	Variable	Unit	Mean error		RMSE	
			Year 2015	Year 2016	Year 2015	Year 2016
Mooring	Temperature	°C	0.15	0.17	0.93	1.26
Sea-Bird profiles	Temperature	°C	0.26	0.37	1.00	1.63
	Conductivity	$\mu\text{S}\cdot\text{cm}^{-1}$	-4.13	-3.66	8.06	8.45
	Turbidity	NTU	0.34	2.04	5.44	6.28
Tributary sampling	Temperature	°C	-0.60	-0.96	0.83	1.57
	Turbidity	NTU	-2.22	4.43	6.53	5.96

13.2 Water temperature

Water temperature in a reservoir is controlled by a variety of factors including: inflows, outflows, heat exchange at the air-water and sediment-water interfaces, solar radiation, light extinction, and mixing processes within the reservoir. Therefore, to accurately model the variation in water temperature within a reservoir, a detailed set of hydrological and meteorological field data are needed to provide the initial conditions and boundary conditions for model calibration.

The most common model parameter to be adjusted is the wind sheltering coefficient (WSC). This parameter adjusts both for differences in wind from shore to water, and for variations in wind along the reservoir. Note the model for Carpenter Reservoir used the wind from a single land-based station at Fivemile located approximately halfway up the reservoir. The model was run varying WSC from 0.5 to 1.0 and a value of 0.7 produced the closest match to the field data.

The surface water temperature was also found to be sensitive to the wind-speed dependence of the evaporation, $f(W)$. This is consistent with the CE-QUAL-W2 Manual which noted that “the most uncertain parameter in the surface heat exchange computations is the evaporative wind speed function, $f(W)$ ” (Cole and Wells 2015, pA-111), and noted that the coefficients of this function depend on the size and shape of the water body, as well as the location of the wind measurements. For Carpenter Reservoir the default function was chosen, $f(W) = AFW + BFW * W^{CFW}$, and the coefficients of this function were adjusted slightly to provide a better match between the measured and modelled surface temperature (Table 19). Similar adjustments were used in other studies, for example, in Kobler et al. (2018) and Bonalumi et al. (2012).

Modelled water temperature in Carpenter Reservoir was compared to two sets of field data: (1) moored data from the thermistor chain at station C2, and (2) vertical profiles from the monthly CTD surveys at stations C1 to C9. The moored and modelled data are compared in Figure 60, with reasonable agreement in both 2015 (RMSE 0.9°C) and 2016 (RMSE 1.3°C). Note, in Figure 60 the measured and modelled temperature are shown for only five depths, whereas the RMSE was computed using daily-averaged data from every 1m over the top 30m depth. The modelled temperature showed similar agreement when compared to the CTD profiles in 2015 (Figure 61, RMSE 1.0°C) and 2016 (Figure 62, RMSE 1.6°C). The agreement between measured and modelled water temperature for Carpenter Reservoir are comparable to those obtained in similar studies (e.g. Gelda et al. 2015, Kobler et al. 2018). Differences between the observations and the model are greatest in the thermocline, as a result of large gradients. Other than the thermocline, the largest differences occurred in June and early July 2016, when water release from Carpenter Reservoir to the lower Bridge River was exceptionally high (Figure 16).

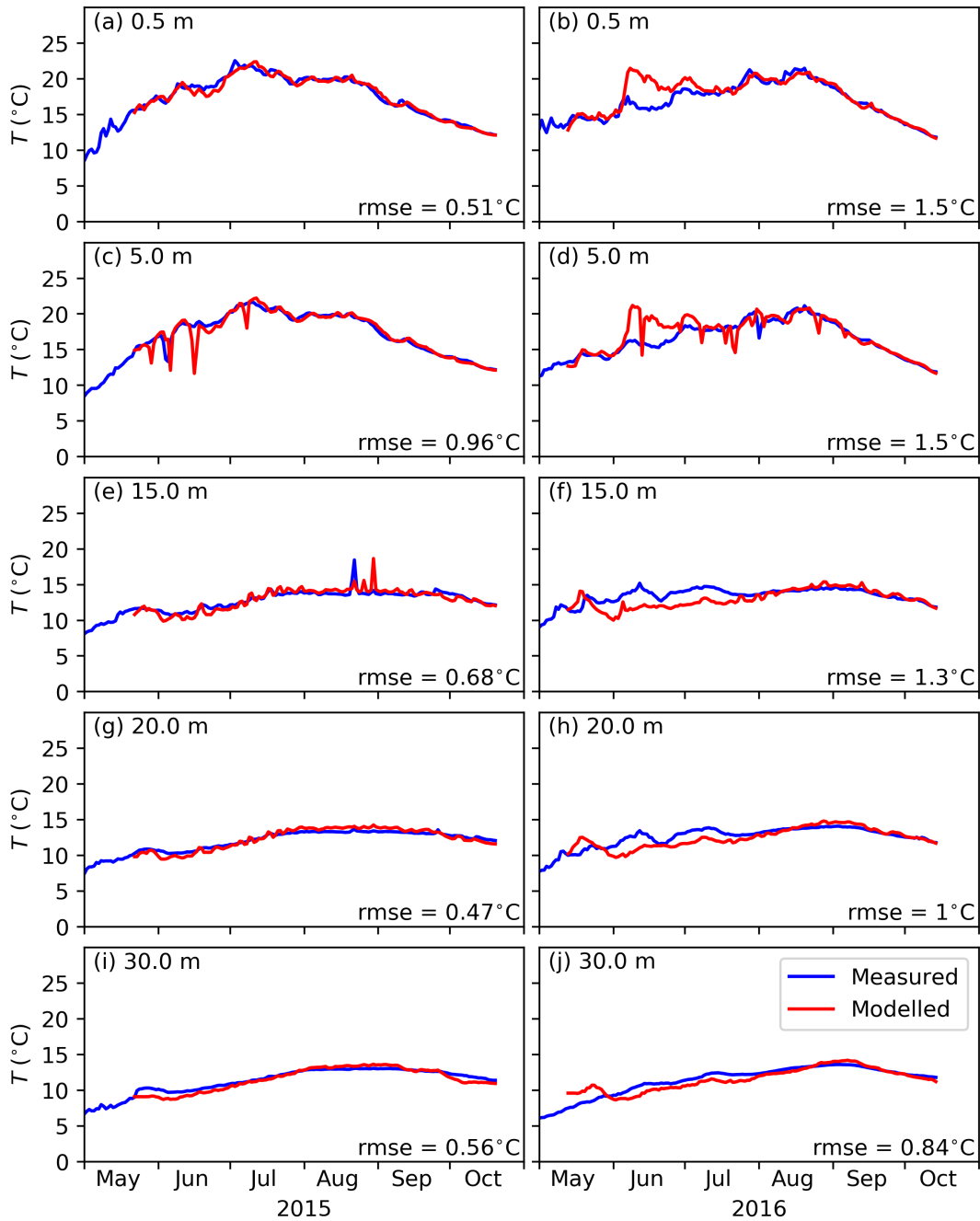


Figure 60. Comparison of the temperature measured at the log boom (blue) and the temperature from segment 53 (station C2) of the model (red) at depths of (a) 0.5, (b) 5, (c) 15, (d) 20 and (e) 30 m during field Year 1 (2015) (left), and Field Year 2 (2016) (right).

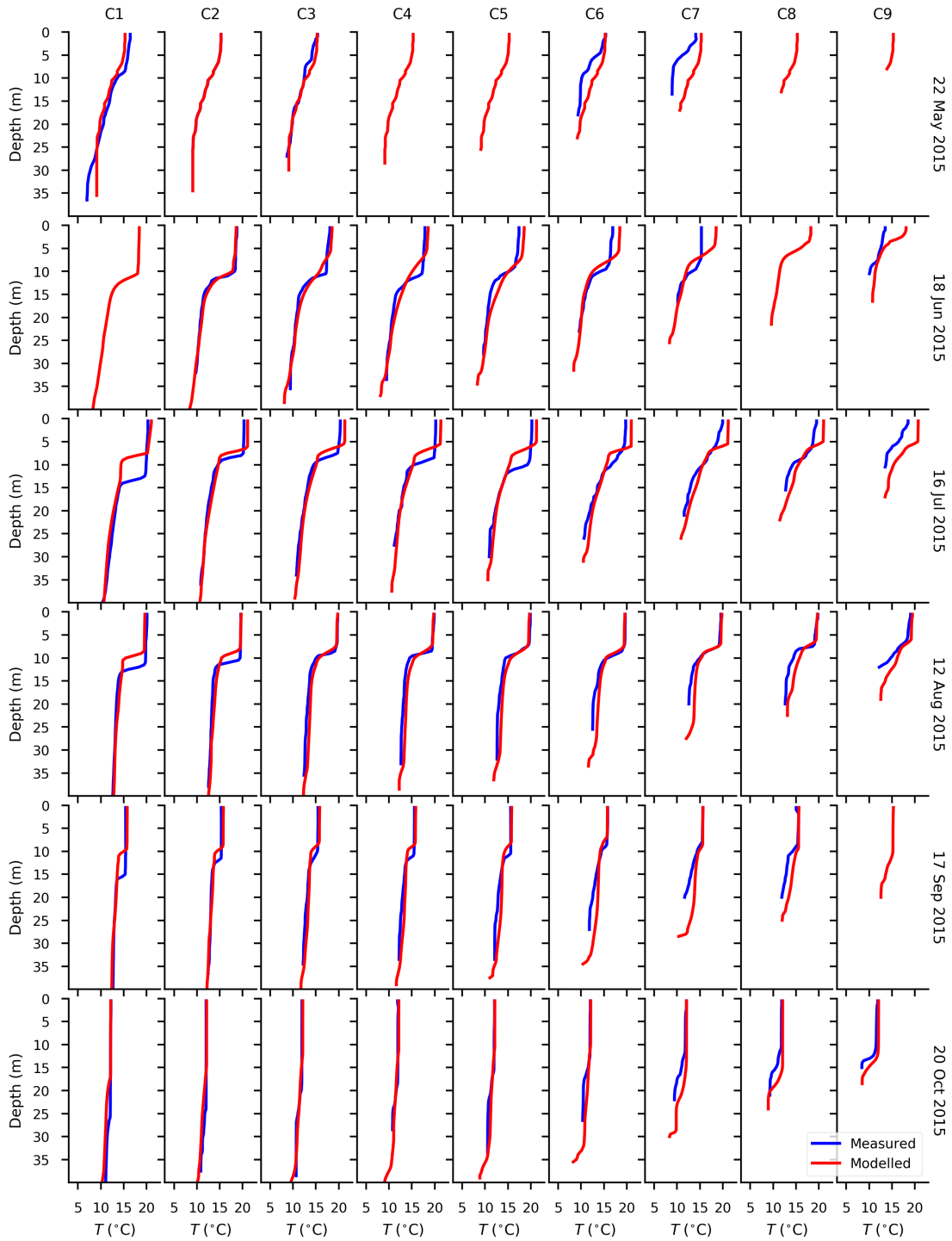


Figure 61. Measured and modelled temperature profiles at station C1--C9 in 2015 (Field Year 1).

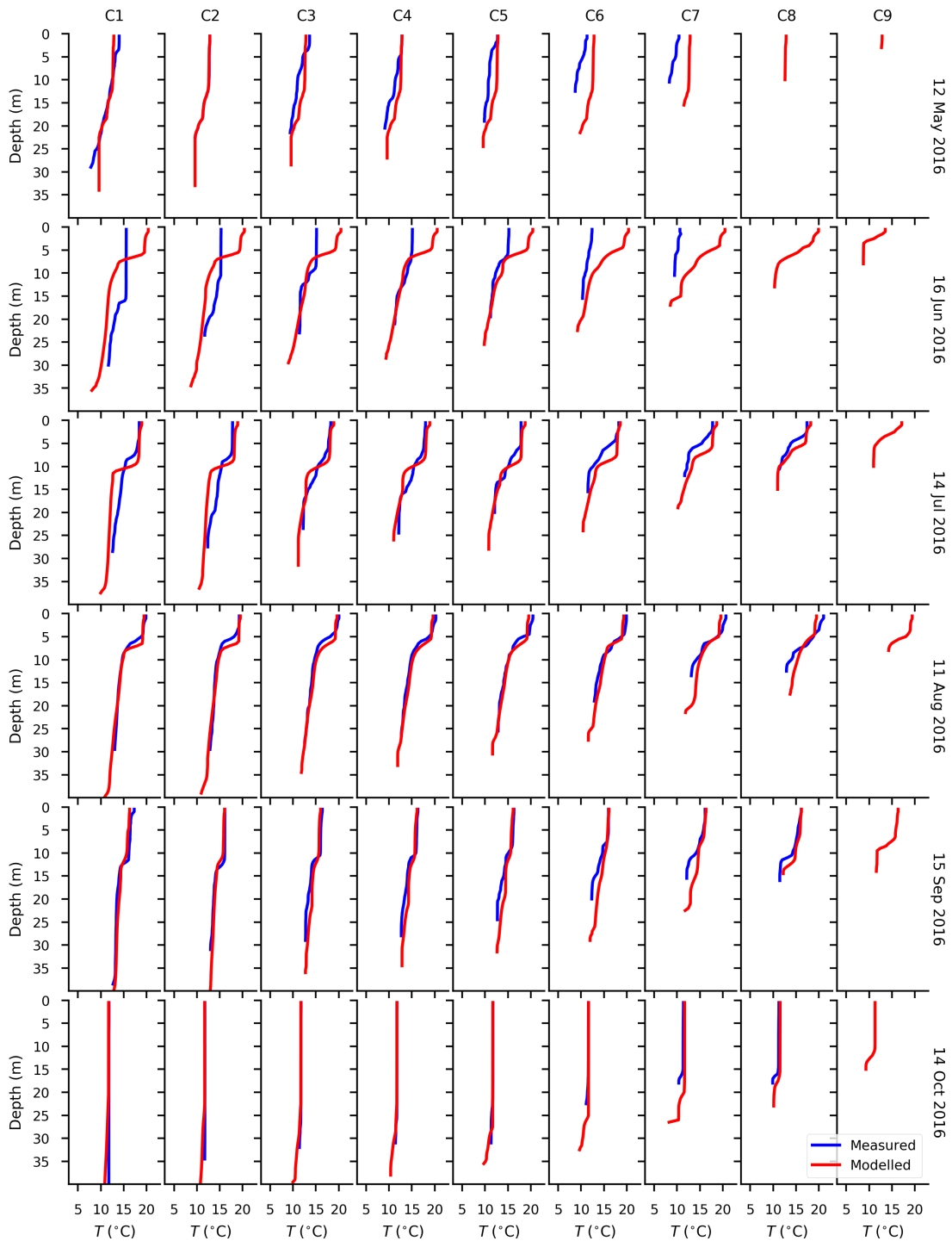


Figure 62. Measured and modelled temperature profiles at station C1--C9 in 2016 (Field Year 2).

13.3 Hypolimnetic Mixing

Comparison of the modelled and observed temperature, conductivity and turbidity in the hypolimnion of Carpenter Reservoir showed that the modelled fields had more horizontal and vertical gradients than observed in the field measurements. Since the inflows were colder than the ambient water they tended to slot in at the reservoir bottom. The resulting gradients appear to arise from either insufficient entrainment as the plunging inflows traverse the hypolimnion or insufficient mixing within the hypolimnion. Changes to a number of model parameters were tried (e.g. turbulence scheme, vertical and horizontal diffusivities), but these had little effect on the gradients in the model results.

The model includes three methods for placing inflows in the water body (CE-QUAL-W2 parameter PTRC):

PTRC=DISTR, distributes the inflow over the entire water column,

PTRC=DENSITY, places the inflow at neutral density in the water column (used in the model for Carpenter Reservoir), and

PTRC=SPECIFY, places the inflow over a range of layer elevations.

Several recent studies have specified the vertical extent of the inflows over a range of depths within the hypolimnion, presumably to achieve appropriate mixing between the inflow and the ambient water (Kobler et al. 2018, Bonalumi et al. 2012). However, this was not an option for our modelling of Carpenter Reservoir because of the dramatic change in water level, and since we were particularly interested in the case which begins with low water level in spring. Specifying a range of elevations that would contribute to mixing in the hypolimnion in the summer would, in some cases, end up distributing the inflow throughout the epilimnion and hypolimnion at low water level in spring. Mixing in the hypolimnion of lake models is a problem that has received comparatively little attention.

To address this problem, the major tributary inflows – Hurley, Gun, and Tyaughton – were inserted into the first active segment, while the inflow from La Joie Dam was placed at the current upstream segment (CUS), which may vary during a simulation, depending on the water level. If the CUS is downstream of a segment receiving tributary inflow, then the tributary inflow was added to the CUS to maintain the water balance. This change had little effect on the evolution of the stratification over the model period but resulted in fewer vertical gradients in the hypolimnion. Note that for much of the time the affected segments receiving water from Gun and Tyaughton Creeks were dewatered or were shallow. The rest of the tributary inflows were inserted at the depth of neutral buoyancy into the segments outlined in Table 4.

13.4 Specific Conductance

Variation in specific conductance, C25, was a useful tracer to determine the origin of water and to estimate the exchange between water masses. Modelled profiles of C25 are compared to the monthly CTD casts at stations C1 to C9 in Figure 63 and Figure 64. The model results agree reasonably well with the field data both in 2015 (RMSE $8.0 \mu\text{S cm}^{-1}$) and in 2016 (RMSE $8.4 \mu\text{S cm}^{-1}$). Given the range of measured C25 in the reservoir ($70\text{-}110 \mu\text{S}\cdot\text{cm}^{-1}$), the model error is approximately 7-12 percent of the measured values. Similar agreement was obtained in Sullivan et al. (2007); while the numerical value of the RMSE was lower (between 2.4 and $3.1 \mu\text{S cm}^{-1}$), the model error was a similar proportion, approximately 5-10 percent of the measured range (27 to $47 \mu\text{S}\cdot\text{cm}^{-1}$).

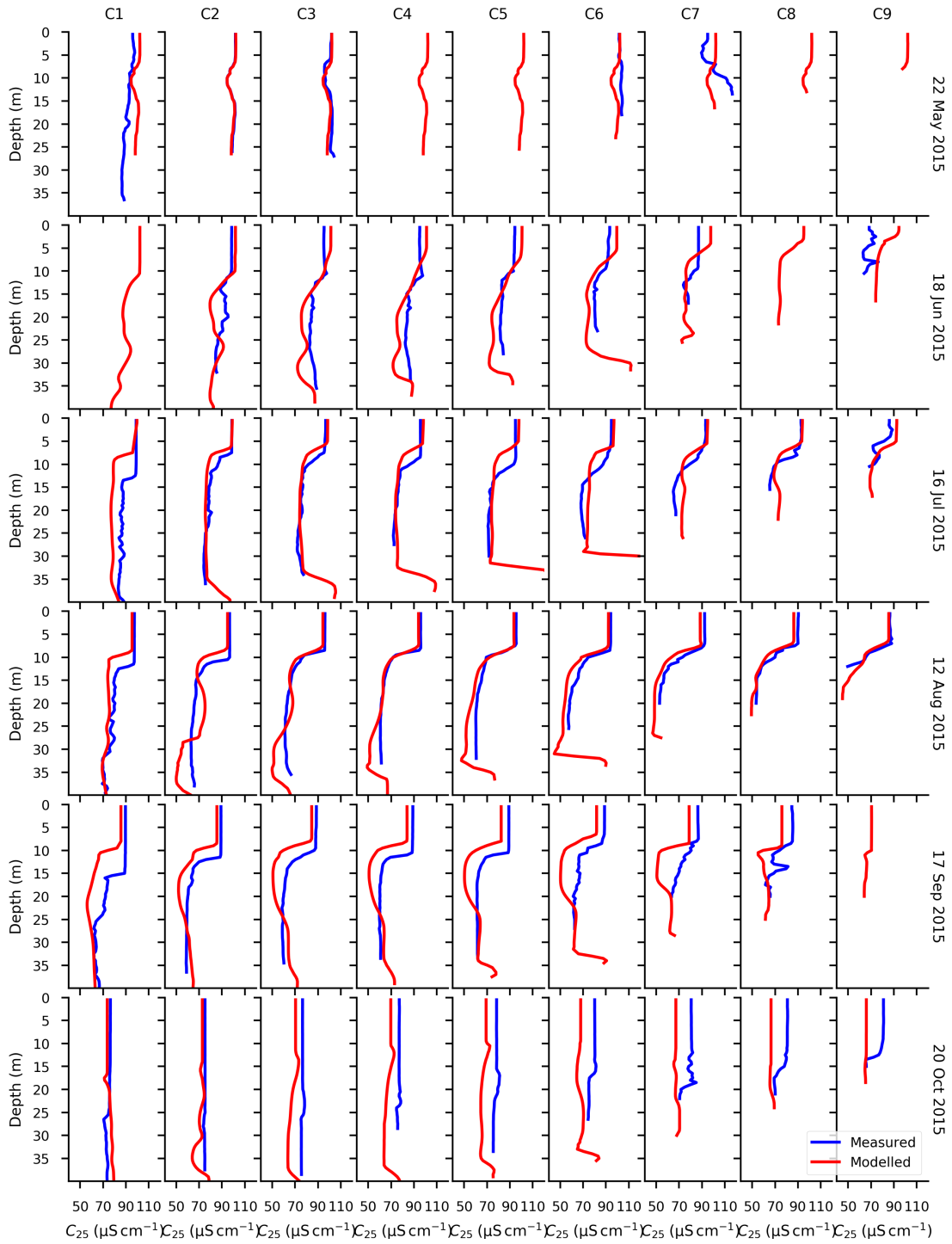


Figure 63. Measured and modelled conductivity profiles at station C1--C9 in 2015 (Field Year 1).

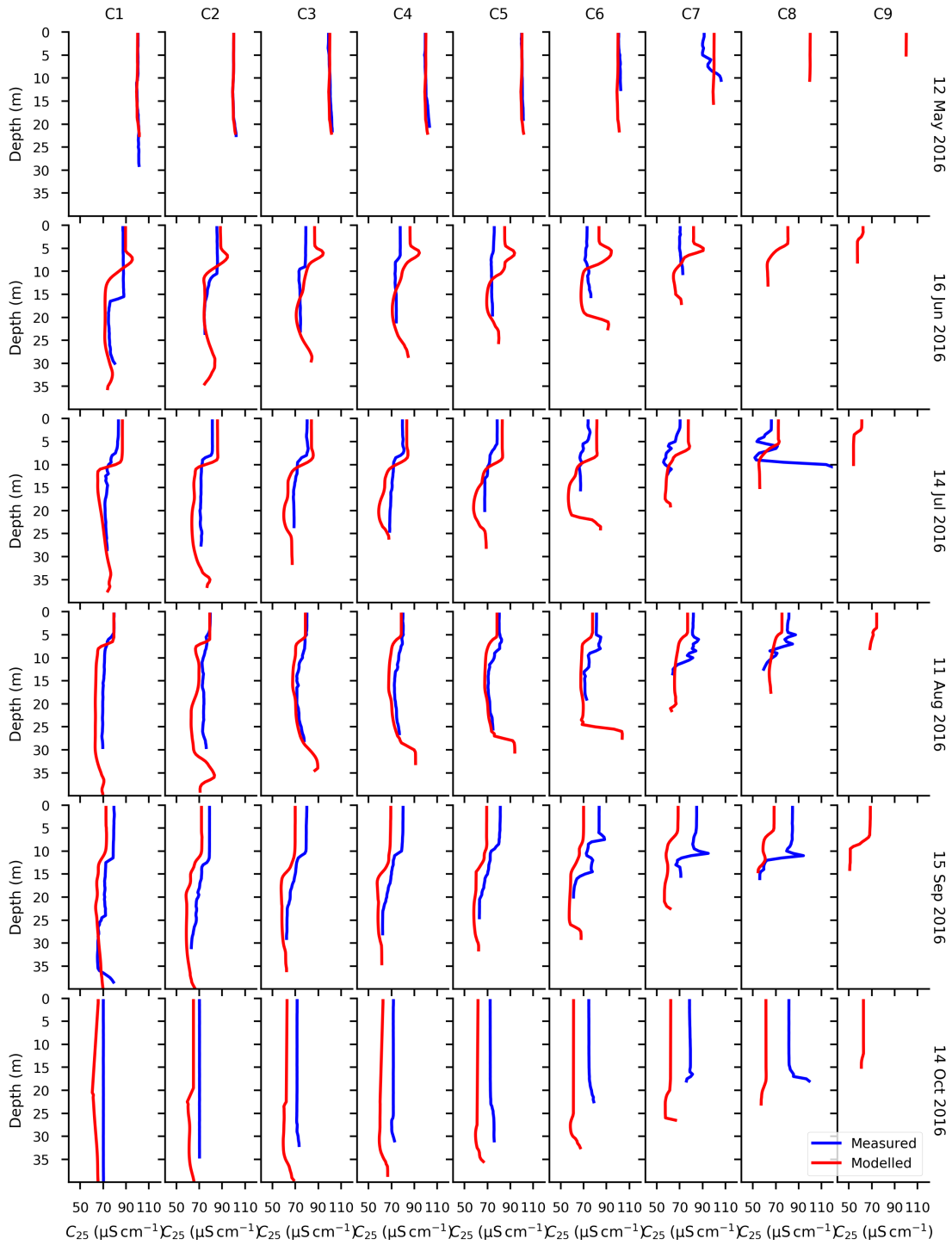


Figure 64. Measured and modelled conductivity profiles at station C1--C9 in 2016 (Field Year 2).

13.5 Turbidity

A variety of factors influence the turbidity in a receiving water body including the stratification of the water body, turbidity and plunge depth of the inflows, suspended particle size, and particle settling rate. Turbidity in the surface water limits light penetration, which reduces the depth of the photic zone and alters the thermal structure of the surface mixed layer. Changes in light availability and water temperature can, in turn, affect primary productivity (See Section 5.2).

During model calibration, the particle settling velocity was adjusted to best match the field data. A settling velocity of $SSS = 0.2 \text{ m}\cdot\text{day}^{-1}$ was selected (Table 19), which corresponds to Stokes settling of particles with a diameter of $\sim 2 \mu\text{m}$. Suspended particles in Carpenter Reservoir have a range of sizes and settling rates, they do not settle under the idealized conditions assumed by Stokes' Law (dilute suspensions of spherical particles in a quiescent fluid), and flocculation may also play a role (Gilbert and Lamoureux 2004, Hodder and Gilbert 2007, Hodder 2009). Therefore, the selected settling rate is not intended to represent a single particle size, rather, it represents the best fit to the distribution of particles giving rise to turbidity in Carpenter Reservoir.

Modelled turbidity profiles are compared to monthly Sea-Bird casts at stations C1 to C9 in Figure 65 and Figure 66. Modelled turbidity agrees reasonably well with measurements in both 2015 (RMSE 5.4 NTU) and 2016 (RMSE 6.3 NTU). Given the range of measured turbidity in the reservoir (0-40 NTU), the model error is approximately 15 percent of the measured values. Similar agreement was obtained in Sullivan et al. (2007); while the numerical value of the RMSE was significantly lower (0.7 NTU), the model error was a similar proportion, approximately 11-12 percent of the measured range (0 to 6 NTU).

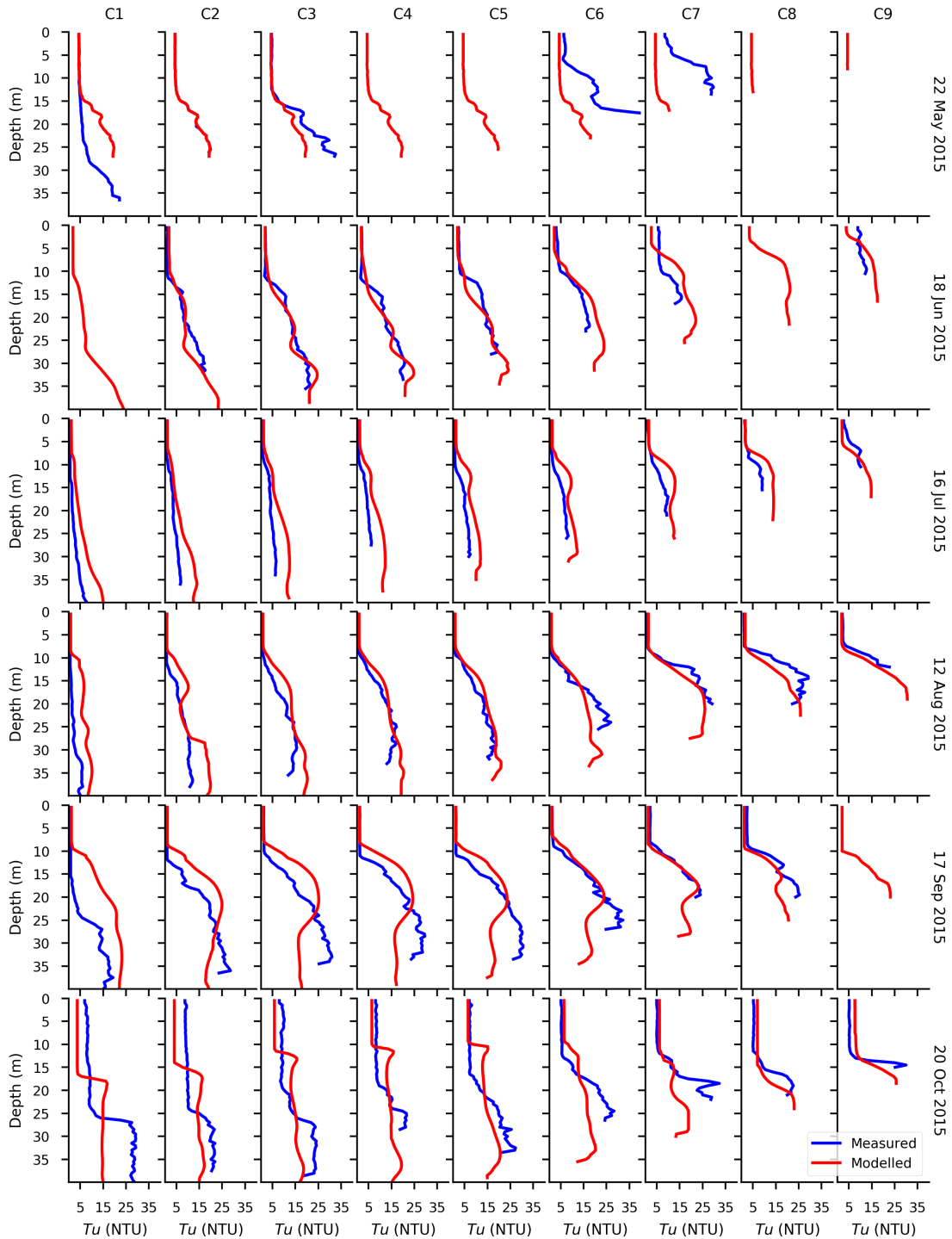


Figure 65. Measured and modelled turbidity profiles at station C1--C9 in 2015 (Field Year 1).

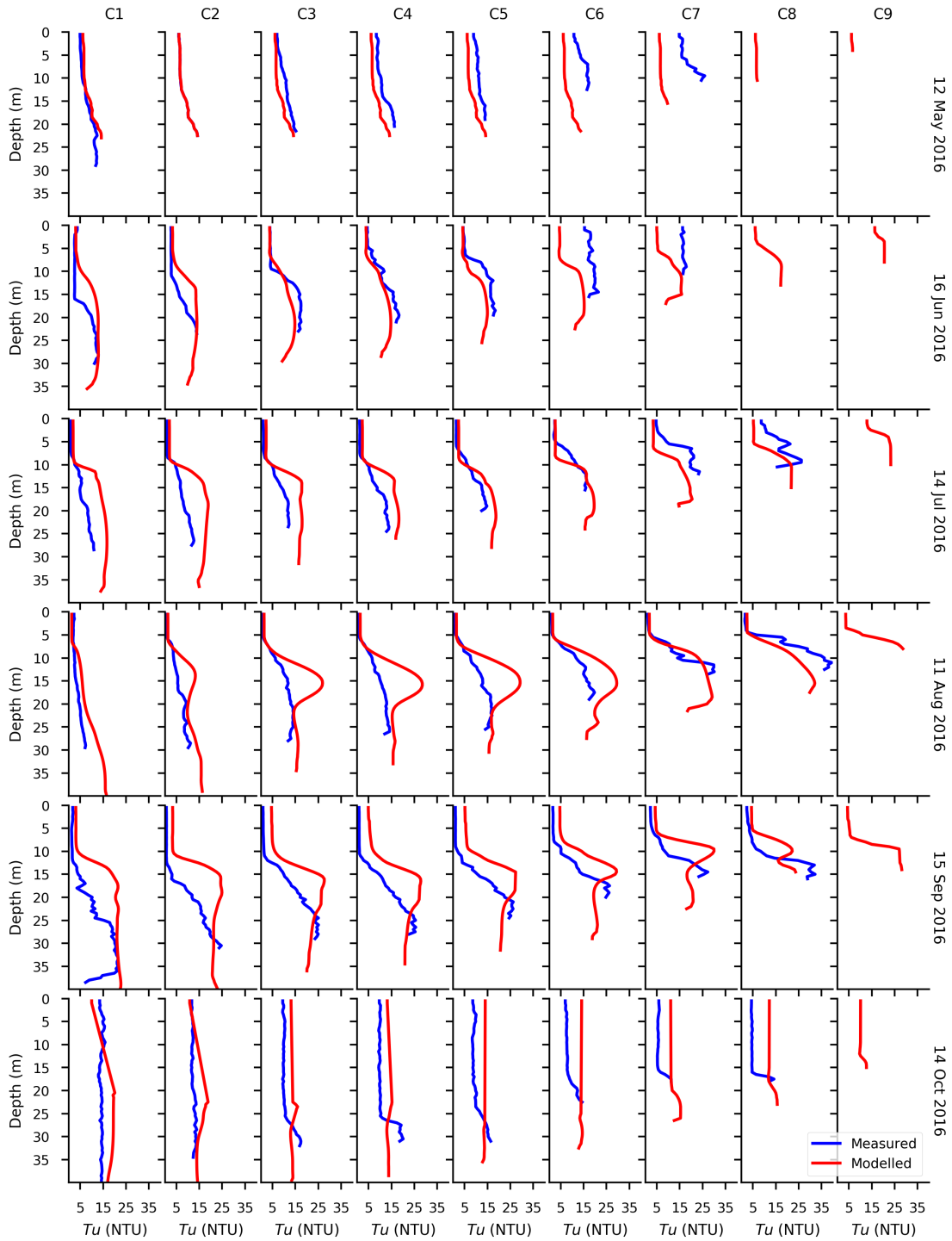


Figure 66. Measured and modelled turbidity profiles at station C1--C9 in 2016 (Field Year 2).

13.6 Outflows

To study the effect of Carpenter Reservoir operations on downstream water bodies, we modelled the outflow temperature and turbidity to (1) the outflows to the Bridge powerhouses on Seton Lake, and (2) the Lower Bridge River. To verify that the model accurately represents observed conditions, it was tested using reservoir operations from field years in 2015 and 2016. Modelled water temperature and turbidity agree reasonably well with measurements, with an RMSE of 0.8°C and 6.5 NTU in 2015, and 1.6°C and 6.0 NTU in 2016, respectively (Figure 67).

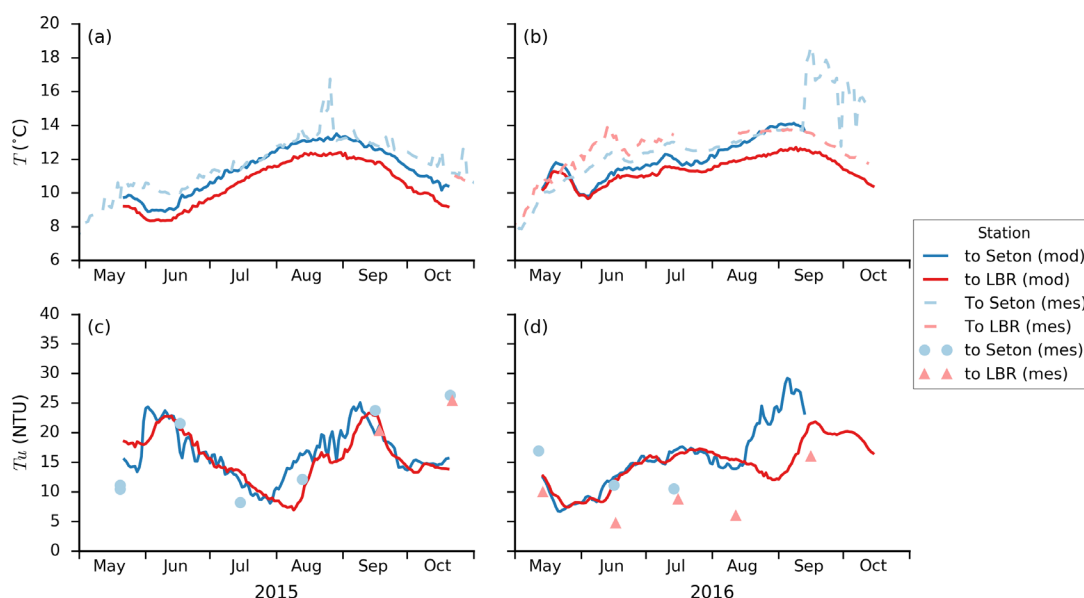


Figure 67. Measured and modelled (a,b) temperature and (c,d) turbidity; in (a,c) 2015 and (b,d) 2016; at (blue) Bridge powerhouse on Seton Lake (to Seton) and (red) the Lower Bridge River downstream of Terzaghi Dam (to LBR); (solid lines) model output; (dashed lines) tributary temperature loggers; (markers) tributary sampling with the YSI probe; (mod) model output; (mes) measured values. The Bridge powerhouse units were shut from mid-September to mid-October which shows up as a data gap for the model output. From 14 Jul to 11 Aug 2016, the tributary temperature logger in the Lower Bridge River was malfunctioning, which shows up as a data gap for the measured data.

The modelled temperature to the Lower Bridge River (LBR) was consistently cooler than to Seton, by as much as $\sim 1^\circ\text{C}$. In contrast, the field data from 2016 suggest that the outflow temperature to LBR was similar or slightly warmer than the outflow to Seton (Figure 67b, ignore from early September onward when there was no outflow to Seton). Since the outlet sills to LBR (599.69m) and to Seton (600.61m for BR1 and 599.54m for BR2) are at the same elevation, the temperature from the two outflows should be similar. A potential reason for the discrepancy is that the model withdraws water from a range of depths depending on the stratification and flow rate, and the range

of depths available includes deeper colder water for the outflow to LBR than for the outflow to Seton.

Other studies have encountered similar challenges; for example, Buccola et al. (2013) used CE-QUAL-W2 to examine how changes in both reservoir operation and changes to the structural release points might affect downstream water temperature. In one case, they modelled a release point as a line source, and the range of depths was adjusted to best matched their field data.

13.7 Light attenuation

A seasonal variation in light attenuation was observed in Carpenter Reservoir, with shallow photic depths in May, followed by increasingly deeper photic depths over the summer months, and finally shallower photic depths again near fall turnover (Figure 17 and Figure 18). A regression between the average measured turbidity in the photic zone and light extinction coefficients computed from the Sea-Bird PAR measurements showed that light extinction and turbidity were highly correlated ($R^2 = 0.91$, Figure 68).

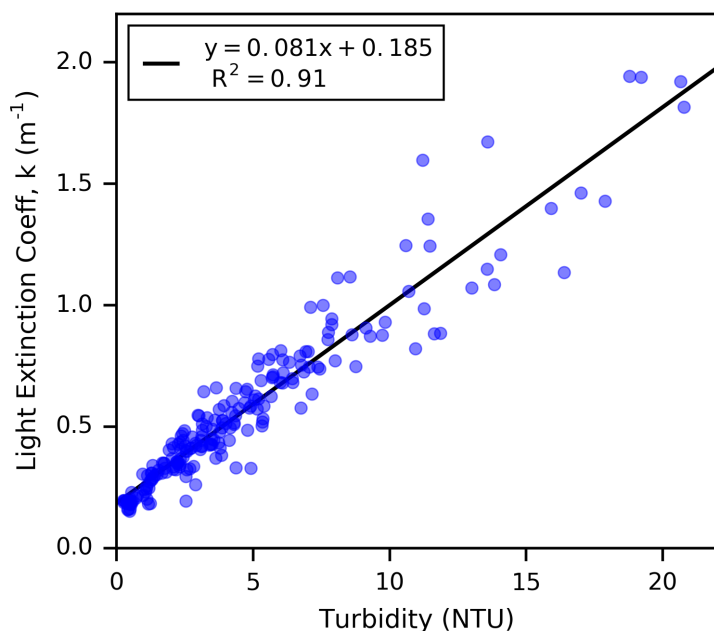


Figure 68. Scatter plot of light extinction coefficient versus turbidity. Each data point corresponds to one Sea-Bird profile where the extinction coefficient was calculated from the PAR measurements and the turbidity was the mean value from the water surface to the 1 percent light level. Measurements from Carpenter Reservoir, Seton Lake, and Anderson Lake are included in the regression.

The regression enabled the parameterization of the extinction coefficient in the CE-QUAL-W2 model as a function of turbidity. The extinction coefficient, k_{total} , was divided into two components: k_{H_2O} for the light extinction due to water without particles,

and k_{ISS} for the light extinction due to inorganic suspended solids (measured as turbidity). k_{H2O} is a constant given by the intercept (0.185 m^{-1}) of the best fit line in Figure 68; and $k_{ISS} = m_{ISS} Tu$, where m_{ISS} is the slope ($0.081 \text{ m}^{-1} \text{ NTU}^{-1}$) of the best fit line in Figure 68 and Tu is turbidity.

13.8 References cited in Appendix F

- Bonalumi, M., Anselmetti, F. S., Wüest, A., & Schmid, M. (2012). Modeling of temperature and turbidity in a natural lake and a reservoir connected by pumped-storage operations. *Water Resources Research*, 48(8).
- Buccola, N. L., Rounds, S. A., Sullivan, A. B., & Risley, J. C. (2012). Simulating potential structural and operational changes for Detroit Dam on the North Santiam River, Oregon, for downstream temperature management. US Department of the Interior, US Geological Survey.
- Cole, T. M., & Wells, S. A. (2015). CE-QUAL-W2: A two-dimensional, laterally averaged, hydrodynamic and water quality model, User's Manual, version 3.72.
- Gelda, R. K., King, A. T., Effler, S. W., Schweitzer, S. A., & Cowen, E. A. (2015). Testing and application of a two-dimensional hydrothermal/transport model for a long, deep, and narrow lake with moderate Burger number. *Inland Waters*, 5(4), 387-402.
- Gilbert, R., & Lamoureux, S. (2004). Processes affecting deposition of sediment in a small, morphologically complex lake. *Journal of Paleolimnology*, 31(1), 37-48.
- Hodder, K. R. (2009). Flocculation: a key process in the sediment flux of a large, glacier-fed lake. *Earth Surface Processes and Landforms*, 34(8), 1151-1163.
- Hodder, K. R., & Gilbert, R. (2007). Evidence for flocculation in glacier-fed Lillooet Lake, British Columbia. *Water research*, 41(12), 2748-2762.
- Kobler, U. G., Wüest, A., & Schmid, M. (2018). Effects of Lake–Reservoir Pumped-Storage Operations on Temperature and Water Quality. *Sustainability*, 10, 1968.
- Sullivan, A. B., Rounds, S. A., Sobieszczyk, S., & Bragg, H. M. (2007). Modeling hydrodynamics, water temperature, and suspended sediment in Detroit Lake, Oregon. US Geological Survey.

14 APPENDIX G: FIGURES SUPPORTING SCENARIOS MODELLED IN CEQUAL-W2

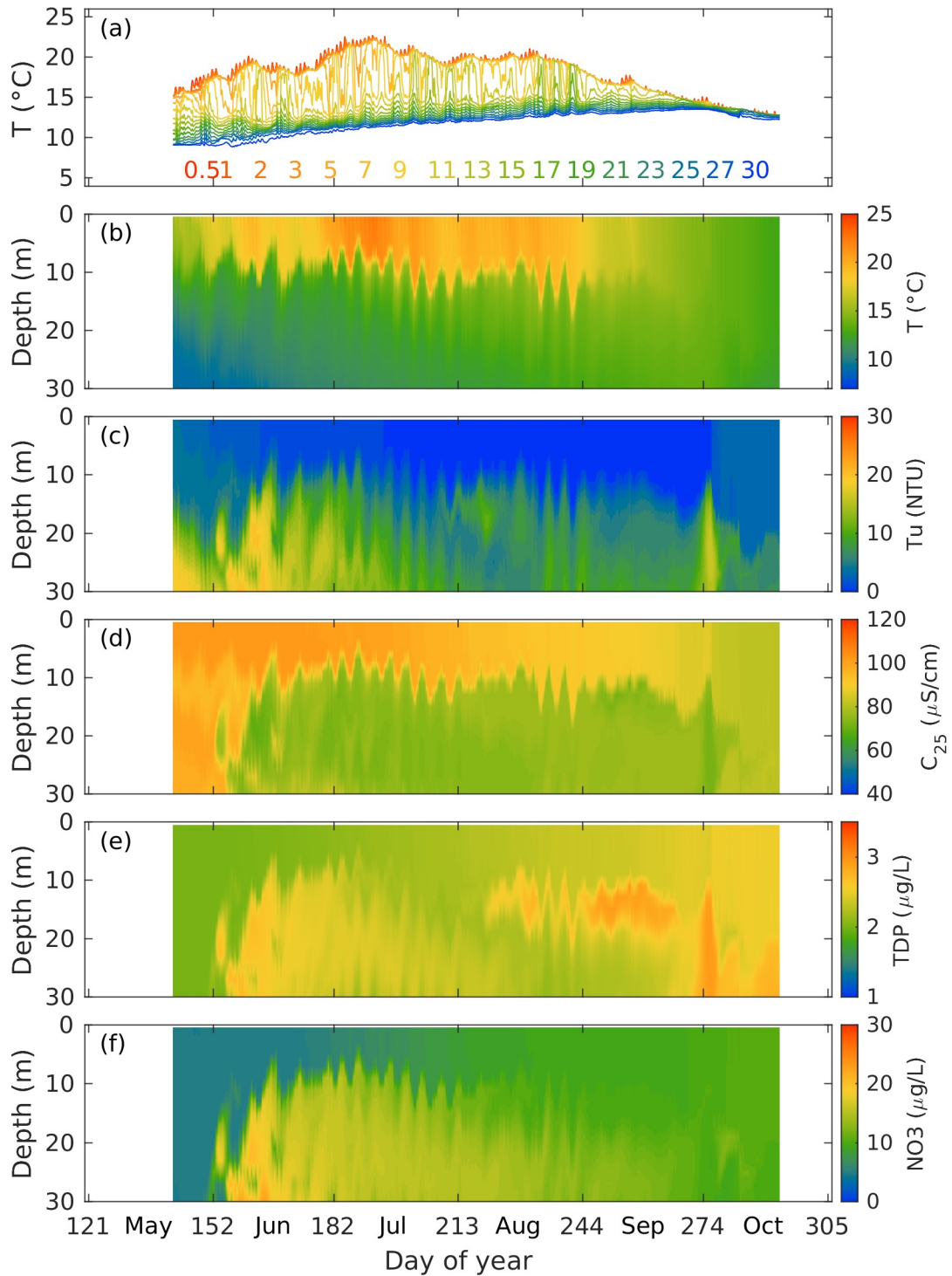


Figure 69. Scenario 1, Clear Surface Layer (1973). Modelled water quality parameters at segment 53 (station C2).

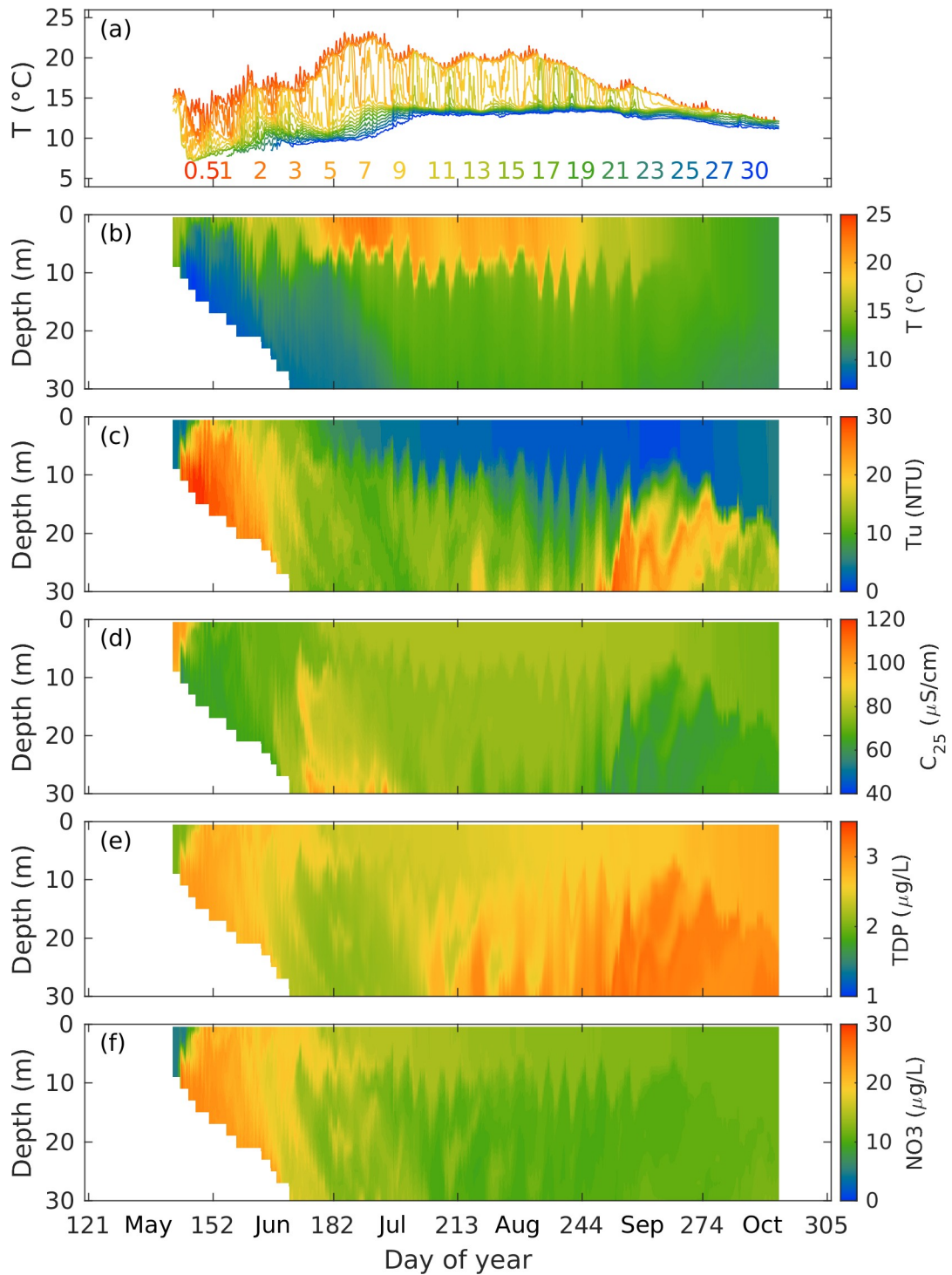


Figure 70. Scenario 2, Turbid Surface Layer (1999). Modelled water quality parameters at segment 53 (station C2).

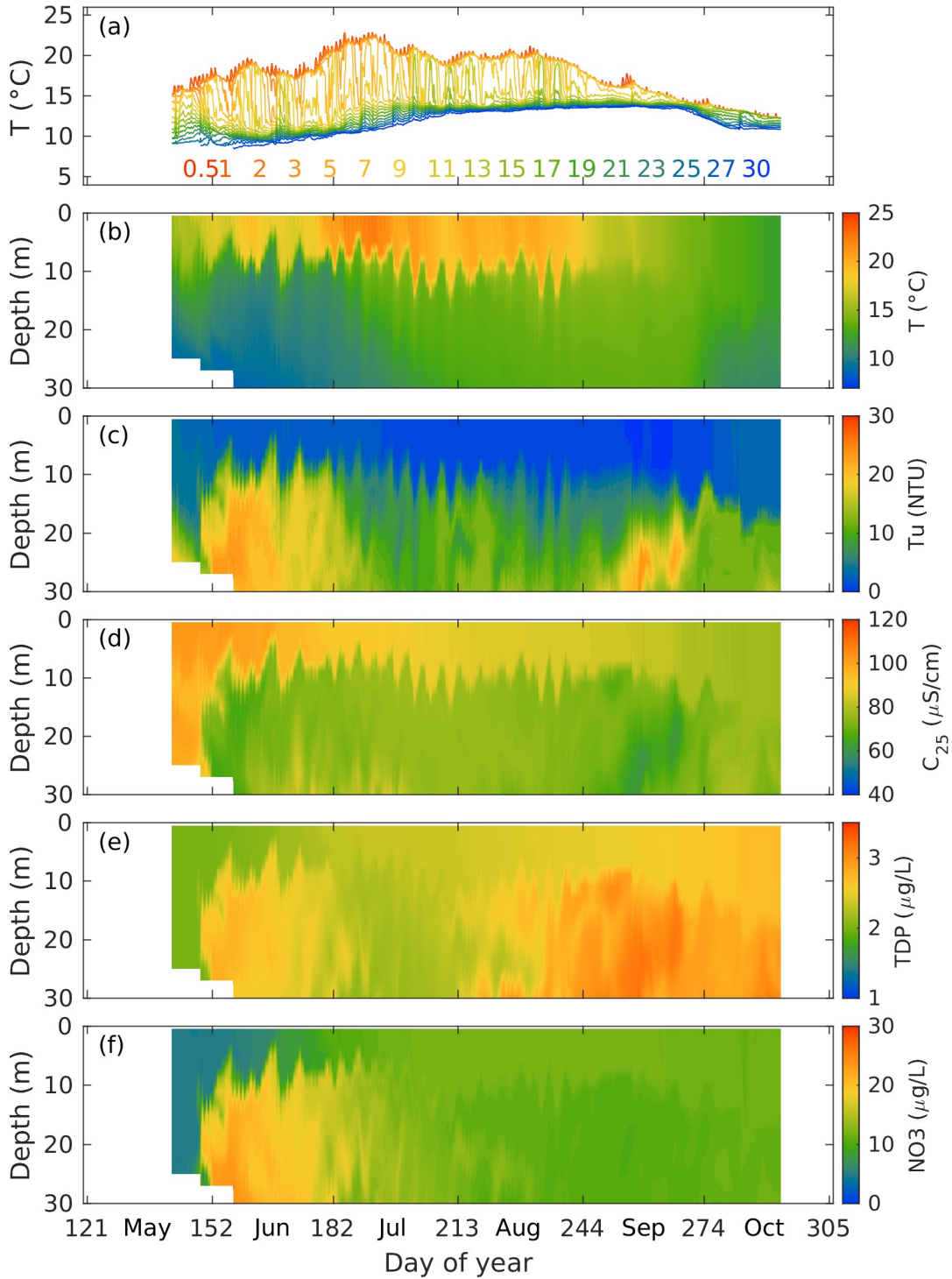


Figure 71. Scenario 3, Normal Operations (2011). Modelled water quality parameters at segment 53 (station C2).

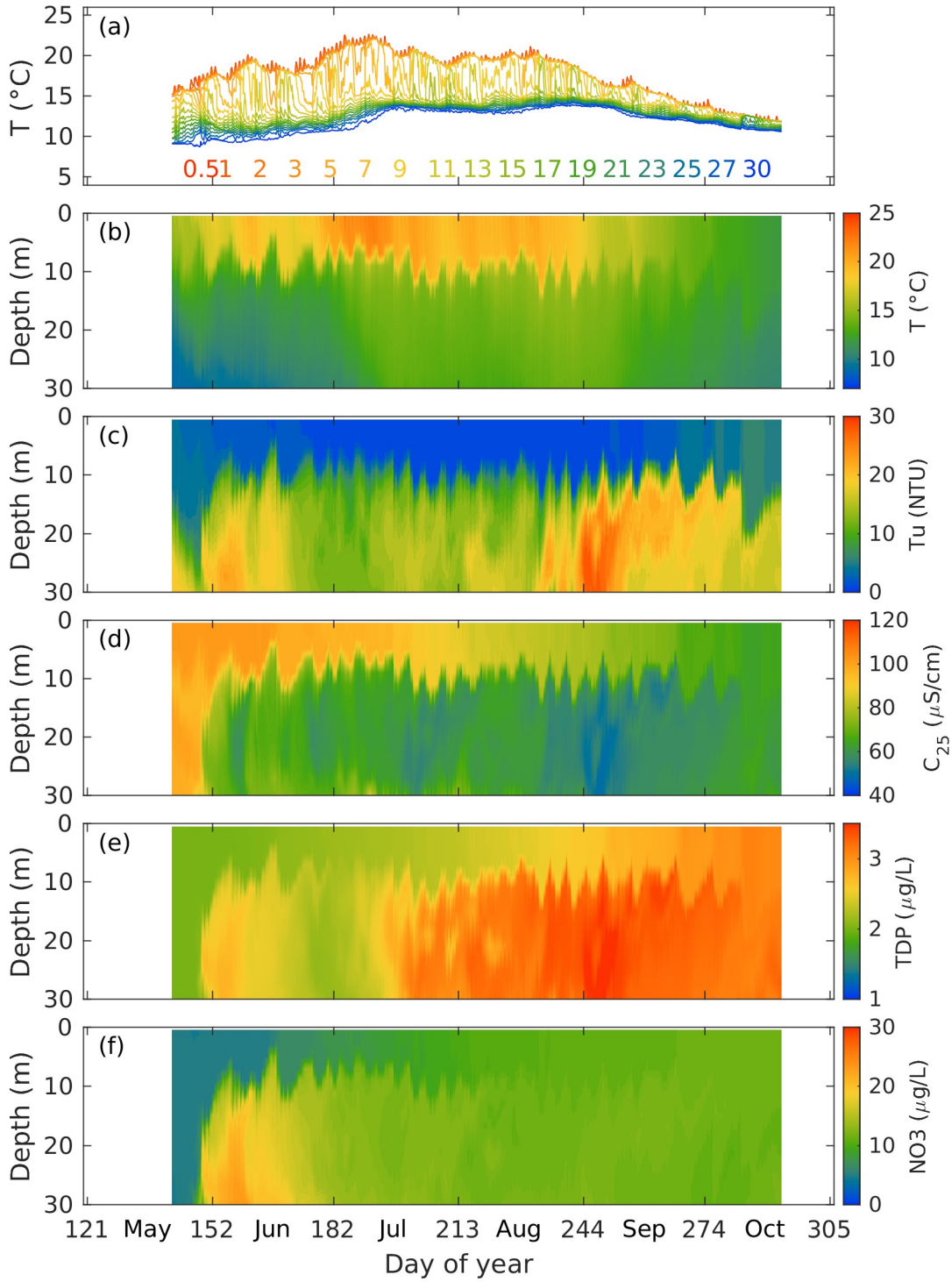


Figure 72. Scenario 4, Low Downton Reservoir (2016). Modelled water quality parameters at segment 53 (station C2).

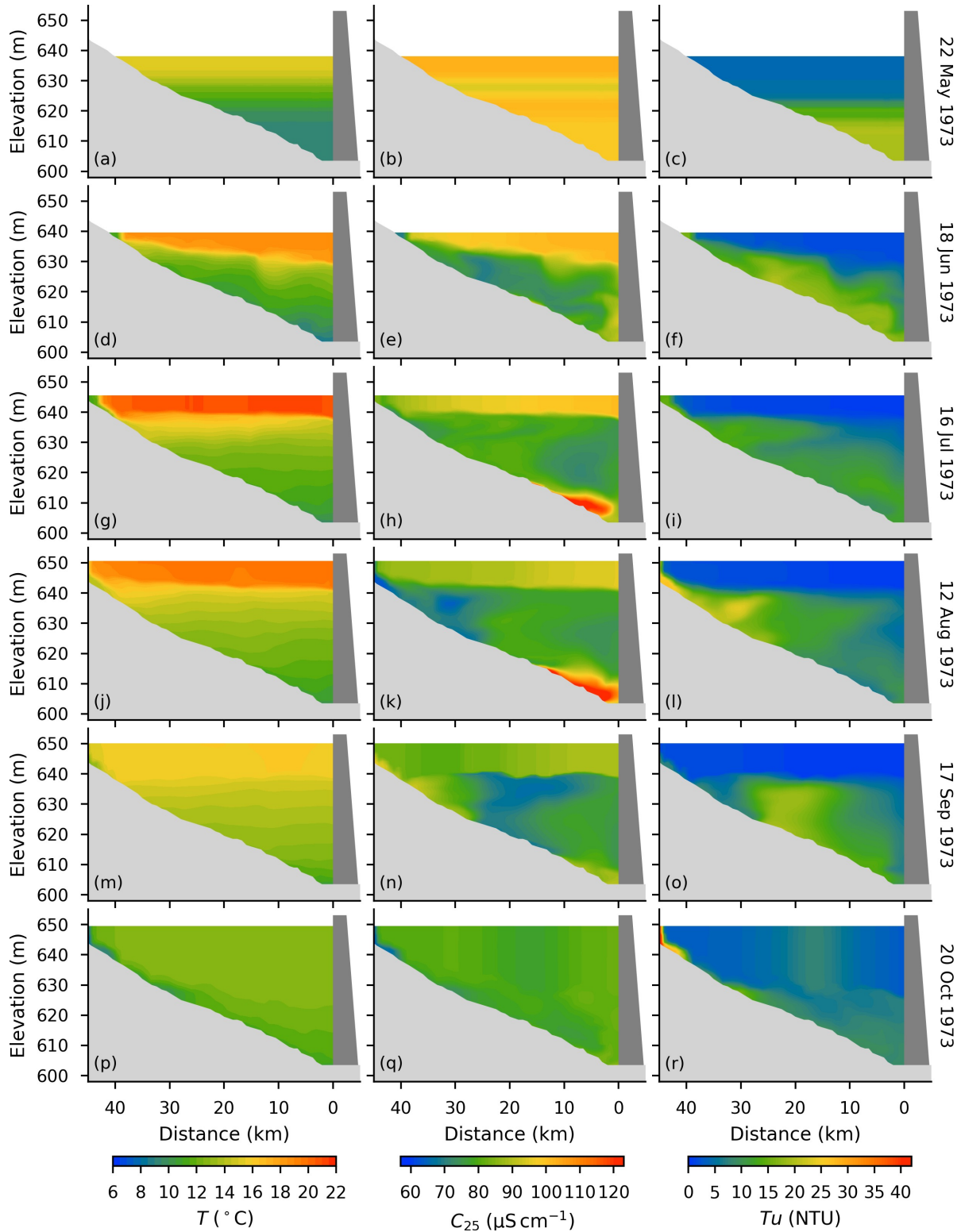


Figure 73. Scenario 1, Clear Surface Layer (1973). Snapshots of modelled temperature T , conductivity C_{25} , and turbidity Tu .

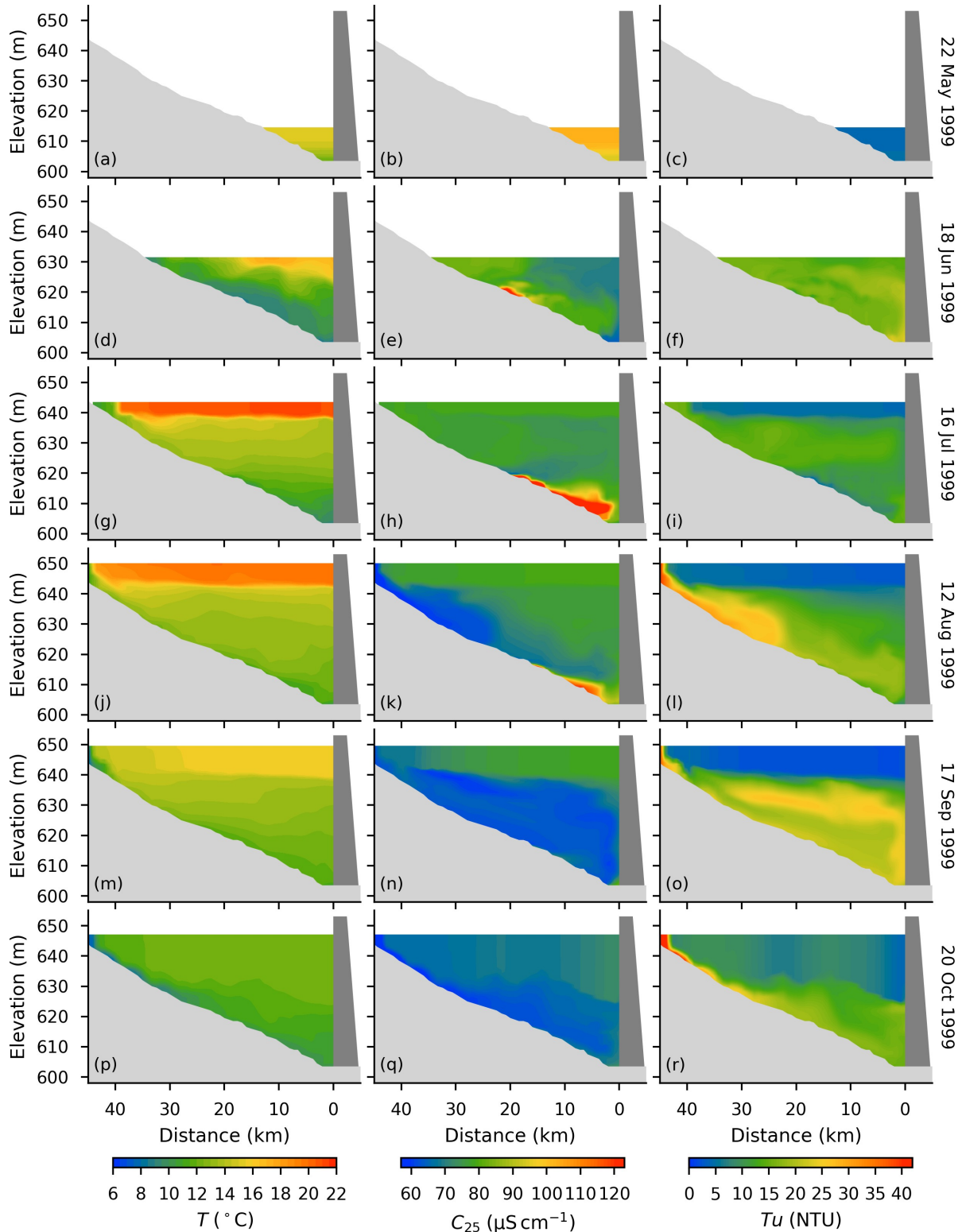


Figure 74. Scenario 2, Turbid Surface Layer (1999). Snapshots of modelled temperature T , conductivity C_{25} , and turbidity Tu .

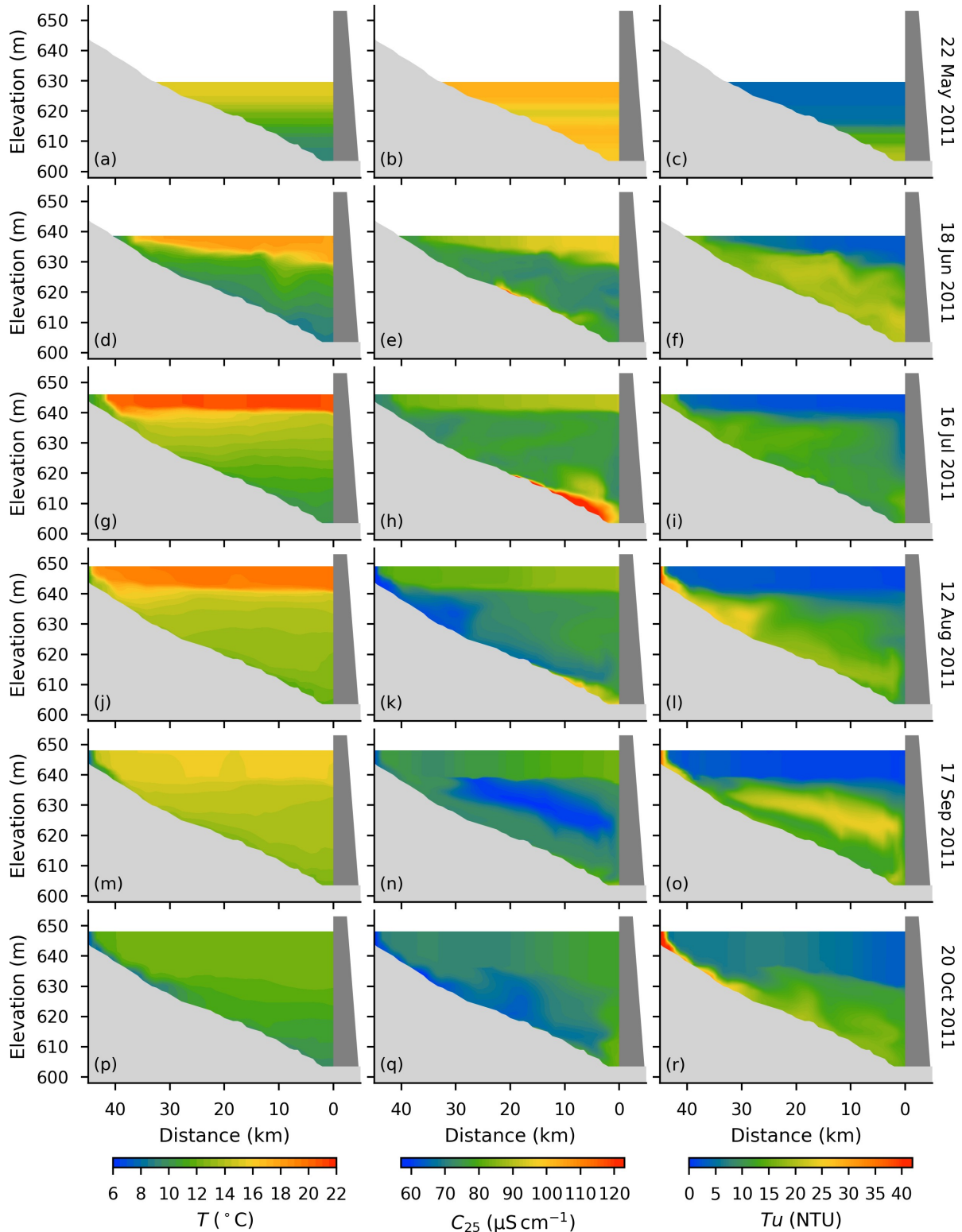


Figure 75. Scenario 3, Normal Operations (2011). Snapshots of modelled temperature T , conductivity C_{25} , and turbidity Tu .

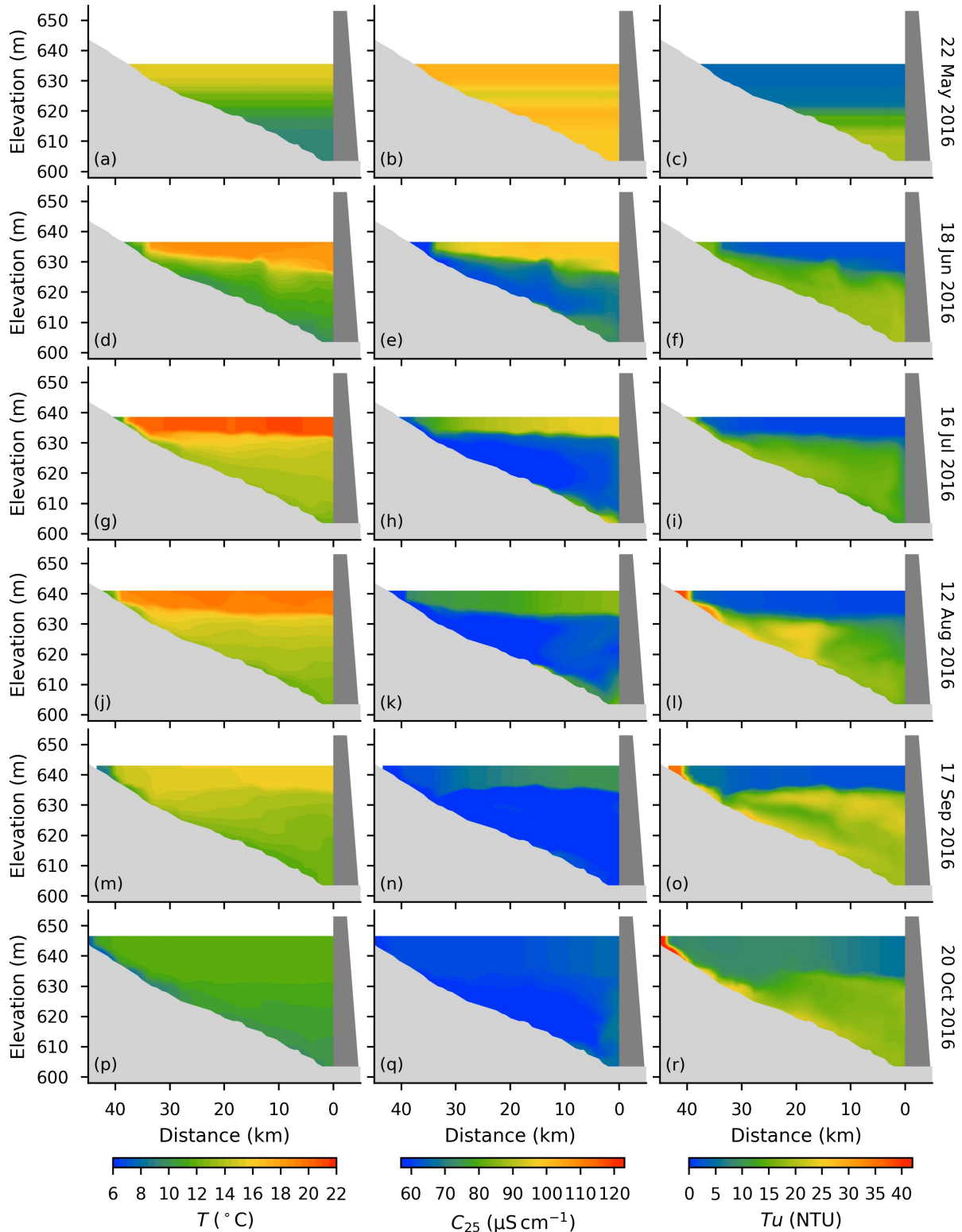


Figure 76. Scenario4, Low Downton Reservoir (2016). Snapshots of modelled temperature T , conductivity C_{25} , and turbidity T_u .

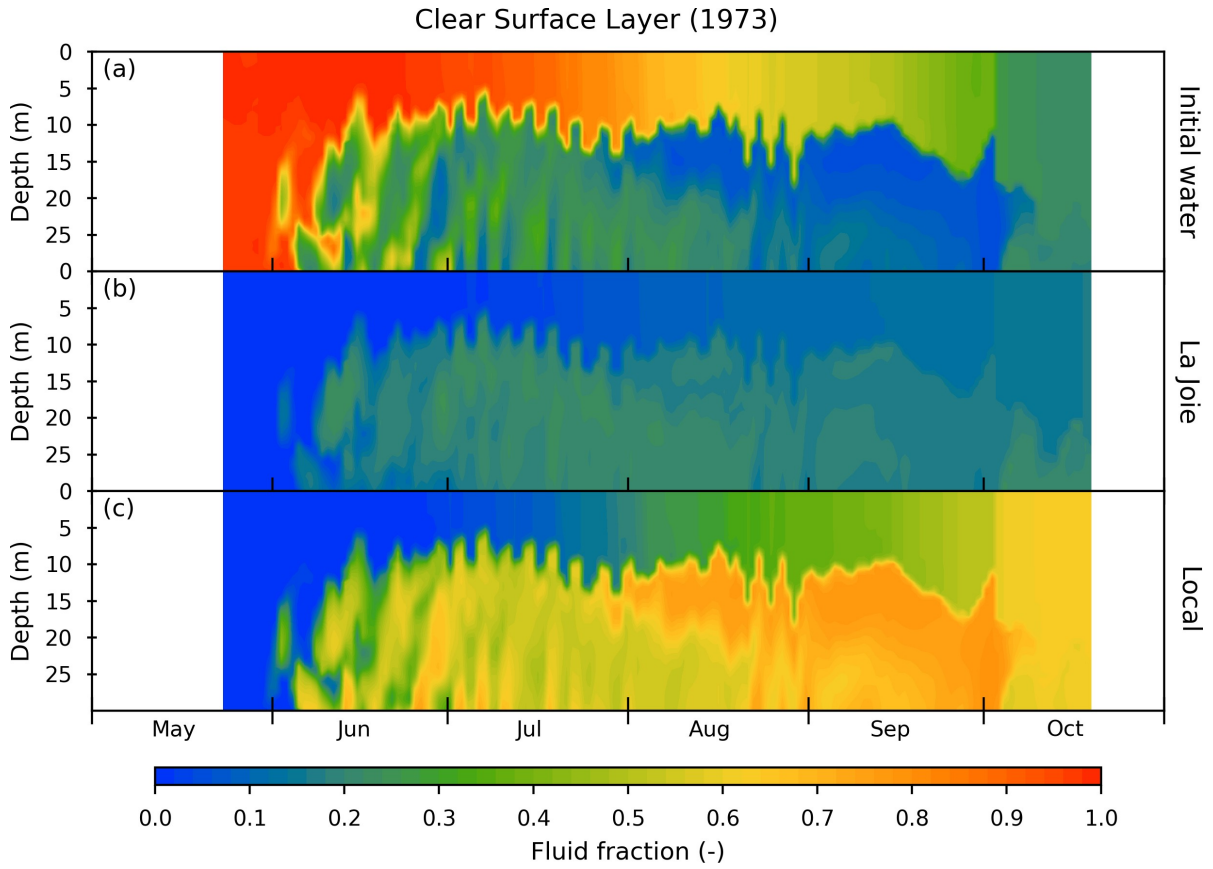


Figure 77. Scenario 1, Clear Surface Layer (1973). Passive conservative tracers at segment 53 (station C2) from (a) Initial water in the reservoir, (b) inflow from La Joie Dam, (c) Local tributary inflow.

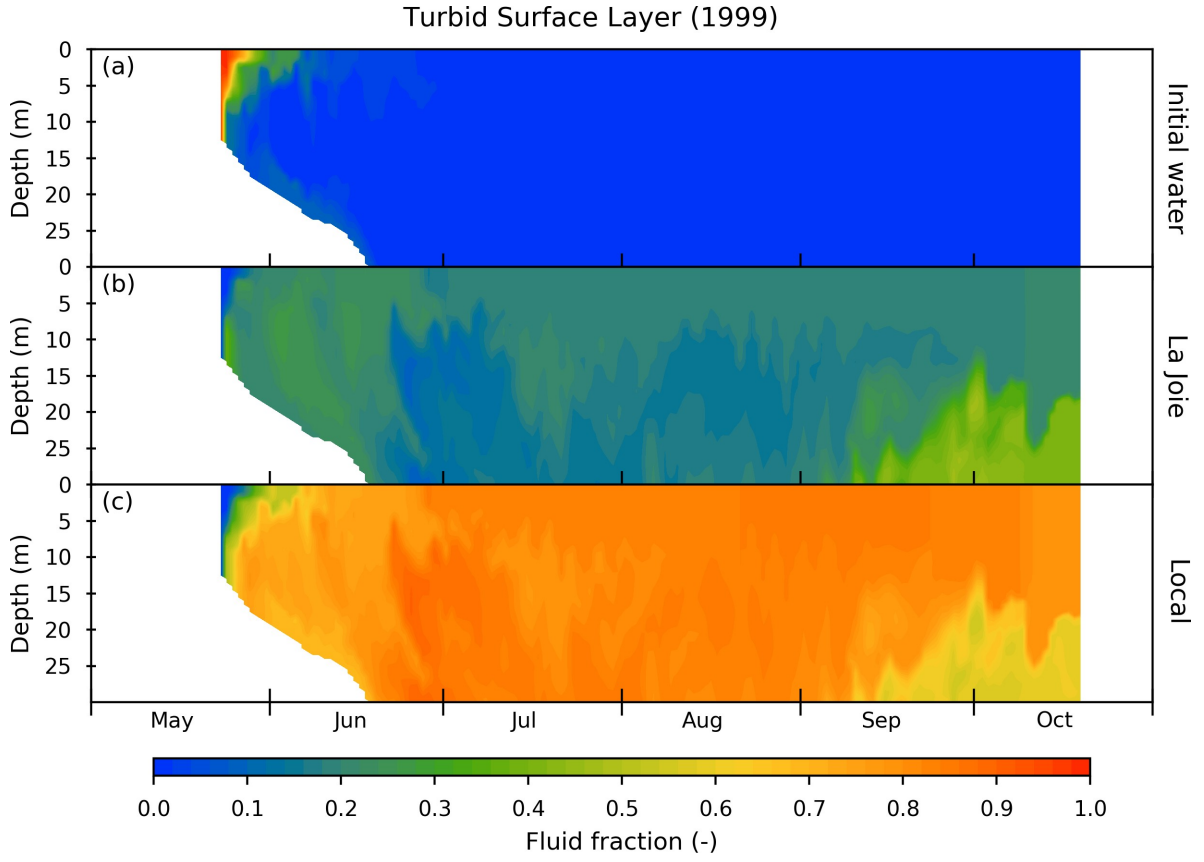


Figure 78. Scenario 2, Turbid Surface Layer (1999). Passive conservative tracers at segment 53 (station C2) from (a) Initial water in the reservoir, (b) inflow from La Joie Dam, (c) Local tributary inflow.

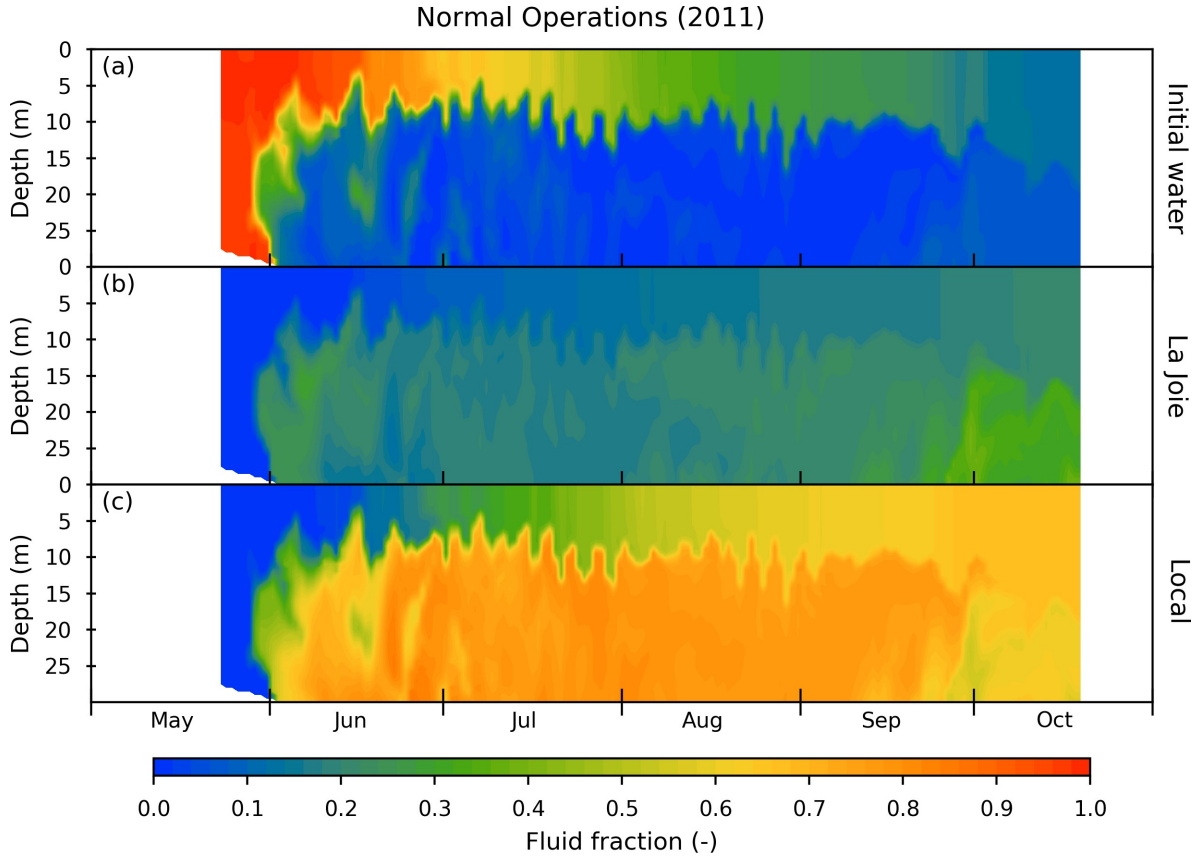


Figure 79. Scenario 3, Normal Operations (2011). Passive conservative tracers at segment 53 (station C2) from (a) Initial water in the reservoir, (b) inflow from La Joie Dam, (c) Local tributary inflow.

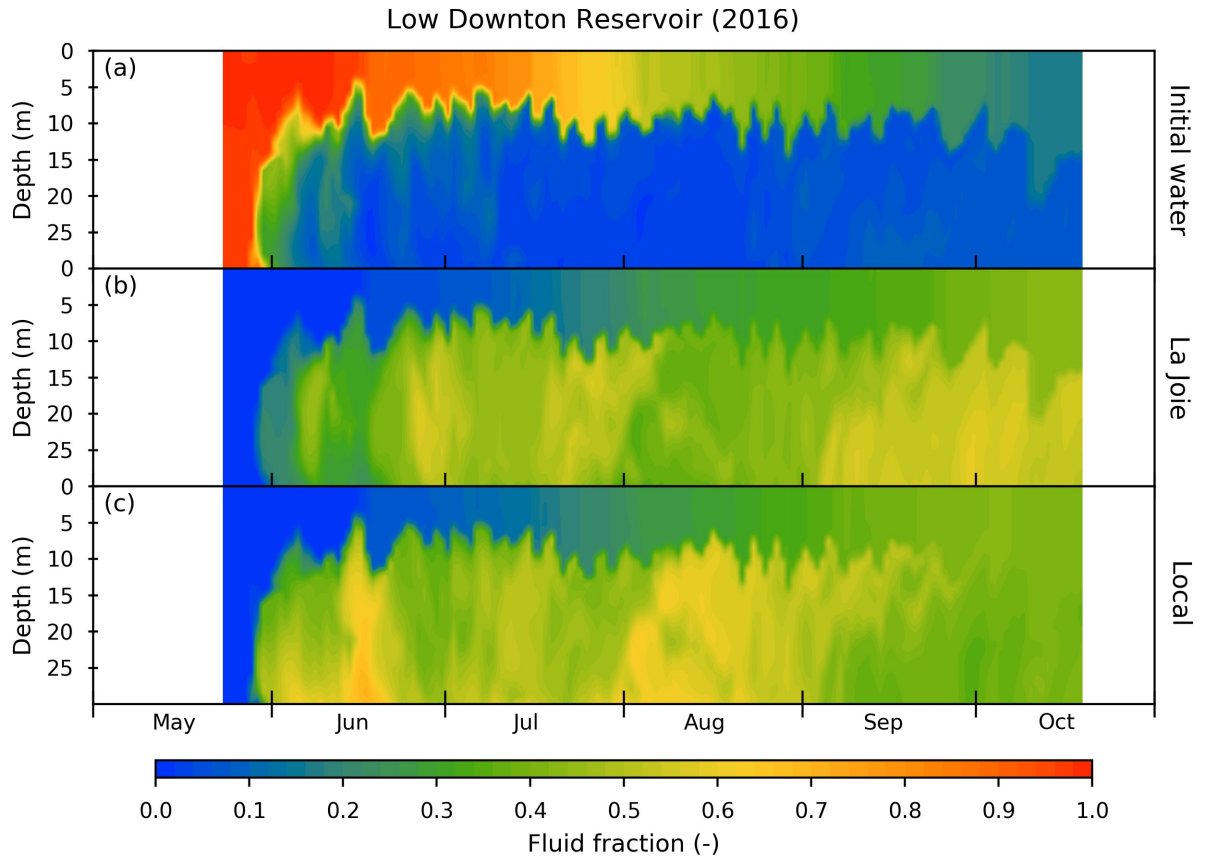


Figure 80. Scenario 4, Low Downton Reservoir (2016). Passive conservative tracers at segment 53 (station C2) from (a) Initial water in the reservoir, (b) inflow from La Joie Dam, (c) Local tributary inflow.